UNIVERSIDADE FEDERAL DE VIÇOSA

Estudo para otimização das propriedades eletromecânicas de compósitos cimentícios nanomodificados sensores e avaliação da compatibilidade mecânica em estruturas

Gustavo Emílio Soares de Lima
Doctor Scientiae

VIÇOSA - MINAS GERAIS
2024

GUSTAVO EMÍLIO SOARES DE LIMA

Estudo para otimização das propriedades eletromecânicas de compósitos cimentícios nanomodificados sensores e avaliação da compatibilidade mecânica em estruturas

Tese apresentada à Universidade Federal de Viçosa, como parte das exigências do Programa de Pós-Graduação em Engenharia Civil, para obtenção do título de *Doctor Scientiae*.

Orientador: Leonardo Goncalves Pedroti

Coorientadores: Jose M. F. de Carvalho
Jose C. Lopes Ribeiro

VIÇOSA - MINAS GERAIS
2024

Ficha catalográfica elaborada pela Biblioteca Central da Universidade Federal de Viçosa - Campus Viçosa

T
L732e
2024

Lima, Gustavo Emílio Soares de, 1985-
Estudo para otimização das propriedades eletromecânicas de compósitos cimentícios nanomodificados sensores e avaliação da compatibilidade mecânica em estruturas / Gustavo Emílio Soares de Lima. – Viçosa, MG, 2024.
1 tese eletrônica (209 f.): il. (algumas color.).

Texto em português e inglês.
Orientador: Leonardo Gonçalves Pedroti.
Tese (doutorado) - Universidade Federal de Viçosa, Departamento de Engenharia Civil, 2024.
Inclui bibliografia.
DOI: https://doi.org/10.47328/ufvbbt.2025.569
Modo de acesso: World Wide Web.

1. Cimento. 2. Nanocompósitos (Materiais). 3. Nanopartículas. 4. Carbono. 5. Nanotubos. I. Pedroti, Leonardo Gonçalves, 1978-. II. Universidade Federal de Viçosa. Departamento de Engenharia Civil. Programa de Pós-Graduação em Engenharia Civil. III. Título.

CDD 22. ed. 620.135

Bibliotecário(a) responsável: Bruna Silva CRB-6/2552

GUSTAVO EMÍLIO SOARES DE LIMA

Estudo para otimização das propriedades eletromecânicas de compósitos cimentícios nanomodificados sensores e avaliação da compatibilidade mecânica em estruturas

Tese apresentada à Universidade Federal de Viçosa, como parte das exigências do Programa de Pós-Graduação em Engenharia Civil, para obtenção do título de *Doctor Scientiae*.

APROVADA: 19 de julho de 2024.

Assentimento:

Gustavo Emílio Soares de Lima
Autor

Leonardo Goncalves Pedroti
Orientador

Para Kelly, Bernardo e Carolina. O verdadeiro motivo para continuar seguindo em frente.

AGRADECIMENTOS

Em primeiro lugar, agradeço a Deus por ter me dado forças para continuar lutando.

A Kelly, por estar ao meu lado e, da sua forma, me incentivar.

Ao Bernardo e Carolina, por estarem aqui. Sem dúvidas, a conclusão mais importante desta Tese.

Aos meus pais, por toda ajuda e compreensão nos momentos de falta.

Ao meu Orientador, pela amizade, incentivo e ensinamentos.

Aos meus Coorientadores, pelo apoio e valiosos conselhos.

Aos amigos Gustavo Nalon e Rodrigo, por toda colaboração e companheirismo.

Ao Técnicos do LMC, por todo suporte e ajuda.

Ao PPGEC, pela oportunidade e suporte.

A UFV, por me ajudar a sonhar.

A todos aqueles que de alguma forma participaram desta jornada, meu muito obrigado!

Este trabalho foi realizado com o apoio das seguintes agências de pesquisa brasileiras: Coordenação de Aperfeiçoamento de Pessoal de Nível Superior – Brasil (CAPES) – Código de Financiamento 001, Fundação de Amparo à Pesquisa do Estado de Minas Gerais (FAPEMIG) e Conselho Nacional de Desenvolvimento Científico e Tecnológico (CNPq).

RESUMO

LIMA, Gustavo Emílio Soares de, D.Sc., Universidade Federal de Viçosa, julho de 2024. **Estudo para otimização das propriedades eletromecânicas de compósitos cimentícios nanomodificados sensores e avaliação da compatibilidade mecânica em estruturas**. Orientador: Leonardo Goncalves Pedroti. Coorientadores: Jose Maria Franco de Carvalho e Jose Carlos Lopes Ribeiro.

O monitoramento da integridade estrutural (SHM) é um campo em expansão que visa avaliar continuamente o comportamento de estruturas por meio de dispositivos sensores. Estes sistemas permitem a coleta em tempo real de parâmetros cruciais como deformação, deslocamentos, temperatura e umidade, viabilizando a detecção precoce de anomalias e o planejamento de intervenções. Neste contexto, a presente pesquisa investigou a otimização de compósitos cimentícios nanomodificados sensores (CCNS), com o objetivo de aprimorar suas propriedades sensoras e sua aplicabilidade no monitoramento de vigas de concreto armado. O estudo teve como objetivo principal o desenvolvimento e a otimização da dispersão de nanopartículas, focando em sua compatibilidade mecânica e desempenho em elementos estruturais. Inicialmente, foi realizada uma revisão abrangente da literatura sobre a produção, os mecanismos de hidratação e as propriedades mecânicas e piezoresistivas de argamassas sensoras. Esta análise permitiu identificar os efeitos de diferentes materiais nos mecanismos de condutividade elétrica e autodetecção, bem como sugerir resíduos industriais e agrícolas como alternativas promissoras para futuras pesquisas em CCNS. Na sequência, foram investigados os efeitos da variação da energia de sonicação na dispersão de nanopartículas de Carbon Black (CBN) e no comportamento eletromecânico e reológico dos CCNS. Através de uma combinação de quatro técnicas de análise, foi possível identificar a energia de 240 J/mL como a mais eficaz para produzir nanosuspensões de alta eficiência, otimizando as propriedades dos compósitos. Em seguida, o foco foi a avaliação do impacto da variação da razão entre aditivo superplastificante (PCE) e CBN no comportamento eletromecânico e reológico. A pesquisa determinou que uma razão de 0.4 otimiza o desempenho dos CCNS, resultando em nanosuspensões com dispersão e estabilidade superiores. Por fim, a compatibilidade mecânica entre os CCNS e um elemento de concreto armado submetido à flexão foi analisada, demonstrando que o sensor desenvolvido possui habilidade satisfatória para automonitoramento de deformações e autodetecção de danos. Os resultados obtidos revelaram que a concentração ideal de 5% de CBN proporcionou a melhor combinação entre piezorresistividade e

propriedades mecânicas adequadas. Além disso, a pesquisa demonstrou que um módulo de elasticidade ligeiramente menor para o sensor, em comparação com a estrutura monitorada, é crucial para a obtenção de uma resposta coerente. A análise comparativa com strain gauges comerciais validou a capacidade do sensor em identificar danos e deformações, consolidando seu potencial para aplicação prática em SHM. As contribuições deste trabalho fornecem diretrizes essenciais para a seleção e aplicação de CCNS, abrindo caminho para o desenvolvimento de soluções mais eficientes e confiáveis no campo do monitoramento de infraestruturas.

Palavras-chave: compósitos cimentícios nanomodificados sensores; nanopartículas de Carbon Black; piezoresistividade; dispersão de nanopartículas; compatibilidade mecânica

ABSTRACT

LIMA, Gustavo Emílio Soares de, D.Sc., Universidade Federal de Viçosa, July, 2024. **Optimization study of electromechanical properties of cementitious composite nanomodified sensors and mechanical compatibility evaluation in structures**. Adviser: Leonardo Goncalves Pedroti. Co-advisers: Jose Maria Franco de Carvalho and Jose Carlos Lopes Ribeiro.

Structural Health Monitoring (SHM) is a growing field that aims to continuously assess the behavior of structures using sensing devices. These systems enable the real-time collection of crucial parameters like strain, displacement, temperature, and humidity, facilitating the early detection of anomalies and the planning of interventions. In this context, the present research investigated the optimization of Cement Composite Nanomodified Sensors (CCNS), with the goal of enhancing their sensing properties and their applicability in monitoring reinforced concrete beams. The main objective of the study was the development and optimization of nanoparticle dispersion, focusing on their mechanical compatibility and performance in structural elements. Initially, a comprehensive literature review was conducted on the production, hydration mechanisms, and the mechanical and piezoresistive properties of sensor-enabled mortars. This analysis identified the effects of different materials on electrical conductivity and self-sensing mechanisms, as well as suggesting industrial and agricultural waste as promising alternatives for future research in CCNS. Subsequently, the effects of varying sonication energy on the dispersion of Carbon Black Nanoparticles (CBN) and the electromechanical and rheological behavior of the CCNS were investigated. Through a combination of four analytical techniques, an energy of 240 J/mL was identified as the most effective for producing high-efficiency nanosuspensions, thereby optimizing the composite's properties. Next, the focus was on evaluating the impact of varying the ratio between superplasticizer additive based on polycarboxylate ether (PCE) and CBN on the electromechanical and rheological behavior. The research determined that a ratio of 0.4 optimizes the performance of the CCNS, resulting in nanosuspensions with superior dispersion and stability. Finally, the mechanical compatibility between the CCNS and a reinforced concrete element subjected to bending was analyzed, demonstrating that the developed sensor possesses satisfactory ability for strain self-monitoring and damage self-sensing. The obtained results revealed that the ideal concentration of 5% of CBN provided the best combination of piezoresistivity and adequate mechanical properties. Furthermore, the research demonstrated that a slightly lower elastic modulus for the sensor,

in comparison to the monitored structure, is crucial for obtaining a coherent response. A comparative analysis with commercial strain gauges validated the sensor's capacity to identify damage and deformation, consolidating its potential for practical application in SHM. The contributions of this work provide essential guidelines for the selection and application of CCNS, paving the way for the development of more efficient and reliable solutions in the field of infrastructure monitoring.

Keywords: cement composite nanomodified sensors; carbon black nanoparticles; piezoresistivity; nanoparticle dispersion; mechanical compatibility

Sumário

1 INTRODUÇÃO GERAL

1.1 CONSIDERAÇÕES INICIAIS

O monitoramento da integridade estrutural (SHM, do inglês *Structural Health Monitoring*) tem como principal objetivo avaliar de forma contínua o comportamento de determinadas características de uma estrutura. Por meio de dispositivos sensores, é possível monitorar em tempo real parâmetros como deformação, deslocamentos, temperatura, umidade, etc. Estas informações são fundamentais para detecção prematura de anomalias e planejamento de intervenções de manutenção, recuperação e reforço [1–3].

Estudos recentes têm proposto o uso de compósitos cimentícios nanomodificados como sensores para monitoramento de deformação, tensão e danos [4–6]. Para obter este efeito, nanomateriais com boa condutividade elétrica são incorporados e adequadamente dispersos na matriz cimentícia, a fim de formar uma extensa rede condutora, reduzindo a resistividade elétrica do compósito para valores próximos àqueles dos semicondutores [7]. Quando este material está sujeito a um carregamento, ele se deforma e apresenta alterações em sua resistividade elétrica. Este comportamento faz com que o compósito funcione como um elemento sensor, possibilitando realizar medições de deformação, tensão e até mesmo de danos causados por fissuração.

Por serem quimicamente inertes e apresentarem elevada condutividade elétrica, nanomateriais à base de carbono são frequentemente utilizados como *fillers* condutivos em materiais cimentícios sensores [8,9]. Neste contexto, nanopartículas de *carbon black* (NCB) têm ganhado destaque em diversas pesquisas relacionadas à aplicação em compósitos cimentícios sensores, por proporcionarem vantagens, tais como: baixo custo, elevada condutividade elétrica, elevada sensibilidade à deformação, boa estabilidade de sinal e facilidade de aplicação [6,10–14]. Além disso, quando adicionado em proporções adequadas, as NCB podem contribuir com o refinamento da matriz cimentícia [8].

Diversos estudos têm se dedicado ao desenvolvimento de compósitos cimentícios nanomodificados sensores (CCNS) utilizando NCB como *filler* condutivo. De forma geral, esses trabalhos adotam dosagens estabelecidas de forma empírica e estão focados no comportamento de diversas propriedades desses sensores associadas à variação do teor das nanopartículas [15–18]. Quanto à aplicação de CCNS em elementos estruturais, atualmente existe número reduzido de referências na literatura, focados principalmente em testar a resposta de sensores com diferentes características [19–21].

Desta forma, buscando contribuir com este promissor campo de pesquisa, o presente trabalho visa investigar a otimização da dispersão de nanopartículas para produção de compósitos cimentícios nanomodificados sensores, com foco na energia ultrassônica aplicada para separação de agregados de CBN e no teor de surfactante (aditivo superplastificante). Assim, espera-se obter um compósito com suas propriedades sensoras potencializadas e, na etapa final desta investigação, verificar a compatibilidade mecânica e aplicabilidade deste compósito no monitoramento de danos em vigas de concreto armado, bem como a confiabilidade de sua resposta de deformação.

1.2 OBJETIVOS

1.2.1. Objetivo geral

Tem-se como objetivo geral o desenvolvimento de um estudo para otimização da dispersão de nanopartículas, visando a potencialização das propriedades de compósitos cimentícios nanomodificados sensores (CCNS) e a avaliação da compatibilidade mecânica destes compósitos em vigas de concreto armado.

1.2.2. Objetivos específicos

Os objetivos específicos do presente estudo são:

a) investigar e sistematizar, o estado da arte para produção, os mecanismos de hidratação e as propriedades mecânicas e piezoresistivas de argamassas sensoras;
b) avaliação dos efeitos da variação da energia ultrassônica aplicada na dispersão das nanopartículas nas propriedades de compósitos cimentícios nanomodificados sensores;
c) avaliação dos efeitos da variação do teor de surfactante utilizado na estabilização da dispersão de nanopartículas nas propriedades de compósitos cimentícios nanomodificados sensores; e
d) verificação da compatibilidade mecânica de nanocompósitos cimentícios sensores embutidos em vigas de concreto armado e seus efeitos no monitoramento de deformações e danos.

1.3 JUSTIFICATIVA

O mercado global do SHM tem se ampliado anualmente, impulsionado principalmente pela construção de novas obras de infraestrutura e pela necessidade de conservar as estruturas já existentes. Essas edificações têm um elevado custo de implementação e manutenção, sendo desejável ampliar sua durabilidade e vida útil. Projeções de empresas especializadas em consultoria de mercado, indicam uma taxa de crescimento anual da ordem de 11.5% entre 2022 e 2030 para os investimentos em SHM, podendo alcançar valores na casa dos US$5.8 bilhões até 2030.

Os CCNS, de forma geral, não apresentam problemas frequentes de compatibilidade química com o concreto, entretanto a compatibilidade mecânica ainda representa um grande desafio. Falhas neste ponto podem significar que a resposta do sensor não será capaz de reproduzir adequadamente os fenômenos que se deseja monitorar. Como as estruturas de concreto armado possuem uma grande variabilidade em suas propriedades mecânicas, os sensores de base cimentícia precisariam ser produzidos com características específicas para apresentar compatibilidade mecânica com a estrutura na qual serão instalados. Outro ponto relevante é que os sensores podem ter exigências de projeto, como por exemplo, uma sensibilidade à deformação mínima ou uma característica mecânica específica.

Devido à tendência de aglomeração dos nanomateriais, uma dispersão adequada dessas partículas dentro da matriz cimentícia é um procedimento essencial para a obtenção de compósitos sensores com respostas elétricas estáveis e reprodutíveis. Além disso, uma dispersão de melhor qualidade e mais estável contribui para reduzir a quantidade de energia mecânica necessária na mistura com os demais materiais constituintes, possibilitando também um aumento no número de caminhos condutivos disponíveis e ganhos para as propriedades elétricas e mecânicas do material. Contudo, não foram identificados na literatura estudos anteriores que investigaram alternativas para a otimização da dispersão de CBN voltados para a produção de argamassas sensoras, que proporcionem uma baixa resistividade elétrica e boa resposta piezoresistiva, sem causar impactos negativos nas propriedades mecânicas. Além disso, também não foram encontrados estudos relacionados a avaliação da compatibilidade mecânica entre os CCNS à base de CBN e um elemento estrutural.

Neste sentido, as três principais contribuições do presente trabalho são: (i) a compreensão dos efeitos do teor de CBN nos mecanismo de hidratação e nas propriedades eletromecânicas de CCNS; (ii) a identificação da energia de sonicação e teor de aditivo superplastificante ótimos

para a produção de CCNS; e (iii) a avaliação da resposta sensora de CCNS embutidos em vigas de concreto armado com diferentes propriedades mecânicas, permitindo verificar adequadamente a compatibilidade mecânica entre o compósito sensor e o concreto.

De forma mais ampla, o presente trabalho irá contribuir com a Linha de Pesquisa relacionada ao desenvolvimento de compósitos cimentícios inteligentes no âmbito da Área de concentração em Engenharia da Construção do Programa de Pós-Graduação em Engenharia Civil da Universidade Federal de Viçosa.

1.4 REFERENCIAL TEÓRICO

1.4.1 Compósitos cimentícios sensores piezoresistivos

1.4.1.1 Generalidades

Um sensor piezoresistivo de base cimentícia é um compósito que consiste de uma fase condutiva e uma fase não condutiva [4,22]. A fase condutiva é formada por *fillers* funcionais como as nanopartículas de *carbon black* (CBN) e nanotubos de carbono (CNT), e a fase não condutiva é formada pela matriz cimentícia do compósito no estado seco (pasta, argamassa ou concreto) [23–28]. A fase condutiva, quando adicionada à fase não condutiva, estabelece as condições para observação do comportamento piezoresistivo no compósito [22]. O fenômeno da piezoresistividade consiste na capacidade do material apresentar mudanças reversíveis na sua resistividade elétrica quando sofre uma pressão [29,30]. De forma geral, sensores baseados neste fenômeno têm despertado grande interesse devido a sua facilidade de produção e facilidade na aquisição do sinal de resposta [31,32].

Dentre as nanopartículas empregadas no desenvolvimento de sensores piezoresistivos, as CBN têm uso frequente na literatura. Esse material é composto por partículas de carbono de formato aproximadamente esférico e com estrutura porosa [33,34]. Além disso, as CBN apresentam elevada superfície específica, elevada condutividade elétrica, baixos custos de produção e boas propriedades mecânicas [8,11].

1.4.1.2 Mecanismos de condutividade elétrica

A condução de eletricidade em CCNS ocorre basicamente de duas formas: a iônica, que está relacionada ao movimento de íons dissolvidos na água contida no interior dos poros do

material cimentício, e a eletrônica, que está relacionada ao movimento de elétrons através do gel e nanopartículas [4,11,35]. No estado seco e à temperatura ambiente, os materiais cimentícios são quase isolantes, apresentando resistividades elétricas da ordem de 10^4 a 10^8 Ωcm [36,37]. Entretanto, após a adição de quantidades adequadas de *fillers* condutivos, esta resistividade pode chegar próximo de 1 Ωcm [38].

De forma geral, com o aumento do teor de *fille*r condutivo na matriz cimentícia, é atingida uma concentração crítica, o chamado limiar de percolação, que separa a curva Resistividade Elétrica x Concentração de *filler* condutivo (Figura 1) em três zonas distintas: isolante, de percolação e de condução [4]. Quando a quantidade de *fillers* condutivos é suficiente para se alcançar o limiar de percolação, fatores como teor de umidade e idade do material deixam de influenciar de forma tão significativa no valor da resistividade elétrica do material, uma vez que o caminho de condução ocorre majoritariamente pelos nanomateriais, e não mais pela água que eventualmente se encontre no interior dos poros [14].

Em compósitos cujo teor de nanopartículas está situado na Zona Isolante (Zona A da Figura 1), o espaço entre os *fillers* condutivos do compósito cimentício é grande, o que dificulta o surgimento de caminhos de condução elétrica entre eles [11,39]. Nesse caso, a condução iônica é dominante quando se encontra no estado úmido, e o material não possui a capacidade de funcionar como um sensor de deformação eficiente.

Figura 1: Mecanismo de condutividade elétrica

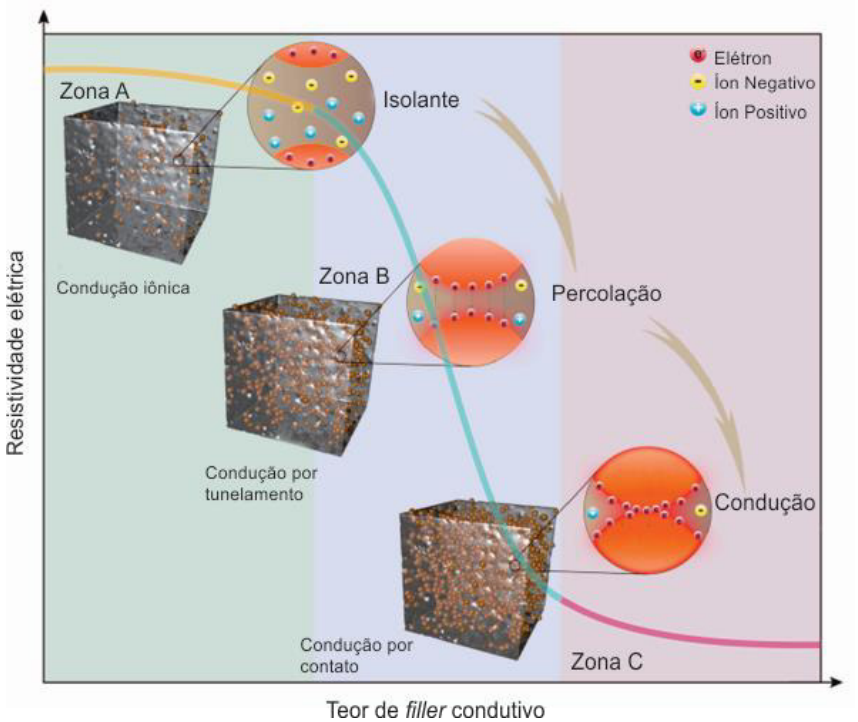

Fonte: Adaptado de Ding et al. [4] (2022).

Quando o teor de nanopartículas situa o compósito na Zona de Percolação (Zona B da Figura 1), o espaço entre *fillers* condutivos diminui, o que aumenta a quantidade de caminhos de condução entre eles, ou seja, a condução eletrônica passa a ser dominante. A condução eletrônica pode ocorrer por contato direto entre as várias partículas que formam a rede condutiva ou pelo efeito de tunelamento, o qual está associado à transmissão de elétrons entre terminações desconectadas das partículas [11]. Em compósitos nessa região, a condução por efeito de tunelamento é dominante, o que culmina em um excelente comportamento piezoresistivo [40]. Pela teoria de tunelamento quântico, quando ocorre deformação de compressão no material, sua resistividade diminui devido ao aumento da densidade de corrente de tunelamento proporcionado pela aproximação entre *fillers* condutivos adjacentes [10]. Logo, as deformações causam mudanças nos caminhos de condução de eletricidade em seu interior, o que provoca mudanças na sua resistividade elétrica.

Já em compósitos na Zona Condutiva (Zona C da Figura 1), existe uma quantidade muito maior de caminhos condutivos entre os *fillers* funcionais. Por esse motivo, a rede condutiva não sofre grande modificação quando ocorrem deformações, de modo que a sensibilidade à deformação do material não é tão elevada, sendo dominante nesses casos a condução por contato ôhmico [40].

1.4.1.3 Fabricação

Na Tabela 1, são apresentadas algumas das principais características de misturas utilizadas para produção de CCNS à base de CBN. Os métodos ultrassônicos são os mais efetivos para se obter uma boa dispersão de nanopartículas condutivas, principalmente associados ao uso de surfactantes, pois reduzem a probabilidade de reaglomeração [22].

Uma boa dispersão dos nanomateriais dentro da matriz cimentícia permite a obtenção de nanocompósitos cimentícios com propriedades estáveis e reprodutíveis e reduz a quantidade de energia mecânica necessária na mistura com os demais materiais constituintes [39]. Li et al. [10] utilizaram um aditivo superplastificante como agente dispersante de CBN e obtiveram um excelente comportamento piezoresistivo em seus compósitos. Coppola et al. [48] também relatam que obtiveram uma melhor piezoresistividade utilizando aditivo superplastificante associado a um banho ultrassônico para dispersar as nanopartículas. Entretanto, uma dispersão homogênea dos nanomateriais na água de amassamento ainda não é garantia de uma adequada dispersão deste material no compósito cimentício [49], pois as nanopartículas conseguem se

mover entre os grãos de cimento antes da formação dos produtos da hidratação do cimento, podendo levar a sua reaglomeração [50].

Tabela 1: Aplicações de CCNS em elementos estruturais

Matriz	CBN (%)[1]	Dispersão	a/c	SP (%)[1]	Referência
Pasta	2.0	Banho ultrassônico	0.40	0.8	[41]
Argamassa	0-6.0	Misturador mecânico	0.27-0.38	0.01-1	[42]
Pasta	3.0	Banho ultrassônico	0.45	0.8	[25]
Pasta	0-2.92	Banho ultrassônico	0.50	0-13.0	[11]
Argamassa	1.0	Misturador mecânico	0.38	6.0	[34]
Argamassa	2.5	Sonda ultrassônica	0.45	var	[43]
Argamassa	0-10.3	Manual	0.50	0-3.0	[44]
Pasta	0.5	Banho ultrassônico	0.40	0.8	[45]
Argamassa	0-10.0	Misturador mecânico	0.45-0.50	0.5-0.8	[46]
Argamassa	0.5-5.0	Manual	0.50	-	[47]
Argamassa	0.5-2.0	Banho ultrassônico	0.32-0.45	0.8	[20]

CBN: Nanopartículas de Carbon Black; a/c: relação água/cimento; SP: superplastificante; var: consumo variável não informado.
(1) teor em relação ao consumo de cimento

Fonte: Autor (2024)

Chen et al. [40] constataram que a trabalhabilidade de concretos no estado fresco diminui com o aumento da quantidade de CBN. Os autores observaram que o *slump* diminui cerca de 47.0% quando um teor de 0.4% de CBN (com relação à massa de aglomerante) é utilizado. Dong et al. [41] observaram uma redução significativa da trabalhabilidade de argamassas com CBN quando foram adicionadas fibras de aço. Os autores sugerem que esta redução da trabalhabilidade pode causar prejuízos a piezoresistividade. Parvan et al. [47] relatam que as CBN podem adsorver parte da água de amassamento, causando uma perda de trabalhabilidade da pasta. Segundo os autores, quando são utilizados teores elevados de CBN, é possível que as nanopartículas se aglomerem na superfície do grão de cimento anidro, impedindo sua hidratação e, levando ao atraso do fim de pega.

1.4.1.4 Propriedades mecânicas

As propriedades mecânicas dos CCNS são diretamente afetadas pelas caraterísticas das nanopartículas utilizadas em sua produção. Por exemplo, Dai et al. [42] utilizaram 5% de CBN

(relação à massa de aglomerante), com diâmetro médio de 33 nm e superfície específica de 1056 m²/g, para produzir CCNS que alcançaram aproximadamente 32 MPa de resistência à compressão aos 28 dias. Os autores argumentam que as CBN preenchem os vasos capilares, proporcionando um refinamento da matriz. Por outro lado, o aumento do teor das nanopartículas pode causar prejuízos às propriedades mecânicas do compósito, pois devido sua elevada superfície específica, essas partículas tendem a adsorver uma fração da água de amassamento, reduzindo a quantidade de água disponível para o processo de hidratação da matriz cimentícia.

Parvan et al. [47] produziram CCNS substituindo 3% e 5% da massa de cimento por CBN, com diâmetro médio de 53 nm e superfície específica de 72 m²/g. Aos 28 dias, os compósitos atingiram resistência à compressão de aproximadamente 47 MPa e 45 MPa, para adições de 3% e 5% de CBN, respectivamente. Aos 90 dias, os autores observaram um aumento da resistência da ordem de 10%, chegando a valores próximos de 52 MPa (3% de CBN) e 50 MPa (5% de CBN). Os autores atribuem a redução da resistência à compressão à redução do consumo de cimento e consequente aumento do teor de CBN. Entretanto, com o aumento da quantidade de nanopartículas, foi observada uma redução da porosidade dos compósitos.

Huang et al. [34] avaliaram o comportamento à tração de CCNS, por meio de um ensaio de tração direta. Os autores produziram os corpos de prova utilizando 2% de fibra PVA (relação ao volume de aglomerante) e 1% (relação à massa de aglomerante) de CBN, com diâmetro médio de 50 nm e superfície específica de 254 m²/g. Os autores observaram a formação da primeira fissura com uma tensão média de 3.28 MPa e uma deformação de 0.021%, enquanto a resistência à tração atingiu valores médios de 5.08 MPa. Os autores relatam que o CBN aderiu à superfície da fibra PVA, o que pode ter resultado em uma maior aderência da fibra com a matriz cimentícia.

1.4.1.5 Resistividade elétrica

A resistividade elétrica de materiais cimentícios representa sua oposição à transferência de corrente elétrica e, em casos convencionais, é função da porosidade, da composição química da solução em seus poros e da interação com o ambiente em que se encontra [51,52]. Quanto maior o tamanho dos poros, a interconectividade entre eles e o teor de água em seu interior, menor é o valor da resistividade elétrica do material cimentício.

O método mais simples de se medir a resistividade elétrica de um material cimentício consiste na aplicação de uma corrente contínua (medição CC) neste material. Medindo-se a

diferença de potencial *U* entre dois eletrodos e a corrente elétrica *i* no circuito, determina-se a resistência interna *R* do compósito pela Eq. (1):

$$R = \frac{U}{i} \tag{1}$$

Conhecendo-se a área *A* do eletrodo que penetra o material cimentício e a distância *L* entre os eletrodos, pode-se estimar a resistividade ρ pela Eq. (2) [53,54]:

$$\rho = \frac{RA}{L} \tag{2}$$

Downey et al. [55], ao utilizarem uma medição CC e calcularem R através da Eq. (1), demostraram que ocorre um aumento exponencial da resistência elétrica do material ao longo do tempo. Tal comportamento capacitivo é indesejável em nanocompósitos a serem empregados em SHM, uma vez que tais variações na resistência elétrica não estão associadas a deformações e danos do material cimentício. Para contornar este problema, alguns autores sugerem que o monitoramento de deformações e danos seja feito apenas a partir do momento em que o valor da resistência elétrica se estabilizar [5,56].

Técnicas mais apropriadas para medição da resistividade elétrica dos nanocompósitos cimentícios são aquelas que os submetem a corrente alternada (medição CA) com picos positivos e negativos de igual magnitude. Hou e Lynch [36] explicam que esses métodos possibilitam que a amostra seja carregada e descarregada ao longo do tempo. Aumentando-se o valor da frequência da corrente alternada, torna-se possível reduzir os impactos do efeito de polarização para níveis aceitáveis. Contudo, a necessidade de medição de parâmetros como reatância, impedância e ângulo de fase exige o uso de equipamentos eletrônicos e processadores mais sofisticados.

Foi proposto por Downey et al. [55] uma abordagem para determinação de valores estáveis de resistência elétrica de compósitos cimentícios, a qual chamaram de medição CC bifásica. Através dessa técnica é possível mitigar os impactos do efeito de polarização. Além disso, apenas equipamentos medidores de tensão com múltiplos canais precisam ser utilizados. A técnica consiste em utilizar ciclos periódicos de carga e descarga elétrica do nanocompósito, por meio da aplicação de tensão na forma de onda quadrada. Em algum instante de tempo de cada semionda positiva faz-se a medição de *U* e *i* para o cálculo de *R* pela Eq. (1). Durante cada

semionda negativa, ocorre a inversão do sentido da corrente elétrica, o que possibilita a despolarização do material e viabiliza seu uso para o monitoramento de efeitos de ações predominantemente estáticas.

1.4.1.6 Monitoramento de deformações

Baseado no fenômeno da piezoresistividade, os compósitos cimentícios dopados com *fillers* condutivos, podem ter a habilidade de monitorar sua própria deformação e de elementos nos quais estão inseridos [57]. Como as deformações produzidas nos materiais cimentícios habitualmente são pequenas, a mudança relativa na resistência elétrica do material pode ser considerada igual à mudança relativa na sua resistividade [14].

Sejam, respectivamente, R_0 e ρ_0 a resistência e a resistividade elétrica inicial do material cimentício e, ΔR e $\Delta\rho$ as variações de sua resistência e resistividade associadas a uma deformação linear ε. O fator *gauge S* de um material, também chamado de coeficiente de deformação ou sensibilidade à deformação, pode ser calculado através da Eq. (3).

$$S = \frac{\frac{\Delta R}{R_0}}{\varepsilon} \approx \frac{\frac{\Delta \rho}{\rho_0}}{\varepsilon} \tag{3}$$

Quando a deformação ε ocorrer devido à uma tensão σ aplicada ao material, pode-se calcular a sensibilidade à tensão Q do material pela Eq. (4).

$$Q = \frac{\frac{\Delta R}{R_0}}{\sigma} \approx \frac{\frac{\Delta \rho}{\rho_0}}{\sigma} \tag{4}$$

1.4.2 Aplicações de CCNS em elementos estruturais

Na literatura ainda existe um número limitado de trabalhos que se dedica a exploração do comportamento de CCNS em elementos estruturais. Na Tabela 2, são apresentados os principais estudos encontrados na literatura. Na análise da tabela, nota-se uma variedade de dimensões dos elementos estruturais e do tipo de *filler* condutivo aplicados. Por outro lado, há uma predominância do uso de ensaios estáticos com flexão a 4 pontos. Quanto à instalação do sensor,

os estudos, em sua maioria, optam por embutir CCNS durante o momento da moldagem do elemento estrutural ou após a cura deste elemento.

Tabela 2: Aplicações de CCNS em elementos estruturais

Elemento estrutural		Sensor		Tipo de ensaio	Referência
Tipo	Dimensões (b x h x c cm)	*Filler*	Instalação		
Viga	4x4x16	CBN	Embutido[1]	Flexão (3p)	[20]
Viga T	12x17x450 (mesa: 60 cm)	CNT	Ancorado na superfície	Dinâmico (2p)	[19]
Viga	2,5x3x25	NCF	Embutido[2]	Flexão (3p)	[58]
Viga	10x15x100	CF+CNT	Embutido[1]	Flexão (4p)	[59]
Viga	10x10x40	SF+CF+CNT	Embutido[2]	Flexão (4p)	[60]
Viga	10x10x40	SF+CF+CBN	Embutido[2]	Flexão (4p)	[61]
Viga	10x15x100	CF+CNT	Embutido[2]	Flexão (4p)	[62]
Viga	5x20x60	GNP	Embutido[1]	Flexão (4p)	[63]
Viga	10x10x40	CNT	Embutido[1]	Flexão (3p)	[64]
Viga	10x10x50	CNT	Embutido[2]	Flexão (4p)	[65]
Viga	10x10x50	CNT	Embutido[2]	Flexão (4p)	[66]
Viga	25x25x200	CNT	Embutido[1]	Dinâmico (2p)	[67]
Viga	3x7x28	CF	Embutido[1]	Flexão (4p)	[68]
Viga	20x30x430	CNT	Ancorado na superfície	Dinâmico (2p)	[69]
Viga	10x10x40	CBN	Embutido[2]	Flexão (3p)	[70]
Viga	15x30x240	CBN	Embutido[1]	Flexão (3p)	[71]

CBN: Nano Carbon Black; CNT: Nanotubos de carbono; NCF: Nanofibra de carbono; CF: Fibra de carbono; SF: Fibra de aço; GNP: Nanoplaquetas de grafite
(1) Sensor embutido na moldagem; (2) Sensor embutido após a moldagem

Fonte: Autor (2024)

Apesar de ainda não existirem muitos estudos relacionados ao comportamento de CCNS em elementos estruturais, as pesquisas realizadas até o momento fizeram observações de grande relevância. Por exemplo, Rao e Sasmal [19] sugerem que a sensibilidade a vibração dos CCNS é altamente influenciada pelo teor de *filler* condutivo. Os autores relatam que com teores da ordem de 0.5% de CNT (% peso de cimento) foi observado um excelente comportamento piezoresistivo. Entretanto, só com concentrações mais elevadas foi possível obter sensibilidade a vibração; Dong et al. [20] monitoraram de forma satisfatória as tensões e o início do colapso de uma viga submetida a flexão em 3 pontos. Segundo os autores, os melhores resultados foram obtidos com sensores com 2% de CB (% peso de cimento). Os sensores instalados na zona comprimida exibiram uma redução gradual da resistividade elétrica com o aumento do carregamento, mas retornaram a valores próximos ao inicial quando a viga se aproximou da falha na flexão. Os sensores posicionados na zona tracionada apresentaram um aumento da resistividade elétrica com o aumento da tensão de flexão; Yang e Sun [58] avaliaram alteração da resistividade elétrica em sensores de NCF em temperaturas variando de -40 ºC a +40 ºC. Os

autores verificaram que a resistividade elétrica diminuiu com o aumento da tensão de flexão para todas as temperaturas testadas. Os autores sugerem que a resistividade máxima obtida (resistividade final) pode ser utilizada como referência para previsão do início do processo de fissuração do elemento estrutural. Liu et al. [63] estudaram o comportamento piezoresistivo de sensores à base de GNP para o monitoramento de deformações em vigas submetidas à flexão. Os autores observaram que os CCNS com adição de 6.4% apresentaram propriedades mecânicas similares as de compósitos cimentícios sem a adição de nanopartículas. Os sensores instalados nas regiões comprimida e tracionada apresentaram resultados compatíveis com extensômetros localizados na mesma região. Downey et al. [65] apresentaram um modelo para detecção, localização e quantificação de dano em elementos estruturais usando CCNS à base de CNT. Aplicando a abordagem CC bifásica para determinação da resistividade elétrica, os autores foram capazes de monitorar as deformações e os danos causados nos elementos estruturais em um ensaio de flexão a quatro pontos. O estudo concluiu que a abordagem utilizada alcançou resultados satisfatórios usando equipamentos simples e de baixo custo.

1.5 ESTRUTURAÇÃO DA TESE

O presente trabalho está dividido nos 6 capítulos a seguir:

Capítulo 1: Introdução geral – apresenta as considerações iniciais, objetivos (principal e específicos), justificativas, referencial teórico e a estrutura da Tese.

Capítulo 2: Recycling waste materials to produce self-sensing concretes for smart and sustainable structures: a review - publicado no periódico *Construction and Building Materials* (DOI: 10.1016/j.conbuildmat.2022.126658) - apresenta uma revisão de literatura abrangente, focada em estudos que investigaram os efeitos da incorporação de materiais reciclados ou resíduos na produção de CCNS.

Capítulo 3: Evaluation of the effects of sonication energy on the dispersion of carbono black nanoparticles (CBN) and properties of self-sensing cementitious composites - publicado no periódico *Journal of Materials Research and Technology* (DOI: 10.1016/j.jmrt.2025.03.122) - apresenta um estudo focado nos efeitos da variação da energia ultrassônica aplicada na dispersão das nanopartículas nas propriedades de CCNS.

Capítulo 4: Avaliação do teor de surfactante na dispersão de CBN para otimização das propriedades eletromecânicas de compósitos cimentícios nanomodificados sensores –

apresenta um estudo focado nos efeitos da variação do teor de surfactante utilizado na estabilização da dispersão de nanopartículas nas propriedades de CCNS.

Capítulo 5: Estudo experimental da compatibilidade mecânica entre compósitos cimentícios nanomodificados sensores e vigas de concreto armado – apresenta um estudo focado no comportamento eletromecânico dos CCNS, como ferramenta para avaliação da compatibilidade mecânica entre o sensor e o elemento estrutural.

Capítulo 6: Conclusão geral – apresenta as considerações finais, contribuições e conclusões finais da Tese.

1.6 REFERÊNCIAS

[1] F. Azhari, N. Banthia, Cement-based sensors with carbon fibers and carbon nanotubes for piezoresistive sensing, Cem. Concr. Compos. 34 (2012) 866–873. https://doi.org/10.1016/j.cemconcomp.2012.04.007.

[2] S. Taheri, A review on five key sensors for monitoring of concrete structures, Constr. Build. Mater. 204 (2019) 492–509. https://doi.org/10.1016/j.conbuildmat.2019.01.172.

[3] C. Wang, J. Xiao, C. Zhang, X. Xiao, Structural health monitoring and performance analysis of a 12-story recycled aggregate concrete structure, Eng. Struct. 205 (2020) 110102. https://doi.org/10.1016/j.engstruct.2019.110102.

[4] S. Ding, S. Dong, A. Ashour, B. Han, Development of sensing concrete: Principles, properties and its applications, J. Appl. Phys. 126 (2019). https://doi.org/10.1063/1.5128242.

[5] A. D'Alessandro, A. Meoni, F. Ubertini, A. Luigi Materazzi, Strain Measurement in a Reinforced Concrete Beam Using Embedded Smart Concrete Sensors, in: 2020: pp. 289–300. https://doi.org/10.1007/978-3-030-23748-6_22.

[6] W. Dong, W. Li, Z. Tao, K. Wang, Piezoresistive properties of cement-based sensors: Review and perspective, Constr. Build. Mater. 203 (2019) 146–163. https://doi.org/10.1016/j.conbuildmat.2019.01.081.

[7] I. You, D.Y. Yoo, S. Kim, M.J. Kim, G. Zi, Electrical and self-sensing properties of ultra-high-performance fiber-reinforced concrete with carbon nanotubes, Sensors (Switzerland). 17 (2017). https://doi.org/10.3390/s17112481.

[8] L. Wang, F. Aslani, A review on material design, performance, and practical application of electrically conductive cementitious composites, Constr. Build. Mater. 229 (2019)

116892. https://doi.org/10.1016/j.conbuildmat.2019.116892.

[9] D.D.L. Chung, Electrical applications of carbon materials, J. Mater. Sci. 39 (2004) 2645–2661. https://doi.org/10.1023/B:JMSC.0000021439.18202.ea.

[10] H. Li, H. Xiao, J. Ou, Effect of compressive strain on electrical resistivity of carbon black-filled cement-based composites, Cem. Concr. Compos. 28 (2006) 824–828. https://doi.org/10.1016/j.cemconcomp.2006.05.004.

[11] A.O. Monteiro, Development of a multifunctional carbon black/cement composite for traffic monitoring, Universidade de Aveiro, 2018.

[12] Y. Huang, H. Li, S. Qian, Self-sensing properties of Engineered Cementitious Composites, Constr. Build. Mater. 174 (2018) 253–262. https://doi.org/10.1016/j.conbuildmat.2018.04.129.

[13] Z. Zhou, N. Xie, X. Cheng, L. Feng, P. Hou, S. Huang, Z. Zhou, Electrical properties of low dosage carbon nanofiber/cement composite: Percolation behavior and polarization effect, Cem. Concr. Compos. 109 (2020) 103539. https://doi.org/10.1016/j.cemconcomp.2020.103539.

[14] D.-Y. Yoo, I. You, H. Youn, S.-J. Lee, Electrical and piezoresistive properties of cement composites with carbon nanomaterials, J. Compos. Mater. 52 (2018) 3325–3340. https://doi.org/10.1177/0021998318764809.

[15] Y. Guo, W. Li, W. Dong, Z. Luo, F. Qu, F. Yang, K. Wang, Self-sensing performance of cement-based sensor with carbon black and polypropylene fibre subjected to different loading conditions, J. Build. Eng. 59 (2022) 105003. https://doi.org/10.1016/j.jobe.2022.105003.

[16] A. Hussain, Y. Xiang, T. Yu, F. Zou, Nanocarbon black-based ultra-high-performance concrete (UHPC) with self-strain sensing capability, Constr. Build. Mater. 359 (2022) 129496. https://doi.org/10.1016/j.conbuildmat.2022.129496.

[17] W. Dong, W. Li, K. Wang, S.P. Shah, D. Sheng, Multifunctional cementitious composites with integrated self-sensing and self-healing capacities using carbon black and slaked lime, Ceram. Int. 48 (2022) 19851–19863. https://doi.org/10.1016/j.ceramint.2022.03.260.

[18] J. Han, J. Pan, J. Cai, Self-sensing properties and piezoresistive effect of high ductility cementitious composite, Constr. Build. Mater. 323 (2022) 126390. https://doi.org/10.1016/j.conbuildmat.2022.126390.

[19] R. kant Rao, S. Sasmal, Smart nano-engineered cementitious composite sensors for vibration-based health monitoring of large structures, Sensors Actuators A. Phys. 311

(2020) 112088. https://doi.org/10.1016/j.sna.2020.112088.

[20] W. Dong, W. Li, Z. Luo, G. Long, K. Vessalas, D. Sheng, Structural response monitoring of concrete beam under flexural loading using smart carbon black / cement-based sensors, (2020).

[21] A. Dinesh, D. Suji, M. Pichumani, Performance evaluation of graphite-integrated smart-engineered cementitious composite for health monitoring of structural components, J. Build. Eng. 69 (2023) 106228. https://doi.org/10.1016/J.JOBE.2023.106228.

[22] W. Dong, W. Li, Z. Tao, K. Wang, Piezoresistive properties of cement-based sensors: Review and perspective, Constr. Build. Mater. 203 (2019) 146–163. https://doi.org/10.1016/j.conbuildmat.2019.01.081.

[23] R. kant Rao, B.S. Sindu, S. Sasmal, Synthesis , design and piezo-resistive characteristics of cementitious smart nanocomposites with different types of functionalized MWCNTs under long cyclic loading, Cem. Concr. Compos. 108 (2020) 103517. https://doi.org/10.1016/j.cemconcomp.2020.103517.

[24] B. Del Moral, I. Mart, R. Navarro, O. Galao, F.J. Baeza, E. Zornoza, The E ff ect of Di ff erent Oxygen Surface Functionalization of Carbon Nanotubes on the Electrical Resistivity and Strain Sensing Function of Cement Pastes, (2020) 1–15.

[25] W. Dong, W. Li, L. Shen, D. Sheng, Piezoresistive behaviours of carbon black cement-based sensors with layer-distributed conductive rubber fi bres, Mater. Des. 182 (2019) 108012. https://doi.org/10.1016/j.matdes.2019.108012.

[26] S. Chen, J. Luo, X. Wang, Q. Li, L. Zhou, C. Liu, Fabrication and Piezoresistive / Piezoelectric Sensing Characteristics of Carbon Nanotube / PVA / Nano-ZnO Flexible Composite, Sci. Rep. (2020) 1–12. https://doi.org/10.1038/s41598-020-65771-x.

[27] A. Meoni, A.D. Alessandro, F. Ubertini, Characterization of the strain-sensing behavior of smart bricks : A new theoretical model and its application for monitoring of masonry structural elements, Constr. Build. Mater. 250 (2020) 118907. https://doi.org/10.1016/j.conbuildmat.2020.118907.

[28] L. Zhang, L. Li, Y. Wang, X. Yu, B. Han, Multifunctional cement-based materials modified with electrostatic self-assembled CNT / TiO 2 composite filler, Constr. Build. Mater. 238 (2020) 117787. https://doi.org/10.1016/j.conbuildmat.2019.117787.

[29] J. He, Y. Zhang, R. Zhou, L. Meng, T. Chen, Recent advances of wearable and fl exible piezoresistivity pressure sensor devices and its future prospects, J. Mater. 6 (2020) 86–101. https://doi.org/10.1016/j.jmat.2020.01.009.

[30] M. Cao, J. Su, S. Fan, H. Qiu, D. Su, L. Li, Wearable piezoresistive pressure sensors

based on 3D graphene, 406 (2021). https://doi.org/10.1016/j.cej.2020.126777.

[31] C.G. Núñez, W.T. Navaraj, E.O. Polat, R. Dahiya, Energy-Autonomous , Flexible , and Transparent Tactile Skin, 27 (2017). https://doi.org/10.1002/adfm.201606287.

[32] T.Q. Trung, N. Lee, Flexible and Stretchable Physical Sensor Integrated Platforms for Wearable Human-Activity Monitoringand Personal Healthcare, Adv. Mater. 28 (2016) 4338–4372. https://doi.org/https://doi.org/10.1002/adma.201504244.

[33] A.O. Monteiro, P.B. Cachim, P.M.F.J. Costa, Electrical Properties of Cement-based Composites Containing Carbon Black Particles, Mater. Today Proc. 2 (2015) 193–199. https://doi.org/10.1016/j.matpr.2015.04.021.

[34] Y. Huang, H. Li, S. Qian, Self-sensing properties of Engineered Cementitious Composites, Constr. Build. Mater. 174 (2018) 253–262. https://doi.org/10.1016/j.conbuildmat.2018.04.129.

[35] B. Han, K. Zhang, X. Yu, E. Kwon, J. Ou, Electrical characteristics and pressure-sensitive response measurements of carboxyl MWNT/cement composites, Cem. Concr. Compos. 34 (2012) 794–800. https://doi.org/10.1016/j.cemconcomp.2012.02.012.

[36] T.-C. Hou, J.P. Lynch, Conductivity-based strain monitoring and damage characterization of fiber reinforced cementitious structural components, in: M. Tomizuka (Ed.), 2005: p. 419. https://doi.org/10.1117/12.599955.

[37] D.D.L. Chung, Electrical Conduction Behavior of Cement-Matrix Composites, J. Mater. Eng. Perform. 11 (2002) 194–204. https://doi.org/10.1361/105994902770344268.

[38] A.P. Singh, B.K. Gupta, M. Mishra, Govind, A. Chandra, R.B. Mathur, S.K. Dhawan, Multiwalled carbon nanotube/cement composites with exceptional electromagnetic interference shielding properties, Carbon N. Y. 56 (2013) 86–96. https://doi.org/10.1016/j.carbon.2012.12.081.

[39] B. Han, S. Ding, X. Yu, Intrinsic self-sensing concrete and structures: A review, Measurement. 59 (2015) 110–128. https://doi.org/10.1016/j.measurement.2014.09.048.

[40] B. Chen, K. Wu, W. Yao, Conductivity of carbon fiber reinforced cement-based composites, Cem. Concr. Compos. 26 (2004) 291–297. https://doi.org/10.1016/S0958-9465(02)00138-5.

[41] W. Dong, W. Li, Y. Guo, X. He, D. Sheng, Effects of silica fume on physicochemical properties and piezoresistivity of intelligent carbon black-cementitious composites, Constr. Build. Mater. 259 (2020) 120399. https://doi.org/10.1016/j.conbuildmat.2020.120399.

[42] Y. Dai, M. Sun, C. Liu, Z. Li, Electromagnetic wave absorbing characteristics of carbon

black cement-based composites, Cem. Concr. Compos. 32 (2010) 508–513. https://doi.org/10.1016/j.cemconcomp.2010.03.009.

[43] A. D'Alessandro, A. Meoni, F. Ubertini, Innovative Composites with Carbon Nanofillers for Self-Sensing Structural RC Beams, Nano Hybrids Compos. 19 (2018) 12–22. https://doi.org/10.4028/www.scientific.net/NHC.19.12.

[44] A.O. Monteiro, P.B. Cachim, P.M.F.J. Costa, Carbon nanoparticles cement-based materials for service life monitoring, in: Conf. Segm. Serv. Life Cem. Mater. Struct., RILEM, Lyngby, 2016: pp. 195–202.

[45] B. Han, L. Zhang, J. Ou, Influence of water content on conductivity and piezoresistivity of cement-based material with both carbon fiber and carbon black, J. Wuhan Univ. Technol. Sci. Ed. 25 (2010) 147–151. https://doi.org/10.1007/s11595-010-1147-z.

[46] H. Dehghanpour, K. Yilmaz, M. Ipek, Evaluation of recycled nano carbon black and waste erosion wires in electrically conductive concretes, Constr. Build. Mater. 221 (2019) 109–121. https://doi.org/10.1016/j.conbuildmat.2019.06.025.

[47] M.-G. Pârvan, G. Voicu, A.-I. Bădănoiu, Study of hydration and hardening processes of self-sensing cement-based materials with carbon black content, J. Therm. Anal. Calorim. 139 (2020) 807–815. https://doi.org/10.1007/s10973-019-08535-8.

[48] L. Coppola, A. Buoso, F. Corazza, Electrical Properties of Carbon Nanotubes Cement Composites for Monitoring Stress Conditions in Concrete Structures, Appl. Mech. Mater. 82 (2011) 118–123. https://doi.org/https://doi.org/10.4028/www.scientific.net/amm.82.118.

[49] C. Stephens, L. Brown, F. Sanchez, Quantification of the re-agglomeration of carbon nanofiber aqueous dispersion in cement pastes and effect on the early age flexural response, Carbon N. Y. 107 (2016) 482–500. https://doi.org/10.1016/j.carbon.2016.05.076.

[50] A. Yazdanbakhsh, Z. Grasley, Utilization of Silica Fume to Stabilize the Dispersion of Carbon Nanofilaments in Cement Paste, J. Mater. Civ. Eng. 26 (2014) 06014010. https://doi.org/10.1061/(ASCE)MT.1943-5533.0001016.

[51] L. Jingjing, Z. Fusheng, X. Long, K. Bo, T. Xiaohui, D. Yongfeng, Y. Chengbin, Mechanism of stabilized / solidified heavy metal contaminated soils with cement-fly ash based on electrical resistivity measurements, Measurement. 141 (2019) 85–94. https://doi.org/10.1016/j.measurement.2019.03.070.

[52] R. Polder, C. Andrade, B. Elsener, Ø. Vennesland, J. Gulikers, R. Weidert, M. Raupach, Test methods for on site measurement of resistivity of concrete, Mater. Struct. 33 (2000)

603–611. https://doi.org/https://doi.org/10.1007/BF02480599.

[53] A.O. Monteiro, A. Loredo, P.M.F.J. Costa, M. Oeser, P.B. Cachim, A pressure-sensitive carbon black cement composite for traffic monitoring, Constr. Build. Mater. 154 (2017) 1079–1086. https://doi.org/10.1016/j.conbuildmat.2017.08.053.

[54] S.-J. Lee, I. You, G. Zi, D.-Y. Yoo, Experimental Investigation of the Piezoresistive Properties of Cement Composites with Hybrid Carbon Fibers and Nanotubes, Sensors. 17 (2017) 1–16. https://doi.org/https://doi.org/10.3390/s17112516.

[55] A. Downey, A. D'Alessandro, F. Ubertini, S. Laflamme, R. Geiger, Biphasic DC measurement approach for enhanced measurement stability and multi-channel sampling of self-sensing multi-functional structural materials doped with carbon-based additives, Smart Mater. Struct. 26 (2017) 065008. https://doi.org/10.1088/1361-665X/aa6b66.

[56] A. Meoni, A. D'Alessandro, A. Downey, S. Laflamme, F. Ubertini, Strain monitoring in masonry structures using smart bricks, in: H. Sohn (Ed.), Sensors Smart Struct. Technol. Civil, Mech. Aerosp. Syst. 2018, SPIE, 2018: p. 66. https://doi.org/10.1117/12.2297526.

[57] S. Zhu, D.D.L. Chung, Analytical model of piezoresistivity for strain sensing in carbon fiber polymer–matrix structural composite under flexure, Carbon N. Y. 45 (2007) 1606–1613. https://doi.org/10.1016/j.carbon.2007.04.012.

[58] N. Yang, Q. Sun, Study on the Self-Monitoring of Bending Fatigue Cumulative Damage for Carbon Nanofiber Polyurethane Cement, Appl. Sci. 9 (2019) 1–20.

[59] M.H. Sarwary, G. Yıldırım, A. Al-Dahawi, Ö. Anıl, K.A. Khiavi, K. Toklu, M. Şahmaran, Self-Sensing of Flexural Damage in Large-Scale Steel-Reinforced Mortar Beams, ACI Mater. J. 116 (2019). https://doi.org/10.14359/51715581.

[60] A. Hussain, Y. Ding, G. Liu, A. Naqi, Study on self-monitoring of multiple cracked concrete beams with multiphase conductive materials subjected to bending, (2019).

[61] Y. Ding, G. Liu, A. Hussain, F. Pacheco-torgal, Y. Zhang, Effect of steel fiber and carbon black on the self-sensing ability of concrete cracks under bending Effect of steel fiber and carbon black on the self-sensing ability of concrete cracks under bending, Constr. Build. Mater. 207 (2019) 630–639. https://doi.org/10.1016/j.conbuildmat.2019.02.160.

[62] G. Yıldırım, M.H. Sarwary, A. Al-Dahawi, O. Öztürk, Ö. Anıl, M. Şahmaran, Piezoresistive behavior of CF- and CNT-based reinforced concrete beams subjected to static flexural loading: Shear failure investigation, Constr. Build. Mater. 168 (2018) 266–279. https://doi.org/10.1016/j.conbuildmat.2018.02.124.

[63] Q. Liu, R. Gao, V.W.Y. Tam, W. Li, J. Xiao, Strain monitoring for a bending concrete beam by using piezoresistive cement-based sensors, Constr. Build. Mater. 167 (2018)

338–347. https://doi.org/10.1016/j.conbuildmat.2018.02.048.

[64] F. Naeem, H.K. Lee, H.K. Kim, I.W. Nam, Flexural stress and crack sensing capabilities of MWNT/cement composites, Compos. Struct. 175 (2017) 86–100. https://doi.org/10.1016/j.compstruct.2017.04.078.

[65] A. Downey, A.D. Alessandro, M. Baquera, E. García-macías, D. Rolfes, F. Ubertini, S. Laflamme, R. Castro-triguero, Damage detection , localization and quantification in conductive smart concrete structures using a resistor mesh model, Eng. Struct. 148 (2017) 924–935. https://doi.org/10.1016/j.engstruct.2017.07.022.

[66] A. Downey, E. Garcia-macias, A.D. Alessandro, S. Laflamme, Continuous and embedded solutions for SHM of concrete structures using changing electrical potential in self-sensing cement-based composites, 10169 (2017) 1–13. https://doi.org/10.1117/12.2261427.

[67] A.D. Alessandro, F. Ubertini, E. García-macías, R. Castro-triguero, A. Downey, S. Laflamme, A. Meoni, A.L. Materazzi, Static and Dynamic Strain Monitoring of Reinforced Concrete Components through Embedded Carbon Nanotube Cement-Based Sensors, 2017 (2017).

[68] Y. Goldfeld, O. Rabinovitch, B. Fishbain, T. Quadflieg, T. Gries, Sensory carbon fiber based textile-reinforced concrete for smart structures, J. Intell. Mater. Syst. Struct. 27 (2016) 469–489. https://doi.org/10.1177/1045389X15571385.

[69] F. Ubertini, A. Luigi, A.D. Alessandro, S. Laflamme, Natural frequencies identification of a reinforced concrete beam using carbon nanotube cement-based sensors, Eng. Struct. 60 (2014) 265–275. https://doi.org/10.1016/j.engstruct.2013.12.036.

[70] Y. Ding, Z. Chen, Z. Han, Y. Zhang, F. Pacheco-torgal, Nano-carbon black and carbon fiber as conductive materials for the diagnosing of the damage of concrete beam, Constr. Build. Mater. 43 (2013) 233–241. https://doi.org/10.1016/j.conbuildmat.2013.02.010.

[71] H. Xiao, H. Li, J. Ou, Strain sensing properties of cement-based sensors embedded at various stress zones in a bending concrete beam, Sensors Actuators A. Phys. 167 (2011) 581–587. https://doi.org/10.1016/j.sna.2011.03.012.

2 RECYCLING WASTE MATERIALS TO PRODUCE SELF-SENSING CONCRETES FOR SMART AND SUSTAINABLE STRUCTURES: A REVIEW

DOI: 10.1016/j.conbuildmat.2022.126658

Abstract: *The construction industry is currently facing the great challenge of applying sustainable materials with suitable mechanical properties and durability performance. Among the different strategies used to meet technical and sustainable criteria, two interesting approaches can be highlighted: the reuse of materials to produce sustainable construction materials and the development of smart concretes for Structural Health Monitoring. The first strategy consists of using recycled materials, co-products, and by-products of industrial processes to replace primary raw materials used to produce blocks, ceramics, mortars, and concrete. The second strategy is associated with the development of multifunctional cementitious and alkali-activated concretes with strain and damage self-sensing properties in response to the growing concerns related to the increase in the durability of civil structures. This paper presents a critical review of previous studies that combine both strategies, i.e., research works investigating smart construction materials that incorporate recycled and waste materials and exhibit self-sensing properties. Sustainable self-sensing composites (SSCs) incorporating different types of recycled and waste materials were presented. These sustainable admixtures provided different benefits to self-sensing composites, such as improvements in the conductive path within the matrices and improvements in the dispersion of other conductive fillers. The effects of silica fume, fly ash, steel slag, red mud, and other recycled materials on the electrical resistivity, strain-sensing properties, and damage-detection properties of SSCs were discussed. Promising SSCs were identified based on comparisons between gauge factor, stress sensibility, linearity, strain amplitude, and stress amplitude of SSCs produced with one single type of waste or combination of various types of wastes. In this sense, SSCs were found to be a viable alternative for modernization and greater sustainability of the construction industry.*

Keywords: *Sustainability; eco-concretes; alkali-activated matrices; Structural Health Monitoring; smart materials.*

2.1 INTRODUCTION

2.1.1 Background information

The construction industry significantly contributes to climate changes and resource scarcity. This sector is responsible for 40-50% of the global greenhouse gas emissions and 40-60% of the worldwide depletion of natural resources [1,2]. At a global level, the cement industry is one of the largest sources of anthropogenic CO_2 emissions [3–5]. In addition, most of the materials used to produce ordinary Portland cement concretes (PCCs) are non-renewable resources [6]. Given the impacts generated by the construction sector, various studies focused on the sustainable development of the construction industry have been carried out. Different technologies have been proposed to solve this critical scenario, such as carbon capture and storage, use of sustainable cementitious materials as partial replacement of clinker, management of industrial waste, improvements in the durability of existing civil structures, use of alternative fuels, and improvements in energy efficiency [7,8]. All these technologies aim to change the way natural resources are exploited, guide investments, and promote technological development and changes in attitudes in the sector. This process can ensure a future in which society's needs and aspirations interact harmoniously, which is, in essence, the definition of sustainable development [9,10].

Since cementitious matrices can incorporate different materials, the addition of recycled and waste materials to concretes is widely studied as an alternative for obtaining benefits in terms of environmental sustainability [11–13]. Materials that would be discarded by different industrial sectors, with high potential to generate pollution, overload deposit areas, and affect the population's quality of life, now have the opportunity to generate new products and be reinserted in the production chain. Thus, the incorporation of wastes into ordinary Portland cement (OPC) matrices for producing eco-concretes has become a strategy that positively affects the sustainability of the construction industry. Extensive literature highlights the beneficial effects of reusing industrial co-products and by-products in PCCs, such as silica fume (SF), fly ash (FA), and blast-furnace slag (BFS) for concrete production, as these admixtures present good pozzolanic activity, hydraulic properties, and filler effects [14–18]. Other waste materials still require further comprehensive research to investigate some details associated with the effects of their application in cementitious matrices, such as red mud (RM), rubber waste (RW), ornamental stone waste (ORW), mining waste (MW), rice husk ash (RHA), oil

fuel ash palm (POFA), sugarcane bagasse ash (SCBA), construction waste (CW), iron ore tailing (IOT), recycled glass waste (RGW), steel slag (SS), among others [6,19–22].

Alkali-activated concretes (AACs) have been developed as potential alternatives to PCCs, since they present satisfactory mechanical properties, resistance to high temperatures, chemical resistance, and lower environmental impacts [23]. Compared to PCCs, AACs provide 26-45% reduction in CO_2 emissions [24]. As AACs result from reactions of a source of aluminosilicates in a highly alkaline medium, their use as alternative materials to enhance eco-efficiency is very promising [25]. In fact, AACs are regarded as an environmentally friendly alternative to OPC [26]. Different recycled and waste materials have been used to produce AACs, such as BFS, MW, FA, GW, CW, among others [27,28].

The construction industry must evaluate the impact of waste materials on physical and mechanical properties of construction materials and analyze their effects on the durability of civil structures. Although construction materials are usually very durable and present excellent strength, especially in the case of large infrastructure, significant degradation can occur due to deficiencies in design and construction, in addition to the lack of proper maintenance [29,30]. Improving the durability of structures is another interesting strategy to increase sustainability in the construction sector, since it increases their service life and reduces life cycle costs. Monitoring different processes that happen in civil structures is a way to increase their service life, ensuring that harmful conditions to construction materials are identified quickly and early. Nowadays, Structural Health Monitoring (SHM) systems have been developed for real-time assessment of strains and damage in response to the growing concerns regarding the durability of civil structures. According to previous literature [31–35], smart structural materials can be defined as elements capable of exhibiting certain functional behavior when they are subjected to different stimuli such as stress/strain and damage. Sensing is a fundamental functional property of smart structural materials, so that they are particularly interesting approaches for SHM. The recent knowledge advance on multifunctional cementitious materials enabled the development of construction materials that work as structural elements and smart systems for self-monitoring of strain and self-detection of damage in smart civil structures [34,36–38]. These self-sensing building materials have numerous advantages in comparison to conventional SHM systems, such as high gauge factor (GF), durability and mechanical properties, in addition to low cost and natural compatibility with elements of civil structures [36,38,39].

Various types of smart concretes, blocks, aggregates, bricks, and pavements have been extensively studied, considering both PCC and AAC sensors [34,40]. These materials can exhibit changes in their electrical resistivity due to deformations or damage [36]. These self-

sensing properties are obtained by adding conductive admixtures to PCCs and AACs matrices, which increases their electrical conductivity and provides suitable conditions for the predominance of electronic conduction mechanisms, as discussed in the following section [34,40]. Different types of conductive fillers have been used for the production of self-sensing composites, such as carbon black nanoparticles (CBN) [41–43], single-walled and multi-walled carbon nanotubes (SWCNT and MWCNT, respectively) [19,44,45], carbon fibers (CF) [26,46], carbon nanofiber (CNF) [47,48], graphene (G) [49], graphite nanofiber (GNF) [50], graphite powder (GP) [51,52], nickel powder (NP) [53], steel slag (SS) [54], steel fibers (STF) [55–57], among others.

Sustainability is often claimed to be a desired outcome of smart construction materials with self-sensing abilities. In fact, smart construction materials can contribute to sustainable development, as they increase the durability and lifespan of civil structures. Although smart materials provide this important contribution, most of them have been produced with conventional raw materials in processes that contribute to climate changes and natural resource scarcity. In order to develop smart materials that are much more sustainable, many papers have recently published different findings concerning the reuse of waste and recycled materials to produce concrete with smart self-sensing properties, which are reviewed in the next sections.

2.1.2 Significance of this literature review

Literature review papers have addressed the influence of different residues on the microstructural properties [58–63], mechanical properties [28,64–68], and durability [69–76] of PCCs and AACs. These reviews demonstrate that incorporating waste materials into construction materials is a viable and important alternative from an economic, social, and environmental point of view. However, these papers did not cover self-sensing properties of construction materials produced with waste materials. Despite the self-sensing properties of PCCs and AACs have been revised in several review papers [31,40,77–81], only self-sensing composites containing conventional conductive admixtures were revised, i.e., self-sensing composites without waste additions. Therefore, it is possible to identify a gap in the current literature: review papers dealing with the incorporation of wastes into PCCs and AACs did not address their self-sensing properties, whereas review papers addressing the production of self-sensing construction materials did not revise the sustainable approach of recycling waste materials. The recent progress on the reuse of waste and recycled materials to produce concrete with smart self-sensing properties calls for an updated review. Then, the present study aimed to

develop a review of recent advances on the development of sustainable self-sensing composites (SSCs), i.e., eco-friendly construction materials with intrinsic strain sensing and damage detection abilities.

This review aimed to provide the following significant contributions: (i) identify the effects of different types of wastes on mechanisms of electrical conductivity and self-sensing response of AACs and PCCs; (ii) discover the waste dosages that have already been used in previous literature to produce SSCs and corresponding percentages of conventional binders eventually replaced by wastes; (iii) identify the highest increases in various self-sensing properties (e.g., gauge factor, stress sensibility, linearity, strain and stress amplitude, damage detection, etc.) provided by the incorporation of wastes into concretes, and find optimal waste contents in SSCs, in terms of improvements in their smart response; (iv) introduce researchers and the general public to possible combinations between different waste materials that were found to improve the self-sensing properties of SSCs; (v) suggest other agricultural, industrial and municipal wastes that are promising alternatives for production of SSCs; and (vi) identify limitations and needs for future research in this field.

This paper has been structured in three sections. Section 2.1 presents a background information on the development of eco-efficient and self-sensing construction materials, in addition to the objectives of the present review paper. Section 2.2 presents a review of self-sensing properties of smart construction materials incorporating one or a combination of different types of wastes. Finally, main conclusions and suggestions for future research are presented in Section 2.3.

2.2 SELF-SENSING PROPERTIES OF SUSTAINABLE CONSTRUCTION MATERIALS

2.2.1. SSCs produced with a single type of waste material

Based on the concentration of conductive fillers, alkali-activated and cementitious matrices can be classified in the three different zones (A, B, and C) indicated in Figure 1. In zone A (insolation zone), the conductive filler content is lower than a critical content called percolation threshold that provides reductions in the electrical resistivity of the material. In zone A, ionic conduction is the dominant conduction mechanism. Since ionic conduction is associated with the movement of ions in the pore water of the matrix, composites at zone A have very high electrical resistivity after drying. Due to the polarization phenomenon, they have lower electrical resistivity in the wet state and exhibit considerable capacitive response. Zone

B (percolation zone) refers to the range in which the increases in conductive filler content provide gradual reductions in electrical resistivity. The beginning of the percolation zone is characterized by ionic conduction over the pore water and electronic conduction over the conductive admixtures. At the end of the percolation zone, the dominant conduction mechanism is electronic conduction by tunneling effect and direct contact between conductive fillers. Composites in zone C (conductive zone) have concentrations of conductive admixtures that reduced the electrical resistivity to a minimum possible value. Electronic conduction by direct contact between conductive fillers is dominant in the conductive zone [34,43,82].

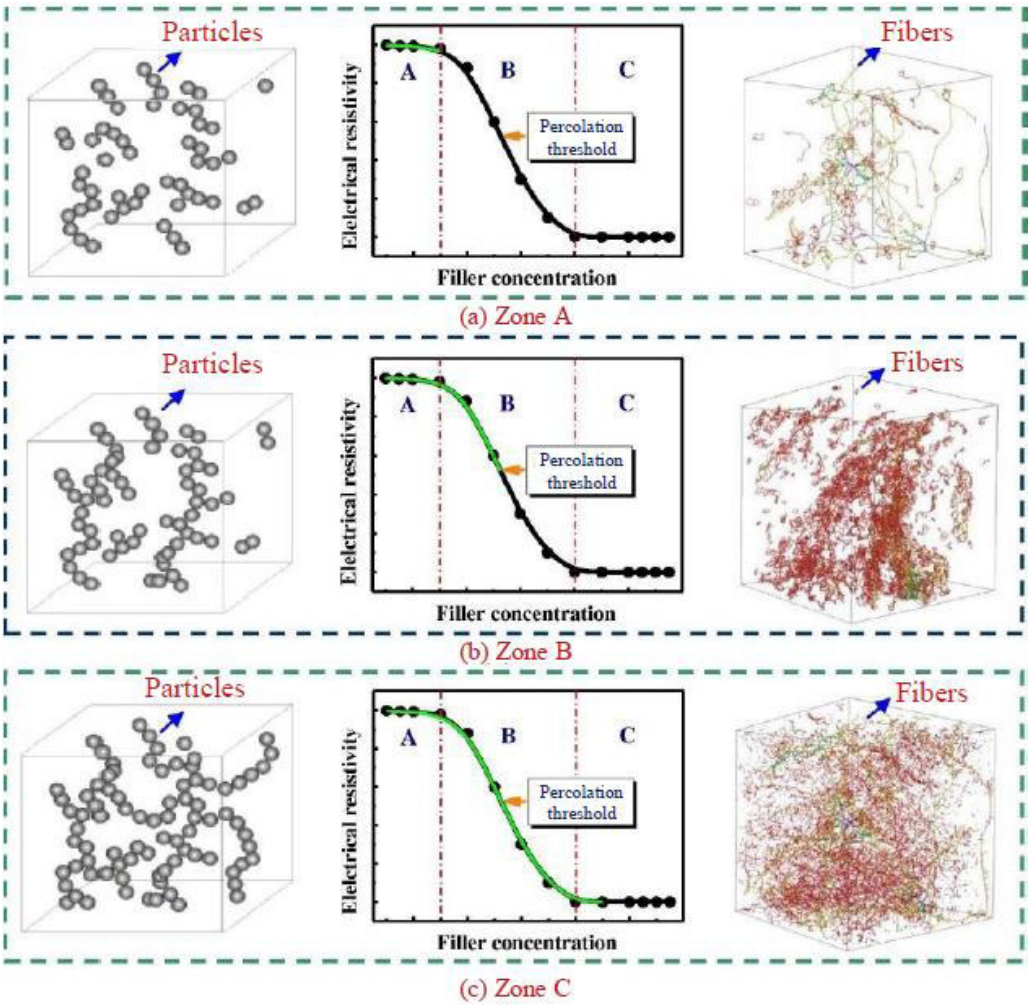

Figure 1. Changes in electrical resistivity with the concentration of conductive admixtures: (a) insulation zone, (b) percolation zone, and (c) conductive zone. Reproduced from Han et al. [34], Copyright 2015, with permission from Elsevier.

Composites in the percolation zone can self-monitor deformations and stresses due to the phenomenon of piezoresistivity, which is characterized by changes in the material's electrical resistivity due to deformations and stresses [36,83]. Han, Ding, and Yu [34] observed that when

these composites are subjected to compression stresses up to about 30% of their ultimate capacity, reversible changes in their electrical resistivity are observed, resulting from the reversible elastic deformations that occur in this stress range. The ratio between the fractional change in electrical resistivity (FCR) and strain (ε) that caused this change is defined as the GF of the composite. Stress sensibility (SST) consists of the ratio between FCR and the respective stress (σ).

A good piezoresistive response is observed in composites in the percolation zone because a compressive deformation decreases their electrical resistivity due to the increase in the tunneling current density provided by the decrease in the distance between adjacent conductive fillers. Then, deformations cause changes in the conduction paths inside the matrix, leading to FCRs [80]. In contrast, composites in the conductive zone have a much greater number of conductive paths between the functional fillers, so that the conductive mesh does not undergo major changes when deformation occurs, and the self-sensing properties of the material are not very high [84].

Another interesting application of PCC and AAC sensors is the self-detection of damage under static or dynamic loading conditions. The development of cracks in the matrix causes interruptions in the conductive paths, so that it is possible to identify damage evolution based on irreversible changes in electrical resistivity [45,85,86]. According to Gull et al. [87], the baseline resistance increases irreversibly at high stress levels, due to the damage-induced resistance increase. Then, the baseline resistance in the plastic regime can provide a measure of extent of damage.

In uniaxial tensile tests of smart self-sensing concretes, progressive increases in positive FCR values are observed, which are associated with the separation between conductive fillers and interruptions in the conductive network due to microcracking propagation [88]. In uniaxial compression tests, FCR values are always negative. Initially, the absolute FCR values increase due to resistivity reductions associated with the decrease in the distance between conductive particles [80]. It is followed by a phase of apparent equilibrium in FCR values, in which the beginning of microcracking tends to destroy the conductive network, but the compression deformations reconstruct conductive paths. Such destruction and reconstruction of conductive paths can be used as indicative of crack generation [89]. Finally, reductions in absolute FCR values are observed due to resistivity increases associated with the progressive cracking evolution, so that the interruption of conductive paths becomes the dominant phenomenon. In simply supported composite sensors subjected to a bending test, FCR variations depend on the position and orientation of electrodes for resistivity measurement, since the normal tensile and

compression stresses are different in each region of the specimen. Consequently, bending tests of cementitious composites can also be developed to investigate their self-sensing ability [90].

The incorporation of waste materials into conventional PCC has been extensively studied, in order to develop more sustainable self-sensing cementitious materials and reduce economic and environmental impacts resulting from their inappropriate disposal. SF is now considered as the mainstream addition agent for improvements in the dispersion of different types of conductive fillers and production of self-sensing PCCs. However, other recycled materials (e.g., RM, SS, RW, etc) containing conductive particles have also been added to PCCs to increase their electrical conductivity, as discussed in the next subsections. Although many studies dealt with self-sensing PCCs, the amount of studies dealing with self-sensing AACs is very limited. This is mainly because AACs are relatively new, and PCCs are still the most widely used construction materials today.

The performance of AACs is strongly influenced by different factors, such as the aluminosilicate source (precursor), alkaline source concentration (activator), and curing temperature. In previous literature, the production of AACs with self-sensing properties has been generally applied to the best-known conditions, with metakaolin [91–94], FA [95,96], and GGBFS [97] as the main precursors. There is great research potential to be explored in this area, since the migration of free alkaline ions resulting from the geopolymerization process is able to improve the conductivity of these composites [98], so that their application for production of SSCs is naturally advantageous.

In the production of self-sensing PCCs and AACs, different recycled and waste materials have been combined or not with conventional conductive fillers, in order to produce SSCs. Table 1 shows the type and dosage of recycled admixtures and/or conductive fillers used in different published studies. These works reported self-sensing properties of SSCs subjected to uniaxial compression tests, with the following exceptions: (i) Huang et al. [99], Deng and Li [100], and Hardy et al. [47] investigated the self-sensing properties of SSCs subjected to uniaxial tensile tests; (ii) Haque et al. [101] explored the self-sensing properties of SSCs subjected to bending tests; and (iii) Belli et al. [57], Dehghanpour et al. [102], Mobili et al. [103], Mobili et al. [104], Dong et al. [105], Kamaluddin et al. [106], and Haque et al. [107] only focused on electrical resistivity measurements (piezoresistive response was not reported).

Table 1. Works dealing with composites containing a single type of waste material.

Composite type	Recycled admixture			Conductive filler			Reference
	Type	Admixture/ binder (or precursor) ratio (% in mass)	Admixture/ composite ratio (% in volume)	Type	Conductive filler/binder (or precursor)* ratio (% in mass)	Conductive filler/composite ratio (% in volume)	
Cement paste	SF	10.00	-	CBN	1.00	-	[108]
Cement paste	SF	10.00	-	CBN	0.50	-	[109]
Cement paste	SF	10.00	-	CBN	0.50	-	[110]
Cement paste	SF	5.00, 10.00, 20.00	-	CBN	2.00	-	[111]
Cement paste	SF	20.00	-	CBN	0.50, 1.00, 2.00	-	[112]
Cement paste	SF	20.00	-	MWCNT	0.25, 0.50	-	[44]
Cement paste	SF	10.00	-	MWCNT	0.50	-	[113]
Cement paste	SF	20.00	-	CBN	3.00	-	[114]
Cement paste	SF	23.08	-	MWCNT; GNF; GO	0.10 (MWCNT); 0.10 (GNF); 0.10 (GO)	-	[115]
Cement paste	SF	30.00	-	MWCNT; GNF; G	0.80 (MWCNT); 1.28 (GNF); 1.33 (G)	-	[50]
Cement mortar	SF	20.00	-	MWCNT; STF	1.20 (MWCNT)	2.00 (STF)	[116]
Cement mortar	SF	10.00	-	CBN + MWCNT	-	0.39; 0.77; 1.41; 2.14	[117]
Cement mortar	SF	20.00	-	MWCNT + STF	-	0.10; 0.30; 0.50 (MWCNT);	[118]

						2 (STF)	
Cement mortar	SF	10.00	-	CBN + MWCNT	-	0.39; 0.77; 1.52; 2.40; 3.12	[119]
Concrete	SF	10.00	-	STF	0.036, 0.063, 0.090, 0.144	-	[56]
Concrete	SF	10.00	-	BF	-	0.80	[120]
Concrete	SF	10.00	-	BF	-	0.35; 0.50; 0.80; 1.00; 1.50	[121]
Cement mortar	FA	5 to 25	-	FA	0.05 to 0.33	-	[122]
Cement mortar	CNTFA	0.4, 0.8, 1.2, 2.0	-	CNTFA	0.4, 0.8, 1.2, 2.0	-	[123]
Cement mortar	FA	16.67	-	BHNCM	6.0	-	[124]
Cement mortar	FA	46.88	-	CBN	0.39	-	[99]
Cement mortar	FA	52.44	-	CBN	0.35	-	[100]
Cement mortar	FA	73.68	-	CNF	4.4, 8.9, 13.2, 26.3	-	[47]
Cement paste	FA	20	-	BHNCM	0, 0.5, 1, 2, 3, 4, 5, 6, 7	-	[125]
Alkali-activated mortar	GGBFS	***	-	CNT; CBN; G; CNF	1.0 (CNT); 1.0 (CB); 1.0 (G); 1.0 (CNF)	-	[48]
Alkali-activated mortar	GGBFS	***	-	GGBFS	**	-	[126]
Alkali-activated mortar	GGBFS	***		GGBFS; GP	** (GGBFS); 1.0 to 30.0 (GP)	-	[51]
Alkali-activated paste	BFS	***	-	CF	0.38, 0.76	-	[127]
Cement mortar	BFS	5 to 25	-	BFS	0.05 to 0.33	-	[122]
Cement mortar	SS	300		CF; SS	1, 2, 3, 4 (CF); 300 (SS)	-	[128]
Concrete	SS	9, 13, 14.5, 17	-	SS	9, 13, 14.5, 17	-	[129]
Polymer concrete	SS	100		SS; GP	100 (SS); 60 (GP)	-	[52]

Cement mortar	RCF	-	0.1 to 1.4	RCF	0.1 to 1.4	-	[130]
Cement mortar	RCF	0.73	-	RCF; G; CF	0.18, 0.73 (RCF); 3.9 (G); 0.18, 0.66 (CF)	-	[131]
Cement mortar	RCF	0.125, 0.25, 0.50, 1.03, 2.01, 3.14, 4.21	0.05, 0.1, 0.2, 0.4, 0.8, 1.2, 1.6	RCF; CF; BSF	0.125, 0.25, 0.50, 1.03, 2.01, 3.14, 4.21 (RCF); 0.125, 0.25, 0.50, 1.03, 2.01, 3.12, 4.21 (CF); 0.56, 1.11, 2.24, 4.47, 8.93, 13.38, 17.82 (BSF)	0.05, 0.1, 0.2, 0.4, 0.8, 1.2, 1.6 (RCF, CF and BSF)	[57]
Cement concrete	RCBN	0.0, 3.0, 6.0, 10.2 (RCBN)	-	CF, STF	0.00, 0.85, 2.10, 4.30 (CF), 11.70 (STF)	-	[102]
Cement mortar	RCF; GCH; UFS	0.176, 0.722 (RCF); 4 (GCH); 4 (UFS)	-	CF; GNP	0.176, 0.722 (CF); 4 (GNP)	-	[103]
Lime mortar	GCH; UFS	0.25, 0.50, 1.00 (GCH); 0.25, 0.50, 1.00 (UFS)	-	PAC; GNP	0.25, 0.50, 1.00 (PAC); 0.25, 0.50, 1.00 (GNP)	-	[104]
Cement mortar	RM	5 to 25	-	RM	0.05 to 0.33	-	[122]
Cement concrete	ING	1, 3, 5	-	NG	1, 3, 5	-	[105]
Cement paste	Rice husk biochar	5, 10, 15	-	Rice husk biochar	5, 10, 15	-	[106]
Cement mortar	SHCP obtained from wood chips biochar	5.26, 11.11	-	SHCP obtained from wood chips biochar	5.26, 11.11	-	[107]
Cement mortar	SHCP obtained from wood chips biochar	0, 2.56, 5.26, 11.11, 17.65	-	SHCP obtained from wood chips biochar	0, 2.56, 5.26, 11.11, 17.65	-	[101]

Notes: SF - silica fume, CBN - carbon black nanoparticle, MWCNT - multi-walled carbon nanotube, GNF - graphite nanofiber, GO - graphite oxide, G - graphene, STF - steel fiber, BF - brass fiber, FA - fly ash, CNTFA - fly ash covered with carbon nanotube, BHNCM - botryoid hybrid nano-carbon material, GGBFS - ground-

granulated blast-furnace slag, CNT - carbon nanotube, CNF - carbon nanofiber, GP - graphite powder, BFS - blast-furnace slag, CF - carbon fiber, SS - steel slag, WWE - waste wire erosion, RCBN - recycled carbon black nanoparticle, RCF - recycled carbon fiber, GCH - gasification char, UFS - used foundry sand, PAC - powdered activated carbon, ING - waste of nano-graphite containing iron particles, NG - nano-graphite, RM - red mud, SHCP - super-hydrophobic carbonaceous powder.
*In ordinary Portland cement concretes, the concentration of conductive admixtures was provided in terms of mass of binders. In alkali-activated concretes, the concentration of conductive admixtures was provided in terms of mass of precursor.
**The precursor used to produce the alkali-activated concrete is the conductive admixture itself.
***The precursor used to produce the alkali-activated concrete is the recycled admixture itself.

Table 2 presents the sensing properties observed in all SSCs that exhibited a piezoresistive behavior characterized by a linear variation of FCR with the compressive stress (or strain). The experimental results of Segura et al. [130] were not included in Table 2 because these authors did not report FCRs values. Despite this, Segura et al. [130] observed a self-sensing behavior discussed in Section 2.1.6. Values of strain and stress amplitude measured in piezoresistive tests were also listed. When enough data was available, the ratio between the stress amplitude □ and the compressive strength *fc* of the material was provided, in order to investigate which fraction of the full SSC strength is associated with a linear piezoresistive response. When available, the coefficients of determination (R^2) obtained from the dataset of FCR vs. strain curves were also reported, since they provide an idea of the magnitude of linearity of the SSCs [132].

Table 2. Sensing properties of composites containing a single type of waste material (linear behavior in FCR vs. strain curves)

Recycled admixture	Conductive filler	Gauge factor	Stress sensibility (MPa^{-1})	Strain amplitude (microns)	Stress amplitude (MPa)	Linearity	Average compressive strength (MPa)	σ/*fc* ratio (%)	Reference
SF	CBN	-	0.004 - 0.009	-	5	-	52.1 - 54.6	9.16 - 9.60	[109]
SF	CBN	-	0.004 - 0.016	-	5	-	51.4 - 54.6	9.16 - 9.73	[110]
SF	MWCNT	168 - 228	0.0118 - 0.0169	700 - 740	10	-	52.5 - 54	18.52 - 19.05	[44]
SF	MWCNT	38 - 183	0.0049 - 0.0265	1200 - 1450	10	0.89 – 0.99	13.5 - 51.4	19.46 - 74.07	[113]
SF	CBN; MWCNT	35 - 202	0.0018 - 0.017	180 - 350	4	-	-	-	[117]
SF	CBN	424.74	0.0491	231.25	2		-	-	[114]
SF	BF	20.8 - 26.9	-	-	-	0.54 - 0.94	59	-	[120]
SF	STF	18.9 - 126.7	-	1000 - 2300	39 - 52	0.93 - 0.99	-	-	[56]

SF	MWCNT; GNF; GO	166.6	0.0125	1500	20	0.97	35.2	56.82	[115]
SF	MWCNT; GNF; G	113.2	0.001 - 0.0085	2500	12	0.49 - 0.93	35.2	34.09	[50]
SF	BF	21 - 60	-	1000 - 2200	-	0.93 - 0.99	-	-	[121]
SF	CBN; MWCNT	116 - 231	0.0271 - 0.0087	300 - 325	8	0.92 - 0.94	61.2 - 65.4	12.22 - 13.07	[119]
FA	FA	-	0.00085 - 0.00841	-	6.5 - 18	-	22.17 - 27.94	26.46 - 81.19	[122]
FA	BHNCM	4.41 - 225.08	0.0004 - 0.0232	900 - 1100	10 - 10.5	0.91 - 0.99	25.6 - 50.2	20.92 - 38.99	[125]
FA	GO	21.6 - 43.87	0.0100 - 0.0138	3100 - 3600	11.4	0.98 - 0.99	-	-	[133]
GGBFS	CNT; CBN; G; CNF	39 - 65	0.0117 - 0.0224	540 - 635	1.8	0.8577 - 0.9852	15.3 - 19.0	9.47 - 11.11	[48]
GGBFS	GGBFS	-	0.00505	-	5	-	57.2	8.74	[126]
BFS	CF	52 - 661.9	0.0043 - 0.0680	415 - 514	5	0.964 - 0.992	-	-	[127]
BFS	BFS		0.00109 - 0.0126	-	8.5 - 18	-	24.45 - 32.58	26.09 - 73.62	[122]
SS	SS	139 - 505	0.0028 - 0.0113	69 - 160	3.55	-	47.5 - 65.4	5.43 - 7.48	[129]
SS	CF; SS	4.73 - 7.24	0.00014 - 0.00017	118 - 145	5	0.7897 - 0.9787	-	-	[128]
RCF	RCF; G; CF	285.71	0.00141	77	15.6	0.94	25	62.4	[131]
RM	RM	-	0.00134 - 0.00629	-	10 - 18	-	25.15 - 32.94	31.98 - 69.69	[122]

Note: SF - silica fume, CBN - carbon black nanoparticle, MWCNT - multi-walled carbon nanotube, BF - brass fiber, STF - steel fiber, GNF - graphite nanofiber, GO - graphite oxide, G - graphene, FA - fly ash, BHNCM - botryoid hybrid nano-carbon material, GGBFS - ground-granulated blast-furnace slag, CNF - carbon nanofiber, CNT - carbon nanotube, BFS - blast-furnace slag, CF - carbon fiber, SS - steel slag, RCF - recycled carbon fiber, RM - red mud.

Some SSCs presented a non-linear relationship between FCR and compressive stresses (or strains). These cases were listed in Table 3, with the stress and strain amplitudes associated with the maximum absolute values of FCR. When enough data was available, the σ/fc ratio was also calculated.

Table 3. Sensing properties of composites containing a single type of waste material (non-linear behavior in FCR vs. strain curves)

Recycled admixture	Conductive filler	Maximum absolute values of FCR amplitude (%)	Strain amplitude (microns)	Stress amplitude (MPa)	Average compressive strength (MPa)	*σ/fc* ratio (%)	Reference
SF	CBN	1.3 - 3.9	-	5	-	-	[108]
SF	CBN	9.0 - 17.5	-	4	-	-	[112]
SF	CBN	11 - 24	-	8	14.2 - 43.4	18.43 - 56.34	[111]
SF	MWCNT; STF	47 - 51	4120 - 4500	181 - 197	181 - 197	100	[116]
SF	MWCNT; GNF; GO	9 - 31	-	24 - 35	32 - 40	60 - 100	[115]
SF	MWCNT; STF	25 - 270	750 - 1800	80 - 120	80 - 120	100	[118]
SF	CBN; MWCNT	6 - 22	320 - 350	8	34.4 - 44.5	17.97 - 23.25	[119]
FA	BHNCM		4500	36.32	36.3	100	[124]
CNTFA	CNTFA	25 - 69	260 - 620	7.5	34 - 41	18.29 - 22.06	[123]
GGBFS	GGBFS; GP	8.6	-	4.5	40 - 57	7.89 - 11.25	[51]
SS	SS; GP	756.5	4819- 5264	-	-	-	[52]

Note: SF - silica fume, CBN - carbon black nanoparticle, MWCNT - multi-walled carbon nanotube, STF - steel fiber, GNF - graphite nanofiber, GO - graphite oxide, FA - fly ash, BHNCM - botryoid hybrid nano-carbon material, CNTFA - fly ash covered with carbon nanotube, GGBFS - ground-granulated blast-furnace slag, GP - graphite powder, SS - steel slag.

Figure 2 presents the different sensing properties (GF, linearity, and SST) and *σ/fc* ratios of SSCs produced with a single type of waste. Figures 2a and 2b show that high contents of SF (10-30% by weight of binders) have been successfully used in many works for the production of SSCs with high values of GF (51-424.74) and SST (0.001-0.049 MPa^{-1}). High contents of FA (5-25% by weight of binders) and SS (9-17% by weight of binders) have also been used as supplementary cementitious materials (SCMs) of different SSC types, which also provides significant gains in terms of decreases in OPC consumption and reductions in environmental impacts. Although this data shows that FA could replace significant amounts of OPC, lower values of GF (40-228) and SST (0.0004-0.0232 MPa^{-1}) were observed in FA-based SSCs compared to SF. In contrast, SS composites usually presented very high GF values (139-505) and moderate SST (0.0028-0.0113 MPa^{-1}). In terms of GF and SST, the optimal recycled admixtures contents were around 20% for SF, 20% for FA, and 15% for SS. A couple of studies

also reported SSCs produced with high concentrations of BFS (5-25% by weight of binders) and RM (5-25% by weight of binders), in order to reduce OPC consumption. However, these composites' GFs were not reported, and their SST values (0.00109-0.0126 MPa^{-1} for BFS-based SSCs and 0.00134-0.00629 MPa^{-1} for RM-based SSCs) were usually lower than those of SSCs containing SF, FA, and SS. Regarding SSCs containing recycled conductive admixtures, piezoresistive properties were only previously investigated in composites containing a very low content (0.73% by weight of cement) of recycled carbon fibers (RCFs). These composites exhibited a high GF (285.71) and low SST (0.00141 MPa^{-1}) compared to the other SSCs presented in Figures 2a and 2b.

The linearity of the piezoresistive response was only investigated in few studies dealing with SSCs produced with FA, SF, and RCF. Figure 2c shows that most of these SSCs presented R^2 values close to 1.0, which indicates that they have electrical outputs with suitable linearity. Finally, Figure 2d shows that the sensing properties of SSCs have been obtained from piezoresistive tests covering compressive stresses up to 81.19% of their compressive strength. The highest σ/fc ratios were reported in FA-based composites (26.46-81.19%), suggesting that these composites can be used to monitor structural elements subjected to a wide range of compression loads. In contrast, the piezoresistive behavior of SS-based composites was mainly investigated at very low compressive loads (5.43-7.48% of their compressive strength). In the case of SSCs produced with SF, a great range of σ/fc ratios (5.77-74.07%) has been investigated in previous research.

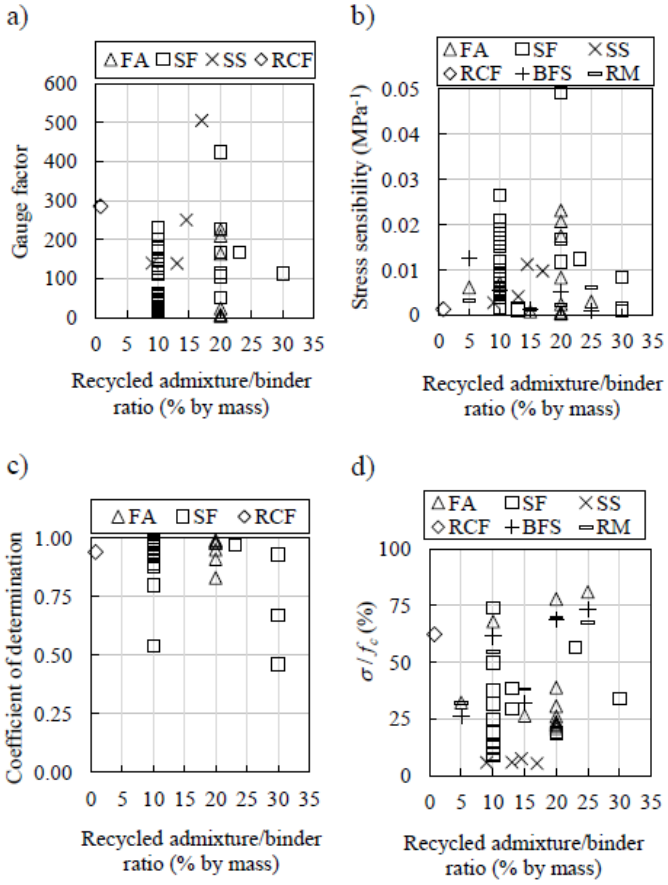

Figure 2. Piezoresistive response of composites containing a single type of waste: a) recycled admixture/binder ratio vs. Gauge factor; b) recycled admixture/binder ratio vs. stress sensibility; c) recycled admixture/binder ratio vs. coefficient of determination; d) recycled admixture/binder ratio vs. σ/f_c. Note: FA - fly ash, SF - silica fume, SS - steel slag, RCF - recycled carbon fiber, BFS - blast-furnace slag, RM - red mud, f_c - compressive strength, σ - compressive stress.

Figure 3 shows the GF, strain amplitude, SST, and stress amplitude of SSCs produced with a single type of waste, considering cases with a linear relationship between FCR and strain (or stress). Figure 3a indicates that SSCs produced with SF as SCM were evaluated in a wide range of compressive strain (up to 2500 με) and presented high GF values (18.9 - 231.25). These properties are particularly interesting when monitoring structures subject to wide deformation ranges. Composites with FA shared this same characteristic, monitoring large deformations (up to 3600 με) with high GF (4.41-225). At the maximum strain of 3600 με, the GF of some FA-based composites was 43.87, a relatively high value. In general, slag residues (SS and GGBFS) provided composites with GF values higher than those of the other wastes (505 and 661.9, respectively). However, they covered a much smaller strain range, up to 160 με for composites with SS and 635 με for GGBFS-based composites. Similar behavior was observed in composites with RCF, which presented a high GF (285.71) and a small amplitude strain of up to 77 με.

Meanwhile, Figure 3b presents the results of studies that evaluated the SST and stress amplitude of SSCs tested over the elastic regime. Again, the piezoresistive response of composites with SF was evaluated over wide stress ranges (up to 60 MPa). Moreover, they exhibited high values of SST (0.001-0.049 MPa^{-1}). Thus, these SSCs could satisfactorily monitor structures made with concretes of conventional and high mechanical strength within their elastic regime. Composites with other types of wastes were evaluated in much lower stress ranges (18 MPa for BFS, FA, and RM; 5 MPa for GGBFS and SS; 15.6 for RCF). It is also worth mentioning the SST values above 0.01 MPa^{-1} of composites with BFS, GGBFS, FA, and SS. The highest SST value (0.068 MPa^{-1}) was verified in GGBFS-based composites, although it covered a small stress amplitude (5 MPa). In general, research on SSCs containing SF is the most advanced so far. Further studies are needed to explore the piezoresistive response of SSCs containing various types of wastes at greater strain and stress amplitudes.

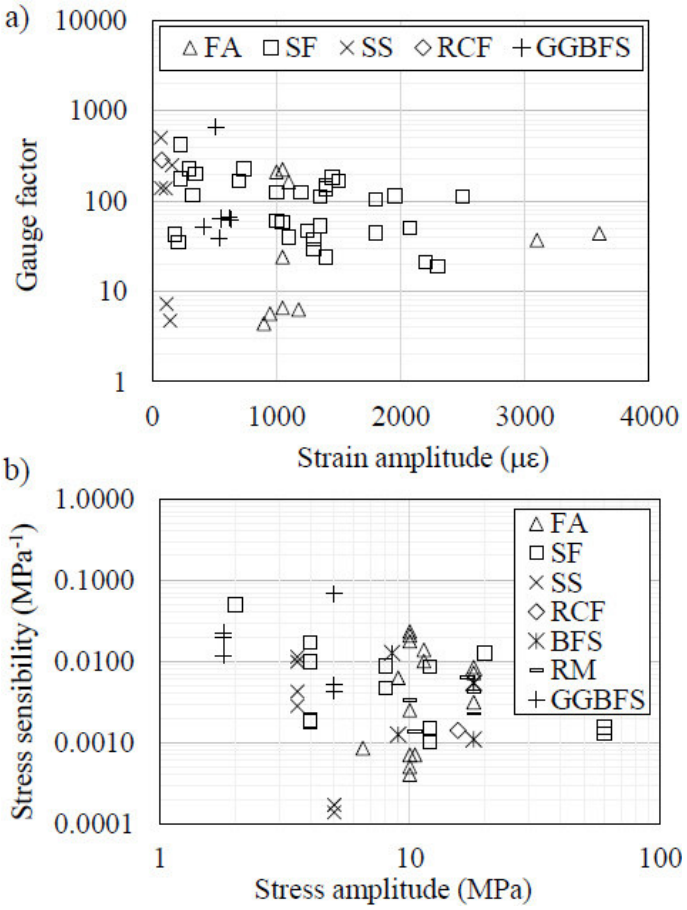

Figure 3. Sensing properties of composites containing a single type of waste with linear behavior in FCR vs. strain (or stress) curves: a) Gauge factor vs. strain amplitude; b) Stress sensibility vs. stress amplitude. Note: FCR - fractional change in electrical resistivity, FA - fly ash, SF - silica fume, SS - steel slag, GGBFS - ground-granulated blast-furnace slag, RCF - recycled carbon fiber, BFS - blast-furnace slag, RM - red mud.

Figure 4 shows the absolute FCR, strain, and stress amplitude of SSCs produced with a single type of waste, considering cases with a non-linear relationship between FCR and strain (or stress). In general, this non-linear relationship can be attributed to the separation of conductive particles due to matrix damage, dispersion of conductive particles, pore distribution in the matrix, and content of conductive materials [50]. Figure 4a clearly shows that composites produced with SS performed better than the other composites, covering the highest strain amplitudes (up to 5263.64 με) and presenting high absolute FCR amplitudes (up to 756.47%). However, the use of FA and SF also provided composites with high strain amplitude and FCR values. Composites with CNTFA presented inferior sensing properties when compared to the others. However, since a modern technique was used to obtain CNTFA, this area has great potential for evolution in future studies.

Regarding the stress amplitude, the piezoresistive response of composites with SF was evaluated up to the highest compressive stress levels (up to 197 MPa), a conclusion similar to that obtained from Figure 3b. In addition, absolute FCR amplitudes reached values up to 270%. Therefore, it is concluded that studies with SF are the most advanced for the production of SSCs for self-detection of damage. FCRs of composites with FA were evaluated at moderate compressive stress amplitudes, reaching 36.32 MPa, whereas those with CNTFA were analyzed up to 8.46 MPa. Finally, FCRs of composites with GGBFS were evaluated up to a compressive stress of 4.5 MPa. Thus, further studies are needed to improve the current understanding of the abilities of damage self-diagnosis of composites with FA, CNTFA, and GGBFS.

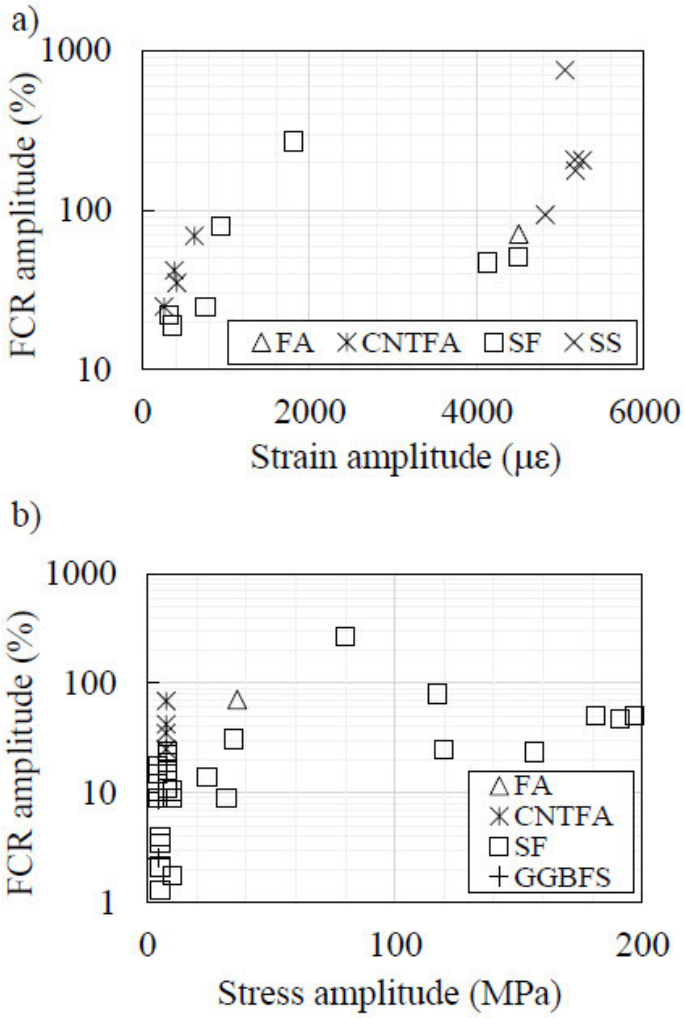

Figure 4. Sensing properties of composites containing a single type of waste with non-linear behavior in FCR vs. strain (or stress) curves: a) absolute FCR amplitude vs. strain amplitude; b) absolute FCR amplitude vs. stress amplitude. Note: FCR - fractional change in electrical resistivity, FA - fly ash, CNTFA - fly ash covered with carbon nanotube, SF - silica fume, SS - steel slag, GGBFS - ground-granulated blast-furnace slag.

Therefore, experimental data of the studies of Tables 1, 2, and 3 suggested that significant progress has been made on the development of modern multifunctional concretes that provide an efficient response to the demand for sustainability and durability of civil infrastructure. As they integrate satisfactory mechanical, self-sensing, and sustainable performance, SSCs are gaining significant importance in the domain of SHM. The next subsections present specific discussions on the research findings reported in the revised studies, which cover the origin of the recycled materials and their effects on the electrical resistivity, strain-sensing properties, and damage-detection properties of SSCs.

2.2.1.1 Silica fume (SF)

SF is a co-product from the production of silicon, ferrosilicon, or zirconium in electric arc furnaces. The reduction of high-purity quartz to silicon generates silicon dioxide vapor that oxidizes at low temperatures and forms SF [134,135]. It is an extremely fine material consisting of amorphous SiO_2 particles with a degree of purity generally greater than 90% [136]. SF was released directly into the atmosphere in the past, being a cause of air pollution. However, the emergence of more austere legislation encouraged the reuse of the material, so that it was first collected for reuse in Norway in 1947 [137]. Nowadays, the application of SF for the production of cementitious compounds is well established, so that SF is one of the most deeply entrenched and accepted industrial co-products in the civil construction sector [136]. This fact reflects the high production and consumption of SF, which is in the order of one million tons per year [138,139]. SF acts as filler, nucleation site, and pozzolanic materials, increasing the mechanical and durability properties of concretes [136,140,141]. However, their workability decreases as the replacement percentage of SF increases, due to the high surface area of this admixture [142].

Regarding the development of concrete sensors, certain concentrations of SF can decrease the electrical resistivity of composites. According to Yazdanbakhsh and Grasley [143], incorporating sufficient proportions of SF can remarkably enhance the dispersion of conductive nanofillers in cement matrices by acting as stabilizing agents that prevent their natural tendency of re-agglomeration. The authors observed that SF particles could fill the space between cement particles due to their small size, restraining the movement and re-agglomeration of CNFs. Kim, Nam, and Lee [144] reported reductions in electrical resistivity up to four orders of magnitude due to the incorporation of 30% of SF into cementitious composites containing 0.3% of MWCNT (by mass of cement). Moreover, this incorporation provided reductions of 3-7% in porosity and an increase of about 87.5% in compressive strength. Although the incorporation of this SF dosage improved the dispersion of MWCNT within the cementitious matrix, higher SF contents can cause a densification of MWCNT around SF fields, leading to agglomeration of the conductive nanoadmixtures. When MWCNT were not used, the lowest electrical resistivity was observed in cementitious composites containing 20% of SF. However, a resistivity decrease of only one order of magnitude was observed, suggesting that a more efficient application of SF for the production of SSCs can be obtained when SF is combined with other conductive fillers.

Kim et al. [145] also observed that incorporating SF into cement-based composites provided improvements in the dispersion of MWCNT by the superplasticizer. Figure 5a shows

that SF was able to fill the gaps between dispersed conductive nanofillers, preventing their re-agglomeration in the fresh mixture and increasing the electrical conductivity of the matrix. A dosage of SF of 20% provided a reduction in the electrical resistivity from 130 Ω.m to 3 Ω.m, which was mainly attributed to the contributions of the recycled admixture in dispersing the conductive nanofillers. In addition, SF filled large matrix voids, reducing ionic conduction through the pore water and improving the conductive pathway inside dried composites (Figure 5b). Similar observations were reported by Dong et al. [111] for cementitious composites containing SF and CBN. The authors reported higher matrix densification due to the filler effect of SF, which provided better dispersion of CBN.

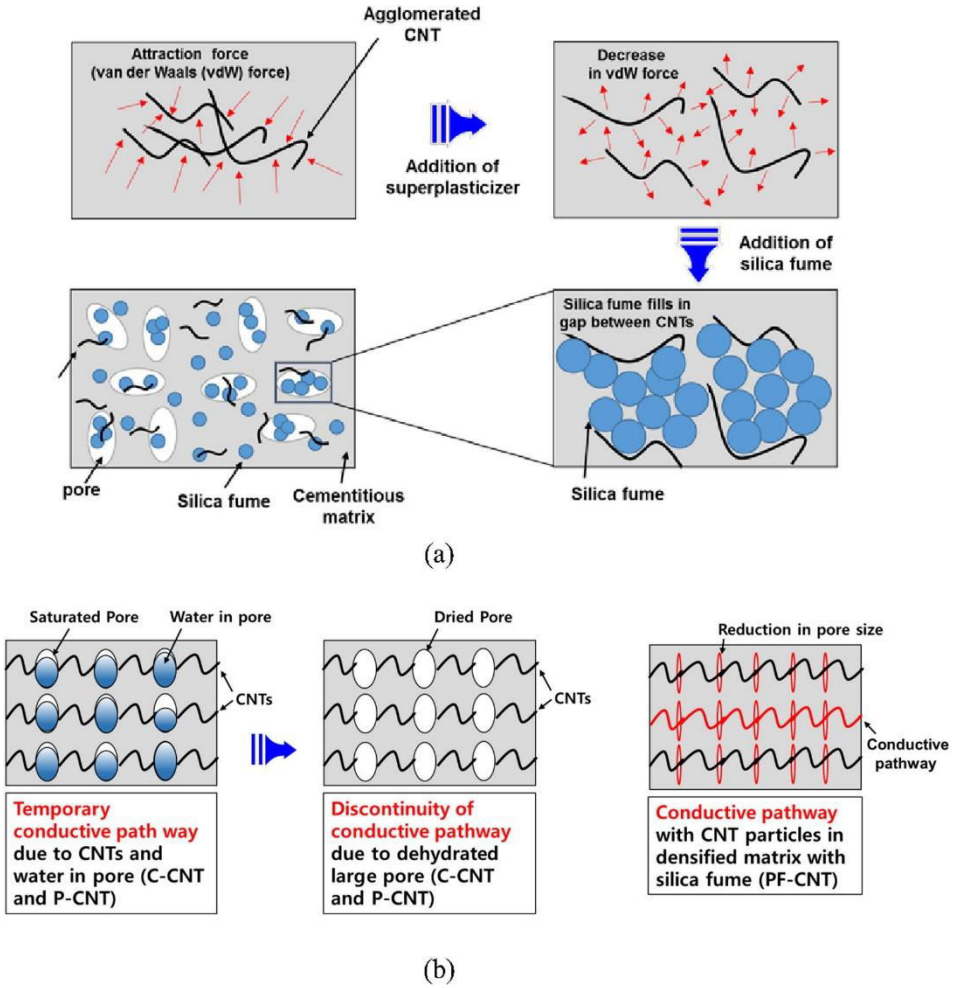

Figure 5. Analysis of the interaction between carbon nanotubes (CNT) and silica fume (SF): (a) Effects of superplasticizer and SF on the dispersion of CNT, and (b) improvement of the conductive pathway over CNTs due to addition of SF. Adapted from Kim et al. [145], Copyright 2017, with permission from Elsevier. Note: C-CNT - composites containing CNT, P-CNT - composites containing CNT and SF, PF-CNT - composites containing CNT, SF, and superplasticizer.

Figure 2 and Table 1 show that SF contents range between 10% and 30% by mass of binders. It clearly demonstrates that one of the great advantages of incorporating SF into concrete materials is the reduction of OPC consumption, since cement production is one of the

highest sources of CO_2 emissions [3–5]. Composites containing SF combined with different conductive admixtures exhibited high values of GF (Figure 2a), SST (Figure 2b), and linearity (Figure 2c). Moreover, they were able to monitor a wide range of strain and stress levels (Figure 3).

Yoo et al. [50] produced cement pastes containing 30% of SF combined with three different conductive admixtures: MWCNT, GNF, and G. MWCNT provided the highest impact on the electrical properties of the pastes, based on high reduction in the electrical resistivity and excellent piezoresistive response with negligible noise. The GF of these composites was 113.2, which is significantly higher than the GF of conventional electrical strain gauges, as commonly observed in other SSCs reported in the present review. In addition, these composites were able to monitor strains up to 2500 με, which is one of the largest strain amplitudes observed in SSCs (Figure 3).

It is also important to highlight recent findings reported by Dong et al. [114] concerning dried cement composites containing 20% of SF and 3% of CBN. These smart composites presented one of the highest GF values (425) observed in SSCs. The authors also evaluated the influence of temperature, moisture content, and freeze-thaw cycles on the piezoresistive behavior of the composites. Specimens subjected to ambient temperature (20 °C) presented good repeatability of electrical outputs during compression loading cycles. An FCR calibration was able to eliminate the effects of thermal changes and provide good repeatability in the piezoresistive response at temperatures between -20 and 100 ºC. The moisture content that provided the highest strain sensitivity (GF of 560) was 8%. Although moisture contents lower than 12% provided suitable repeatability in piezoresistive tests, higher moisture contents provided FCR fluctuations due to polarization effects in the pore water, changes in pore water content, and changes in the number of pores filled with water. Finally, freeze-thaw cycles caused slight impacts on the piezoresistivity of dried specimens and significant damage to saturated composites. Therefore, it is possible to conclude that the moisture content of SSCs with SF and CBN affects their self-sensing properties. For practical engineering applications, the use of compensation circuits [33] or protections against undesirable variations in water content [146,147] are strongly recommended.

Dong et al. [111] reported that incorporating various contents of SF into cement-based composites containing CBN caused a strong non-linear behavior in FCR vs. compressive stress curves since the beginning of the loading process, as presented in Figure 6a. However, this non-linear behavior was not attributed to the development of damage in the cementitious matrix. It was actually associated with the filling effect provided by SF particles. Small compressive

stresses changed the position of CBN and resulted in rapid FCRs. With the increase in the compressive stresses, the authors observed variations in the porosity filled with SF, which reduced the FCRs. They also observed that increasing the SF content up to 10% (by weight of binders) improved the sensing properties of the cement matrices, which is mainly due to the improvements in the CBN dispersion provided by the recycled admixtures. However, a higher SF dosage (20% by weight of binders) caused significant agglomeration of CBN and SF (Figure 6b), leading to reductions of FCR values in the piezoresistivity tests. Specimens with different SF contents presented some FCR fluctuation at the constant stress of 4 MPa (Figure 6a). Then, Dong et al. [111] concluded that these SSCs could also provide their stability to fatigue damages, since those FCR fluctuations are liable to cause such damages inside the CBN-cementitious composites.

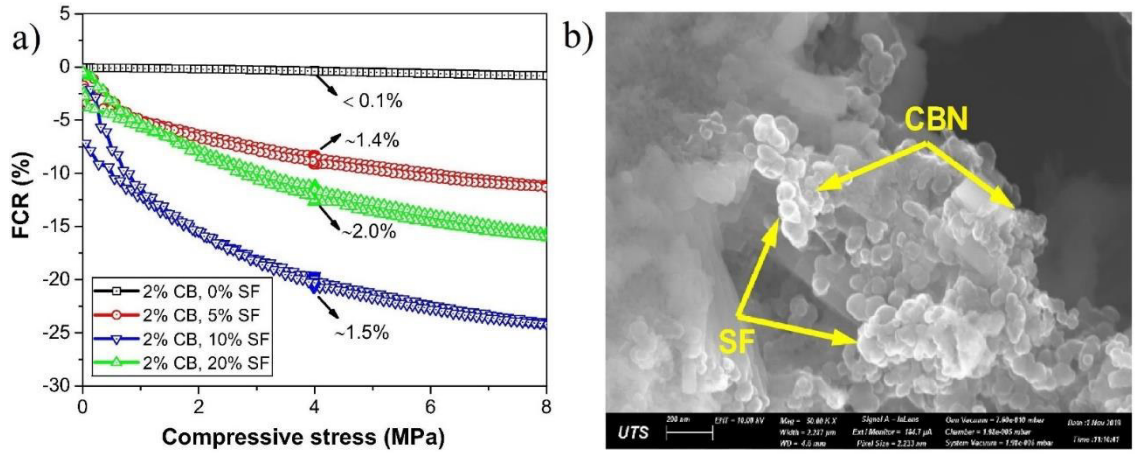

Figure 6. Cement-based composites containing carbon black (CB) nanoparticles (CBN) and silica fume (SF): (a) Fractional change in electrical resistivity (FCR) vs. compressive stress curves and (b) scanning electron microscope image showing agglomerations of recycled and conductive admixtures. Adapted from Dong et al. [111], Copyright 2020, with permission from Elsevier.

A non-linear behavior in FCR vs. compressive stress curves since the beginning of the loading process was also observed by Dong et al. [112] in composites containing 20% of SF (by weight of binders) and different CBN contents. However, the increase in the CBN concentration from 0.5% to 2.0% (by mass of binders) increased the linearity in FCR vs. compressive stress. Then, higher contents of conductive admixtures seem to decrease the effects of instability of the SF that filled the pore system of the composites. Dong et al. [112] also mentioned that higher CBN concentration can eliminate FCR fluctuations induced by small water content remaining in the pores after oven-drying at 60 ºC for one day.

Previous studies also reported that SSCs containing SF combined with different conductive fillers have a self-sensing ability to diagnose damage propagation in structural

elements. For instance, Yoo et al. [50] observed that the FCR of cement-based composites containing SF, MWCNT, and STF suddenly increased at compressive stresses close to their compressive strength. It was mainly attributed to the increases in the distances between the conductive fillers due to cracking localization phenomena. The conductive pathways mainly formed by MWCNT and STF were disrupted with the increases in crack width. Composites containing 20% of SF (by weight of binders) presented one of the highest FCR amplitudes (~270% at the peak stress of 80 MPa) reported in the literature (Figure 4), which suggests the effectiveness of combining SF, MWCNT, and STF to produce SSCs that present high compressive strength and detect the evolution of severe damage.

Jung et al. [116] also used SF as chemical binders (concentration of 20 % by weight of binders), and MWCNT and STF as conductive fillers to produce ultra-high performance concretes with crack sensing ability. They obtained high compressive strength values (181-197 MPa), but the maximum FCR amplitudes (47-51%) observed at the peak stress were lower than those reported by Yoo et al. [50].

A review of previous works suggested that the incorporation of SF contents between 10% and 30% (by weight of binders) is strongly recommended to decrease the porosity of cementitious matrices, reduce cement consumption and greenhouse gas emissions, and increase the dispersion of various conductive admixtures. Consequently, this approach can improve mechanical, durability, sustainable, and electrical properties of structural elements. The natural tendency of agglomeration of different types of conductive admixtures can be avoided, as they can be densely dispersed in SF fields inside cementitious matrices. Then, the use of SF has assumed great importance in the development of multifunctional civil infrastructures, including structural elements with electromagnetic shielding and self-sensing behavior.

2.2.1.2 Fly ash (FA)

FA is a coal combustion product with an annual generation of about 900 Mt. About one-third of this amount is currently used to produce cement-based materials, as the main limitation for expanding FA use is its great quality variability [148,149]. The chemical composition of FA varies according to its source materials and the conditions of the combustion process, although the resulting material is predominantly formed by Al_2O_3, CaO, MgO, Fe_2O_3, and SiO_2 [150,151]. Low-calcium FA has been widely used as a concrete admixture, due to its pozzolanic properties [152]. However, since pozzolanic reactions are usually slow, the mechanical properties of composites containing FA can be negatively affected at early ages. The use of FA

as SCM provides many positive effects, such as reductions in hydration heat and increases in durability [153]. In contrast, the application of high-calcium fly ash in concrete has been hindered because it significantly changes the cement hydration, so that future research is needed to support the full use of high-calcium FA in concrete [154].

According to Kang et al. [155], the effects of FA on the electrical resistivity of cement-based materials are not easy to predict due to the diverse sources of FAs and their varying reactivity. For example, FAs with high SiO_2 contents have a good source to form calcium silicate hydrates (C-S-H) with OPC particles. Consequently, concretes produced with these FAs present a higher amount of C-S-H phases, lower capillary porosity, and lower connectivity of capillary pores, resulting in higher electrical resistivity. Moreover, Tran et al. [156] reported that the improvements in pozzolanic reactions provided by FA resulted in increases in the electrical resistivity of FA concretes. Similar behavior was observed by Vo et al. [157] in slag AACs: the incorporation of FA contributed not only to the improvement in hydration reactions but also to the filling effect, which created a structure that was denser than that of control mixtures, which resulted in electrical resistivity increases. In contrast, Konkanov et al. [122] reported reductions in electrical resistivity of SSCs due to the addition of FA, which was attributed to the presence of iron oxides in the recycled materials.

The FA concentrations used to produce SSCs varied from 5% to 75%, as presented in Table 1 and Figure 2. Figures 2a and 2b indicate that FA contents around 20% provided the highest GF values (200) and linearity (R^2 of 0.99). The highest SST values were observed in composites containing 25% of FA (Figure 2c). The environmental benefits provided by FA are similar to those discussed for SF, as the incorporation of FA into smart composites provides reductions in cement consumption and greenhouse gas emissions.

In a recent experimental work developed by Zhan et al. [123], MWCNTs were synthesized in situ on the surface of FA particles using a one-spot microwave heating method. Different contents (0.4, 0.8, 1.2, and 2.0% by weight of binders) of these conductive FA particles (CNTFA) were then used to produce cement mortars. A piezoresistive behavior was observed in composites with well-dispersed CNTFA. The increase in the compressive stress caused increases in the number of contacts between the MWCNT synthesized on the FA particles' surface and decreased the gaps between them, which improved electronic conduction. Figure 7 shows that in a complete conductive path formed by CNTFA, there should be much more MWCNT junctions or contacting points than a conductive path constructed by conventional MWCNT. Consequently, the unique morphology of CNTFA provided many possible locations for triggering MWCNT contacts, which improved the sensing ability of the

cement mortars. Nevertheless, nonlinear relationships between FCR and compressive strain were observed in mortars containing CNTFA. Although very high sensitivity was observed for lower strain levels, while reasonable FCR amplitudes ranging between 25% and 69% were observed at the ultimate stress.

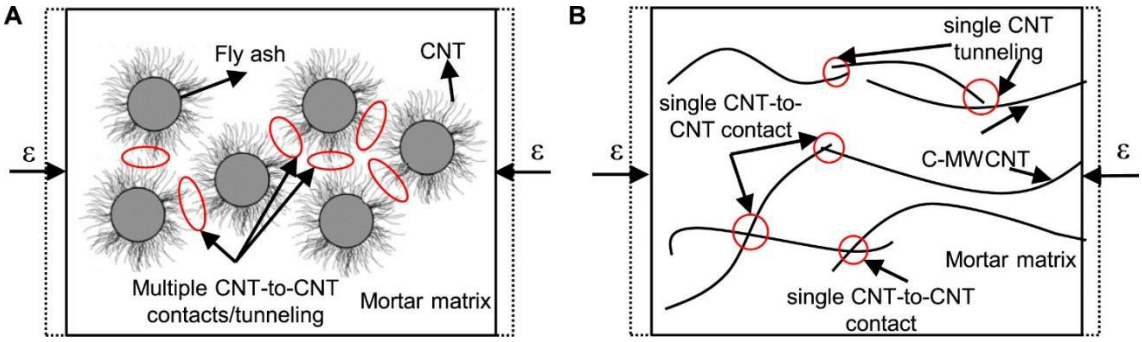

Figure 7. Schematic comparison of possible electronic conduction occurring in cement-based composites containing (a) carbon nanotubes (CNTs) covering fly ash or (b) conventional CNTs under compression. Adapted from Zhan et al. [123], Copyright 2020, with permission from Elsevier.

Ding et al. [124] also observed a nonlinear behavior in FCR vs. strain curves of cement mortars containing 16.67% (by mass of cement) of conventional FA and 6% (by mass of binders) of BHNCM (botryoid hybrid nano-carbon material). This nonlinearity is mainly related to the development of cracks in the region between the electrodes of the cement-based sensor. The maximum absolute FCR value was 71%, one of the highest values reported by the works reviewed in the present paper (Figure 4). After reaching the ultimate stress, the absolute FCR values of the sensor remained basically unchanged and then slightly decreased in the latter period, as also observed by Han, Ding, and Yu [34].

The electrical response of cement-based composites with FA and different conductive admixtures (CBN and CNF) under uniaxial tension tests has also been investigated. A strong piezoresistive behavior within the elastic regime was observed in some composites. For instance, Deng and Li [100] observed high sensing ability from the elastic regime to the first cracking stage in composites containing 0.4% of CBN and 60% of FA (by mass of binders). Huang, Li, and Qian [99] also observed a very interesting sensitive response to first cracking in cement mortars produced with 0.45% of CBN and 54.54% of FA (by mass of binders). All authors also observed that the electrical resistivity of the composites significantly increased with the propagation of cracks between the electrodes, which indicates that they are suitable for strain-sensing applications even in the inelastic regime. Hardy et al. [47] found that the incorporation of a CNF concentration of 0.088% (by mass of binders) into cement mortars

containing a high amount of FA (73.7% by mass of binders) provided the optimal results in terms of enhanced mechanical properties and self-sensing behavior.

2.2.1.3 Red mud (RM)

RM is a waste generated from the Bayer process used for the processing of bauxite into alumina. About 160 Mt of RM is generated per year [158]. An amount between 1.0 and 1.5 tons of dry weight waste is generated for each ton of alumina produced [159–161]. RM is mainly composed of oxides and hydroxides of silicon, aluminum, iron, calcium, titanium and others, so that the high alkalinity (pH 9.2-12.8) of the material is a challenge for its suitable management [162]. Several applications of RM as a construction material have been studied to promote the valorization of this residue and reduce the environmental impacts resulting from its inappropriate disposal. In studies of incorporation of RM in cement matrices, Dodoo-Arhin et al. [163] observed that the fine granulometry of RM provided decreases in workability, but improved the bulk density and reduced the porosity of the composites. Moreover, the presence of hydroxides of aluminum and sodium in RM tend to decrease the setting time of cementitious composites [122]. In addition, high concentrations of RM usually lead to decreases in mechanical properties of concretes [164].

Raghu and Kondraivendhan [165] measured the electrical resistivity of concretes with RM exposed to different moisture contents over 270 days. Concretes made with RM presented lower electrical resistivity than reference concretes without RM. Ribeiro et al. [166] reported that concrete specimens containing RM presented higher electrical resistivity in a humid environment than control specimen without RM. However, after a drying process, concretes with RM showed resistivity values lower than the reference samples. According to the authors, this difference can be related to the existing highly conductive Na^+, OH^-, Ca^{2+} and K^+ ions in RM, which contributes to decrease the electrical resistivity of concrete when it loses moisture. The effects of these compounds on the electrical conductivity became more pronounced and active only when the moisture content decreased. Konkanov et al. [122] also observed that incorporating RM into cement mortars decreased their electrical resistivity by a third at the end of the curing period. It was attributed to the relatively high content of metal oxides (Fe_2O_3) found in these waste materials. In fact, a comprehensive review of previous studies indicates that RM is composed of different residual minerals, such as Fe_2O_3, α-FeO(OH), and γ-AlO(OH) [167].

Research on the electrical resistivity and piezoresistivity of construction materials containing RM is very scarce. Salih et al. [168] studied the stress-strain-resistivity of RM waste incorporated in soils and subjected to dry-wet cycles. Composites containing an optimal RM content of 77% presented an electrical resistivity decrease higher than 60%. In a recent study developed by Konkanov et al. [122], the self-sensing properties of SSCs produced with different RM contents varying from 5% to 25% were investigated (by mass of binders). After a 28-days curing period, the authors did not observe a significant difference in the electrical resistivity of the composites. The maximum absolute FCR value was observed in composites containing 25% of RM subjected to a compressive stress of 18 MPa. The SST varied from 0.001 MPa^{-1} to 0.01 MPa^{-1} (Figure 3b), reaching values close to those observed in SSCs containing FA, SF, and BFS, for example. Although RM is regarded as a resource of multiple metals [169], no investigation of GF, linearity, and strain amplitude of RM-based SSCs was found in previous literature. The investigation of the ability of self-detection of damage of RM-based SSCs is also recommended for further research.

2.2.1.4 Blas-furnace slag (BFS)

GGBFS has been one of the most used SCMs for the production of PCCs and one of the most used precursors of AACs. GGBFSs are co-produced with pig iron, have an annual production of 360 billion tons [142], and have a chemical composition formed mostly by oxides of calcium, silica, and alumina [170]. In most of the cases, the mechanical properties at early age decrease with increases in the GGBS content. However, the mechanical performance increases with the increase in percentage of GGBS at later ages [171]. In fact, GGBFS can form additional C-S-H, thus providing mechanical performance improvements, porosity reductions, greater durability, and increased resistance to corrosion, chloride entry, and fire [172]. Moreover, inclusions of GGBFS beyond the optimal dosage may negatively affect the strength and durability of concrete [173]. In comparison to conventional PCCs, the use of GGBFS as precursors of AACs provides significant reductions in environmental impacts associated with CO_2 emissions from clinker production, in addition to 30-40% reductions in depletion of natural raw materials [48]. GGBFS is used as a source of aluminosilicates and calcium, and a series of chemical reactions take place to form the composite matrix when this residue is mixed with alkaline solutions [40]. The alkaline activation of GGBFS consists of a disruption of the waste and subsequent polycondensation with formation of calcium-aluminosilicate hydrates [174], which provides materials with good mechanical performance and durability [175].

Alkali-activated GGBFS shows improved electrical conductivity properties due to the presence of mobile hydrated Na^+ ions and metallic iron particles [126]. The incorporation of BFS on CPCs also provides improvements in electrical conductivity. Konkanov et al. [122] verified that the replacement of OPC with BFS provided gradual reductions of electrical resistivity for BFS contents up to 25% (by mass of binders).

D'Alessandro et al. [48] carried out an alkaline activation of GGBFS. Incorporating 1% (by mass of GGBFS) of CBN and CNF provided reductions in electrical resistivity of 28.6% and 42.9%, respectively. In contrast, the incorporation of GNP (graphene nanoplatelets) caused an increase in the electrical resistivity of 65.7% due to a possible increase in the porosity of the composite. Rovnaník et al. [51] studied the combination of GP and alkali-activated GGBFS. They observed improvements in electrical conductivity for GP contents up to 10% of GGBFS mass, while higher GP contents did not provide additional improvements in electrical conductivity, but caused a strong deterioration of mechanical properties of the sustainable material.

Some alkali-activated mortars produced by Rovnanik et al. [126] were compared to OPC mortars, in terms of self-sensing properties. Although no conventional conductive filler was added to the alkali-activated specimens, they presented a remarkable sensing behavior due to the iron particles existing in the GGBFS. The combination between ionic and electronic conduction provided a high SST (0.00505 MPa^{-1}) to the alkali-activated mortars, so that their piezoresistive response was more significant than that of conventional OPC mortars.

D'Alessandro et al. [48] demonstrated that incorporating conductive carbon nanofillers (CBN, CNF, MWCNT, and G) enhances the piezoresistive behavior of alkali-activated mortars produced with GGBFS, with special attention on improvements in linearity and reductions in hysteresis. They presented GF from 39 to 65 and SST from 0.017 MPa^{-1} to 0.023 MPa^{-1} (Table 2 and Figure 2). Vilaplana et al. [127] added CF to BFS alkali-activated pastes and observed positive effects of the conductive fibers on the sensing properties of the materials, so that GF between 52 and 661.9 and SST between 0.0043 MPa^{-1} and 0.0680 MPa^{-1} were obtained. Then, alkali-activated matrices containing waste materials as precursors are promising alternatives for SSCs. Their piezoresistive effects can also be optimized with the addition of conductive fillers.

Regarding the slag-modified cementitious composites, Konkanov et al. [122] used BFS to partially replace cement. Specimens produced with the replacement of 20% of cement by BFS presented good repeatability in piezoresistivity tests, with average absolute values of FCR around 6%. Figure 2b compares the sensing properties of these composites with those reported in other works dealing with different types of waste materials. Reasonable SST values were

obtained because BFS was not combined with other conventional conductive fillers to optimize the sensing behavior, which was the approach used in most of the works presented in Figure 2b.

Studies on the ability of self-detection of damage of GGBFS-based composites are scarce. In this context, a non-linear relationship between FCR and compressive stress was reported by Rovnaník et al. [51] in alkali-activated mortars produced with GGBFS and different contents of GP (0 to 30% by mass of GGBFS). Figure 4 shows that absolute FCR values up to 8.6% were verified in composites subjected to cycle piezoresistive tests. The authors stated that the decreases in electrical resistivity with the increases in the compressive stresses were mainly related to the closure of microcracks and initial defects in the matrix. During unloading, the electrical resistivity increased as the defects were aggravated again. A non-linear behavior was also observed in FCR vs. stress curves of the evaluated composites because conductive particles became very close to each other at a certain compressive stress level, so that the system reached maximum conductivity.

2.2.1.5 Steel slag (SS)

SS is a waste generated from steelmaking and refining processes with an annual production of about 130 million tons. Most of the SS has been deposited in landfills or incorporated as aggregate for different construction purposes [176]. With some physicochemical properties similar to those of GGBFS, SS also provides improvements to the mechanical performance of construction materials, in addition to interesting positive responses when incorporated into self-sensing building materials [52,54,55]. Hydration of free lime (CaO) and free periclase (MgO) and oxidation of iron existing in SS can cause volumetric instability and expansion issues, so that long periods of aging and quality control are required before the incorporation of SS into building materials [177,178].

Heat treatments and the composition of SS affect its electrical properties. Farahat et al. [179] observed that the electrical conductivity of the used electric arc furnace (EAF) slags increases exponentially with temperature increases, due to the fragility of silicate structures and increased ion mobility, being non-conductive for temperatures below 135 °C. However, the authors noticed that the electrical conductivity increases as the FeO and CaO contents increase and SiO_2 content decreases. According to the authors, CaO breaks the silicate network, reduces the slag viscosity, and increases ion mobility, while SiO_2 increases the silicate network, which prevents the movement of ions and increases the viscosity, thereby reducing the electrical

conductivity of the material. FeO has the lowest melting point among the SS constituents, which makes its effect on electrical conductivity very deep. FeO was found to provide improvements in both ionic and electronic conductivity. For instance, the magnetite (Fe_3O_4) of SS is a material classified as a semiconductor, enabling the formation of conductive channels when SS is incorporated into composite matrices.

According to Ding et al. [52], the continuous state of solid solutions of iron oxides in SS can be destroyed after ground, so that the conductive components are exposed. Therefore, different grinding procedures lead to various exposure levels of conductive components. Moreover, high heterogeneity is usually observed in SS materials. Consequently, the conductive phase distribution has great randomness. For an accurate assessment of the environmental benefits provided by the incorporation of SS into cement-based materials, energy consumption during the grinding procedures need to be taken into consideration while calculating greenhouse gas emissions.

Two different approaches have been used to incorporate SSs into cement-based materials: they have been added as SCMs or aggregates. For instance, Baeza et al. [128] used EAF steel slags as fine aggregates of OPC and CF mixtures. They observed that SS increased the compressive strength and electrical conductivity of the composites, so that the percolation threshold was reached with lower CF contents (CF volume fractions lower than 0.97%), compared to composites produced with conventional limestone aggregates (CF volume fraction of approximately 1.1%).

Hong et al. [129] evaluated the effects of different contents of SS (9, 13, 14.5, and 17% by mass of binders) content and moisture content on the electrical properties of PCCs. After a 28-days curing period, the authors verified that the electrical resistivity of non-dried and dried concrete mixtures without SS was about 1600 Ω.cm and 3600 Ω.cm, respectively. Non-dried and dried concrete specimens produced with 17% of SS (by mass of binders) presented electrical resistivity of 1200 Ω.cm and 2400 Ω.cm, respectively. These results indicated the effects of ionic conduction inside the material, in addition to improvements in electrical conductivity. The high amount of iron oxide in the waste (SS with 40% of Fe_2O_3) was distributed evenly within the concrete matrix, forming many electrical conductive paths.

A piezoresistive behavior was also observed in SSCs containing SS. For example, Baeza et al. [128] also measured the piezoresistive response of their OPC mortars produced with different types of fine aggregate (SS and limestone) and various concentrations and types of CF. Among their experimental results, it is important to highlight those observed in specimens

containing SS and 4% of oxidized CF, which presented the best value of linearity in the FCR vs. strain curves, represented by an R^2 of 0.98 (Table 1).

Regarding the piezoresistive behavior, Hong et al. [129] also observed that non-dried and dried specimens presented higher absolute FCR values in piezoresistive tests when the SS concentration increased. In fact, Figure 2a shows that composites with SS present very high GF values compared to those reported for other types of wastes. Higher moisture content also tends to affect the piezoresistive response, increasing the GF of cement-based sensors [120]. However, Hong et al. [129] observed higher GF values in dried specimens with SS contents of 9, 13, and 17%, which was attributed to the expansion effects of SS in the presence of water. According to the authors, during the cycles of compressive loads, the water pore reacts with the free lime (CaO) of the SS, forming hydrated compounds of higher volume that cause microcracks in the waste particles (Figure 8). This degradation causes interruptions and changes in the conductive pathways inside the matrix of SSCs, decreasing their self-sensing properties. Due to this phenomenon, non-dried SSCs containing 9, 13, and 17% of SS presented increases in GF of 37, 27, and 135%, respectively, after a drying process.

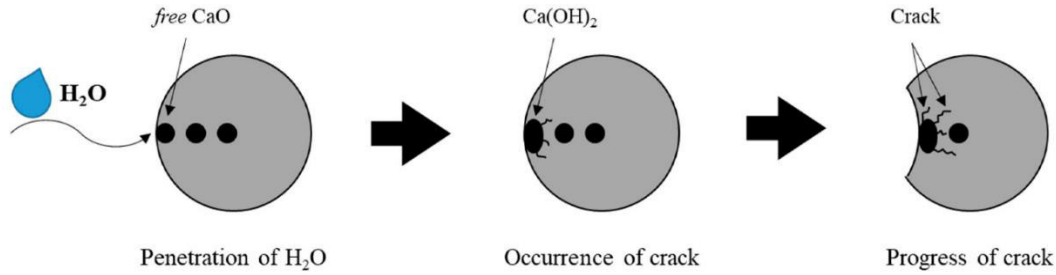

Figure 8. Cracking development in SS particles due to the presence of water. Reproduced from Hong et al. [129], as permitted under the Creative Commons Attribution License Agreement.

SSs can form conductive channels inside the matrix of an SSC not only when used as SCM, but also when applied as aggregates. Lee, Le, and Kim [55] evaluated the piezoresistive behavior of SSCs produced with SS and micro STF. As the compressive stress increased, the conductive network of these SSCs enhanced owing to the contact of SS and STF, causing approximately linear decreases in the electrical resistivity. An image of SS and STF inside these composites is presented in Figure 9, together with some sketches showing the formation of a new conductive path inside the matrix due to the compression load Δ applied to the specimen.

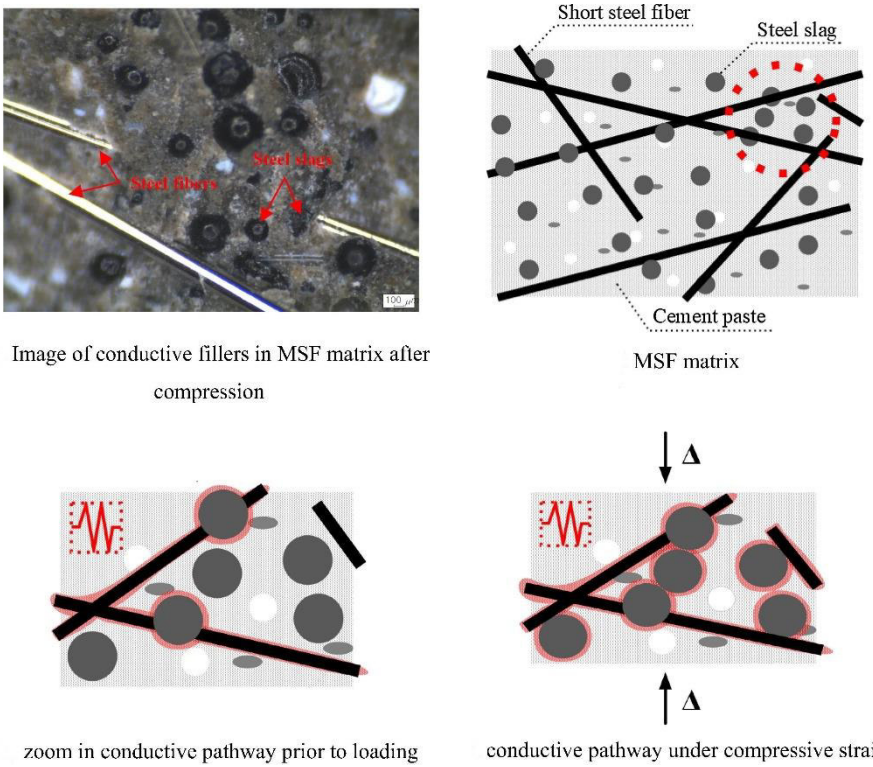

Figure 9. Formation of conductive pathways in a cementitious matrix containing steel slag aggregates and steel fibers (MSF) due to compressive loading. Adapted from Lee et al. [55], Copyright 2019, with permission from Elsevier.

Ding et al. [52] produced epoxy resin concretes with SS and 60% of graphite (by mass of SS). The authors verified that the SS improved the system's electrical conductivity, playing the role of providing a conductive interface layer that interacts with the epoxy conductive adhesive and forms a conductive path. When the composite was subjected to increasing compressive load, the conductive phase of SS and the epoxy conductive adhesive were separated and the conductive path was broken, which provided a pressure sensitivity to the composite. This monotonous increase in the electrical resistivity since the beginning of the compression test is not in agreement with results of previous works. In the elastic regime, all studies revised in this paper reported gradual decreases in the electrical resistivity due to decreases in the distance between adjacent conductive particles. The distinct behavior observed in composites of Ding et al. [52] suggested poor bond conditions between the epoxy resin concrete matrix and the SS, so that low levels of transversal deformation due to compressive loading were enough to cause lateral microcracks and interruptions in the conductive network. At the later loading stage, the electrical resistance increased rapidly with the increase of the compressive stress due to the expansion of pores and the development of cracks. Then, these composites also presented some sensitivity to damage evolution. The experimental data of SS-based composites indicated in Figure 4b were those obtained by Ding et al. [52]. They indicated that high sensing properties

were verified at the end of the uniaxial compression tests, since FCR amplitudes up to 756.5% were observed.

2.2.1.6 Recycled carbon fiber (RCF)

RCFs are promising alternatives for the production of SSCs, since their incorporation into construction materials can decrease waste landfilling and provide conductive admixtures with reduced costs. RCFs can enhance the compressive, flexural, and tensile splitting strength of the cementitious matrices, mainly due to the bridging effects. The presence of carbon micro-fragments on the surface of RCF can increase the roughness and act as nucleation points for C–S–H, improving the adhesion between RCFs and the composite matrix [57]. However, increases in the dosage of RCFs caused significant workability reductions, which eventually affected the compaction of the samples, increased porosity, and decreased the mechanical properties [180].

Segura et al. [130] and Faneca et al. [180] investigated the electrical properties of cement-based materials produced with RCF obtained from aerospace composite scrap with processes that allow high retention of the properties exhibited by virgin CF. High electrical conductivity values were reported by Segura et al. [130] for cementitious matrices with RCF contents above the capacitance threshold. They also observed that the incorporation of monofilament RCF (mRCF) provided a seven-fold increase in the electrical conductivity of the cementitious matrices, while a nineteen-fold increase was observed in cementitious matrices containing RCF supplied as fibrillated sheets (fsRCF). Faneca et al. [180] also verified that incorporating mRCF and fsRCF increased the electrical conductivity of concretes. However, they observed that higher RCF dosage caused an inversion phenomenon, and the electrical conductivity slightly decreased again. It was mainly attributed to the inadequate dispersion of recycled fillers when high RCF concentrations were used. These experimental results indicate that, in general, the electrical behavior of concrete manufactured with RCF did not differ significantly from that observed in concrete produced with virgin CF, which suggests that the use of RCF for the production of multifunctional concretes will enhance the sustainability of infrastructures.

Belli et al. [57] evaluated cement mortars made with RCF derived from the cutting and processing of CF panels. The authors developed a comparison between the electrical behavior of cement mortars produced with RCF, virgin CF, and BSF (brass-plated steel fiber). They reported a percolation threshold at fiber volume fractions between 0.1% and 0.2% for both CF and RCF. BSF presented lower electrical effectiveness, with a percolation threshold at fiber volume fractions between 0.4% and 0.8%. The incorporation of CF, RCF, and BSF provided

electrical resistivity decreases up to 65%, 75%, and 52%, respectively, compared to reference mortars without conductive fibers.

Although the effects of RCF on the electrical resistivity of concretes have been reported in the works mentioned above, systematic investigation of the GF and SST of these conductive concretes is very limited. Also, the application of RCF for self-diagnosis of damage of concrete elements is not covered in previous literature. Consequently, further research is recommended to investigate properties for self-monitoring of strain and damage of SSCs made with RCF.

2.2.1.7 Rubber waste (RW)

The production process of different rubber materials (e.g., tires, belts, hoses, shoe soles, among others) and their disposal after their service life are responsible for generating large amounts of RW [181,182]. Since the main products of the rubber industry are vehicle tires, the growing prevalence of automotive transportation has increased the generation of RW, which poses an enormous environmental problem due to its non-biodegradability and flammability [183,184]. Every year, almost 1 billion tires end their service life and, out of that, more than 50% are disposed in landfills or garbage without any treatment [185]. This critical scenario and the strong environmental awareness movement have stimulated the recycling of RW in various civil engineering applications, such as cement production and the replacement of natural aggregates for the production of concrete [14,186]. In general, the incorporation of RW into concretes tends to decrease their mechanical and durability properties. This tendency increases with the increase in the dosage and particle size of RW. Nevertheless, the incorporation of RW increases the ductility, energy-absorbing capacity, impact resistance, sound-absorbing capacity, and thermal insulation of concrete materials [187–189].

RW can also be subjected to thermal decomposition in the absence of oxygen (pyrolysis) to produce recycled carbon black nanoparticles (RCBN) and oil/gas that can be used as an alternative fuel in cement kilns [65,190]. For instance, recycled RW obtained by the pyrolysis method from waste tires has been used to produce electrically conductive concretes. With increasing demands on electromagnetic shielding materials, conductive rubber containing small conductive particles (e.g., conductive carbon black, aluminum powder, silver powder) has been widely used in the aerospace, precision instruments, military, and automobiles industry [43,102,191,192]. Consequently, conductive RWs have also been investigated as promising admixtures for the production of SSCs.

For instance, Dehghanpour et al. [102] produced electrically conductive concretes using RCBN obtained by the pyrolysis of RW. When only RCBN was incorporated into cementitious matrices, their bulk electrical resistivity did not decrease. Actually, RCBN only decreased the electrical resistivity of cement-based composites when used in combination with CF (around 0, 0.85, 2.1, and 4.3% by mass of cement) or STF (around 11.7% by mass of cement). Among specimens containing RCBN and 11.7% of STF, the minimum bulk electrical resistivity (5218.62 □.cm) was observed when the concentration of RCBN was equal to 6% (by mass of cement). Results also indicated that increases in the RCBN clearly decreased the percolation threshold of cementitious composites containing CF. Then, the combination between RW and conventional conductive fillers is a promising alternative for the future development of SSCs.

2.2.1.8 Biochar

Biochar is a carbon-rich and low-cost material obtained from the pyrolysis of biomass and biodegradable waste materials, such as animal, agricultural, and forestry wastes. Recent studies have explored the potential application of biochar to enhance eco-efficiency, mechanical, and self-sensing properties of cementitious composites. Biochar has a high concentration of carbon, so that its incorporation into cementitious composites ensures sequestration of relevant amount of carbon that cannot get back to the atmosphere [101,193,194]. The addition of biochar to cement-based materials improves their compressive strength, flexural strength ductility, and fracture toughness [195]. Moreover, workability is reduced by biochar addition and high contents of biochar cause decreases in mechanical strength [196].

Kamaluddin et al. [106] investigated cement pastes containing biochar obtained from the pyrolysis of rice husks at a controlled environment. Electrical resistivity decreases were observed with increases in biochar content. The use of 15% (by weight of cement) of rice husk biochar provided pastes with electrical resistivity values comparable to those of cementitious composites containing conventional conductive fillers, such as graphite. Haque et al. [107] recently proposed a chemo-mechanical modification of biochar that can enhance the durability, sustainability, and electrical properties of cement mortars. Using 11.11% (by weight of cement) of a super-hydrophobic carbonaceous powder (SHCP), the authors increased the electrical conductivity of cement mortars by 33% and decreased their CO_2 emissions by 28%.

The self-sensing properties of SSCs containing biochar were only observed by Haque et al. [101], based on bending tests of mortars beams containing biochar produced by pyrolysis of

wood chips. Their SHCP biochar contained around 80% by weight of carbon particles that acted as conductive inclusions in the cementitious matrices. A concentration of 17.65% (by weight of cement) of SHCP increased the electrical conductivity of mortar beams by 23%. Flexural stresses up to 1.5 MPa caused FCR up to 0.14%. Moreover, a strong linear correlation of FCR with flexural stress was observed (R^2 of 0.996). Thus, biodegradable waste materials are promising alternatives for the production of self-sensing cementitious composites.

2.2.1.9 Gasification char (GCH)

The thermal treatment of biomasses in gasification processes also generates a by-product called gasification char (GCH). Gasification is a thermochemical process in which biomass can be converted into syngas, a mixture of different gases (e.g., CO, H_2, CH_4, and lighter hydrocarbons) that can be used for the cogeneration of heat and electricity or for production of fuels. GCH is one of the by-products of the process and is mainly composed of carbon [197]. Mobili et al. [104] observed that the incorporation of small contents of these carbonaceous fillers (up to 1% by weight of binder) into cement-based composites can increase their compressive and tensile strength. The high surface area of GCH particles provided new locations for the growth of hydration products and leads to the accelerating effect on the hydration kinetics at early ages. However, experimental results of Mobili et al. [103] indicated that high dosage of GCH (5% by weight of binder) can slightly decrease the workability and the compressive strength of cementitious composites.

Mobili et al. [104] evaluated the electrical resistivity of lime mortars containing 0%, 0.25%, 0.50%, and 1.00% of GCH (by weight of binder). Their GCH was a by-product of the gasification process of natural wood chips. The electrical resistivity of GCH-based mortars was about 60% lower than that of reference mortars, regardless of the GCH dosage. Electrical resistivity decreases were attributed to the high carbon content of the wastes and their effective dispersion in the composite matrix. Similar observations were observed in other recent experimental study developed by Mobili et al. [103], in which the addition of 5% of GCH (by weight of binder) to cement mortars provided electrical resistivity reductions of 31% and 42%, according to direct current and alternating current measurements, respectively. Although self-sensing properties of composites containing GCH were not investigated in previous research, these findings could be interesting for the future development of GCH-based SSCs.

2.2.1.10 Waste of nano-graphite containing iron particles (ING)

A new type of conductive cementitious material was recently investigated by Dong et al. [105], based on the incorporation of wastes of nano-graphite containing iron particles (INGs) into PCCs. INGs are by-products generated during the hydrogen production process. The authors investigated the compressive strength of concretes with different contents (1%, 3%, and 5% by mass of binder) of ING or conventional nano-graphite (NG). Their application in concrete production had a negative impact on the compressive strength since all mixtures containing nano-graphite particles had lower compressive strengths than that of the plain concrete. Strength reductions were attributed to lubrication effects of nano-graphite particles that negatively affected the transition zone between aggregates and hydration products.

The experimental study of Dong et al. [105] also covered the electrical resistivity of concretes containing ING or NG. They observed a clear trend of reducing electrical resistivity as the proportion of conductive admixtures increases. However, resistivity reductions provided by ING were much more significant than those provided by conventional NG. The incorporation of 1% of ING and NG (by mass of binder) reduced the electrical resistivity by 70.3% and 11.3%, respectively. Therefore, it is evident that composites produced with ING reached the percolation threshold more quickly than composites fabricated with NG. The contributions of ING in enhancing the concrete electrical conductivity are directly associated with the presence of additional iron particles that were not found in pure NG. More free electrons were able to pass through conductive tunnels between these iron particles, so that electrical resistivity decreases were higher in composites containing ING. An experimental study of self-sensing properties of PCCs and AACs containing ING is recommended as a follow-up of this work. Then, implementing ING into SSCs will provide a beneficial way of recycling the industrial by-product of hydrogen production.

2.2.1.11 Used foundry sand (UFS)

Used foundry sand (UFS) is an industrial waste generated by the ferrous and non-ferrous metal casting industries. Actually, moulding sands are reused multiple times in this manufacturing process. After many cycles, the UFS degrades to the state that it can no longer be reused in the casting process, so that it is discarded as a waste. Although UFS has been successfully used as a land filling material since many years, this approach is becoming a problem due to increases in disposal costs [198]. UFS is generally composed of silica, carbon-based additions, and several metals, so that it is an interesting candidate for production of SSCs [103,104,198]. Results of Mobili et al. [104] indicated that small contents of UFS (up to 1% by

weight of binder) can increase the compressive and tensile strength of cementitious materials. This increase was attributed to the presence of alkaline salts in UFS, which acted as quick setting agents. In contrast, Mobili et al. [103] observed that high dosage of UFS (5% by weight of binder) decreased both compressive and tensile strength of cementitious composites.

The electrical resistivity of lime mortars with 0%, 0.25%, 0.50%, and 1.00% of UFS (by weight of binder) was determined by Mobili et al. [104]. After a curing period of 28 days, the authors observed that increases in the UFS content provided decreases in electrical resistivity up to 65%, which were attributed to the carbon-based particles and metals of the UFS and their effective dispersion in the mortar specimens. In contrast, recent studies carried out by Mobili et al. [103] indicated that the addition of 5% of UFS (by weight of binder) to cement mortars increased their electrical resistivity by 43% and 28% in direct current and alternating current measurements, respectively. Then, future studies are needed to improve the understanding of the mechanisms behind the electrical resistivity and self-sensing properties of composites incorporating UFS.

2.2.2 SSCs produced with a combination of waste materials

The combination of different types of wastes for the production of SSCs is a relevant strategy that allows the complementation of properties of different materials and provides a higher rate of waste incorporation. This section presents the studies that combined various recycled admixtures for the production of cementitious and alkali-activated composites. Table 4 presents the types and concentrations of the different combined wastes and/or conductive admixtures used in various research projects. Detailed discussions on these works are presented in the following subsections. All of these works reported self-sensing properties of SSCs subjected to uniaxial compression tests, except the studies of Dong et al. [191], Dehghanpour et al. [102], and Wang et al. [199], who only focused on electrical resistivity measurements (piezoresistive response was not reported). In the following subsections, grouping was made according to the waste combinations already investigated in previous literature.

Table 4. Works dealing with composites made with a combination of various waste materials.

Composite type	Recycled admixture content			Conductive filler content			Reference
	Type	Admixture/ binder (or precursor) ratio (% in mass)	Admixture/ composite ratio (% in volume)	Type	Conductive filler/binder (or precursor)* ratio (% in mass)	Conductive filler/composite ratio (% in volume)	
Concrete	FA; BFS	30 (BFS); 20 (FA)	-	CMF; CNT	0.2 (CNT); 0.18, 0.35, 0.70, 1.41, 3.0 (CMF)	-	[200]
Alkali-activated mortar	FA; GGBFS	*** (FA; GGBFS)	-	FA; GGBFS; CF	** (FA; GGBFS)	0.1, 0.2, 0.3, 0.4, 0.5 (CF)	[46]
Alkali-activated mortar	FA; GGBFS	70/30, 50/50, 30/70, 0/100 (FA/GGBFS)	-	CF, CC	-	0.1, 0.2, 0.3, 0.4 (CF); 25, 30, 35, 40 (CC)	[26]
Reactive powder concrete	SF; FA	17.24 (SF); 13.79 (FA)	-	SSSW	-	0.10, 0.50, 1.00, 1.50	[201]
Cement mortar	SF; GGBFS	4.8 (SF); 54.54 (GGBFS)	-	CF	0.10, 0.30, 0.50, 0.70	-	[172]
Cement paste	SF; GGBFS	10 (SF); 20 (GGBFS)	-	CNF	-	2.25% by volume of binder	[199]
Cement mortar	SF; RW	10 (SF); 20, 40, 60, 80 (RW)	-	RW	20, 40, 60, 80	-	[202]
Cement paste	SF; SF+RW	10 (SF)	0, 0.32, 0.64, 0.96, 1.28, 1.60, 2.24 (RW)	RW	-	0.32, 0.64, 0.96, 1.28, 1.60, 2.24	[192]
Cement paste	SF; SF+RW	20 (SF)	0.32, 0.64, 0.96, 1.25, 1.60, 2.24 (RW)	RW	-	0.32, 0.64, 0.96, 1.25, 1.60, 2.24	[191]
Cement paste	SF; SF+RW	20 (SF)	0, 0.32, 0.64, 1.27 (RW)	RW; CBN	0.1, 0.5, 1.0, 2.0, 4.0 (CBN)	0.32, 0.64, 1.27 (RW)	[43]
Cement mortar	SF; SF+GGBFS	52, 57, 61 (GGBFS); 4.8 (SF)	-	GGBFS	52, 57, 61	-	[203]
Cement mortar	SF; SS+SF	13 (SF); 87 (SS)	-	MWCNT, SS, STF	0.25 (MWCNT); 100 (SS)	2.0 (STF)	[55]

Concrete	SF; SS+SF	13 (SF); 43, 87, 130, 174 (SS)	-	SS; STF	50, 100, 150, 200 (SS)	1.0, 2.0 (STF)	[54]
Cement mortar	SF + FA + GGBF	33.7 (FA); 21.2 (GGBFS); 7.2 (SF)	-	SMAF; CF; STF	-	0.25, 0.50, 0.75, 1.00, 1.25, 1.50 (SMAF and STF) 0.1, 0.2, 0.3, 0.4, 0.5, 0.6 (CF)	[170]
Concrete	WWE+RCBN	8.5, 3.2, 2.1 (WWE); 6.3 (RCBN)	-	CF	0, 0.85, 0.91 (CF)	-	[204]
Cement mortar	SF+IOT	10 (SF); 0, 33, 66 (IOT)	-	CF	-	0, 0.3, 0.6	[205]
Cement mortar	SF+RGW coated by MWCNTs	11.1 (SF)	-	RGW coated by MWCNTs	0, 55.5, 111.1, 166.7, 222.2	-	[206]

Notes: FA - fly ash, BFS - blast-furnace slag, CMF - carbon micro fiber, CNT - carbon nanotube, GGBFS - ground-granulated blast-furnace slag, CF - carbon fiber, CC - conductive ceramsite, SF - silica fume, SSSW - short-cut super-fine stainless wire, CNF - carbon nanofiber, RW - rubber waste, CBN - carbon black nanoparticle, SS - steel slag, MWCNT - multi-walled carbon nanotube, STF - steel fiber, SMAF - shape memory alloy fiber, WWE - waste wire erosion, RCBN - recycled carbon black nanoparticle, IOT - iron ore tailing, RGW - recycled glass waste.
*In ordinary Portland cement concretes, the concentration of conductive admixtures was provided in terms of mass of binders. In alkali-activated concretes, the concentration of conductive admixtures was provided in terms of mass of precursor.
**The precursor used to produce the alkali-activated concrete is the conductive admixture itself.
***The precursor used to produce the alkali-activated concrete is the recycled admixture itself.

Some self-sensing properties (e.g., GF, SST, linearity, FCR amplitude) exhibited by SSCs produced with a combination of various types of wastes are presented in Tables 5 and 6. Table 5 lists composites that presented a linear relationship between FCR and compressive stresses (or strains), while Table 6 shows the cases in which this relationship was non-linear. Again, σ/fc ratios were calculated when possible. Based on these tables, one can notice that the combination of different recycled admixtures provided SSCs with high values of GF, SST, strain amplitude, and stress amplitude.

Table 5. Sensing properties of composites made with a combination of various waste materials (linear behavior in FCR vs. strain curves).

Recycled admixture	Conductive filler	Gauge factor	Stress sensibility (MPa^{-1})	Strain amplitude (microns)	Stress amplitude (MPa)	Linearity	Average compressive strength (MPa)	σ/*fc* ratio (%)	Reference
FA; GGBFS	CF; CC	624.45 - 2609.86	0.0007 - 0.0083	14 - 44	12.5	0.94 - 0.99	30.7	40.69	[26]
SF; FA	SSSW	42 - 94.9	-	1600 - 2100	60 - 80	-	105 - 155	50.00 - 63.64	[201]
SF; FA; GGBFS	SMAF; CF; STF	241	0.0074 - 0.0410	417 - 452	10	0.12 - 0.95	32.1 - 37.6	26.60 - 31.15	[170]
SF; RW	RW	54.9 - 87.9	0.0050 - 0.0066	236 - 485	4	-	15.1 - 41.9	9.54 - 26.47	[202]
SF; RW	RW; CBN	51 - 482	-	1733 - 24593	-	-	17 - 51	-	[43]
SF; SS	MWCNT; SS; STF	-	0.0013 - 0.0021	-	60	-	155 - 202	29.7 - 38.71	[55]
SF; IOT	CF	-	0.0033 - 0.0140	-	5.4	-	39 - 45	-	[205]
SF; RGW coated by MWCNT	RGW coated by MWCNT	52.1 - 149.2	0.0027 - 0.0082	200 - 225	4	0.82 - 0.96	40.5 - 46.2	8.66 - 9.66	[206]

Note: FA - fly ash, GGBFS - ground-granulated blast-furnace slag, CF - carbon fiber, CC - conductive ceramsite, SF - silica fume, SSSW - short-cut super-fine stainless wire, SMAF - shape memory alloy fiber, STF - steel fiber, RW - rubber waste, CBN - carbon black nanoparticle, SS - steel slag, MWCNT - multi-walled carbon nanotube, IOT - iron ore tailing, RGW - recycled glass waste.

Table 6. Sensing properties of composites made with a combination of various waste materials (non-linear behavior in FCR vs. strain curves).

Recycled admixture	Conductive filler	Maximum absolute values of FCR amplitude (%)	Strain amplitude (microns)	Stress amplitude (MPa)	Average compressive strength (MPa)	σ/*fc* ratio (%)	Reference
SF; GGBFS	CF	26 - 220	-	10	39.2 - 41.6	24.04 - 25.51	[172]
SF; GGBFS	GGBFS	1.75 - 21.41	-	10	22.8 - 50.8	19.69 - 43.9	[203]
SF; RW	RW	4.4 - 23.85	-	10	21 - 55	18.18 - 47.62	[192]
SF; SS	SS; STF	15.5 - 42.9	-	131.9 - 180.5	178 - 199	70.16 - 93.04	[54]
FA; GGBFS	FA; GGBFS; CF	6 - 22	-	48 - 56	66 - 67	71.64 - 84.85	[46]

BFS; FA	CMF; CNT	0.77 - 7	-	8.2 - 9.1	51	16.04 - 17.75	[200]
SF; RGW coated by MWCNT	RGW coated by MWCNT	42 - 76	2000 - 2400	40.5 - 46.2	40.5 - 46.2	100	[206]

Note: SF - silica fume, GGBFS - ground-granulated blast-furnace slag, CF - carbon fiber, RW - rubber waste, SS - steel slag, STF - steel fiber, FA - fly ash, BFS - blast furnace slag, CMF - carbon micro fiber, CNT - carbon nanotube, RGW - recycled glass waste, MWCNT - multi-walled carbon nanotube.

Table 5 shows that only a few studies investigated the linearity of SSCs. Ma et al. [26] verified very high values of R^2 (94-99%) in composites containing SS and FA as recycled admixtures, in addition to CF and conductive ceramsite (CC) as conductive admixtures. In contrast, Dehghani and Aslani [170] investigated SSCs produced with SF, FA, and GGBFS, but only observed electrical outputs with suitable linearity when combined with CF. Table 5 also shows that GF and SST of SSCs produced with various types of wastes have been obtained from piezoresistive tests covering compressive stresses up to 63.64% of their compressive strength. The highest σ/fc ratios were reported in SSCs containing FA and SF (50-63.64%), which indicates that these concrete sensors can monitor stresses on structural elements subjected to a wide range of compression loads.

On the other hand, the piezoresistive response of SSCs produced with RW and SF was investigated at lower compressive loads (9.54-26.47% of their compressive strength). Table 6 indicates that a non-linear relationship between FCR and compressive stress was observed in piezoresistive tests covering compressive stresses up to 93.04% of the SSCs' compressive strength. In this case, the highest σ/fc ratios were verified in SSCs containing SF and SS (70.16-93.04%), suggesting that these concrete sensors can monitor damage of concretes subjected to a wide range of compression loads. In contrast, the non-linear relationship of FCR vs. stress curves of SSCs produced with BFS and FA was investigated at the lowest compressive load levels (16.04-17.75% of their compressive strength).

Figure 10 shows the GF, strain amplitude, SST, and stress amplitude of SSCs produced with a combination of various types of wastes, considering cases with a linear relationship between FCR and strain (or stress). Figure 10a shows that the combination between FA and SS provided composites with the highest GF values (up to 2610), but covered a low strain range (14-44 με). The combination of FA, GGBFS, and SF provided composites with the same pattern: high GF values (up to 935) covering reasonable strain amplitude (419-452 με). It demonstrates that future research is recommended to seek composites that present higher GF at wider strain ranges, which would make these SSCs extremely functional and versatile for SHM

applications. Sensors produced with FA and SF presented lower GF than the previous ones, but could monitor a large strain amplitude (up to 2100 με). Finally, the sensors produced with SF and RW associate high GF (up to 482) and a wide strain range (236-2459 με), being thus promising candidates for self-monitoring of sustainable structures.

Figure 10b shows that studies dealing with the association of FA and SF, or FA, GGBFS, and SF, have so far reported sensors capable of monitoring small stresses within the elastic regime. For example, the highest SST value (0.041 MPa^{-1}) was observed in SSCs containing FA, GGBFS, and SF. However, this stress sensibility was only evaluated for compressive stresses up to 10 MPa. It reinforces the need to investigate the behavior of these SSCs at greater stress amplitudes, in order to demonstrate whether they would still exhibit good piezoresistive properties. In contrast, sensors produced with SF and SS showed adequate stress sensibility up to 60 MPa, thus demonstrating their great application potential.

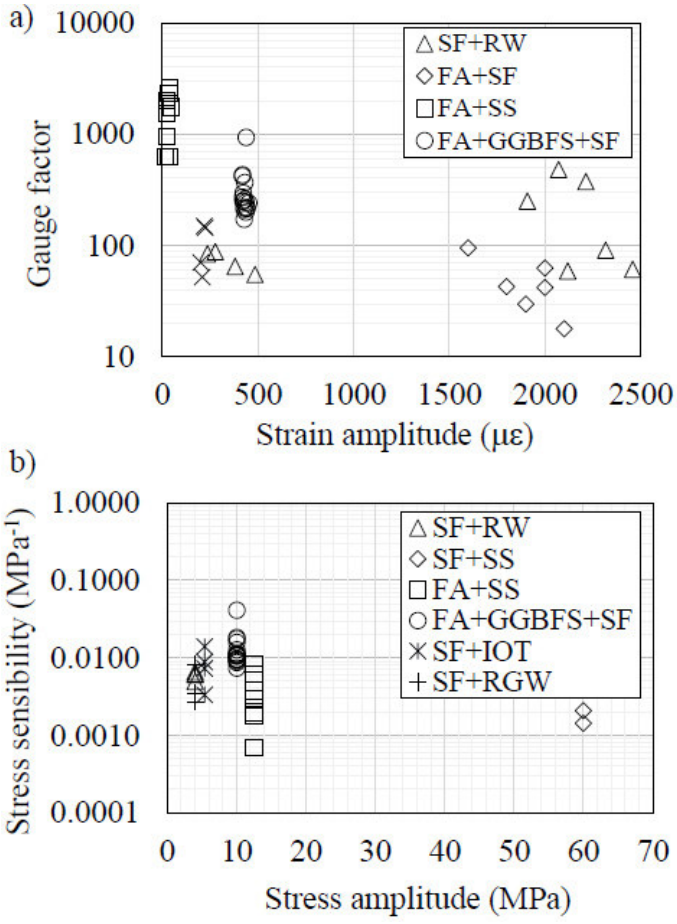

Figure 10. Sensing properties of composites containing combinations of various types of wastes with linear behavior in FCR vs. strain (or stress) curves: a) Gauge factor vs. strain amplitude; b) Stress sensibility vs. stress amplitude. Note: FCR - fractional change in electrical resistivity, SF - silica fume, RW - rubber waste, FA - fly ash, SS - steel slag, GGBFS - ground-granulated blast-furnace slag.

Figure 11 shows the values of absolute FCR amplitude and stress amplitude of SSCs produced with various types of wastes, considering cases with a non-linear relationship between FCR and stress. In this case, most of the works reported the non-linear piezoresistive behavior for compressive stresses up to 10 MPa. For example, composites containing BFS and FA presented absolute FCR amplitudes up to 10%. Composites produced with SF and RW exhibited slightly higher values of maximum absolute FCR amplitudes, ranging between 4.49% and 21.41%. The highest values of absolute FCR amplitude (220%) were observed in piezoresistive tests of composites containing SF and GGBFS. Since these piezoresistive tests covered such small stress amplitude (10 MPa), further research is needed to investigate the self-sensing properties of these SSCs at higher compressive stress levels. An interesting sensing behavior was observed in composites containing GGBFS and FA, since they presented reasonable values of absolute FCR amplitude (6-22%) for higher stress amplitudes (48-56 MPa). High values of maximum absolute FCR amplitude were also observed in compression tests of composites containing SF and SS, as they exhibited high absolute FCR amplitudes (15.5-42.9%) for very high stress amplitude values (131.9-180.5 MPa).

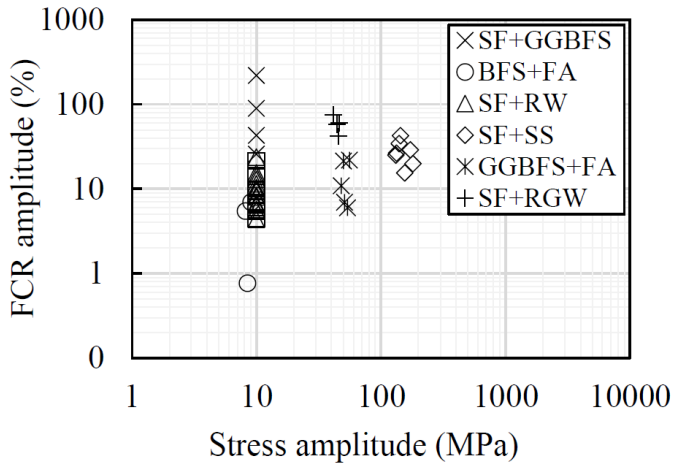

Figure 11. Sensing properties (absolute FCR amplitude vs. stress amplitude) of composites containing combinations of various types of wastes with a non-linear behavior in FCR vs. stress curves. Note: FCR - fractional change in electrical resistivity, SF - silica fume, GGBFS - ground-granulated blast-furnace slag, BFS - blast-furnace slag, FA - fly ash, RW - rubber waste, SS - steel slag.

2.2.2.1 Combination of silica fume (SF), fly ash (FA) and ground-granulated blast-furnace slag (GGBFS)

Table 4 indicates that some previously investigated combinations of recycled materials for the production of SSCs were SF and/or FA with GGBFS. Both SF and FA have been extensively incorporated into cementitious matrices in order to improve cement hydration,

matrix refinement, and mechanical properties [136,140,141,154]. Previous studies also indicated that these recycled admixtures improve the dispersion of conventional conductive fillers [124,199]. In contrast, BFS was found to directly affect the self-sensing properties of SSCs by decreasing their electrical resistivity and improving their piezoresistive response, given the presence of conductive compounds in their chemical composition [122]. In this sense, the combination of SF and/or FA with GGBFS tends to enable the production of very efficient SSCs, in the presence or not of other conventional conductive fillers.

For example, excellent SSCs were recently produced by Dehghani and Aslani [170] using FA, SF, and GGBFS, combined with different types of conductive fibers: CF, STF, or shape memory alloy fibers (SMAF). Among the various results obtained by the authors, it is worth highlighting the high GF (935) and linearity (0.95) observed in SSCs produced with FA, SF, GGBFS, and 0.6% of CF (by volume of composite). Ma et al. [26] also reported excellent results with the combination between FA and GGBFS as precursors of alkali-activated mortars, in addition to CF and CC (ceramsite impregnated with agar, GP, and alkaline chemicals like KOH, $Ca(OH)_2$, and $Al(OH)_3$). The authors reported extremely high GF values, varying between 624.45 and 2609.86. The optimal composition in view of mechanical properties and piezoresistivity was found to be a mixture between 30% of FA and 70% of GGBFS as precursors, combined with 0.3% of CF and 25-30% of CC. It is worth mentioning the contribution of a greater incorporation of GGBFS to avoid significant decreases in mechanical properties caused by the incorporation of CC, thus demonstrating the value of the recycled admixtures as both conductive and structural materials.

Wang and Aslani [172,203] also combined SF and GGBFS to produce SSCs. However, a non-linear increase in the absolute FCR values with the increase in the compressive stress was observed. The authors also observed that when the compressive stress was beyond the elastic regime, the propagation of microcracking caused reductions in the piezoresistive behavior of the material. Even without adding any other conductive material, Wang and Aslani [203] obtained composites with high FCR amplitudes (21.41%). Adding CF to the cementitious composites, Wang and Aslani [172] increased the FCR amplitude values to up to 220% (Figure 11). Moreover, Wang and Aslani [203] observed that the self-sensing properties of non-dried specimens decreased with the increase in the GGBFS content due to increases in the consumption of calcium hydroxide existing in the matrix, leading to a less conductive porous solution.

Non-linear relationships between FCR and compressive stress were also observed in SSCs made with FA and GGBFS. For instance, Deng et al. [46] used FA and GGBFS to produce

alkali-activated mortars with various CF contents. The piezoresistive response of these composites was mainly attributed to the decrease in the distance between adjacent CFs when the compressive stress increased, reducing the electrical resistivity of the material. However, when the compressive stress reached a critical value of around 50 MPa, some cracks occurred inside the specimens, so that the reconstruction and destruction of the conductive network reached balance. Beyond the critical value, cracks developed and caused a breakdown of the conductive network, leading to significant increases in electrical resistivity. Based on these observations, the authors also concluded that their alkali-activated mortars exhibited self-sensing properties to detect cracks with less CF contents than cement-based mortars.

2.2.2.2 Combination of silica fume (SF) and steel slag (SS)

SS, a waste generated from the steelmaking industry, was also found to be a good option for combination with SF, as reported by Lee, Le, and Kim [55]. These authors observed that mortars with SF and Portland cement as binders and SS as aggregates presented FCRs under compression load similar to those observed in conventional mixtures produced with STF and MWCNT, conductive materials widely used in the production of concrete sensors. This observation reinforces the potential of using SS in the production of sensor materials. The authors also demonstrated that the incorporation of STF to mortars containing SF and SS optimized the self-sensing properties of the composites, which was evidenced by the high linearity observed in the relationship between FCR and compressive stress (R^2 of 0.9977).

Le, Lee, and Kim [54] also observed a piezoresistive behavior in ultra-high-performance concretes produced with a combination of SF and SS aggregates, and reinforced with STF. The addition of SS aggregates in the matrix composition improved the compressive strength and workability, and decreased the initial electrical resistivity of the material. Finer SS aggregates provided higher FCR changes under compression. It happened because coarser SS aggregates generated a non-uniform distribution of STF in the concrete matrix, decreasing the piezoresistive response. The smart composites presented a quasi-linear relationship between FCR and compressive stress, and high absolute FCR amplitudes (15.5-42.9%) at compressive levels around 70-90% of the peak stress, as indicated in Figure 11.

2.2.2.3 Combination of waste wire erosion (WWE) and rubber waste (RW)

Wire-electro discharge machining is an important non-traditional machining process that has been widely used in the aerospace, nuclear, and automotive industries [207]. By passing electrical current through the wire erosion, the workpiece is abraded and cutting takes place [102]. Wire used in eroding machine is deformed during the cutting process, so that it must be discarded or reused after long recycling processes of high costs [204]. Dehghanpour et al. [102] combined recycled waste wire erosion (WWE) and recycled carbon black nanoparticles (RCBN) obtained by pyrolysis of RW to produce sustainable concrete mixtures. In this study, different concentrations (2.1, 3.2, and 8.5% by mass of cement) of yellow colored CuZn37 alloy WWE with diameter of 0.25 mm and length of 25 mm were investigated. The authors observed that WWE provided increases in compressive strength, flexural strength, and impact absorption of RCBN-based concretes. In contrast, the addition of CF (0.85-0.91% by mass of cement) to these concretes decreased the benefits provided by the WWE, in terms of mechanical strength and energy absorption.

When a low electrical resistivity cannot be supplied by a single recycled waste, a combination between different wastes are required to get the desired conductivity. In this context, Dehghanpour et al. [102] also observed that WWE effectively reduced the electrical resistivity when combined with RCBN (6.3% by mass of cement) or both RCBN (6.3% by mass of cement) and CF (0.85-0.91% by mass of cement). The bulk electrical resistivity of all mixtures containing WWE was lower than 1700 Ω.cm, whereas the electrical resistivity of control specimens was above 22000 Ω.cm, which clearly shows how effective WWE is in reducing electrical resistance. This results suggest that one of the most promising topics for future research on this field would be an experimental investigation of the piezoresistive response and the determination of self-sensing properties of SSCs fabricated with WWE.

Interestingly, when only RBCN was used, the electrical resistivity of PCCs did not decrease (Section 2.2.1.7). In contrast, the combination of recycled conductive particles at the nanoscale (RCBN) and recycled conductive fillers at the macroscale (WWE) seems to provide an interconnected conductive hierarchical network inside the cementitious composites, decreasing their electrical resistivity. Therefore, synergistic effects of recycled admixtures of different average particle sizes seem to be an interesting strategy to improve the conductive network of SSCs produced with combinations of waste materials.

2.2.2.4 Combination of silica fume (SF) and rubber waste (RW)

Another waste that has been combined with SF to produce SSCs is the rubber waste (RW), as observed in Tables 4, 5, and 6. Some studies have incorporated SF into cement-based composites to improve mechanical properties, in addition to conductive RW to decrease electrical resistivity and improve self-sensing properties. For example, Dong et al. [191] reported that after a 28-days curing period, an eight-fold decrease in electrical resistivity was observed in composites containing 2.24% of RW fibers (by volume of composite) and 20% of SF (by weight of binders). Although the conductive passages were mainly made up by the overlapped or intersected RW fibers, they were slightly affected by the curing age, water content, and hydration degree. Dong et al. [43] studied the combination of different contents of CBN and RW added to cement-based composites produced with 20% of SF (by weight of binders). Although the increase of RW fiber contents caused decreases in the compressive strength of the material, they improved the electrical conductivity of the composites. Figure 12 shows that the reductions in electrical resistivity provided by rubber fibers were more evident in composites containing lower CBN contents. For example, the electrical resistivity of composites without CBN and RW was about 1.63 x 10^4 Ω.cm. After adding 1.27% of RW fibers to these composites, the electrical resistivity decreased to 2.50 x 10^3 Ω.cm.

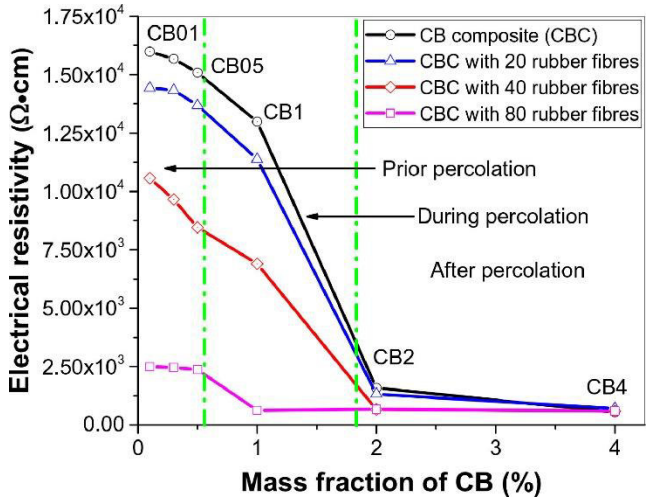

Figure 12. Variation of electrical resistivity in cementitious composites as a function of carbon black (CB) dosage and amount of rubber fibers. Adapted from Dong et al. [43], Copyright 2019, with permission from Elsevier.

Figure 10a shows that composites containing SF and RW presented significant GF values and were able to monitor significant deformation ranges. Dong et al. [202] recently produced cement-based sensors using different contents of conductive rubber crumbs (0-40% by mass of

fine aggregates) and 10% of SF (by mass of binders). Excellent repeatability was observed in the piezoresistive response of RW-based composites. The authors verified that the aggregate replacement levels must be higher than 10% in order to ensure suitable connectivity between rubber crumbs and form conductive networks inside the composites. Moreover, RW improved the ductility of the mortars. As presented in Table 5, the GF of the mortars varied from 54.9 to 87.9. The best results were observed in mixtures with a 20% replacement of aggregates by RW and a water/binder ratio of 0.42.

Regarding self-sensing properties, Dong et al. [43] also reported improvements in the piezoresistive behavior of composites containing SF and RW with the addition of conventional conductive nanofillers. As presented in Figure 13a, the combination of CBN and RW as conductive admixtures provided a higher amount of conductive pathways inside the cementitious matrix. In addition, the authors also reported that the SF decreased the porosity of the material, which improved their mechanical properties and provided higher GF values. Therefore, RW, SF, and CBN provided SSCs with high strain sensitivity, which clearly shows the great potential of this technical combination strategy. Some details on the piezoresistive mechanism of SSCs containing RW and SF were also discussed by Dong et al. [192]. They observed that the electrical conductivity and the piezoresistive behavior of the SSCs were significantly affected by the movement of ions (Ca^{+}, SO_4^{2-}, OH^{-}) in the pore solution of the matrix. When non-dried specimens are subjected to compressive loads, the RW fibers tend to be connected to the pore solution (Figure 13b), forming new conductive pathways that affect the piezoresistive response of the composite.

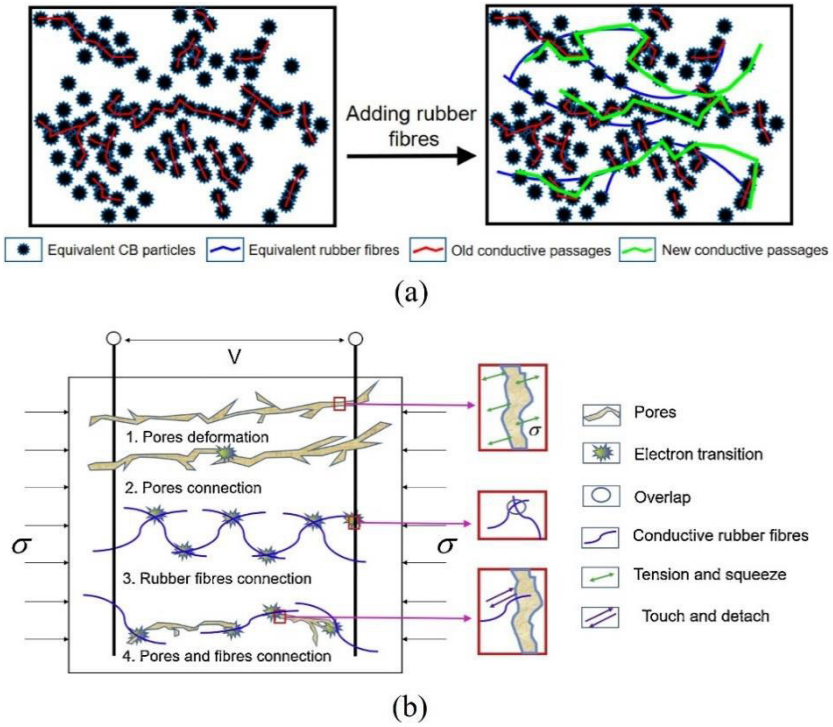

Figure 13. Effects of the incorporation of rubber waste fibers on the formation of conductive pathways inside (a) composites containing silica fume and carbon black (CB) nanoparticles, and (b) composites containing silica fume (without CB nanoparticles) subjected to a compressive stress σ. Adapted from Dong et al. [43], Copyright 2019, and Dong et al. [192], Copyright 2020, with permissions from Elsevier.

Dong et al. [192] developed a novel cement-based sensor produced with 10% SF (by mass of binders) and layer-distributed conductive RW. A novel rubber installation process was proposed for the production of these smart cementitious composites. At first, a small amount of fresh mixture of cement, water, and SF was poured into molds and vibrated to compaction. After that, rubber fibers were directionally allocated in the center of the composite. Then, the mold was filled with a new layer of fresh mixture, and the same distribution method was applied for the rest of the rubber fibers. Finally, the last layer of the fresh mixture was added, and copper mesh electrodes were symmetrically embedded into the composite. A non-linear relationship between FCR and compressive stress was observed in piezoresistive tests with compressive stress amplitude ranging between 18% and 48% of the compressive strength of the composites, with maximum FCR amplitudes from 4.4% to 23.9% (Figure 11). According to the authors, it mainly happened because the cement-based sensors were significantly non-homogeneous and anisotropic due to this distinct rubber installation process.

2.2.2.5 Combination of iron ore tailing (IOT) and silica fume (SF)

IOT is a solid waste generated during the beneficiation process of iron ore. Increases in the demand for iron lead to the mining of iron ores with lower iron contents, which increases the generation of tailings. Consequently, disposal of IOTs has become a major challenge for industry owners and local government, due to environmental impacts, health issues, and land scarcity [208–210]. According to a review paper of Zhao et al. [211], the replacement of natural sand with low contents of IOT usually provided increases in the mechanical strength and carbonation resistance due to the filling effect of the waste. However, strength decreases were observed when the dosage of IOT exceeded the optimal replacement ratio. When substituting cement by IOT, the compressive strength and the carbonation resistance usually decreased with the increase in the IOT dosage.

According to Table 4, the contribution of IOTs for the development of SSCs was only investigated in a recent work of Quan et al. [205]. The authors investigated the piezoresistive response of mortars with 10% of SF (by weight of cement), different replacement levels of silica sand with IOT (0%, 30%, and 60% by weight), and different contents of CF (0%, 5.25%, and 10.5% by volume of composite). Resistivity decreases provided by the addition of CF were higher than those provided by the IOTs. Despite this, increases in the content of IOTs provided reasonable decreases in the electrical resistivity of the composites. The enhancement in the conductive network provided by IOTs is attributed to a certain amount of conductive iron particles existing in IOTs.

The synergistic effects of CF and IOTs on the self-sensing properties of cement-based materials containing SF are illustrated in Figure 14. Electrical conduction through iron particles is the dominant conductive mechanism in mortars with small contents of IOT and without CF (Figure 14a), which was defined as “contact point mode” by Quan et al. [205]. Some iron particles are connected when the composite is subjected to compressive stress, and the electrical resistivity slightly decreases. However, it is not easy to form contact points between spherical IOT particles, so that these mortars presented a low SST value (around 0.0033 MPa^{-1}). The increase in the CF contents (Figure 14b and Figure 14c) enabled the formation of new conductive paths between fibers of high aspect ratio, which was defined as “bridging mode” by Quan et al. [205]. When the compressive stress increased, the increased contact conductive points between CFs and IOTs particles exceeded the decreased conductive points, so that higher SST values were observed (around 0.0073 MPa^{-1} and 0.0089 MPa^{-1} for composites of Figure 14b and Figure 14c, respectively). When a high dosage of CF is combined to a high

concentration of IOTs (Figure 14d), a SST around 0.0140 MPa^{-1} was verified, which suggested increases in the probability of changes in electrical resistivity due to eventual contacts between IOTs and CFs with the compressive load. Since composites containing SF and IOTs presented interesting high pressure-sensitivity properties, further studies are also recommended to investigate the ability of self-diagnosis of damage of SSCs incorporating these recycled materials.

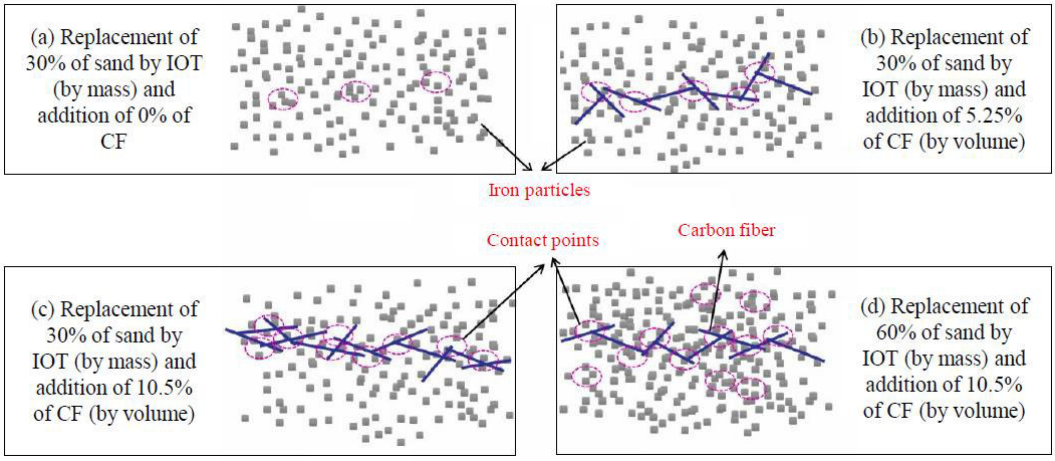

Figure 14. Conductive mechanisms in PCCs with (a) replacement of 30% of sand with iron ore tailing (IOT) (by mass) and addition of 0% of carbon fiber (CF); (b) replacement of 30% of sand with IOT (by mass) and addition of 5.25% of CF (by volume); (c) replacement of 30% of sand with IOT (by mass) and addition of 10.5% of CF (by volume); and (d) replacement of 60% of sand with IOT (by mass) and addition of 10.5% of CF (by volume). Adapted from Quan et al. [205], Copyright 2022, Copyright 2022, with permissions from Elsevier.

2.2.2.6 Combination of recycled glass waste (RGW) and silica fume (SF)

Glass is one of the most used materials around the globe due to its excellent and versatile characteristics. Quality requirements for glass remanufacturing have been a limitation for complete recycling of glass wastes, as they must be strictly sorted and cleaned before being melted. Consequently, the non-recyclable fraction is commonly disposed in landfills, leading to wasting of resources, massive occupation of land, and environmental pollution [63,212,213]. According to Mehta and Ashish [142], replacement levels of cement by RGW powder up to 20% can improve the mechanical properties of concretes, including compressive, tensile, and flexural strength. RGW can also provide durable cement and geopolymer concretes against shrinkage, chemical attack, and freeze-thaw action, in addition to electrical and thermal insulation properties. However, cementitious materials containing RGW can be vulnerable to alkali-silica reaction and expansive gel formation [71].

Although many studies [71,212–214] have widely reported the mechanical and durability properties of cementitious composites containing RGW, the pioneering investigation of the potential use of waste glass as conductive fillers was recently reported by Dong et al. [206]. The high bond strength and refined microstructure of concretes containing RGW effectively increase their resistance to the passage of electrical charges [71]. Since RGWs are insulating materials, Dong et al. [206] covered the surface of RGWs with conductive MWCNTs. A simple procedure of immersion of the alkali washed waste glass in a suspension of MWCNTs was carried out, followed by a drying process that evaporated the water molecules and left the conductive nanomaterials onto the surface of RGWs.

The combined use of SF as SCM and RGW as aggregate provides the amplification of the compressive strength of concretes, which is mainly attributed to the high amount of amorphous silica in these residues [215]. Thus, Dong et al. [206] investigated cement mortars containing 11.1% of SF (by weight of cement) and 0%, 25%, 50%, 75%, and 100% of MWCNT-coated RGWs as replacement (by weight) of natural sand. Experimental results indicated that the replacement of low amount of natural sand with MWCNT-coated RGW (25% by weight) failed to improve the electrical conductivity of the mortars. In this situation, glass particles were enclosed by non-conductive materials (e.g., SF, natural sand, and cement hydrates) that blocked the conductive passages. Nevertheless, replacement levels of natural sand with MWCNT-coated RGW higher than 25% caused later decreases in electrical resistivity, as increases in the RGW content improved the connections among conductive MWCNT-coated glass particles.

Dong et al. [206] investigated the piezoresistive response of their composites under an elastic regime of uniaxial compression up to 4 MPa. In mortars without MWCNT-coated RGWs, FCRs almost had no relationship to the compressive stress/strain. However, the piezoresistive response was enhanced by the addition of MWCNT-coated RGW. Piezoresistive tests of these mortars revealed coherent decreases and increases in electrical resistivity in loading and unloading processes, respectively. Moreover, the GF increased with the growth of RGW content from 52.1 (mortars with 25% of RGW by weight of natural sand) to 149.2 (mortars with 100% of RGW), as indicated in Figure 10a.

Finally, the ability of self-diagnosis of damage of composites containing SF and different dosages of MWCNT-coated RGW was also investigated by Dong et al. [206]. FCR measurements of specimens subjected to uniaxial compression indicated that mortars without MWCNT-coated RGW exhibited a poor correlation between FCR and compressive stresses and unsatisfactory ability to monitor the failure. The replacement of low amount of natural sand

with MWCNT-coated RGW (25% by weight) was not able to provide composites with the ability of damage self-detection, since they presented sudden and irreversible reduction of electrical resistivity during the increase of compressive load due to abruptly formed conductive passages. Similar issue was not observed when the replacement level of natural sand with CNT-coated RGW was over 75%. Results indicated that satisfactory percolation meshwork can be provided by higher contents of CNT-coated RGWs, as they can omit non-uniformity effects of the cement composite. Therefore, SSCs produced with high concentration of CNT-coated RGW were found to be promising eco-efficient alternatives to monitor stress and strain magnitude and failure condition of concrete structures.

2.3 GENERAL OVERVIEW AND PROMISING WASTES FOR PRODUCTION OF SSC

The previous section aimed to organize and describe details on the main findings of previous literature on the incorporation of different recycled materials into SSCs. In order to summarize these findings, a general overview of the revised literature is presented Table 7. The advantages, limitations, and specific uses of recycled materials in production of SSCs are clearly summarized in this table. It is important to highlight that all specific uses are directly dependent on the concentration of recycled admixtures, as discussed in the previous subsections.

Table 7. Advantages, limitations, and specific uses of recycled admixtures incorporated into SSCs

Type of recycled admixture	Advantages	Limitations for application in SSCs	Specific uses in SSCs already reported in previous literature*			
			Production of composites with higher electrical conductivity	Production of SSCs with self-stress sensibility	Production of SSCs with self-strain sensibility	Production of SSCs with self-diagnosis of damage
Silica fume (SF)	Recycling of a co-product generated in electric arc furnaces; replacement of OPC; acting as filler, nucleation site, and pozzolanic material; improvements in mechanical performance and durability; improvement of dispersion of other conductive admixtures; stabilizing agents that prevent re-agglomeration of other conductive admixtures.	Workability of SSCs decreases as the dosage of SF increases, due to its high surface area. Variations in the porosity filled with SF can cause strong non-linear behavior in FCR vs. compressive stress curves since the beginning of the loading process, which can impair the calibration of a constant GF or SST value for the SSC.	✓	✓	✓	✓
Fly ash (FA)	Recycling of a coal combustion product; reductions in OPC consumption; FA can act as a pozzolanic material; reductions in hydration heat; improvements in mechanical performance and durability; improvements in electrical conductivity when FA presents iron oxides; conductive admixtures can be synthesized on the surface of FA particles, providing locations for triggering contacts between	Mechanical properties of composites with FA can be negatively affected at early ages. The great quality variability of FA is the main limitation for expanding its use in production of SSCs. FA with high SiO_2 content have a good source to form C-S-H with OPC particles, resulting in significant increases in electrical resistivity that can eventually impair the	✓	✓	✓	✓

	the conductive fillers when the composite is subjected to loading, which improves its self-sensing ability.	self-sensing properties of SSCs. The use of high-calcium fly ash in concrete has been hindered because it significantly changes the cement hydration.				
Red mud (RM)	Recycling of a waste generated during the processing of bauxite into alumina; reductions in OPC consumption; suitable RM contents can increase the bulk density and reduce the porosity of composites; presence of metal oxides in RM can decrease the electrical resistivity.	High concentrations of RM usually lead to decreases in mechanical properties. The fine granulometry of RM can provide decreases in workability. Presence of highly conductive ions in RM (e.g., Na^+, OH^-, Ca^{2+} and K^+) can increase the dependence of electrical conductivity on the moisture content of the composite.	✓	✓	×	×
Blast furnace slag (BFS)	Recycling of a product generated by iron industries; replacement of OPC or natural aggregates; reactivity and/or pozzolanicity; reductions in porosity; mechanical and durability improvements; mobile hydrated Na^+ ions and metallic iron particles of BFS can increase electrical conductivity	Mechanical properties at early age decrease with increases in the GGBS content. Inclusions of GGBFS beyond the optimal dosage may negatively affect the strength and durability of concrete.	✓	✓	✓	✓
Steel slag (SS)	Recycling of a waste generated from steelmaking and refining processes; replacement of OPC or natural aggregates; SS fines can exhibit pozzolanic activity; filler effect; mechanical performance improvements; iron compounds of SS can enable the formation of conductive channels within SSCs; the presence of CaO can break the silicate network, which reduces the slag viscosity and increases ion mobility.	Hydration of free CaO and MgO and oxidation of iron of SS can lead to expansion issues. High contents of SiO_2 in SS increase the silicate network, which prevents the movement of ions, increases the viscosity, and decreases the electrical conductivity of the material. When the compressive load increases, the water pore of non-dried SSCs can react with CaO of SS, forming hydrated compounds of higher	✓	✓	✓	✓

		volume that cause microcracks and changes in the piezoresistive response.				
Recycled carbon fiber (RCF)	Recycling of discarded CF (e.g., CF of aerospace composite scrap, cutting and processing of CF panels); improvement of compressive, flexural, and tensile splitting strength due to the bridging effects; decreases in electrical resistivity, based on the same conductive mechanisms of virgin CF.	High dosage of RCF cause workability reductions, changes in specimen compaction, increases in porosity, and decreases in mechanical properties.	✓	×	×	×
Rubber waste (RW)	Recycling of various types of rubber materials disposed in landfills or garbage; improvements in ductility, energy-absorbing capacity, impact resistance, sound-absorbing capacity, and thermal insulation; increases in electrical conductivity due to the presence of small conductive particles (e.g., carbon black, aluminum powder, and silver powder).	Increases in the dosage and particle size of RW usually decrease mechanical and durability properties.	✓	✓	✓	×
Biochar	Recycling of biodegradable waste materials (e.g., animal, agricultural, and forestry wastes); sequestration of carbon that cannot get back to the atmosphere; improvements in mechanical strength, ductility, and fracture toughness; decreases in electrical resistivity due to the presence of carbon particles that acted as conductive inclusions.	Workability is reduced by biochar addition and high contents of biochar cause decreases in mechanical strength.	✓	×	×	×
Gasification char (GCH)	Recycling of by-products of industrial gasification processes; improvements in nucleation effects; increases in compressive and tensile strength; decreases in electrical resistivity due to the high carbon content of the GCH and its effective dispersion.	High dosage of GCH can slightly decrease the workability and the compressive strength of cementitious composites.	✓	×	×	×

Waste of nano-graphite with iron particles (ING)	Recycling of a by-product generated in the hydrogen production process; decreases in electrical resistivity due to the presence of conductive nano-graphite and iron particles.	ING caused decreases in the compressive strength due to lubrication effects of nano-graphite particles that negatively affected the transition zone between aggregates and hydrated cement paste.	✓	×	×	×
Used foundry sand (UFS)	Recycling of a waste generated by ferrous and non-ferrous metal casting industries; increases in compressive and tensile strength; electrical resistivity decreases are eventually observed, due to carbon-based additions and several metals of UFS.	High dosage of UFS caused decreases in the compressive and tensile strength of cementitious composites.	✓	×	×	×
Waste wire erosion (WWE)	Recycling of a waste generated in metal cutting processes of aerospace, nuclear, and automotive industries; increases in compressive strength, flexural strength, and impact absorption; formation of conductive hierarchical networks when combined with other small conductive admixtures.	Research on cement-based materials incorporating WWE is scarce. Based on few results reported in the literature, the incorporation of CF into concretes containing WWE can be a limitation due to decreases in their compressive strength.	✓	×	×	×
Iron ore tailing (IOT)	Recycling of a waste generated in the beneficiation process of iron ore; reduction of environmental impacts, health issues, and land scarcity; increases in compressive strength and carbonation resistance when IOT replaces natural aggregates; increases in electrical conductivity and self-sensing properties due to the presence of conductive iron particles in IOT.	Mechanical properties decrease when the replacement level of natural aggregates with IOT exceeds the optimal dosage. When substituting cement by IOT, the compressive strength and the carbonation resistance usually decrease with increases in IOT contents.	✓	✓	×	×
Recycled glass waste (RGW)	Recycling of glass waste commonly disposed in landfills; replacement of natural aggregates; decreases in occupation of land, environmental pollution, and depletion of natural resources; conductive admixtures can be synthesized on the	SSCs containing RGW are vulnerable to alkali-silica reaction and formation of expansive products. Since RGW are insulating materials, they need to be covered by conductive admixtures to improve the electrical conductivity of concrete materials.	✓	✓	✓	✓

surface of RGW, which improves electrical conductivity and self-sensing performance	

Notes: SSC - sustainable self-sensing composite, SF - silica fume, OPC - ordinary Portland cement, FCR - fractional change in electrical resistivity, GF - gauge factor, SST - stress sensibility, FA - fly ash, C-S-H - calcium silicate hydrates, RM - red mud, BFS - blast-furnace slag, SS - steel slag, RCF - recycled carbon fiber, CF - carbon fiber, RW - rubber waste, GCH - gasification char, ING - waste of nano-graphite with iron particles, UFS - used foundry sand, WWE - waste wire erosion, IOT - iron ore tailing, RGW - recycled glass waste

*The symbol ✓ indicates that the corresponding use on SSCs was investigated in previous literature, whereas the symbol ✕ indicates that the corresponding use on SSCs was not investigated in previous literature (promising topics for future research).

Further research is needed to extend the range of types of wastes applied to the preparation of SSCs. Based on the content revised in this section, it is possible to infer that some promising wastes are those with an elevated content of conductive compounds. For instance, materials that are rich in conductive metal particles can be considered as recycled conductive fillers for the production of SSCs, such as industrial waste ashes [216,217], municipal solid waste incinerator ashes [218,219], and sewage sludge ashes [217,220]. Other promising wastes are those containing conductive carbon particles, which can be obtained from wastes of the tire industry [221], petroleum industry [222], leather industry [223], oil refineries [224], among others. Moreover, various waste materials can be used to produce recycled conductive nanoparticles, such as graphene produced from waste tire rubber [225]; CBN produced from carbon-based waste ashes [226]; graphene produced from RHA [227,228]; MWCNT derived from coal combustion ashes [229]; MWCNT obtained from SCBA [230]; carbon-based nanomaterials obtained from plastic, industrial, and biomass wastes [231,232]; conductive nanoparticles derived from crop, food, and industrial wastes [233]; nano-sized iron oxide particles obtained from steelmaking industry wastes [234–236]; metal- oxide nanoparticles from electronic and metal industry wastes [237]; among others.

In addition, there is no previous investigation of self-sensing properties of PCCs and AACs containing battery wastes. High amount of battery waste is generated in many developing countries, so that the application of this residue for production of multifunctional composites is an alternative to decrease environmental impacts, contributing to the circular economy. These byproducts of the primary batteries grinding process (alkaline and zinc carbon batteries) are promising candidates for fabrication of SSCs for monitoring of civil infrastructures, as they are mainly composed of conductive particles, such as graphite, manganese oxide, and zinc oxide [238].

Birgin et al. [239] also suggested another sustainable material with promising application for the development of self-sensing composites: an eco-friendly synthetic binder material called EVIzero that is fabricated with polymers and industrial by-products. SSCs produced with EVIzero and carbon microfibers (CMFs) were not included in Table 2, Table 3, and Figures 2, 3, and 4 because Birgin et al. [239] did not determine their sensing and mechanical properties, such as GF, SST, FCR amplitude, linearity, compressive strength, etc. Despite this, initial studies based on a tailored data acquisition setup with distributed line electrodes indicated that these SSCs were sensitive to hammer impact loads, rapid loading-unloading tests with, and traffic loads associated with light vehicles at various speeds. Further research must be

developed for optimization of the composite for mechanical and electrical properties, as well as field validation on existing infrastructures.

2.4 CONCLUSIONS AND PERSPECTIVIES FOR FUTURE RESEARCH

This work presented a detailed review of the recent progress on the development of smart sustainable building materials, focusing on the effects of different recycled admixtures on their self-sensing properties for monitoring strains and detecting damage in civil structures. Various contributions derived from this review:

(1) Experimental data revised in this paper indicated that the incorporation of waste materials into AACs and PCCs can provide significant reductions in Portland cement consumption, decrease the depletion of natural resources, avoid inappropriate waste disposal, and cause interesting effects on mechanisms of electrical conductivity and self-sensing behavior. Various types of wastes (SF, FA, RM, BFS, SS, RCF, RCBN, WWE, biochar, ING, RW, IOT, RGW) were able to provide or improve self-sensing properties of AACs and CPCs, based on different mechanisms carefully revised in this paper.

(2) High contents of SF (10-30% by weight of binders) and FA (5-25% by weight of binders) have been successfully used to produce SSCs, which provided gains in terms of decreases in Portland cement consumption and reductions in environmental impacts. In contrast, few studies reported SSCs containing high concentrations of BFS (5-25% by weight of binders) or RM (5-25% by weight of binders). Regarding the use of recycled conductive admixtures, piezoresistive properties were only investigated in composites containing a low content (0.73% by weight of cement) of RCFs.

(3) The highest self-sensing properties and optimal waste dosages reported in SSCs containing a single type of waste were identified in this work. High values of GF and SST were reported in the revised literature, covering a wide range of strain and stress values. Strong non-linear sensing response was also observed in many SSCs, which eventually represented the damage conditions of structural elements.

(4) Combinations between different recycled admixtures were found to be an interesting alternative to simultaneously improve their self-sensing and mechanical properties and provide environmental gains. In addition, synergistic effects of wastes of different average particle sizes seem to be an interesting strategy to provide hybrid SSCs with a hierarchical multi-scale conductive architecture. This work also identified the highest values of self-sensing properties reported in SSCs containing two or more types of wastes. Some SSCs produced with a

combination of different types of wastes also presented a non-linear relationship between FCR and stress in their piezoresistive tests, which was mainly associated with an intrinsic ability of damage detection.

(5) Wastes with promising application in the production of SSCs were identified in this review, such as recycled materials that are rich in metallic conductive particles, wastes containing conductive carbon particles, and wastes that can be used to produce recycled conductive nanoparticles

In addition, some open questions were identified over the present review process. The following issues on this topic call for further research:

(1) Most studies have only investigated the self-sensing properties of SSC subjected to uniaxial compression or uniaxial tensile tests. Therefore, relevant future investigations would be evaluations of the practical application of SSCs for monitoring different structural elements over time (e.g., beams, columns, and walls built in the laboratory or existing buildings).

(2) Experimental evaluations of different approaches for applying SSCs in structural elements have not yet been carried out. Therefore, studies of SSCs applied in different conditions are desirable, such as the embedding, bonding, sandwich, and bulk approach. Extensive investigation on the bulk approach would be of great interest, as it enables greater consumption of waste and offers the best solution to scalability issues recently verified in conventional SHM architectures.

(3) Although fixed dosages of SF and certain types of FA have been added to SSCs, further investigations on the effects of different concentrations and compositions of these recycled admixtures on the self-sensing properties of composites are needed. (4) Studies of SSCs containing RM, RCF, biochar, GCH, ING, and UFS are still in their initial phase, mainly focused on the electrical conductivity. It is pertinent to expand the investigations regarding their self-sensing properties.

(4) Previous works have shown that the sensing properties of PCCs and AACs can be improved by incorporating wastes containing conductive compounds in their composition or improving the dispersion of other conductive fillers existing in the matrix. It is important to investigate other waste materials (e.g., RHA, POFA, ORW, GW, and SCBA) that can also provide direct increases in the electrical conductivity of SSCs (e.g., SS, GGBFS, RCF, RW, RCBN, IOT, biochar, GCH, and WWE) and/or that can improve the dispersion of conventional conductive filers (e.g., FA and SF).

(5) The studies developed to date have mainly focused on evaluating the mechanical and self-sensing performance of SSCs. Therefore, it is necessary to develop life cycle assessment

(LCA) and life cycle cost (LCC) of SSCs, demonstrating and reinforcing the environmental and economic gains provided by waste incorporation.

(6) Previous studies have already synthesized conductive nanomaterials on the surface of recycled admixtures (e.g., CTNFA) or produced conductive nanomaterials from waste materials. The investigation of the self-sensing properties of composites produced with these innovative types of materials is strongly recommended.

(7) The dispersion of conductive fillers in the composite matrix is a key point for obtaining a suitable piezoresistive effect. However, previous studies did not investigate promising strategies to improve dispersion of conductive waste materials within the matrix of SSCs. Future works are recommended to evaluate the effects of simplified and efficient dispersion techniques of conductive waste materials on the sensing properties of PCCs and AACs, aiming at their large-scale production.

The improvements in self-sensing properties provided by waste materials indicated that incorporating SSCs into SHM systems is one of the key approaches that smart cities can apply to decrease environmental impacts of the construction sector, ensure the structural safety of buildings, and increase their life span. However, some policy implications exist for ensuring a successful application of SSCs for construction of intelligent and sustainable infrastructure, such as the development of effective collaborative partnerships among universities, research institutes, state-owned enterprises, and private enterprises; monetary incentives (e.g., tax exemption, government subsidy, and special loans) to stimulate waste recycling in the construction industry; sharing of knowledge between scientists and market players; inclusion of sustainable SHM technologies in eco-labeling and green building certifications; financial support to defray the costs of maturing research on SSCs; and provision of technical support and consultancy services for practical application of SSCs in the construction sector.

2.5 REFERENCES

[1] D.R. Vieira, J.L. Calmon, F.Z. Coelho, Life cycle assessment (LCA) applied to the manufacturing of common and ecological concrete: A review, Construction and Building Materials. 124 (2016) 656–666. https://doi.org/10.1016/j.conbuildmat.2016.07.125.

[2] B. Xia, T. Ding, J. Xiao, Life cycle assessment of concrete structures with reuse and recycling strategies: A novel framework and case study, Waste Management. 105 (2020) 268–278. https://doi.org/10.1016/j.wasman.2020.02.015.

[3] R.M. Andrew, Global CO2 emissions from cement production, Earth System Science

Data. 10 (2018) 195–217. https://doi.org/10.5194/essd-10-195-2018.

[4] A. Adesina, Recent advances in the concrete industry to reduce its carbon dioxide emissions, Environmental Challenges. 1 (2020) 100004. https://doi.org/10.1016/j.envc.2020.100004.

[5] E. Benhelal, E. Shamsaei, M.I. Rashid, Challenges against CO2 abatement strategies in cement industry: A review, Journal of Environmental Sciences. 104 (2021) 84–101. https://doi.org/10.1016/j.jes.2020.11.020.

[6] J. de Brito, R. Kurda, The past and future of sustainable concrete: A critical review and new strategies on cement-based materials, Journal of Cleaner Production. 281 (2021) 123558. https://doi.org/10.1016/j.jclepro.2020.123558.

[7] A. Bakchan, K.M. Faust, Construction waste generation estimates of institutional building projects: Leveraging waste hauling tickets, Waste Management. 87 (2019) 301–312. https://doi.org/10.1016/j.wasman.2019.02.024.

[8] International Energy Agency, Technology Roadmap - Low-Carbon Transition in the Cement Industry, 2018.

[9] United Nations, Report of the World Commission on Environment and Development: Our Common Future, (1987) 374. https://digitallibrary.un.org/record/139811.

[10] UNESCO, UNESCO and Sustainable Development Goals, 70th Session of the UN General Assembly. (2015). https://en.unesco.org/sustainabledevelopmentgoals (accessed September 4, 2021).

[11] J.M. Franco de Carvalho, W.C. Fontes, C.F. de Azevedo, G.J. Brigolini, W. Schmidt, R.A.F. Peixoto, Enhancing the eco-efficiency of concrete using engineered recycled mineral admixtures and recycled aggregates, Journal of Cleaner Production. 257 (2020). https://doi.org/10.1016/j.jclepro.2020.120530.

[12] C.M.M.E. Torres, C.M. Silva, L.G. Pedroti, W.E.H. Fernandes, F.C. Ballotin, A.J.V. Zanuncio, Dregs and grits from kraft pulp mills incorporated to Portland cement clinker, Journal of Material Cycles and Waste Management. 22 (2020) 851–861. https://doi.org/10.1007/s10163-020-00983-x.

[13] L.G. Pedroti, C.M.F. Vieira, J. Alexandre, G. de Castro Xavier, V.S. Candido, S.N. Monteiro, Granite Waste from Diamond Wire Sawing Addition into Concrete for Civil Construction, Materials Science Forum. 820 (2015) 503–508. https://doi.org/10.4028/www.scientific.net/MSF.820.503.

[14] L. Liu, G. Cai, J. Zhang, X. Liu, K. Liu, Evaluation of engineering properties and environmental effect of recycled waste tire-sand/soil in geotechnical engineering: A

compressive review, Renewable and Sustainable Energy Reviews. 126 (2020) 109831. https://doi.org/10.1016/j.rser.2020.109831.

[15] K. He, C. Ye, Y. Deng, J. Zhou, B. Liao, R. Gong, Y. Bi, W. Ji, Study on the microscale structure and anti-seepage properties of plastic concrete for cut-off walls modified with silica fume: Experiment and modelling, Construction and Building Materials. 261 (2020) 120489. https://doi.org/10.1016/j.conbuildmat.2020.120489.

[16] P. Kara De Maeijer, B. Craeye, R. Snellings, H. Kazemi-Kamyab, M. Loots, K. Janssens, G. Nuyts, Effect of ultra-fine fly ash on concrete performance and durability, Construction and Building Materials. 263 (2020) 120493. https://doi.org/10.1016/j.conbuildmat.2020.120493.

[17] M.T. Hasholt, K.U. Christensen, C. Pade, Frost resistance of concrete with high contents of fly ash - A study on how hollow fly ash particles distort the air void analysis, Cement and Concrete Research. 119 (2019) 102–112. https://doi.org/10.1016/j.cemconres.2019.02.013.

[18] K. Onoue, Energy consumption characteristics of concrete using granulated blast-furnace slag sand related to nucleation and propagation of microcracks, Construction and Building Materials. 218 (2019) 404–412. https://doi.org/10.1016/j.conbuildmat.2019.05.141.

[19] D. Hou, D. Wu, X. Wang, S. Gao, R. Yu, M. Li, P. Wang, Y. Wang, Sustainable use of red mud in ultra-high performance concrete (UHPC): Design and performance evaluation, Cement and Concrete Composites. 115 (2021) 103862. https://doi.org/10.1016/j.cemconcomp.2020.103862.

[20] S. Ramdani, A. Guettala, M. Benmalek, J.B. Aguiar, Physical and mechanical performance of concrete made with waste rubber aggregate, glass powder and silica sand powder, Journal of Building Engineering. 21 (2019) 302–311. https://doi.org/10.1016/j.jobe.2018.11.003.

[21] M.S. Savadkoohi, M. Reisi, Environmental protection based sustainable development by utilization of granite waste in Reactive Powder Concrete, Journal of Cleaner Production. 266 (2020) 121973. https://doi.org/10.1016/j.jclepro.2020.121973.

[22] A. El Machi, S. Mabroum, Y. Taha, A. Tagnit-Hamou, M. Benzaazoua, R. Hakkou, Use of flint from phosphate mine waste rocks as an alternative aggregates for concrete, Construction and Building Materials. 271 (2021) 121886. https://doi.org/10.1016/j.conbuildmat.2020.121886.

[23] N.B.Singh, S.K.Saxena, M. Kumar, Effect of nanomaterials on the properties of

geopolymer mortars and concrete, Materials Today: Proceedings. 5 (2018) 9035–9040. https://doi.org/10.1016/j.matpr.2017.10.018.

[24] L.K. Turner, F.G. Collins, Carbon dioxide equivalent (CO2-e) emissions: A comparison between geopolymer and OPC cement concrete, Construction and Building Materials. 43 (2013) 125–130. https://doi.org/10.1016/j.conbuildmat.2013.01.023.

[25] M.H. Samarakoon, P.G. Ranjith, T.D. Rathnaweera, M.S.A. Perera, Recent advances in alkaline cement binders: A review, Journal of Cleaner Production. 227 (2019) 70–87. https://doi.org/10.1016/j.jclepro.2019.04.103.

[26] Y. Ma, W. Liu, J. Hu, J. Fu, Z. Zhang, H. Wang, Optimization on the piezoresistivity of alkali-activated fly ash/slag mortar by using conductive aggregates and carbon fibers, Cement and Concrete Composites. 114 (2020) 103735. https://doi.org/10.1016/j.cemconcomp.2020.103735.

[27] J.L. Provis, A. Palomo, C. Shi, Advances in understanding alkali-activated materials, Cement and Concrete Research. 78 (2015) 110–125. https://doi.org/10.1016/j.cemconres.2015.04.013.

[28] B.C. Mendes, L.G. Pedroti, C.M.F. Vieira, M. Marvila, A.R.G. Azevedo, J.M. Franco de Carvalho, J.C.L. Ribeiro, Application of eco-friendly alternative activators in alkali-activated materials: A review, Journal of Building Engineering. 35 (2021) 102010. https://doi.org/10.1016/j.jobe.2020.102010.

[29] B. Suhendro, The Role of Structural Health Monitoring in Sustainability of Civil Engineering Structures, in: Proceedings of the 1st International Conference on Sustainable Civil Engineering Structures and Construction Materials, Yogyakarta, 2012: pp. 16–25.

[30] J. Xu, T. Yin, Y. Wang, L. Liu, Anisotropic electrical and piezoresistive sensing properties of cement-based sensors with aligned carbon fibers, Cement and Concrete Composites. 116 (2021) 103873. https://doi.org/10.1016/j.cemconcomp.2020.103873.

[31] D.D.L. Chung, Self-sensing concrete: from resistance-based sensing to capacitance-based sensing, International Journal of Smart and Nano Materials. 12 (2021) 1–19. https://doi.org/10.1080/19475411.2020.1843560.

[32] D.D.L. Chung, Electrical applications of carbon materials, Journal of Materials Science. 39 (2004) 2645–2661. https://doi.org/10.1023/B:JMSC.0000021439.18202.ea.

[33] B. Han, X. Yu, J. Ou, Self-Sensing Concrete in Smart Structures, Elsevier, 2015. https://doi.org/10.1016/C2013-0-14456-X.

[34] B. Han, S. Ding, X. Yu, Intrinsic self-sensing concrete and structures: A review,

Measurement. 59 (2015) 110–128. https://doi.org/10.1016/j.measurement.2014.09.048.

[35] L. Liu, J. Xu, T. Yin, Y. Wang, H. Chu, Improved conductivity and piezoresistive properties of Ni-CNTs cement-based composites under magnetic field, Cement and Concrete Composites. 121 (2021) 104089. https://doi.org/10.1016/j.cemconcomp.2021.104089.

[36] F. Ubertini, A. D'Alessandro, Concrete with self-sensing properties, in: Eco-Efficient Repair and Rehabilitation of Concrete Infrastructures, Elsevier, 2018: pp. 501–530. https://doi.org/10.1016/B978-0-08-102181-1.00018-6.

[37] A.I. Madbouly, M.M. Mokhtar, M.S. Morsy, Evaluating the performance of rGO/cement composites for SHM applications, Construction and Building Materials. 250 (2020) 118841. https://doi.org/10.1016/j.conbuildmat.2020.118841.

[38] A.V. Gaumet, R.J. Ball, A. Nogaret, Graphite-polydimethylsiloxane composite strain sensors for in-situ structural health monitoring, Sensors and Actuators A: Physical. 332 (2021) 113139. https://doi.org/10.1016/j.sna.2021.113139.

[39] D.D.L. Chung, Multifunctional Cement-Based Materials, CRC Press, New York, 2018. https://doi.org/10.1201/9781315273235.

[40] C. Vlachakis, M. Perry, L. Biondi, Self-Sensing Alkali-Activated Materials: A Review, Minerals. 10 (2020) 885. https://doi.org/10.3390/min10100885.

[41] G. Nalon, J. Ribeiro, E. Araújo, L. Pedroti, J. Carvalho, R. Santos, A. Aparecido-Ferreira, Effects of different kinds of carbon black nanoparticles on the piezoresistive and mechanical properties of cement-based composites, Journal of Building Engineering. 32 (2020) 101724. https://doi.org/10.1016/j.jobe.2020.101724.

[42] H. Li, H. Xiao, J. Ou, Effect of compressive strain on electrical resistivity of carbon black-filled cement-based composites, Cement and Concrete Composites. 28 (2006) 824–828. https://doi.org/10.1016/j.cemconcomp.2006.05.004.

[43] W. Dong, W. Li, L. Shen, D. Sheng, Piezoresistive behaviours of carbon black cement-based sensors with layer-distributed conductive rubber fibres, Materials & Design. 182 (2019) 108012. https://doi.org/10.1016/j.matdes.2019.108012.

[44] W. Dong, W. Li, K. Wang, B. Han, D. Sheng, S.P. Shah, Investigation on physicochemical and piezoresistive properties of smart MWCNT/cementitious composite exposed to elevated temperatures, Cement and Concrete Composites. 112 (2020) 103675. https://doi.org/10.1016/j.cemconcomp.2020.103675.

[45] A. Downey, E. Garcia-Macias, A. D'Alessandro, S. Laflamme, R. Castro-Triguero, F. Ubertini, Continuous and embedded solutions for SHM of concrete structures using

changing electrical potential in self-sensing cement-based composites, in: H.F. Wu, A.L. Gyekenyesi, P.J. Shull, T.-Y. Yu (Eds.), 2017: p. 101691G. https://doi.org/10.1117/12.2261427.

[46] L. Deng, Y. Ma, J. Hu, S. Yin, X. Ouyang, J. Fu, A. Liu, Z. Zhang, Preparation and piezoresistive properties of carbon fiber-reinforced alkali-activated fly ash/slag mortar, Construction and Building Materials. 222 (2019) 738–749. https://doi.org/10.1016/j.conbuildmat.2019.06.134.

[47] D.K. Hardy, M.F. Fadden, M.J. Khattak, A. Khattab, Development and characterization of self-sensing CNF HPFRCC, Materials and Structures. 49 (2016) 5327–5342. https://doi.org/10.1617/s11527-016-0863-z.

[48] A. D'Alessandro, D. Coffetti, E. Crotti, L. Coppola, A. Meoni, F. Ubertini, Self-Sensing Properties of Green Alkali-Activated Binders with Carbon-Based Nanoinclusions, Sustainability. 12 (2020) 9916. https://doi.org/10.3390/su12239916.

[49] J. Tao, X. Wang, Z. Wang, Q. Zeng, Graphene nanoplatelets as an effective additive to tune the microstructures and piezoresistive properties of cement-based composites, Construction and Building Materials. 209 (2019) 665–678. https://doi.org/10.1016/j.conbuildmat.2019.03.173.

[50] D.-Y. Yoo, I. You, S.-J. Lee, Electrical Properties of Cement-Based Composites with Carbon Nanotubes, Graphene, and Graphite Nanofibers, Sensors. 17 (2017) 1064. https://doi.org/10.3390/s17051064.

[51] P. Rovnaník, I. Kusák, P. Bayer, P. Schmid, L. Fiala, Electrical and Self-Sensing Properties of Alkali-Activated Slag Composite with Graphite Filler, Materials. 12 (2019) 1616. https://doi.org/10.3390/ma12101616.

[52] Y. Ding, Y. Yang, R. Liu, T. Xiao, J. Tian, Study on pressure sensitivity of smart polymer concrete based on steel slag, Measurement. 140 (2019) 14–21. https://doi.org/10.1016/j.measurement.2019.03.040.

[53] B.G. Han, B.Z. Han, J.P. Ou, Experimental study on use of nickel powder-filled Portland cement-based composite for fabrication of piezoresistive sensors with high sensitivity, Sensors and Actuators A: Physical. 149 (2009) 51–55. https://doi.org/10.1016/j.sna.2008.10.001.

[54] H.V. Le, D.H. Lee, D.J. Kim, Effects of steel slag aggregate size and content on piezoresistive responses of smart ultra-high-performance fiber-reinforced concretes, Sensors and Actuators A: Physical. 305 (2020) 111925. https://doi.org/10.1016/j.sna.2020.111925.

[55] S.Y. Lee, H.V. Le, D.J. Kim, Self-stress sensing smart concrete containing fine steel slag aggregates and steel fibers under high compressive stress, Construction and Building Materials. 220 (2019) 149–160. https://doi.org/10.1016/j.conbuildmat.2019.05.197.

[56] E. Demircilioglu, E. Teomete, O.E. Ozbulut, Strain sensitivity of steel-fiber-reinforced industrial smart concrete, Journal of Intelligent Material Systems and Structures. 31 (2020) 127–136. https://doi.org/10.1177/1045389X19888722.

[57] A. Belli, A. Mobili, T. Bellezze, F. Tittarelli, Commercial and recycled carbon/steel fibers for fiber-reinforced cement mortars with high electrical conductivity, Cement and Concrete Composites. 109 (2020) 103569. https://doi.org/10.1016/j.cemconcomp.2020.103569.

[58] V.W.Y. Tam, H. Wattage, K.N. Le, A. Buteraa, M. Soomro, Methods to improve microstructural properties of recycled concrete aggregate: A critical review, Construction and Building Materials. 270 (2021) 121490. https://doi.org/10.1016/j.conbuildmat.2020.121490.

[59] R. Wang, N. Yu, Y. Li, Methods for improving the microstructure of recycled concrete aggregate: A review, Construction and Building Materials. 242 (2020) 118164. https://doi.org/10.1016/j.conbuildmat.2020.118164.

[60] C. Karakurt, Microstructure properties of waste tire rubber composites: an overview, Journal of Material Cycles and Waste Management. 17 (2015) 422–433. https://doi.org/10.1007/s10163-014-0263-9.

[61] Q. Fu, M. Bu, Z. Zhang, W. Xu, Q. Yuan, D. Niu, Hydration Characteristics and Microstructure of Alkali-Activated Slag Concrete: A Review, Engineering. (2021). https://doi.org/10.1016/j.eng.2021.07.026.

[62] H.M. Magbool, Utilisation of ceramic waste aggregate and its effect on Eco-friendly concrete: A review, Journal of Building Engineering. 47 (2022) 103815. https://doi.org/10.1016/j.jobe.2021.103815.

[63] P. Guo, W. Meng, H. Nassif, H. Gou, Y. Bao, New perspectives on recycling waste glass in manufacturing concrete for sustainable civil infrastructure, Construction and Building Materials. 257 (2020) 119579. https://doi.org/10.1016/j.conbuildmat.2020.119579.

[64] Z. Xu, Z. Huang, C. Liu, X. Deng, D. Hui, S. Deng, Research progress on mechanical properties of geopolymer recycled aggregate concrete, Reviews on Advanced Materials Science. 60 (2021) 158–172. https://doi.org/10.1515/rams-2021-0021.

[65] R. Roychand, R.J. Gravina, Y. Zhuge, X. Ma, O. Youssf, J.E. Mills, A comprehensive review on the mechanical properties of waste tire rubber concrete, Construction and

Building Materials. 237 (2020) 117651. https://doi.org/10.1016/j.conbuildmat.2019.117651.

[66] G. Bai, C. Zhu, C. Liu, B. Liu, An evaluation of the recycled aggregate characteristics and the recycled aggregate concrete mechanical properties, Construction and Building Materials. 240 (2020) 117978. https://doi.org/10.1016/j.conbuildmat.2019.117978.

[67] J. Anne Mary, R. Gobinath, G. Shyamala, K. Rajesh Chary, Waste Products as an Alternative Construction Material-A Review, IOP Conference Series: Materials Science and Engineering. 981 (2020) 032086. https://doi.org/10.1088/1757-899X/981/3/032086.

[68] H.U. Ahmed, R.H. Faraj, N. Hilal, A.A. Mohammed, A.F.H. Sherwani, Use of recycled fibers in concrete composites: A systematic comprehensive review, Composites Part B: Engineering. 215 (2021) 108769. https://doi.org/10.1016/j.compositesb.2021.108769.

[69] M. Amran, S. Debbarma, T. Ozbakkaloglu, Fly ash-based eco-friendly geopolymer concrete: A critical review of the long-term durability properties, Construction and Building Materials. 270 (2021) 121857. https://doi.org/10.1016/j.conbuildmat.2020.121857.

[70] M. Wasim, T.D. Ngo, D. Law, A state-of-the-art review on the durability of geopolymer concrete for sustainable structures and infrastructure, Construction and Building Materials. 291 (2021) 123381. https://doi.org/10.1016/j.conbuildmat.2021.123381.

[71] A. Siddika, A. Hajimohammadi, M.A. Al Mamun, R. Alyousef, W. Ferdous, Waste Glass in Cement and Geopolymer Concretes: A Review on Durability and Challenges, Polymers. 13 (2021) 2071. https://doi.org/10.3390/polym13132071.

[72] K.H. Mo, B.S. Thomas, S.P. Yap, F. Abutaha, C.G. Tan, Viability of agricultural wastes as substitute of natural aggregate in concrete: A review on the durability-related properties, Journal of Cleaner Production. 275 (2020) 123062. https://doi.org/10.1016/j.jclepro.2020.123062.

[73] K.L. Jain, G. Sancheti, L.K. Gupta, Durability performance of waste granite and glass powder added concrete, Construction and Building Materials. 252 (2020) 119075. https://doi.org/10.1016/j.conbuildmat.2020.119075.

[74] Z. Ma, Q. Tang, D. Yang, G. Ba, Durability Studies on the Recycled Aggregate Concrete in China over the Past Decade: A Review, Advances in Civil Engineering. 2019 (2019) 1–19. https://doi.org/10.1155/2019/4073130.

[75] P.K. Priya, S. Vanitha, P. Meyyappan, Utilization of waste for building materials - a review, IOP Conference Series: Materials Science and Engineering. 955 (2020) 012048. https://doi.org/10.1088/1757-899X/955/1/012048.

[76] C.O. Nwankwo, G.O. Bamigboye, I.E.E. Davies, T.A. Michaels, High volume Portland cement replacement: A review, Construction and Building Materials. 260 (2020) 120445. https://doi.org/10.1016/j.conbuildmat.2020.120445.

[77] P. Cassese, C. Rainieri, A. Occhiuzzi, Applications of Cement-Based Smart Composites to Civil Structural Health Monitoring: A Review, Applied Sciences. 11 (2021) 8530. https://doi.org/10.3390/app11188530.

[78] Z. Bekzhanova, S.A. Memon, J.R. Kim, Self-Sensing Cementitious Composites: Review and Perspective, Nanomaterials. 11 (2021) 2355. https://doi.org/10.3390/nano11092355.

[79] M.T. Mohammadi, M. Yeganeh, M. Eskandari, S.R. AlaviZaree, H. Salemi, Nano self-sensing concretes (NSsCs), in: Nanosensors for Smart Manufacturing, Elsevier, 2021: pp. 373–395. https://doi.org/10.1016/B978-0-12-823358-0.00019-8.

[80] A. Dinesh, S.T. Sudharsan, S. Haribala, Self-sensing cement-based sensor with carbon nanotube: Fabrication and properties – A review, Materials Today: Proceedings. 46 (2021) 5801–5807. https://doi.org/10.1016/j.matpr.2021.02.722.

[81] J. Han, J. Pan, J. Cai, X. Li, A review on carbon-based self-sensing cementitious composites, Construction and Building Materials. 265 (2020) 120764. https://doi.org/10.1016/j.conbuildmat.2020.120764.

[82] L. Wang, F. Aslani, A review on material design, performance, and practical application of electrically conductive cementitious composites, Construction and Building Materials. 229 (2019) 116892. https://doi.org/10.1016/j.conbuildmat.2019.116892.

[83] S. Zhu, D.D.L. Chung, Theory of piezoresistivity for strain sensing in carbon fiber reinforced cement under flexure, Journal of Materials Science. 42 (2007) 6222–6233. https://doi.org/10.1007/s10853-006-1131-3.

[84] G. Nalon, J.C.L. Ribeiro, L.G. Pedroti, E.N.D. de Araújo, J.M. Franco de Carvalho, G.E.S. Lima, D.S. Oliveira, Self-Sensing Mortars: Effect of Moisture and Nanocarbon Black Content, ACI Materials Journal. 118 (2021) 131–141. https://doi.org/10.14359/51732636.

[85] S. Wen, D.D.L. Chung, Electrical-resistance-based damage self-sensing in carbon fiber reinforced cement, Carbon. 45 (2007) 710–716. https://doi.org/10.1016/j.carbon.2006.11.029.

[86] F. Azhari, N. Banthia, Cement-based sensors with carbon fibers and carbon nanotubes for piezoresistive sensing, Cement and Concrete Composites. 34 (2012) 866–873. https://doi.org/10.1016/j.cemconcomp.2012.04.007.

[87] I. Gull, M.A. Tantray, Self-damage sensing of electrically conductive self-compacting

concrete incorporating short carbon fibers, Structural Control and Health Monitoring. 28 (2021). https://doi.org/10.1002/stc.2735.

[88] X. Li, M. Li, Multifunctional self-sensing and ductile cementitious materials, Cement and Concrete Research. 123 (2019) 105714. https://doi.org/10.1016/j.cemconres.2019.03.008.

[89] L. Qiu, S. Dong, X. Yu, B. Han, Self-sensing ultra-high performance concrete for in-situ monitoring, Sensors and Actuators A: Physical. 331 (2021) 113049. https://doi.org/10.1016/j.sna.2021.113049.

[90] H. Wang, F. Shi, J. Shen, A. Zhang, L. Zhang, H. Huang, J. Liu, K. Jin, L. Feng, Z. Tang, Research on the self-sensing and mechanical properties of aligned stainless steel fiber-reinforced reactive powder concrete, Cement and Concrete Composites. 119 (2021) 104001. https://doi.org/10.1016/j.cemconcomp.2021.104001.

[91] J. McAlorum, M. Perry, C. Vlachakis, L. Biondi, B. Lavoie, Robotic spray coating of self-sensing metakaolin geopolymer for concrete monitoring, Automation in Construction. 121 (2021) 103415. https://doi.org/10.1016/j.autcon.2020.103415.

[92] C. Mizerová, I. Kusák, P. Rovnaník, P. Bayer, Conductive Metakaolin Geopolymer with Steel Microfibres, Solid State Phenomena. 321 (2021) 59–64. https://doi.org/10.4028/www.scientific.net/SSP.321.59.

[93] C. Mizerová, P. Rovnaník, I. Kusák, P. Schmid, Self-sensing performance of metakaolin geopolymer with carbon nanotubes subjected to repeated compressive loading, IOP Conference Series: Materials Science and Engineering. 1209 (2021) 012043. https://doi.org/10.1088/1757-899X/1209/1/012043.

[94] J. McAlorum, M. Perry, A.C. Ward, C. Vlachakis, ConcrEITS: An Electrical Impedance Interrogator for Concrete Damage Detection Using Self-Sensing Repairs, Sensors. 21 (2021) 7081. https://doi.org/10.3390/s21217081.

[95] L. Biondi, M. Perry, J. McAlorum, C. Vlachakis, A. Hamilton, G. Lo, Alkali-Activated Cement Sensors for Sodium Chloride Monitoring, IEEE Sensors Journal. 21 (2021) 21197–21204. https://doi.org/10.1109/JSEN.2021.3100582.

[96] C. Mizerová, I. Kusák, L. Topolář, P. Schmid, P. Rovnaník, Self-Sensing Properties of Fly Ash Geopolymer Doped with Carbon Black under Compression, Materials. 14 (2021) 4350. https://doi.org/10.3390/ma14164350.

[97] W.-J. Long, X.-H. Zhang, B.-Q. Dong, Y. Fang, T.-H. Ye, J. Xie, Investigation of Graphene Derivatives on Electrical Properties of Alkali Activated Slag Composites, Materials. 14 (2021) 4374. https://doi.org/10.3390/ma14164374.

[98] X.-M. Cui, G.-J. Zheng, Y.-C. Han, F. Su, J. Zhou, A study on electrical conductivity of chemosynthetic Al2O3-2SiO2 geoploymer materials, Journal of Power Sources. 184 (2008) 652–656. https://doi.org/10.1016/j.jpowsour.2008.03.021.

[99] Y. Huang, H. Li, S. Qian, Self-sensing properties of Engineered Cementitious Composites, Construction and Building Materials. 174 (2018) 253–262. https://doi.org/10.1016/j.conbuildmat.2018.04.129.

[100] H. Deng, H. Li, Assessment of self-sensing capability of Carbon Black Engineered Cementitious Composites, Construction and Building Materials. 173 (2018) 1–9. https://doi.org/10.1016/j.conbuildmat.2018.04.031.

[101] M.I. Haque, R.I. Khan, W. Ashraf, H. Pendse, Production of sustainable, low-permeable and self-sensing cementitious composites using biochar, Sustainable Materials and Technologies. 28 (2021) e00279. https://doi.org/10.1016/j.susmat.2021.e00279.

[102] H. Dehghanpour, K. Yilmaz, M. Ipek, Evaluation of recycled nano carbon black and waste erosion wires in electrically conductive concretes, Construction and Building Materials. 221 (2019) 109–121. https://doi.org/10.1016/j.conbuildmat.2019.06.025.

[103] A. Mobili, C. Giosuè, T. Bellezze, G.M. Revel, F. Tittarelli, Gasification Char and Used Foundry Sand as Alternative Fillers to Graphene Nanoplatelets for Electrically Conductive Mortars with and without Virgin/Recycled Carbon Fibres, Applied Sciences. 11 (2020) 50. https://doi.org/10.3390/app11010050.

[104] A. Mobili, A. Belli, C. Giosuè, M. Pierpaoli, L. Bastianelli, A. Mazzoli, M.L. Ruello, T. Bellezze, F. Tittarelli, Mechanical, durability, depolluting and electrical properties of multifunctional mortars prepared with commercial or waste carbon-based fillers, Construction and Building Materials. 283 (2021) 122768. https://doi.org/10.1016/j.conbuildmat.2021.122768.

[105] W. Dong, Y. Huang, B. Lehane, F. Aslani, G. Ma, Mechanical and electrical properties of concrete incorporating an iron-particle contained nano-graphite by-product, Construction and Building Materials. 270 (2021) 121377. https://doi.org/10.1016/j.conbuildmat.2020.121377.

[106] S. Kamaluddin, D. Kurniawan, M.S. Abu Bakar, Z. Abu Samah, Biochar as a Conducting Filler to Enhance Electrical Conduction Monitoring for Concrete Structures, Key Engineering Materials. 847 (2020) 149–154. https://doi.org/10.4028/www.scientific.net/KEM.847.149.

[107] M.I. Haque, R.I. Khan, W. Ashraf, H. Pendse, Utilization of Biochar as a Multifunctional Additive in Cement-Based Materials, in: Springer (Ed.), Proceedings of the 3rd RILEM

Spring Convention and Conference, RILEM Book, 2021: pp. 343–353. https://doi.org/10.1007/978-3-030-76551-4_31.

[108] W. Dong, W. Li, L. Shen, S. Zhang, K. Vessalas, Integrated self-sensing and self-healing cementitious composite with microencapsulation of nano-carbon black and slaked lime, Materials Letters. 282 (2021) 128834. https://doi.org/10.1016/j.matlet.2020.128834.

[109] W. Li, W. Dong, L. Shen, A. Castel, S.P. Shah, Conductivity and piezoresistivity of nano-carbon black (NCB) enhanced functional cement-based sensors using polypropylene fibres, Materials Letters. 270 (2020) 127736. https://doi.org/10.1016/j.matlet.2020.127736.

[110] W. Dong, W. Li, K. Wang, Y. Guo, D. Sheng, S.P. Shah, Piezoresistivity enhancement of functional carbon black filled cement-based sensor using polypropylene fibre, Powder Technology. 373 (2020) 184–194. https://doi.org/10.1016/j.powtec.2020.06.029.

[111] W. Dong, W. Li, Y. Guo, X. He, D. Sheng, Effects of silica fume on physicochemical properties and piezoresistivity of intelligent carbon black-cementitious composites, Construction and Building Materials. 259 (2020) 120399. https://doi.org/10.1016/j.conbuildmat.2020.120399.

[112] W. Dong, W. Li, Z. Luo, G. Long, K. Vessalas, D. Sheng, Structural response monitoring of concrete beam under flexural loading using smart carbon black/cement-based sensors, Smart Materials and Structures. 29 (2020) 065001. https://doi.org/10.1088/1361-665X/ab7fef.

[113] W. Dong, W. Li, Z. Luo, Y. Guo, K. Wang, Effect of layer-distributed carbon nanotube (CNT) on mechanical and piezoresistive performance of intelligent cement-based sensor, Nanotechnology. 31 (2020) 505503. https://doi.org/10.1088/1361-6528/abb503.

[114] W. Dong, W. Li, N. Lu, F. Qu, K. Vessalas, D. Sheng, Piezoresistive behaviours of cement-based sensor with carbon black subjected to various temperature and water content, Composites Part B: Engineering. 178 (2019) 107488. https://doi.org/10.1016/j.compositesb.2019.107488.

[115] D.-Y. Yoo, I. You, H. Youn, S.-J. Lee, Electrical and piezoresistive properties of cement composites with carbon nanomaterials, Journal of Composite Materials. 52 (2018) 3325–3340. https://doi.org/10.1177/0021998318764809.

[116] M. Jung, J. Park, S. Hong, J. Moon, Electrically cured ultra-high performance concrete (UHPC) embedded with carbon nanotubes for field casting and crack sensing, Materials & Design. 196 (2020) 109127. https://doi.org/10.1016/j.matdes.2020.109127.

[117] L. Zhang, S. Ding, B. Han, X. Yu, Y.-Q. Ni, Effect of water content on the piezoresistive

property of smart cement-based materials with carbon nanotube/nanocarbon black composite filler, Composites Part A: Applied Science and Manufacturing. 119 (2019) 8–20. https://doi.org/10.1016/j.compositesa.2019.01.010.

[118] I. You, D.-Y. Yoo, S. Kim, M.-J. Kim, G. Zi, Electrical and Self-Sensing Properties of Ultra-High-Performance Fiber-Reinforced Concrete with Carbon Nanotubes, Sensors. 17 (2017) 2481. https://doi.org/10.3390/s17112481.

[119] B. Han, L. Zhang, S. Sun, X. Yu, X. Dong, T. Wu, J. Ou, Electrostatic self-assembled carbon nanotube/nano carbon black composite fillers reinforced cement-based materials with multifunctionality, Composites Part A: Applied Science and Manufacturing. 79 (2015) 103–115. https://doi.org/10.1016/j.compositesa.2015.09.016.

[120] E. Demircilioğlu, E. Teomete, E. Schlangen, F.J. Baeza, Temperature and moisture effects on electrical resistance and strain sensitivity of smart concrete, Construction and Building Materials. 224 (2019) 420–427. https://doi.org/10.1016/j.conbuildmat.2019.07.091.

[121] E. Teomete, E. Demircilioğlu, S. Kahraman, The strain sensitivity of brass fiber reinforced concrete, Challenge Journal of Structural Mechanics. 3 (2017) 134. https://doi.org/10.20528/cjsmec.2017.02.008.

[122] M. Konkanov, T. Salem, P. Jiao, R. Niyazbekova, N. Lajnef, Environment-Friendly, Self-Sensing Concrete Blended with Byproduct Wastes, Sensors. 20 (2020) 1925. https://doi.org/10.3390/s20071925.

[123] M. Zhan, G. Pan, F. Zhou, R. Mi, S.P. Shah, In situ-grown carbon nanotubes enhanced cement-based materials with multifunctionality, Cement and Concrete Composites. 108 (2020) 103518. https://doi.org/10.1016/j.cemconcomp.2020.103518.

[124] S. Ding, Y. Ruan, X. Yu, B. Han, Y.-Q. Ni, Self-monitoring of smart concrete column incorporating CNT/NCB composite fillers modified cementitious sensors, Construction and Building Materials. 201 (2019) 127–137. https://doi.org/10.1016/j.conbuildmat.2018.12.203.

[125] B. Han, Y. Wang, S. Ding, X. Yu, L. Zhang, Z. Li, J. Ou, Self-sensing cementitious composites incorporated with botryoid hybrid nano-carbon materials for smart infrastructures, Journal of Intelligent Material Systems and Structures. 28 (2017) 699–727. https://doi.org/10.1177/1045389X16657416.

[126] P. Rovnaník, I. Kusák, P. Bayer, P. Schmid, L. Fiala, Comparison of electrical and self-sensing properties of Portland cement and alkali-activated slag mortars, Cement and Concrete Research. 118 (2019) 84–91. https://doi.org/10.1016/j.cemconres.2019.02.009.

[127] J. Vilaplana, F. Baeza, O. Galao, E. Zornoza, P. Garcés, Self-Sensing Properties of Alkali Activated Blast Furnace Slag (BFS) Composites Reinforced with Carbon Fibers, Materials. 6 (2013) 4776–4786. https://doi.org/10.3390/ma6104776.

[128] F.J. Baeza, O. Galao, I.J. Vegas, M. Cano, P. Garcés, Influence of recycled slag aggregates on the conductivity and strain sensing capacity of carbon fiber reinforced cement mortars, Construction and Building Materials. 184 (2018) 311–319. https://doi.org/10.1016/j.conbuildmat.2018.06.218.

[129] S.-H. Hong, T.-F. Yuan, J.-S. Choi, Y.-S. Yoon, Effects of Steelmaking Slag and Moisture on Electrical Properties of Concrete, Materials. 13 (2020) 2675. https://doi.org/10.3390/ma13122675.

[130] I. Segura, G. Faneca, J.M. Torrents, A. Aguado, Self-sensing concrete made from recycled carbon fibres, Smart Materials and Structures. 28 (2019) 105045. https://doi.org/10.1088/1361-665X/ab3d59.

[131] A. Belli, A. Mobili, T. Bellezze, F. Tittarelli, P. Cachim, Evaluating the Self-Sensing Ability of Cement Mortars Manufactured with Graphene Nanoplatelets, Virgin or Recycled Carbon Fibers through Piezoresistivity Tests, Sustainability. 10 (2018) 4013. https://doi.org/10.3390/su10114013.

[132] L. Duan, D.R. D'hooge, L. Cardon, Recent progress on flexible and stretchable piezoresistive strain sensors: From design to application, Progress in Materials Science. 114 (2020) 100617. https://doi.org/10.1016/j.pmatsci.2019.100617.

[133] M. Saafi, L. Tang, J. Fung, M. Rahman, F. Sillars, J. Liggat, X. Zhou, Graphene/fly ash geopolymeric composites as self-sensing structural materials, Smart Materials and Structures. 23 (2014) 065006. https://doi.org/10.1088/0964-1726/23/6/065006.

[134] P.-C. Aïtcin, Supplementary cementitious materials and blended cements, in: Science and Technology of Concrete Admixtures, Elsevier, 2016: pp. 53–73. https://doi.org/10.1016/B978-0-08-100693-1.00004-7.

[135] D.K. Panesar, Supplementary cementing materials, in: Developments in the Formulation and Reinforcement of Concrete, Elsevier, 2019: pp. 55–85. https://doi.org/10.1016/B978-0-08-102616-8.00003-4.

[136] R. Siddique, Kunal, Utilization of industrial by-products and natural ashes in mortar and concrete, in: Nonconventional and Vernacular Construction Materials, Elsevier, 2016: pp. 159–204. https://doi.org/10.1016/B978-0-08-100038-0.00007-X.

[137] American Concrete Institute, ACI PRC-234-06: Guide for the Use of Silica Fume in Concrete, Farmington Hills, 2012.

[138] V.M. Malhotra, P.K. Mehta, Pozzolanic and Cementitious Materials, CRC Press, 2017. https://doi.org/10.1201/9781482296761.

[139] S. Samad, A. Shah, Role of binary cement including Supplementary Cementitious Material (SCM), in production of environmentally sustainable concrete: A critical review, International Journal of Sustainable Built Environment. 6 (2017) 663–674. https://doi.org/10.1016/j.ijsbe.2017.07.003.

[140] W. Meng, P. Lunkad, A. Kumar, K. Khayat, Influence of Silica Fume and Polycarboxylate Ether Dispersant on Hydration Mechanisms of Cement, The Journal of Physical Chemistry C. 120 (2016) 26814–26823. https://doi.org/10.1021/acs.jpcc.6b08121.

[141] L.A. Qureshi, B. Ali, A. Ali, Combined effects of supplementary cementitious materials (silica fume, GGBS, fly ash and rice husk ash) and steel fiber on the hardened properties of recycled aggregate concrete, Construction and Building Materials. 263 (2020) 120636. https://doi.org/10.1016/j.conbuildmat.2020.120636.

[142] A. Mehta, D.K. Ashish, Silica fume and waste glass in cement concrete production: A review, Journal of Building Engineering. 29 (2020) 100888. https://doi.org/10.1016/j.jobe.2019.100888.

[143] A. Yazdanbakhsh, Z. Grasley, Utilization of Silica Fume to Stabilize the Dispersion of Carbon Nanofilaments in Cement Paste, Journal of Materials in Civil Engineering. 26 (2014) 06014010. https://doi.org/10.1061/(ASCE)MT.1943-5533.0001016.

[144] H.K. Kim, I.W. Nam, H.K. Lee, Enhanced effect of carbon nanotube on mechanical and electrical properties of cement composites by incorporation of silica fume, Composite Structures. 107 (2014) 60–69. https://doi.org/10.1016/j.compstruct.2013.07.042.

[145] G.M. Kim, B.J. Yang, K.J. Cho, E.M. Kim, H.K. Lee, Influences of CNT dispersion and pore characteristics on the electrical performance of cementitious composites, Composite Structures. 164 (2017) 32–42. https://doi.org/10.1016/j.compstruct.2016.12.049.

[146] H. Li, H. Xiao, J. Ou, Electrical property of cement-based composites filled with carbon black under long-term wet and loading condition, Composites Science and Technology. 68 (2008) 2114–2119. https://doi.org/10.1016/j.compscitech.2008.03.007.

[147] H. Xiao, H. Li, A study on the application of CB-filled cement-based composite as a strain sensor for concrete structures, in: M. Tomizuka, C.-B. Yun, V. Giurgiutiu (Eds.), 2006: p. 61742T. https://doi.org/10.1117/12.660787.

[148] K.L. Scrivener, V.M. John, E.M. Gartner, Eco-efficient cements: Potential economically

viable solutions for a low-CO2 cement-based materials industry, Cement and Concrete Research. 114 (2018) 2–26. https://doi.org/10.1016/j.cemconres.2018.03.015.

[149] Y. Xing, F. Guo, M. Xu, X. Gui, H. Li, G. Li, Y. Xia, H. Han, Separation of unburned carbon from coal fly ash: A review, Powder Technology. 353 (2019) 372–384. https://doi.org/10.1016/j.powtec.2019.05.037.

[150] F.O. Ochedi, Y. Liu, A. Hussain, A review on coal fly ash-based adsorbents for mercury and arsenic removal, Journal of Cleaner Production. 267 (2020) 122143. https://doi.org/10.1016/j.jclepro.2020.122143.

[151] F. Mushtaq, M. Zahid, I.A. Bhatti, S. Nasir, T. Hussain, Possible applications of coal fly ash in wastewater treatment, Journal of Environmental Management. 240 (2019) 27–46. https://doi.org/10.1016/j.jenvman.2019.03.054.

[152] P. Mehta, P. Monteiro, Concrete: Microstructure, Properties and Materials (in Portuguese), São Paulo, 2014.

[153] Y. Ogawa, K. Uji, A. Ueno, K. Kawai, Contribution of fly ash to the strength development of mortars cured at different temperatures, Construction and Building Materials. 276 (2021) 122191. https://doi.org/10.1016/j.conbuildmat.2020.122191.

[154] G. Xu, X. Shi, Characteristics and applications of fly ash as a sustainable construction material: A state-of-the-art review, Resources, Conservation and Recycling. 136 (2018) 95–109. https://doi.org/10.1016/j.resconrec.2018.04.010.

[155] S. Kang, M. Tyler Ley, Z. Lloyd, T. Kim, Using the Particle Model to predict electrical resistivity performance of fly ash in concrete, Construction and Building Materials. 261 (2020) 119975. https://doi.org/10.1016/j.conbuildmat.2020.119975.

[156] D.V.P. Tran, P. Sancharoen, P. Klomjit, S. Tangtermsirikul, Electrical resistivity and corrosion potential of reinforced concrete: influencing factors and prediction models, Journal of Adhesion Science and Technology. (2020) 1–13. https://doi.org/10.1080/01694243.2020.1750784.

[157] D.-H. Vo, C.-L. Hwang, K.-D. Tran Thi, M.D. Yehualaw, W.-C. Chen, Effect of Fly Ash and Reactive MgO on the Engineering Properties and Durability of High-Performance Concrete Produced with Alkali-Activated Slag and Recycled Aggregate, Journal of Materials in Civil Engineering. 32 (2020) 04020332. https://doi.org/10.1061/(ASCE)MT.1943-5533.0003420.

[158] International Aluminium Institute, Opportunities for use of bauxite residue in special cements, London, 2020.

[159] Y. Wu, B. Lu, T. Bai, H. Wang, F. Du, Y. Zhang, L. Cai, C. Jiang, W. Wang,

Geopolymer, green alkali activated cementitious material: Synthesis, applications and challenges, Construction and Building Materials. 224 (2019) 930–949. https://doi.org/10.1016/j.conbuildmat.2019.07.112.

[160] R. Zhang, S. Zheng, S. Ma, Y. Zhang, Recovery of alumina and alkali in Bayer red mud by the formation of andradite-grossular hydrogarnet in hydrothermal process, Journal of Hazardous Materials. 189 (2011) 827–835. https://doi.org/10.1016/j.jhazmat.2011.03.004.

[161] M.A. Khairul, J. Zanganeh, B. Moghtaderi, The composition, recycling and utilisation of Bayer red mud, Resources, Conservation and Recycling. 141 (2019) 483–498. https://doi.org/10.1016/j.resconrec.2018.11.006.

[162] M. Gräfe, G. Power, C. Klauber, Bauxite residue issues: III. Alkalinity and associated chemistry, Hydrometallurgy. 108 (2011) 60–79. https://doi.org/10.1016/j.hydromet.2011.02.004.

[163] D. Dodoo-Arhin, R.A. Nuamah, B. Agyei-Tuffour, D.O. Obada, A. Yaya, Awaso bauxite red mud-cement based composites: Characterisation for pavement applications, Case Studies in Construction Materials. 7 (2017) 45–55. https://doi.org/10.1016/j.cscm.2017.05.003.

[164] C. Venkatesh, M. Chand, R. Nerella, A State of the Art on Red Mud as a Substitutional Cementitious Material, Annales de Chimie - Science Des Matériaux. 43 (2019) 99–103. https://doi.org/10.18280/acsm.430206.

[165] U. Raghu Babu, B. Kondraivendhan, Influence of bauxite residue (red mud) on corrosion of rebar in concrete, Innovative Infrastructure Solutions. 5 (2020) 108. https://doi.org/10.1007/s41062-020-00356-1.

[166] D.V. Ribeiro, J.A. Labrincha, M.R. Morelli, Effect of the addition of red mud on the corrosion parameters of reinforced concrete, Cement and Concrete Research. 42 (2012) 124–133. https://doi.org/10.1016/j.cemconres.2011.09.002.

[167] Z. Liu, H. Li, Metallurgical process for valuable elements recovery from red mud—A review, Hydrometallurgy. 155 (2015) 29–43. https://doi.org/10.1016/j.hydromet.2015.03.018.

[168] W.T. Salih, W. Yu, X. Dong, W. Hao, Study on stress-strain-resistivity and microscopic mechanism of red mud waste modified by desulphurization gypsum-fly ash under drying-wetting cycles, Construction and Building Materials. 249 (2020) 118772. https://doi.org/10.1016/j.conbuildmat.2020.118772.

[169] G. Li, M. Liu, M. Rao, T. Jiang, J. Zhuang, Y. Zhang, Stepwise extraction of valuable

components from red mud based on reductive roasting with sodium salts, Journal of Hazardous Materials. 280 (2014) 774–780. https://doi.org/10.1016/j.jhazmat.2014.09.005.

[170] A. Dehghani, F. Aslani, Piezoresistive sensing of cementitious composites reinforced with shape memory alloy, steel, and carbon fibres, Construction and Building Materials. 267 (2021) 121046. https://doi.org/10.1016/j.conbuildmat.2020.121046.

[171] E.D. Shumuye, Z. Jun, A Review on Ground Granulated Blast Slag GGBS in Concrete, in: Eighth International Conference On Advances in Civil and Structural Engineering, Institute of Research Engineers and Doctors, 2018: pp. 5–10. https://doi.org/10.15224/978-1-63248-145-0-14.

[172] L. Wang, F. Aslani, Mechanical properties, electrical resistivity and piezoresistivity of carbon fibre-based self-sensing cementitious composites, Ceramics International. (2020). https://doi.org/10.1016/j.ceramint.2020.11.133.

[173] M. Amran, G. Murali, N.H.A. Khalid, R. Fediuk, T. Ozbakkaloglu, Y.H. Lee, S. Haruna, Y.Y. Lee, Slag uses in making an ecofriendly and sustainable concrete: A review, Construction and Building Materials. 272 (2021) 121942. https://doi.org/10.1016/j.conbuildmat.2020.121942.

[174] P. Awoyera, A. Adesina, A critical review on application of alkali activated slag as a sustainable composite binder, Case Studies in Construction Materials. 11 (2019) e00268. https://doi.org/10.1016/j.cscm.2019.e00268.

[175] B.C. Mendes, L.G. Pedroti, C.M.F. Vieira, M. Marvila, A.R.G. Azevedo, J.M. Franco de Carvalho, J.C.L. Ribeiro, Application of eco-friendly alternative activators in alkali-activated materials: A review, Journal of Building Engineering. 35 (2021) 102010. https://doi.org/10.1016/j.jobe.2020.102010.

[176] P.S. Humbert, J. Castro-Gomes, CO2 activated steel slag-based materials: A review, Journal of Cleaner Production. 208 (2019) 448–457. https://doi.org/10.1016/j.jclepro.2018.10.058.

[177] A.C.P. Martins, J.M. Franco de Carvalho, L.C.B. Costa, H.D. Andrade, T.V. de Melo, J.C.L. Ribeiro, L.G. Pedroti, R.A.F. Peixoto, Steel slags in cement-based composites: An ultimate review on characterization, applications and performance, Construction and Building Materials. 291 (2021) 123265. https://doi.org/10.1016/j.conbuildmat.2021.123265.

[178] E.C. Lopes, T.O. da Silva, H.N. Pitanga, L.G. Pedroti, J.M. Franco de Carvalho, G.H. Nalon, G.E.S. de Lima, M.H.R. Rodrigues, Application of electric arc furnace slag for

stabilisation of different tropical soils, International Journal of Pavement Engineering. (2021) 1–12. https://doi.org/10.1080/10298436.2021.1990289.

[179] R. Farahat, M. Eissa, G. Megahed, A. Fathy, S. Abdel-Gawad, M.S. El-Deab, Effect of EAF Slag Temperature and Composition on its Electrical Conductivity, ISIJ International. 59 (2019) 216–220. https://doi.org/10.2355/isijinternational.ISIJINT-2018-507.

[180] G. Faneca, I. Segura, J.M. Torrents, A. Aguado, Development of conductive cementitious materials using recycled carbon fibres, Cement and Concrete Composites. 92 (2018) 135–144. https://doi.org/10.1016/j.cemconcomp.2018.06.009.

[181] C.B.B. Luna, D.D. Siqueira, E.M. Araújo, D.D. de S. Morais, E.B. Bezerra, Toughening of polystyrene using styrene-butadiene rubber (SBRr) waste from the shoe industry, REM - International Engineering Journal. 71 (2018) 253–260. https://doi.org/10.1590/0370-44672017710090.

[182] T. Weber, A. Zanchet, J.S. Crespo, M.G. Oliveira, J.C.M. Suarez, R.C.R. Nunes, Caracterização de artefatos elastoméricos obtidos por revulcanização de resíduo industrial de SBR (copolímero de butadieno e estireno), Polímeros. 21 (2011) 429–435. https://doi.org/10.1590/S0104-14282011005000066.

[183] L.-J. Li, G.-R. Tu, C. Lan, F. Liu, Mechanical characterization of waste-rubber-modified recycled-aggregate concrete, Journal of Cleaner Production. 124 (2016) 325–338. https://doi.org/10.1016/j.jclepro.2016.03.003.

[184] K. Strukar, T. Kalman Šipoš, I. Miličević, R. Bušić, Potential use of rubber as aggregate in structural reinforced concrete element – A review, Engineering Structures. 188 (2019) 452–468. https://doi.org/10.1016/j.engstruct.2019.03.031.

[185] B.S. Thomas, R.C. Gupta, A comprehensive review on the applications of waste tire rubber in cement concrete, Renewable and Sustainable Energy Reviews. 54 (2016) 1323–1333. https://doi.org/10.1016/j.rser.2015.10.092.

[186] X. Shu, B. Huang, Recycling of waste tire rubber in asphalt and portland cement concrete: An overview, Construction and Building Materials. 67 (2014) 217–224. https://doi.org/10.1016/j.conbuildmat.2013.11.027.

[187] A. Siddika, M.A. Al Mamun, R. Alyousef, Y.H.M. Amran, F. Aslani, H. Alabduljabbar, Properties and utilizations of waste tire rubber in concrete: A review, Construction and Building Materials. 224 (2019) 711–731. https://doi.org/10.1016/j.conbuildmat.2019.07.108.

[188] Y. Li, S. Zhang, R. Wang, F. Dang, Potential use of waste tire rubber as aggregate in

cement concrete – A comprehensive review, Construction and Building Materials. 225 (2019) 1183–1201. https://doi.org/10.1016/j.conbuildmat.2019.07.198.

[189] A.M. Aly, M.S. El-Feky, M. Kohail, E.-S.A.R. Nasr, Performance of geopolymer concrete containing recycled rubber, Construction and Building Materials. 207 (2019) 136–144. https://doi.org/10.1016/j.conbuildmat.2019.02.121.

[190] F. Pacheco-Torgal, Y. Ding, S. Jalali, Properties and durability of concrete containing polymeric wastes (tyre rubber and polyethylene terephthalate bottles): An overview, Construction and Building Materials. 30 (2012) 714–724. https://doi.org/10.1016/j.conbuildmat.2011.11.047.

[191] W. Dong, W. Li, G. Long, Z. Tao, J. Li, K. Wang, Electrical resistivity and mechanical properties of cementitious composite incorporating conductive rubber fibres, Smart Materials and Structures. 28 (2019) 085013. https://doi.org/10.1088/1361-665X/ab282a.

[192] W. Dong, W. Li, K. Wang, Z. Luo, D. Sheng, Self-sensing capabilities of cement-based sensor with layer-distributed conductive rubber fibres, Sensors and Actuators A: Physical. 301 (2020) 111763. https://doi.org/10.1016/j.sna.2019.111763.

[193] J. Villarreal, F. Wang, Feasibility Study on Biochar-Treated Expansive Soils, International Journal of Geosynthetics and Ground Engineering. 7 (2021) 27. https://doi.org/10.1007/s40891-021-00277-8.

[194] A.M.P. Madhubashani, D.A. Giannakoudakis, B.M.W.P.K. Amarasinghe, A.U. Rajapaksha, P.B.T. Pradeep Kumara, K.S. Triantafyllidis, M. Vithanage, Propensity and appraisal of biochar performance in removal of oil spills: A comprehensive review, Environmental Pollution. 288 (2021) 117676. https://doi.org/10.1016/j.envpol.2021.117676.

[195] K.-H. Tan, T.-Y. Wang, Z.-H. Zhou, Y.-H. Qin, Biochar as a Partial Cement Replacement Material for Developing Sustainable Concrete: An Overview, Journal of Materials in Civil Engineering. 33 (2021) 03121001. https://doi.org/10.1061/(ASCE)MT.1943-5533.0003987.

[196] A. Sirico, P. Bernardi, C. Sciancalepore, F. Vecchi, A. Malcevschi, B. Belletti, D. Milanese, Biochar from wood waste as additive for structural concrete, Construction and Building Materials. 303 (2021) 124500. https://doi.org/10.1016/j.conbuildmat.2021.124500.

[197] V. Benedetti, F. Patuzzi, M. Baratieri, Gasification Char as a Potential Substitute of Activated Carbon in Adsorption Applications, Energy Procedia. 105 (2017) 712–717. https://doi.org/10.1016/j.egypro.2017.03.380.

[198] B. Bhardwaj, P. Kumar, Waste foundry sand in concrete: A review, Construction and Building Materials. 156 (2017) 661–674. https://doi.org/10.1016/j.conbuildmat.2017.09.010.

[199] H. Wang, X. Gao, R. Wang, The influence of rheological parameters of cement paste on the dispersion of carbon nanofibers and self-sensing performance, Construction and Building Materials. 134 (2017) 673–683. https://doi.org/10.1016/j.conbuildmat.2016.12.176.

[200] A. Maria Cruz, P. Javier, Self-Compacted Concrete with Self-Protection and Self-Sensing Functionality for Energy Infrastructures, Materials. 13 (2020) 1106. https://doi.org/10.3390/ma13051106.

[201] S. Dong, B. Han, J. Ou, Z. Li, L. Han, X. Yu, Electrically conductive behaviors and mechanisms of short-cut super-fine stainless wire reinforced reactive powder concrete, Cement and Concrete Composites. 72 (2016) 48–65. https://doi.org/10.1016/j.cemconcomp.2016.05.022.

[202] W. Dong, W. Li, K. Wang, K. Vessalas, S. Zhang, Mechanical strength and self-sensing capacity of smart cementitious composite containing conductive rubber crumbs, Journal of Intelligent Material Systems and Structures. 31 (2020) 1325–1340. https://doi.org/10.1177/1045389X20916788.

[203] L. Wang, F. Aslani, Electrical resistivity and piezoresistivity of cement mortar containing ground granulated blast furnace slag, Construction and Building Materials. 263 (2020) 120243. https://doi.org/10.1016/j.conbuildmat.2020.120243.

[204] M. Ipek, Analysis of Usability of Waste Erosion Wires as Fiber in Reactive Powder Concrete, Journal of Polytechnic. 20 (2017) 451–457. https://doi.org/10.2339/2017.20.2.

[205] X. Quan, S. Wang, K. Liu, J. Xu, K. Zhang, N. Zhao, B. Li, Influence of iron ore tailings by-product on the mechanical and electrical properties of carbon fiber reinforced cement-based composites, Journal of Building Engineering. 45 (2022) 103567. https://doi.org/10.1016/j.jobe.2021.103567.

[206] W. Dong, Y. Guo, Z. Sun, Z. Tao, W. Li, Development of piezoresistive cement-based sensor using recycled waste glass cullets coated with carbon nanotubes, Journal of Cleaner Production. 314 (2021) 127968. https://doi.org/10.1016/j.jclepro.2021.127968.

[207] S. Kuriakose, K. Mohan, M.. Shunmugam, Data mining applied to wire-EDM process, Journal of Materials Processing Technology. 142 (2003) 182–189. https://doi.org/10.1016/S0924-0136(03)00596-X.

[208] N. Zhang, B. Tang, X. Liu, Cementitious activity of iron ore tailing and its utilization in

cementitious materials, bricks and concrete, Construction and Building Materials. 288 (2021) 123022. https://doi.org/10.1016/j.conbuildmat.2021.123022.

[209] M. Gou, L. Zhou, N.W.Y. Then, Utilization of tailings in cement and concrete: A review, Science and Engineering of Composite Materials. 26 (2019) 449–464. https://doi.org/10.1515/secm-2019-0029.

[210] T. HK, N. Hossiney, A short review on environmental impacts and application of iron ore tailings in development of sustainable eco-friendly bricks, Materials Today: Proceedings. (2021). https://doi.org/10.1016/j.matpr.2021.09.522.

[211] J. Zhao, K. Ni, Y. Su, Y. Shi, An evaluation of iron ore tailings characteristics and iron ore tailings concrete properties, Construction and Building Materials. 286 (2021) 122968. https://doi.org/10.1016/j.conbuildmat.2021.122968.

[212] W. Dong, W. Li, Z. Tao, A comprehensive review on performance of cementitious and geopolymeric concretes with recycled waste glass as powder, sand or cullet, Resources, Conservation and Recycling. 172 (2021) 105664. https://doi.org/10.1016/j.resconrec.2021.105664.

[213] Y. Jiang, T.-C. Ling, K.H. Mo, C. Shi, A critical review of waste glass powder - Multiple roles of utilization in cement-based materials and construction products, Journal of Environmental Management. 242 (2019) 440–449. https://doi.org/10.1016/j.jenvman.2019.04.098.

[214] E.T. Bueno, J.M. Paris, K.A. Clavier, C. Spreadbury, C.C. Ferraro, T.G. Townsend, A review of ground waste glass as a supplementary cementitious material: A focus on alkali-silica reaction, Journal of Cleaner Production. 257 (2020) 120180. https://doi.org/10.1016/j.jclepro.2020.120180.

[215] M.A. Keerio, S.A. Abbasi, A. Kumar, N. Bheel, K. ur Rehaman, M. Tashfeen, Effect of Silica Fume as Cementitious Material and Waste Glass as Fine Aggregate Replacement Constituent on Selected Properties of Concrete, Silicon. (2020). https://doi.org/10.1007/s12633-020-00806-6.

[216] S. Zhang, C. Saha, Y. Yang, S. Bhattacharya, R. Xiao, Use of Fe2O3-Containing Industrial Wastes As the Oxygen Carrier for Chemical-Looping Combustion of Coal: Effects of Pressure and Cycles, Energy & Fuels. 25 (2011) 4357–4366. https://doi.org/10.1021/ef2011595.

[217] K. Yin, A. Ahamed, G. Lisak, Environmental perspectives of recycling various combustion ashes in cement production – A review, Waste Management. 78 (2018) 401–416. https://doi.org/10.1016/j.wasman.2018.06.012.

[218] C. Lam, J. Barford, G. McKay, Utilization of Incineration Waste Ash Residues in Portland Cement Clinker, Chemical Engineering Transactions. 21 (2010) 757–762.

[219] E. Allegrini, A. Maresca, M.E. Olsson, M.S. Holtze, A. Boldrin, T.F. Astrup, Quantification of the resource recovery potential of municipal solid waste incineration bottom ashes, Waste Management. 34 (2014) 1627–1636. https://doi.org/10.1016/j.wasman.2014.05.003.

[220] M. Cyr, M. Coutand, P. Clastres, Technological and environmental behavior of sewage sludge ash (SSA) in cement-based materials, Cement and Concrete Research. 37 (2007) 1278–1289. https://doi.org/10.1016/j.cemconres.2007.04.003.

[221] R.I. Sugatri, Y.C. Wirasadewa, K.E. Saputro, E.Y. Muslih, R. Ikono, M. Nasir, Recycled carbon black from waste of tire industry: thermal study, Microsystem Technologies. 24 (2018) 749–755. https://doi.org/10.1007/s00542-017-3397-6.

[222] P.F. Andrade, T.F. Azevedo, I.F. Gimenez, A.G.S. Filho, L.S. Barreto, Conductive carbon–clay nanocomposites from petroleum oily sludge, Journal of Hazardous Materials. 167 (2009) 879–884. https://doi.org/10.1016/j.jhazmat.2009.01.070.

[223] N. Konikkara, L.J. Kennedy, U. Aruldoss, J.J. Vijaya, Electrical Conductivity Studies of Nanoporous Carbon Derived from Leather Waste: Effect of Pressure, Temperature and Porosity, Journal of Nanoscience and Nanotechnology. 16 (2016) 8829–8838. https://doi.org/10.1166/jnn.2016.11652.

[224] P. Dong, T. Maneerung, W.C. Ng, X. Zhen, Y. Dai, Y.W. Tong, Y.-P. Ting, S.N. Koh, C.-H. Wang, K.G. Neoh, Chemically treated carbon black waste and its potential applications, Journal of Hazardous Materials. 321 (2017) 62–72. https://doi.org/10.1016/j.jhazmat.2016.08.065.

[225] P.A. Advincula, D.X. Luong, W. Chen, S. Raghuraman, R. Shahsavari, J.M. Tour, Flash graphene from rubber waste, Carbon. 178 (2021) 649–656. https://doi.org/10.1016/j.carbon.2021.03.020.

[226] R. Striani, E. Stasi, A. Giuri, M. Seiti, E. Ferraris, C. Esposito Corcione, Development of an Innovative and Green Method to Obtain Nanoparticles in Aqueous Solution from Carbon-Based Waste Ashes, Nanomaterials. 11 (2021) 577. https://doi.org/10.3390/nano11030577.

[227] I. Rhee, J.S. Lee, Y.A. Kim, J.H. Kim, J.H. Kim, Electrically conductive cement mortar: Incorporating rice husk-derived high-surface-area graphene, Construction and Building Materials. 125 (2016) 632–642. https://doi.org/10.1016/j.conbuildmat.2016.08.089.

[228] I. Rhee, Y.A. Kim, G.-O. Shin, J.H. Kim, H. Muramatsu, Compressive strength

sensitivity of cement mortar using rice husk-derived graphene with a high specific surface area, Construction and Building Materials. 96 (2015) 189–197. https://doi.org/10.1016/j.conbuildmat.2015.08.016.

[229] O.M. Dunens, K.J. MacKenzie, A.T. Harris, Synthesis of Multiwalled Carbon Nanotubes on Fly Ash Derived Catalysts, Environmental Science & Technology. 43 (2009) 7889–7894. https://doi.org/10.1021/es901779c.

[230] K. Mugadza, P.G. Ndungu, A. Stark, V.O. Nyamori, Conversion of residue biomass into value added carbon materials: utilisation of sugarcane bagasse and ionic liquids, Journal of Materials Science. 54 (2019) 12476–12487. https://doi.org/10.1007/s10853-019-03800-5.

[231] C. Zhuo, Y.A. Levendis, Upcycling waste plastics into carbon nanomaterials: A review, Journal of Applied Polymer Science. 131 (2014) n/a-n/a. https://doi.org/10.1002/app.39931.

[232] J. Deng, Y. You, V. Sahajwalla, R.K. Joshi, Transforming waste into carbon-based nanomaterials, Carbon. 96 (2016) 105–115. https://doi.org/10.1016/j.carbon.2015.09.033.

[233] P. Samaddar, Y.S. Ok, K.-H. Kim, E.E. Kwon, D.C.W. Tsang, Synthesis of nanomaterials from various wastes and their new age applications, Journal of Cleaner Production. 197 (2018) 1190–1209. https://doi.org/10.1016/j.jclepro.2018.06.262.

[234] B. Prasad, C. Ghosh, A. Chakraborty, N. Bandyopadhyay, R.K. Ray, Adsorption of arsenite (As3+) on nano-sized Fe2O3 waste powder from the steel industry, Desalination. 274 (2011) 105–112. https://doi.org/10.1016/j.desal.2011.01.081.

[235] J. Yu, G. Kim, T. Kim, J. Kim, Fabrication of Nano-Sized Powders from Waste Solution by Spray Pyrolysis Process, MATERIALS TRANSACTIONS. 46 (2005) 1695–1700. https://doi.org/10.2320/matertrans.46.1695.

[236] J. Tang, Y. Pei, Q. Hu, D. Pei, J. Xu, The Recycling of Ferric Salt in Steel Pickling Liquors: Preparation of Nano-sized Iron Oxide, Procedia Environmental Sciences. 31 (2016) 778–784. https://doi.org/10.1016/j.proenv.2016.02.071.

[237] G. Bhattacharya, S.J. Fishlock, J.A. McLaughlin, S.S. Roy, Metal-oxide nanomaterials recycled from E-waste and metal industries: a concise review of applications in energy storage, catalysis, and sensing, International Journal of Energy Research. 45 (2021) 8091–8102. https://doi.org/10.1002/er.6336.

[238] N. Cardona-Vivas, M.A. Correa, H.A. Colorado, Multifunctional composites obtained from the combination of a conductive polymer with different contents of primary battery

waste powders, Sustainable Materials and Technologies. 28 (2021) e00281. https://doi.org/10.1016/j.susmat.2021.e00281.

[239] H.B. Birgin, A. D'Alessandro, S. Laflamme, F. Ubertini, Innovative Carbon-Doped Composite Pavements with Sensing Capability and Low Environmental Impact for Multifunctional Infrastructures, Journal of Composites Science. 5 (2021) 192. https://doi.org/10.3390/jcs5070192.

3 EVALUATION OF THE EFFECTS OF SONICATION ENERGY ON THE DISPERSION OF CARBON BLACK NANOPARTICLES (CBN) AND PROPERTIES OF SELF-SENSING CEMENTITIOUS COMPOSITES

DOI: 10.1016/j.jmrt.2025.03.122

Abstract: *Good dispersion of nanomaterials within cementitious matrices provides cementitious nanocomposites with stable and replicable properties. Improved dispersion also increases the number of conductive paths and improves the material's mechanical properties. Despite this, there has been no previous research investigating the effects of variation of sonication energy on the electromechanical properties of self-sensing mortars. Thus, the aim of this study was to carry out a combined evaluation of the electromechanical and rheological behavior of cementitious sensors, supported by a comprehensive analysis of the dispersion quality of nanosuspensions using four different techniques: Dynamic Light Scattering (DLS), Zeta Potential, Ultraviolet-visible Spectroscopy (UV-VIS) and Field Emission Gun – Scanning Electron Microscope (FEG-SEM). The electromechanical and rheological behavior of the Cement Composite Nanomodified Sensors (CCNSs) performed best in the sonication energy range of 120 J/mL to 240 J/mL. The zeta potential, UV-VIS absorption and DLS measurements used to analyze the nanosuspensions enabled a satisfactory assessment of the degree of CBN dispersion. All results suggested that sonication energies of around 240 J/mL were responsible for producing nanosuspensions with the most efficient dispersions. Sonication energies of this magnitude were also able to optimize the electromechanical and rheological characteristics of the CCNSs. The main contributions originated from this work are related to the combined evaluation of the mechanical, electrical, and rheological behavior of mortars produced with CBN, the analysis of the quality of the CBN dispersion provided by different sonication energy levels and identification of the optimum sonication energy for the production of CCNS containing CBN.*

.

Keywords: *self-sensing cementitious materials, carbon black nanoparticles, nanoparticle dispersion, sonication energy, piezoresistivity*

3.1 INTRODUCTION

Smart cementitious composites have been produced by adding functional nanomaterials to their matrices, making them capable of monitoring strains, stresses and damage in building structures [1–3]. Cementitious materials with self-sensing capabilities provide an alternative to traditional Structural Health Monitoring (SHM) systems, simplifying the design of SHM architectures and allowing better integration between the sensors and the structure [2,4,5].

Several studies have focused on investigating the mechanical and sensing properties of functionalized composites through the incorporation of different types of conductive materials [6–10]. In this context, Carbon Black Nanoparticles (CBN) have been the subject of interest for many researchers. CBN are small spheres with diameters ranging from approximately 13 nm to 100 nm, which usually join together to form aggregates with sizes of 200 to 1000 nm. These aggregates tend to aggregate due to Van der Waals forces, which leads to the formation of CBN agglomerates with sizes greater than 1000 nm [11]. CBN have several characteristics that make them relevant for application in the development of self-sensing cement composites, such as small average particle size, high specific surface area, low electrical resistivity and lower production costs compared to other materials with similar characteristics [6,12,13].

Due to the tendency for nanomaterials to agglomerate, their appropriate dispersion within the cementitious matrix is an essential procedure for obtaining self-sensing composites with stable and reproducible electrical responses, as well as reducing the amount of mechanical energy required when mixing with the other constituent materials [14]. Improved dispersion also increases the number of conductive paths available and enhances the material's electrical and mechanical properties [15–17]. Uniform dispersion of the conductive filler is essential to ensure the formation of a continuous and homogeneous conductive network throughout the cementitious matrix [18].

Among the main dispersion methods, sonication is one of the most widely used techniques [19]. Sonication acts by applying ultrasonic waves into the nanosuspensions, generating high-frequency mechanical vibrations. These vibrations create cavitation bubbles that collapse with significant energy, causing shear stresses to the nanoparticle clusters and breaking them up into smaller aggregates. [20]. Such procedure has already been used in different studies [21–23] to enable the adsorption of different surfactants on nanostructures, breaking up the agglomerates by steric or electrostatic repulsion mechanisms. In this way, the sonication process has proved effective for dispersing different types of nanomaterials

incorporated into cementitious matrices, such as carbon nanotubes [24–26], nanofibrillated cellulose [27] and graphene nanoplatelets [28].

Previous studies have sought to identify suitable contents of CBN to improve the piezoresistive response of cementitious materials [29–32], but have not yet evaluated the optimization of the dispersion of these types of nanoparticles to improve the sensing abilities of nanomodified cementitious composite sensors (NCCS). Furthermore, determining an optimum sonication energy is a difficult task, mainly because research on this subject is diffuse and even incomplete [19]. The effects of sonication energy on the electromechanical properties of self-sensing mortars produced with CBN remain unknown. No previous research has investigated the optimum sonication energy applied to a CBN nanosuspension, in order to obtain composites with low electrical resistivity and good piezoresistive response, without significant losses in mechanical properties.

Therefore, this study has investigated the effects of sonication energy on the dispersion of CBN and its impact on the properties of CCNS. The following contributions originated from this work: (i) combined evaluation of the electromechanical and rheological behavior of mortars produced with CBN dispersed with different levels of sonication energy; (ii) analysis of the quality of the CBN dispersion provided by different sonication energy levels, using a combination of four different microscale evaluation techniques; and (iii) identification of the optimum sonication energy for the production of CCNS containing CBN.

3.2 MATERIALS AND METHODS

3.2.1. Materials

Portland cement CP V-ARI, provided by Holcim, equivalent to ASTM C150 Type III Portland cement, was used in this study. Quartz natural sand was used in this work, with a specific mass of 2.64 g/cm³ and a maximum diameter of 2.38 mm. CBN type N234 (Birla Carbon) was used as the conductive nanofiller, with an average particle size of 20 nm and a specific surface area of 120 m²/g. In order to adjust the workability of the mixtures and improve the stability of the nanoparticles dispersion, a superplasticizer additive based on polycarboxylate ether (PCE), provided by MC-Bauchemie, with a density of 1.12 g/cm³ was selected. In addition, distilled water with a pH of 6.5 was used in all production stages.

3.2.2. Production of specimens

The sonication energies investigated in this research cover a broad range, encompassing different values reported in previous studies [2,33–36]. Nanomodified mortars were produced with nanosuspensions prepared using a probe-type sonicator with an ultrasonic frequency of 20 kHz and a power of 50 W. Five different sonication energies were applied to produce different series of specimens, as shown in Table 1. Due to the high degree of agglomeration of the nanoparticles, producing specimens without the sonication process was not feasible. Thus, it was necessary to apply a minimum amount of energy to allow appropriate mixing procedures. Table 1 also shows the mix proportions of raw materials used to produce the self-sensing mortars. All series were produced with a sand/cement ratio of 1.95 (by mass), water/cement ratio of 0.56 and a CBN content of 9% (by weight of cement).

Table 1 – Variation in sonication energy and mix proportions

Series	Sonication energy (J/mL)	Mix proportions (kg/m³)				
		Cement	Sand	Water	CBN	PCE
T020	20	585.75	1142.26	326.91	52.72	21.09
T060	60					
T120	120					
T240	240					
T480	480					

The nanosuspension was prepared by mixing CBN, water and PCE and applying the sonication time compatible with the energy of each different series. The nanosuspension was then taken to a mechanical planetary mixer where the cement and sand were added and mixed for around 10 minutes. In order to assess the rheological aspects of the mixture, a portion of the material was used to carry out the mini-flow test, using a Kantro-type truncated cone mold [37,38].

Then, the fresh mortar was poured into oiled molds and then compacted on a vibrating table for 10 seconds. In composites prepared for the electromechanical tests, two copper electrodes (1.4 cm x 3.0 cm x 0.1 cm) were embedded in the central region, about 0.8 cm apart. The molds were placed in a moist chamber with a relative humidity higher than 85% and ambient temperature of 20 ± 5 ºC. After 72 hours, the specimens were demolded and left to cure in the moist chamber for 28 days. For each of the series, three prisms of self-sensing mortars with dimensions of 2.5 cm x 2.5 cm x 7.5 cm (with electrodes) were produced for the

electrical resistivity and piezoresistive tests, three cubes with a 2.5 cm edge (without electrodes) for the compressive strength tests and one 3.5 cm x 7.0 cm cylinder for microstructural analysis.

3.2.3. Electromechanical Analysis

In order to eliminate the possible effects of ionic conduction during the tests, the specimens were dried in an oven at approximately 60 ºC for 72 hours, after which they were removed and cooled to room temperature [39,40]. In the sequence, two different electrical tests were carried out on the composites: a direct current (DC) test to assess electrical resistivity and a biphasic direct current (B-CC) test, accompanied by the application of mechanical loading cycles, to measure the piezoresistivity of the composites.

The specimens were connected in series to a 1 kΩ (R_{ref}) reference resistor. In the DC test, a constant voltage of 5 V was applied using an Arduino Mega board, model 2560 R3. In the B-CC test, to mitigate the effects of polarization, the same board was used to generate a periodic signal in the form of a square wave of ±5 V and a frequency of 6 Hz [5,41].

The voltage drops between the self-sensing composite (U_m) and the reference resistor (U_{ref}) were measured using a virtual instrument developed in Labview, in addition to two NI-9219 modules connected to an NI cDAQ-9178 data acquisition system. Using Equations 1 and 2, the electric current in the circuit (i) and the composite's electric resistance (R_m) were determined. In the B-CC test, i and R_m were obtained using the values of U_m and U_{ref} measured at 80% of the positive constant range of the generated square wave [41–43]. Using the distance between the electrodes (L) and their effective area in contact with the mortar (A), the electrical resistivity was calculated using Equation 3.

Equation 1
$$i = \frac{U_{ref}}{R_{ref}}$$

Equation 2
$$R_m = \frac{U_m}{i}$$

Equation 3
$$\rho = \frac{R_m \ A}{L}$$

Evaluation of the piezoresistive behavior of self-sensing mortars was carried out using compression cycles in a universal testing machine EMIC DL-60000, with a constant loading

rate of 0.50 MPa/s. The longitudinal strains were recorded using EMIC clip-gauges installed symmetrically in relation to the central axis of the mortar prisms. Relative changes in electrical resistivity (FCR) due to loading/unloading cycles were obtained using the B-CC method. The Gauge factor (GF) of the self-sensing mortars was calculated as the angular coefficient obtained from the FCR vs Strain curve.

At the beginning of the test, the specimens were positioned in the testing machine between electrically insulating films and then a preload was applied. The composites were submitted to three loading/unloading cycles with amplitude corresponding to 30% of the predicted rupture load. In the next stage, a progressive loading cycle was carried out with three levels, applying compressive loads of 10%, 20% and 30% of the estimated compressive strength. Finally, the specimens were subjected to rupture in order to determine their compressive strength.

The experimental results for electrical resistivity, Gauge factor and compressive strength were subjected to the Grubbs test at a 5% significance level to check for outliers in the sample data.

3.2.4. Rheological Analysis

In addition to the mini-flow test with a Kantro-type truncated cone mentioned in section 3.2.2, the rheological characteristics of the material were assessed by means of viscosity measurements, using a Fann model 35A viscometer. Due to the limitations of the equipment used in this research, the evaluation could not be carried out on mortars. Therefore, it was necessary to remove the sand from the mixtures and carry out the test on cement pastes. However, the ratio between the materials mentioned in section 3.2.2 was not altered in order to establish a better correlation between the tests. The test was carried out in an air-conditioned room with a relative humidity of 60 ± 3% and an ambient temperature of 21 ± 1 ºC. Approximately 500 mL of paste were prepared for each of the series, following the same procedures described in section 3.2.2 for producing the mortars.

The paste was poured in the equipment jug until it reached the pre-established volume (350 mL) in this container. The equipment was then driven at a speed of 200 RPM and once the reading had stabilized, the torque was recorded. Torque measures for the speeds of 100 RPM, 6 RPM and 3 RPM, were also carried out. The Bingham model was used to describe the rheological behavior of the pastes , and the analysis was carried out using the slope of the Torque vs Angular Velocity curves (correlated with plastic viscosity) and the point at which the curves intercepted the ordinate axis (correlated with yield strength) [44].

3.2.5. Analysis of CBN dispersion quality

Different techniques were used for the evaluation of the dispersion quality of nanosuspensions of distilled water, CBN and PCE used in the production of cementitious composites. Initially, a mass of 0.200 g of PCE was added to 100.000 g of water in a beaker. Next, a mass of 0.025 g of CBN was placed in a test tube. Then 5.000 g of the PCE solution and 19.975 g of water were added to the test tube. This resulted in a mixture with a mass of 25.000 g and a PCE/CBN ratio equal to that used in the production of all mortars (Table 1).

Finally, the mixture was subjected to five successive sonication processes that corresponded, cumulatively, to the five different sonication energy levels (in J/mL) presented in Table 1. In order to enable the application of the techniques described below, the samples had to be diluted 125 times. To do this, an aliquot of just 0.200 mL was removed from the nanosuspension after the sonication process, and added to another capped test tube containing 25 mL of water. After manually shaking the test tube, the diluted sample was subjected to the tests described below:

Dynamic Light Scattering (DLS)

The DLS technique was used to determine the hydrodynamic radius and the size distribution of the CBN aggregates for each of the sonication energies. A Brookhaven Instruments DLS spectrometer with a 522-channel Turbocorr correlator, 90º angular positioning and a 75 mW HeNe laser (632.8 nm) was used.

Ultraviolet-visible Spectroscopy (UV-VIS)

UV-VIS analysis was used to determine the light absorbed by the CBN for the different dispersions. A HORIBA FluoroMax UV-VIS spectrometer was used, with the monochromator selecting a lamp with a wavelength of 350 nm, in the range between 250 nm and 750 nm. In order to eliminate the PCE effects on the CBN absorption spectrum, reference samples were prepared containing only distilled water and the additive, subjected to the same sonication energies applied to the samples containing PCE. By using the equipment's own software, this undesirable effect was subtracted from the spectrum used in this work.

Zeta Potential

A Malvern Zetasizer Nano ZS Zeta Potential Analyzer was used to assess the stability of the suspensions. Water was selected as the dispersant, with a dielectric constant of 78.5 and a viscosity of 0.8872 cP. As the samples could be considered aqueous media with a moderate

concentration of electrolytes, Smoluchowski's approximation (1.5) was adopted for the Henry Function. The Zeta Potential (ζ) adopted was obtained from the average of three determinations for each of the samples analyzed.

Field Emission Scanning Electron Microscopy (FEG-SEM)

After the curing period, the specimens produced for microstructural analysis were cut using a disk saw in order to remove a slice with a thickness of approximately 0.4 cm. This slice was extracted from the central portion of the cylinder in order to obtain a more representative sample of the material [45]. In order to interrupt the mortar hydration process, the slices were immersed in isopropanol and stored in individual airtight containers.

To carry out the microscopy test, the slices were removed from the isopropanol and a small cube with an edge of about 0.4 cm was immediately extracted from the central portion. This sample was placed on a stub prepared with carbon conductive tape and then sputter-coated with a thin layer of gold, using a Quorum Q150RS equipment. A silver-based conductive paste was also applied to optimize the sample conductivity and consequently, the quality of the obtained images. The samples' secondary electrons images were obtained from a Field Emission Scanning Electron Microscope (FEG-SEM) TESCAN MIRA, with 1.2 nm resolution for 30 keV. This analysis aimed to qualitatively assess the effects of sonication energy on the interaction between CBN and the hardened cementitious matrix.

3.3 RESULTS AND DISCUSSION

3.3.1. Electromechanical Behavior

Figure 1 shows the correlation between electrical resistivity and compressive strength as a function of the variation in sonication energy, whereas Table 2 shows the average values obtained for the electromechanical properties. The Grubbs test was applied to check for outliers in the sample data used to construct Table 2. However, for a significance level of 5%, no influential points were detected in the sample.

Figure 1 – Correlation between electrical resistivity and compressive strength as a function of sonication energy.

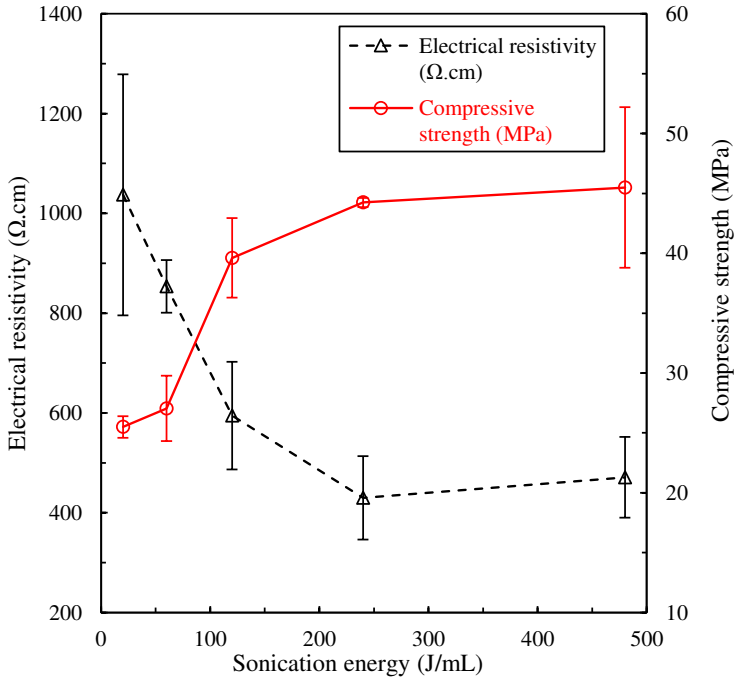

The electrical resistivity values were of the same order of magnitude as other reported in previous studies that also investigated cementitious matrices with self-sensing properties [46,47]. The electrical resistivity averages ranged from 1037.08 Ω.cm to 429.87 Ω.cm with the increase of sonication energy, which represented a reduction of approximately 60%. However, the electrical resistivity results showed a high degree of variability, especially the T020 series, which presented a coefficient of variation (percentage ratio of standard deviation to the mean) of 23.28% (Table 2). This high variation in results may be related to the fact that lower sonication energies were not able to break down the CBN aggregates in sufficient quantities to guarantee the reproducibility of the conductive network in the different samples of this series. This issue will be dealt with in greater detail in section 3.3.3 (Analysis of CBN dispersion quality).

The average compressive strength increased by more than 70% from the T020 series to the T480 series. For this property, the highest coefficient of variation occurred in the T480 series: 14.74% (Table 2). The inadequate workability identified in the mini-flow test may be the cause of the greater dispersion of the results for this series. Inappropriate plasticity during the molding process may cause severe defects in the cement matrix, with a direct impact on the mechanical properties of the material. This discussion will be done in a more appropriate way in section 3.3.2 (Rheological behavior).

Table 2 – CCNS electromechanical properties

Series	Sonication energy (J/mL)	Electrical resistivity (Ω.cm)		Compressive strength (MPa)		Gauge factor	
		Average	Standard deviation	Average	Standard deviation	Average	Standard deviation
T020	20	1037.08	241.40	25.49	0.90	107.00	51.45
T060	60	853.72	52.79	27.04	2.73	134.00	28.16
T120	120	594.60	107.96	39.61	3.32	88.00	9.17
T240	240	429.87	83.79	44.24	0.39	161.33	31.01
T480	480	470.96	80.74	45.49	6.71	155.00	45.71

The relations between FCR and strain verified in the piezoresistive tests of the composites are shown in Figure 2. To better visualize and compare the results, the data obtained from the three replicates (S1, S2 and S3) of each series were plotted together (S1 – Blue; S2 – Orange; S3 – Green), using the same scale of horizontal and vertical axes for all graphs. The tests were conducted within the elastic-linear regime and the electrical response showed good repeatability and a low level of hysteresis. To better interpret the piezoresistive response, linear regression models were fitted to the data set for each FCR vs. Strain curve, with the determination coefficients (R^2) also presented in Figure 2. The GF values shown in Table 2 were taken as the angular coefficient of the regression models. The linear regression models showed excellent correlation with the sample data. Then, it was not necessary to use more complex regression models as reported in other works in the literature [48–50].

The highest value for R^2 (0.9976) was observed in the T060-S1 and T240-S1 composites. However, the T240 series presented a wider range of FCR values for each different level of strain and, consequently, an average GF (Table 2) around 17% higher than the T060 series. The T020, T060 and T120 series reached similar levels of FCR. The T020 series showed the highest standard deviation, possibly due to the low sonication energy applied. On the other hand, the T120 series presented the lowest standard deviation in GF values, but reached the highest strains, which implied a lower GF.

Figure 2 – Relationship between FRC and compressive strain (Color coding: S1 - Blue; S2 - Orange; S3 - Green): (A) T020; (B) T060; (C) T120; (D) T240; (E) T480.

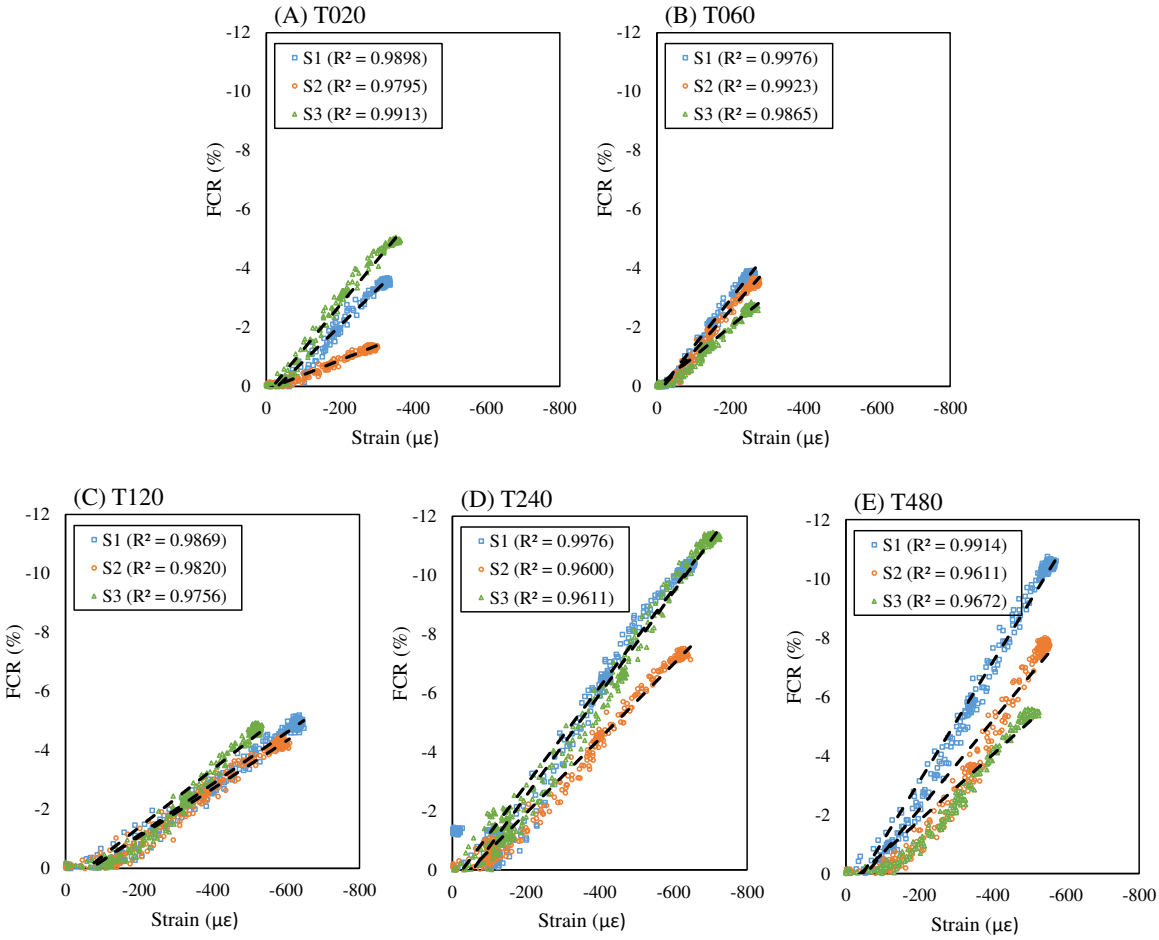

The correlation between electrical resistivity and GF as a function of sonication energy is shown in Figure 3. The average values obtained for GF ranged from 88.00 (T120) to 161.33 (T240), and are in line with those found by other authors [5,13,51–53]. In the range of sonication energy from 20 J/mL to 60 J/mL, the increase in energy caused a drop in the average electrical resistivity and an increase in the average GF, with the coefficient of variation of the GF of the T020 series being around 48%. On the other hand, increasing the sonication energy from 240 J/mL to 480 J/mL did not lead to significant changes in the electrical resistivity and GF values, and the coefficient of variation for GF was 19.22% for the T240 series and 29.49% for the T480 series. The more pronounced dispersion of the data has already been discussed in this section and will be dealt with in more depth in later sections.

Figure 3 – Correlation between electrical resistivity and Gauge factor as a function of sonication energy.

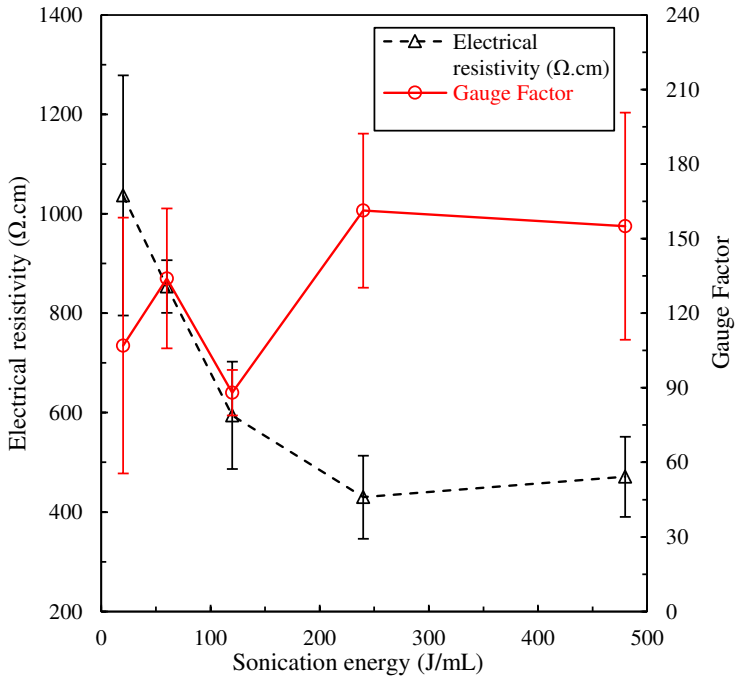

For the sonication energy of 120 J/mL (T120) an unexpected reduction of average GF was observed, in comparison to the previous series (T060). On the other hand, the T120 series had the lowest coefficient of variation (10.41%) for the GF among all the analyzed series. This apparently anomalous response may be associated with changes in the predominant conduction mechanism caused by the increase in sonication energy and consequent reduction in the size of the CBN aggregates and their better dispersion in the cementitious matrix. Taking into consideration the high standard deviation associated with the GF results in the T020 series, it is possible to notice that there was no relevant change in the sensing ability of the composites when the sonication energy increased from 20 J/mL to 120 J/mL. On the contrary, a significant percentual increase on the average value of GF (approximately 83%) was observed when the sonication energy increased from 120 J/mL to 240 J/mL. Therefore, the results suggest that the sonication energy of 240 J/mL was responsible for the breaking up of a greater amount of CBN aggregates, and, consequently, by the appearance of as many tunneling gaps as possible between adjacent nanoparticles, which increased the GF [54]. In other words, the sonication energy of 240 J/mL apparently optimized the quality of the dispersion, which tends to increase electronic conduction by quantum tunneling and improve the piezoresistive behavior of the material. The increase in the sonication energy from 240 J/mL to 480 J/mL did not cause a significant change in the GF and electrical resistivity values, which suggests that the maximum possible level of CBN dispersion had already been provided by the 240 J/mL energy.

It is worth mentioning that the maximum strain values observed in the piezoresistive tests increased with the sonication time. This is because the compressive strength of the composites also increased with the sonication time, as shown in Figure 1. As the loading amplitude of the loading/unloading cycles used in the piezoresistive tests was approximately 30% of the estimated strength of the material, it was to be expected that stronger composites would be subjected to greater compressive load amplitudes and, consequently, would show greater compressive strain, as shown in Figure 2.

The results of the electromechanical tests indicate that reducing the size of the CBN aggregates generally improves the sensing properties of the CCNS. Sonication caused an increase in the free surface area of the CBN aggregates, an improvement in the quantum tunneling conduction mechanisms and a densification of the cementitious matrix. The quality of the piezoresistive response suggests that electronic conduction (quantum tunneling and contact conduction) was the dominant electron transport mechanism in the mortars. The good quality of this response is directly related to the adequate dispersion of the CBN in the cementitious matrix [5,53].

The electromechanical behavior of the CCNS was highly influenced by varying the sonication energy. For lower sonication energy ranges (20 J/mL to 120 J/mL), the poorer dispersion quality had a negative impact on the piezoresistive and sensing behavior of the mortars, especially for the T020 and T060 series. For higher energy ranges (240 J/mL to 480 J/mL), excellent mechanical and sensing performance was observed, but the T480 series showed that excessive sonication energy has a negative effect on the material's mechanical properties. Thus, the analysis of the electromechanical behavior of CCNS suggests that the sonication energy range of 120 J/mL to 240 J/mL is the most suitable for the production of these composites.

3.3.2. Rheological Behavior

The Torque vs. Angular Velocity curves of the pastes and the rheological behavior as a function of the variation in sonication energy are shown in Figure 4. In this analysis, it was considered that the pastes and mortars behave according to the Bingham model [55,56]. In Figure 4A, the slope of the Torque vs. Angular Velocity curves is directly related to the plastic viscosity of the material, and the point of intercept of the ordinate axis is correlated with the yield stresses [44].

The effects of varying the sonication energy were evident in the change in the angular coefficient of the Torque vs. Angular Velocity curves (Figure 4A). The T020 series, which received the lowest sonication energy (20 J/mL), showed the curve with the lowest slope, which suggests a lower plastic viscosity. On the T240 and T480 series, on the other hand, the increase in sonication energy made the material significantly more viscous. The angular coefficient of the T240 and T480 series was about 4 times higher than the one observed in the T020 series, which is possibly related to the breakdown of the CBN aggregates and an increase in the specific surface area, which caused a reduction in the water available in the system caused by the adsorption phenomenon, as well as a decrease in the amount of PCE molecules acting in the surface of the cement grains. As for the point of intersection of the curve with the ordinate axis, in all the pastes this point was close to a torque equal to zero, indicating a low yield stress, possibly related to the presence of PCE in the mixtures [44].

Figure 4 – Torque vs. angular velocity curves of the pastes studied (A) and rheological behavior as a function of sonication energy (B).

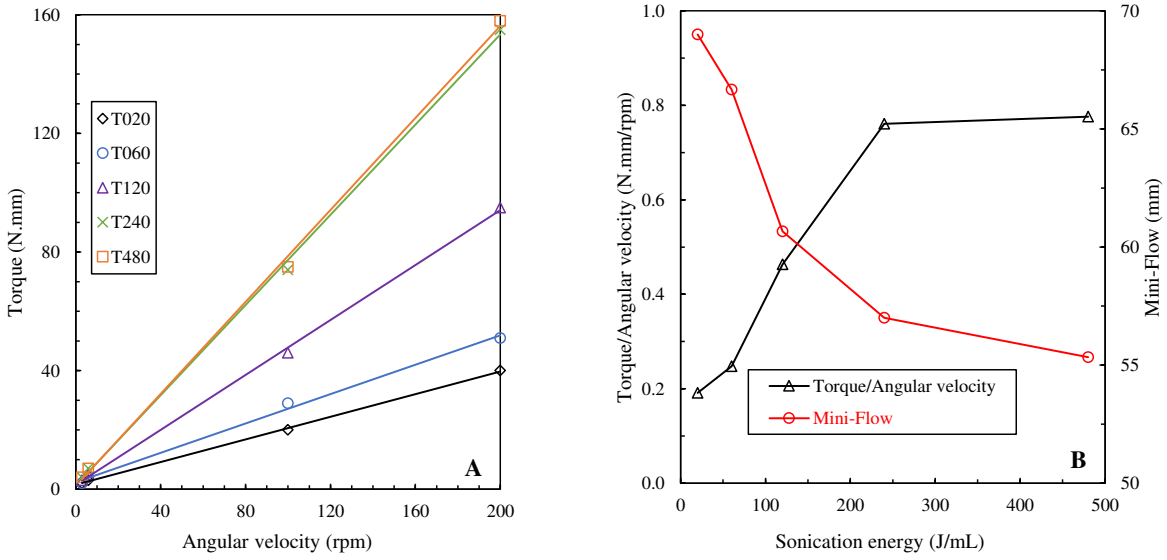

Figure 4B shows the rheological behavior by means of the relationships between the Torque/Angular Velocity ratio (correlated to plastic viscosity), spreading (mini-flow) and the variation in sonication energy. In general, increasing the sonication energy led to an increase in the Torque/Angular Velocity ration and a decrease in spreading. For example, the Torque/Angular Velocity ratio of the T480 series was about 300% higher than the one in the T020 series, whereas the spreading in the T480 series was around 20% lower than the one in the T020 series. The T020 and T060 series presented difficulties in proper electrodes positioning due to their low viscosity. The T480 series also presented inadequate workability

(gelatinous consistency), causing problems during the molding and densification process. The most suitable molding conditions were observed in the T120 and T240 series, with spreading in the range of 57 mm to 61 mm and Torque/Angular Velocity ratio varying from 0.46 N.mm/rpm to 0.76 N.mm/rpm.

Similar behavior has been observed in previous studies that also investigated the workability of cementitious matrices containing different types of nanomaterials, such as carbon nanotubes and halloysite nanotubes [24,25,57]. These studies have also reported that increasing the sonication energy caused a drop in workability. According to the authors, the nanomaterials have high hydrophilicity, so that improvements in dispersion cause an increase in the specific surface area of the nanomaterials and a reduction in the amount of free water in the mixture in the fresh state, which compromises the workability of the material. In addition, the authors state that nanomaterials that are more dispersed in the matrix adsorb more superplasticizer molecules on their surface, which compromises their effects on the cement particles and causes reductions in the fluidity of the mixture.

Varying the sonication energy caused significant changes in the material's rheological behavior. Lower energies caused molding problems that have a direct impact on the piezoresistive effect and the sensing abilities of the material. Higher energies caused problems that affected the material’s mechanical properties. From the point of view of rheological behavior, the energy range that was most suitable for producing CCNS ranged from 120 J/mL to 240 J/mL.

3.3.3. Analysis of CBN dispersion quality

Figure 5 shows the relationship between the size of the CBN aggregates and the zeta potential as a function of the variation in sonication energy. The DLS results showed that increasing the sonication energy proved to be an efficient tool for breaking up the CBN aggregates, reducing their approximate average size from 296.20 nm (T020) to 192.60 nm (T240). Such breaking tends to allow the adsorption of PCE molecules on the surface of carbon nanomaterials, which prevents their re-agglomeration [21,22,28,58]. In the T480 series, the aggregates size was about 196.30 nm, a small increase of 1.9% in relation to the T240 series, which suggests that the excessive increase in sonication energy may cause possible re-agglomeration [15].

This behavior is in good agreement with that reported in the literature for other different types of conductive carbon-based materials [26,28,59]. Thus, with increasing sonication

energy, the zeta potential (in module) started at 21.83 mV in the T020 series, and reached 30.67 mV in the T480 series, which represents an increase of more than 40%. The zeta potential results are related to the dispersion stability of the nanosuspensions and represent the degree of repulsion between the particles in a solution [59]. Thus, the higher the value of the zeta potential (in modulus), the greater the force of repulsion between the particles. If the zeta potential is high, the repulsion force is dominant and the particles tend to disperse. On the other hand, if the value of the zeta potential is small, the force of attraction dominates and the particles tend to agglomerate.

Figure 5 – Relationship between CBN aggregate size and zeta potential as a function of sonication energy.

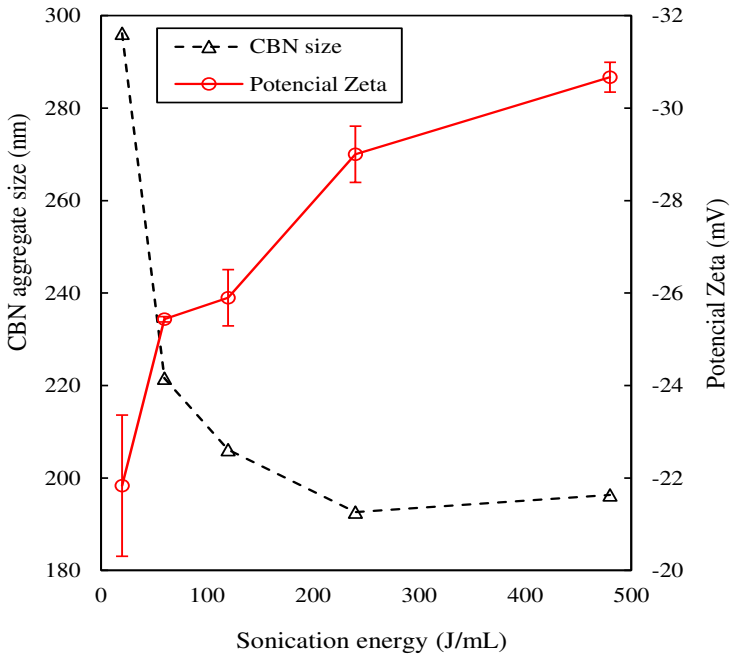

Figure 6 shows the absorbance spectra measured in the UV-VIS analyses of samples subjected to different sonication energy levels. The comparison of the concentrations was conducted within the validity range of the Lambert-Beer Law. The results show that increasing the sonication energy caused an increase in the light absorption of the solutions, indicating that there are more dispersed particles in the system. Maximum light absorption occurred in the 250 nm to 280 nm wavelength range, followed by a gradual reduction until it reached its minimum value at 750 nm. Similar behavior has been observed in other studies dealing with carbon-based materials [15,60,61]. The maximum absorption in the 180 nm to 260 nm range is related to electronic transitions π-π^* associated with carbon nanomaterials [61,62]. The better the quality of the scattering, the greater the surface area of CBN exposed to radiation, which results in a greater number of excitations π-π^*.

The T020 series showed the lowest levels of light absorption, indicating a smaller surface area of CBN absorbing radiation, which is in line with the results observed in Figure 5. On the other hand, the T240 and T480 series reached very close maximum levels of light absorption, which suggests that these series presented the best conditions for CBN scattering.

Figure 6 – UV-VIS absorbance spectra for different sonication energy levels.

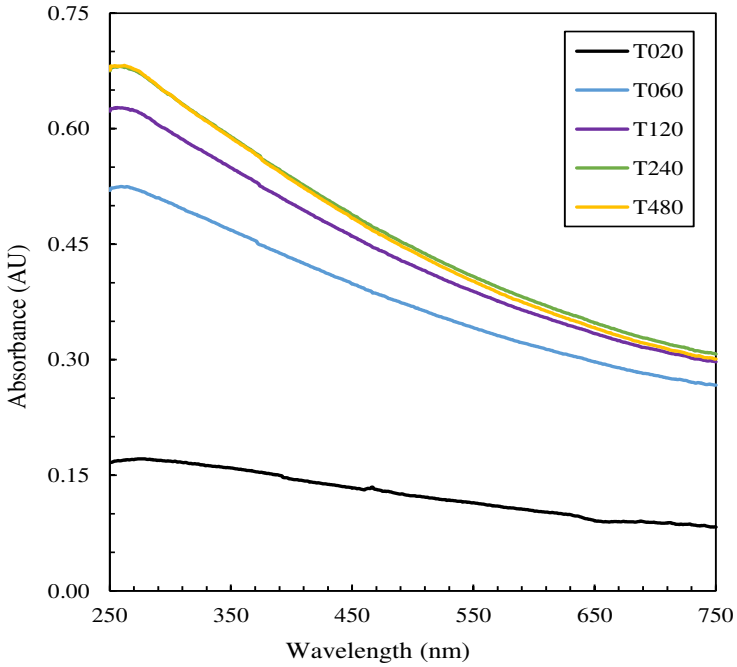

In order to complement the analysis of the effects of sonication energy on the dispersion of nanosuspensions in aqueous media, a qualitative assessment of the microstructure of the CCNS was carried out. The aim of this analysis was to verify the interaction between the CBN and the cementitious matrix in the hardened state.

The FEG-SEM images of the mortars, with a magnification of 80 kx and a graphic scale of 1 μm, are shown in Figure 7. Crystalline structures typical of cementitious matrices were identified, such as calcium hydroxide (CH) and calcite ($CaCO_3$). Furthermore, it was possible to observe many small spheres dispersed in the flocculated structure typically observed in the hydrated calcium silicate (C-S-H) gel, which indicates that the CBN aggregates have a clear interaction with the cementitious matrix. In general, the increase in sonication energy brought benefits to the material, causing an apparent refinement of the matrix, which was evidenced in the significant gain in mechanical strength of around 40% from the T020 to T480 series. The nanofiller effect and the enhancement of the hydration process provided by different levels of CBN have also been reported in previous studies [63–65]. Further evidence of this refinement is related to the change in electrical resistivity (a reduction of up to 58.5%), suggesting that

better dispersion of CBN caused pores filling and enabled the formation of a greater number of conductive paths.

Figure 7 – Micrographs of the mortars at 80 kx magnification (graphic scale of 1 μm): (A) T020; (B) T060; (C) T120; (D) T240; (E) T480.

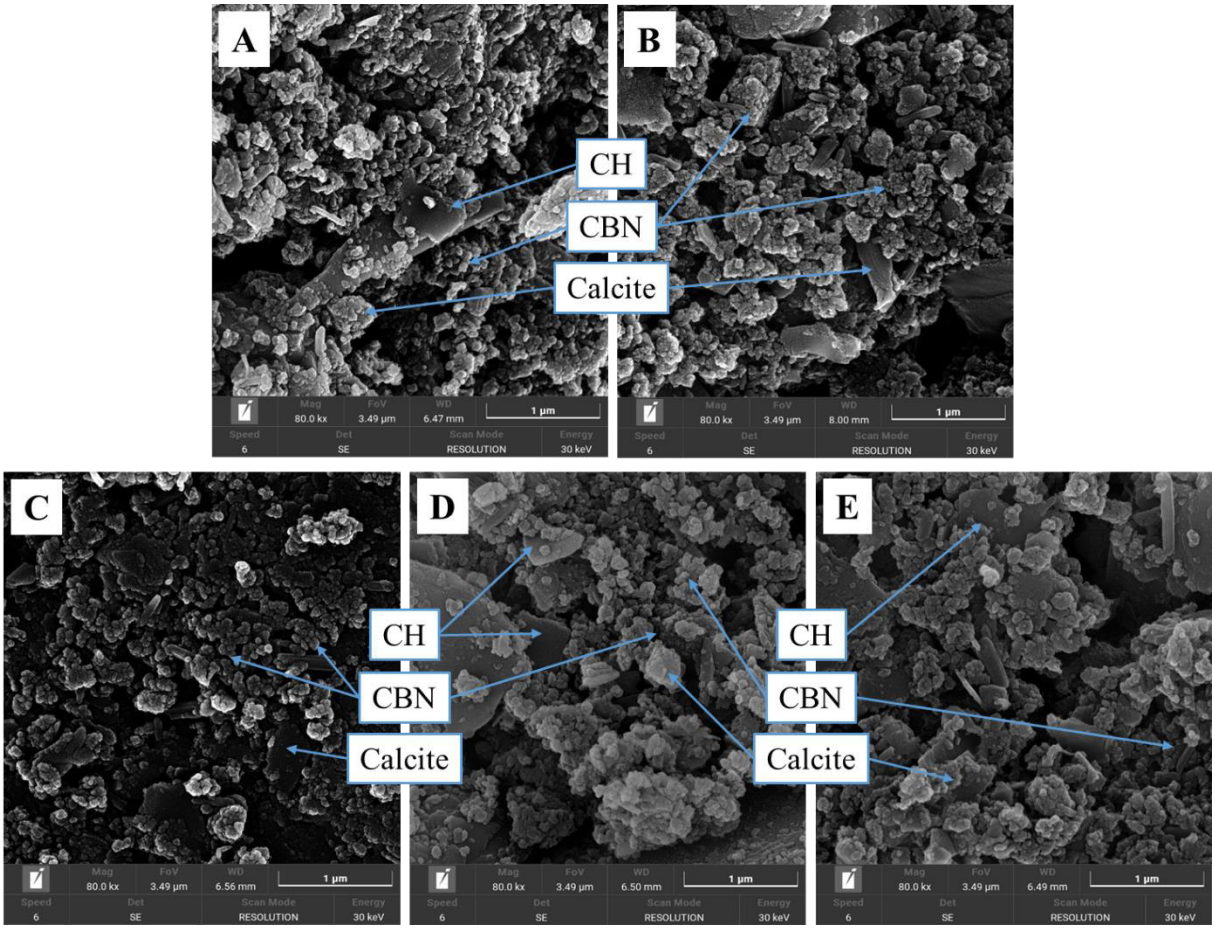

Figure 8 shows the FEG-SEM images of the mortars at a magnification of 200 kx and a graphic scale of 200 nm. The reduction in the size of the CBN aggregates with increasing sonication energy is evident, in line with what was observed in the dynamic light scattering technique (Figure 5), already discussed in the previous sections. The progressive reduction in electrical resistivity observed in the 20 J/mL to 120 J/mL range (Figure 1) may also have been the result of the refinement of the conductive network provided by the breaking up of CBN aggregates associated with the better dispersion quality of these nanomaterials. Reductions in agglomerations of carbon nanotubes, halloysite nanotubes or graphene nanoplatelets due to the sonication process have also been observed in microscopy analyses reported in previous works [25,57,66].

Figure 8 – Micrographs of the mortars at 200 kx magnification (200 nm graphic scale): (A) T020; (B) T060; (C) T120; (D) T240; (E) T480.

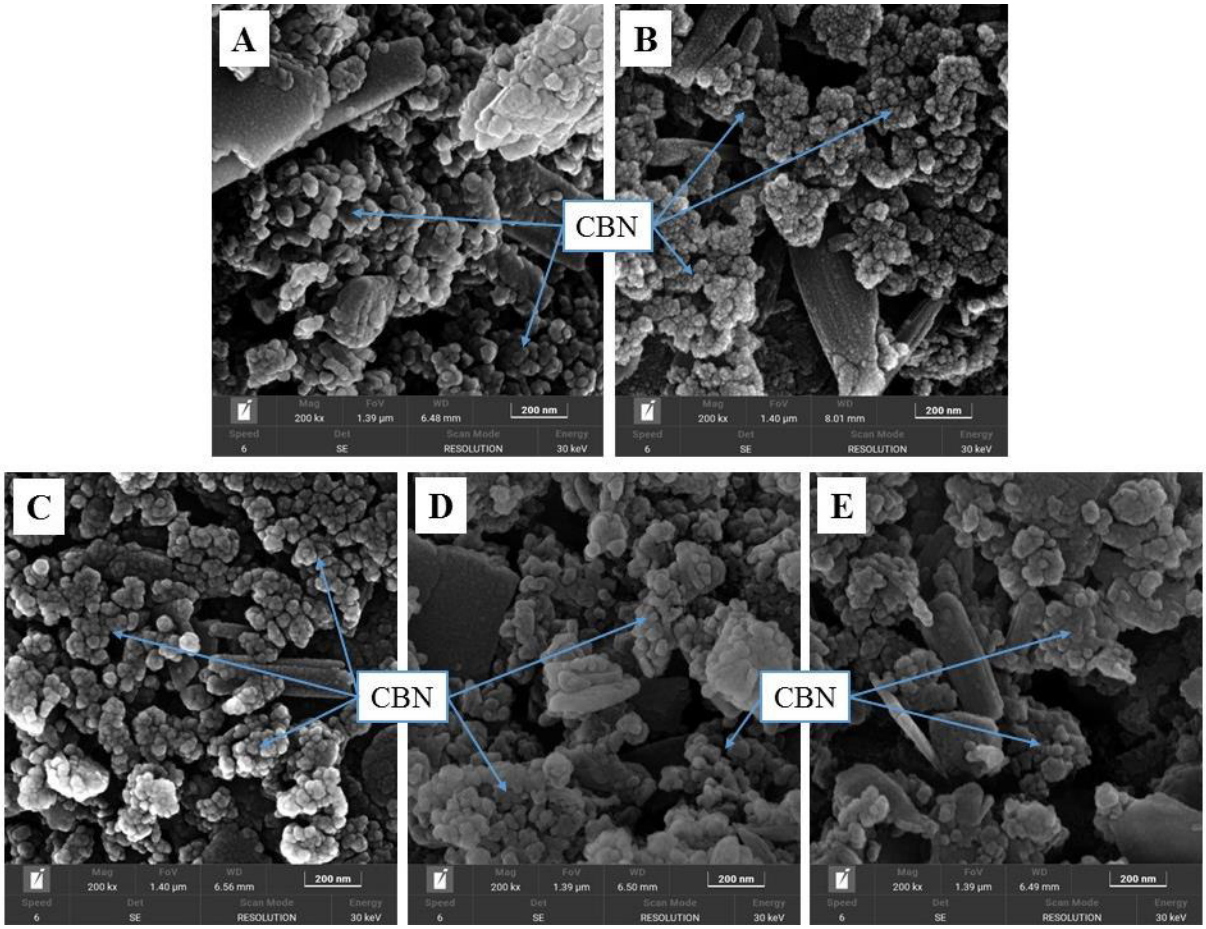

Another relevant aspect is that reducing the size of the aggregates creates favorable conditions for increasing the nucleation points of cement hydrates [67–69], making the matrix more compact and improving the mechanical properties of the composites. However, an excessive increase in nucleation points can cause damage to the electrical conductivity and sensing properties of CCNS, due to the increase in the distance between adjacent conductive particles, reducing the probability of tunneling conduction mechanisms. To some extent, this may explain the 8.7% increase in electrical resistivity and the 4.0% reduction in GF of the T480 series compared to T240 series.

The reduction in the size of the CBN aggregates caused by the variation of the sonication energy led to significant changes in the microstructure morphology of the CCNS matrix. For lower energies (20 J/mL to 120 J/mL), sonication refined the conductive network inside the cement matrix and reduced the material's electrical resistivity, but not to the point of optimizing the self-sensing abilities of the composites. On the other hand, the sonication energy of 240 J/mL increased the average GF value and reduced the electrical resistivity of the material.

However, the use of elevated sonication energy (480 J/mL) may limit gains or lead to problems with the material's electrical and sensing properties.

Studying the behavior of the nanosuspensions via DLS, zeta potential and UV-VIS enabled a satisfactory assessment of the degree of CBN dispersion after applying different levels of sonication energy. Sonication energies in the range of 20 J/mL to 120 J/mL led to lower zeta potential values, thus presenting a lower quality of dispersion when compared to the use of sonication energies equal to or greater than 240 J/mL. The T480 series showed similar results to the T240 series in the DLS and UV-VIS analyses, indicating that the energy of 480 J/mL does not provide significant gain that would justify its use. Thus, the analysis of the nanosuspensions indicates that the sonication energy of 240 J/mL was the most suitable for the production of CCNS. Finally, qualitative evaluation through FEG-SEM analyses proved to be an important complementary tool for better understanding the interaction between CBN and the hardened cementitious matrix.

3.4 CONCLUSIONS

The effects of sonication energy on the dispersion of CBN and on the electromechanical and rheological behavior of CCNS were investigated in this study. The mechanical and self-sensing performance of cementitious composites were explained by analyzing the dispersion quality of nanosuspensions prepared with different techniques. The main conclusions of the study are as follows:

(1) Sonication energy significantly influenced the electromechanical behavior of CCNS. Low sonication energy (20-120 J/mL) negatively impacted mechanical and self-sensing properties due to poor dispersion. Higher energy (240-480 J/mL) improved performance, but excessive energy increased variability in compressive strength. Optimal CCNS electromechanical behavior was observed in the 120-240 J/mL range.

(2) Varying the sonication energy caused significant changes in the rheological behavior of the material. Lower energies led to problems with electrode positioning during molding, which had a direct impact on the self-sensing abilities of the material. Higher energies caused problems in the densification process during molding, which affected the material's mechanical properties. The sonication energy range of 120 J/mL to 240 J/mL provided the best results for the rheological behavior of the CCNS.

(3) The zeta potential, UV-VIS absorption and DLS measurements enabled a satisfactory assessment of the degree of CBN dispersion. A sonication energy in the range of 20 J/mL to 120 J/mL led to poorer dispersion quality when compared to a sonication energy equal to or greater than 240 J/mL. The T240 and T480 series showed similar DLS and UV-VIS results. Consequently, from an operational and economic point of view, it is more efficient to use a sonication energy of 240 J/mL to produce CCNS.

(4) FEG-SEM images revealed the impact of sonication energy on CCNS microstructure morphology. While lower energies (20-120 J/mL) improved the conductive network and reduced resistivity, they did not optimize self-sensing abilities. In contrast, 240 J/mL enhanced the conductive network, increasing the average Gauge Factor and maximizing resistivity reduction. However, 480 J/mL limited the gains in mechanical and sensing properties.

(5) All the results suggest that sonication energies of around 240 J/mL were responsible for producing the nanosuspensions with the most efficient dispersions, suggesting a refinement of the cementitious matrix and an increase in the conductive network. Energies of this order were also able to optimize the electromechanical and rheological characteristics of the CCNS.

In order to complement the findings of this study, future studies should test the recommended sonication procedures to alternative raw materials, considering their specific properties and potential adjustments to optimize the overall performance of the self-sensing composites. In another line of research, future studies should also investigate the effects of pH, temperature, admixtures, and setting time on the stability of CBN suspensions in cementitious matrices, validating their effects and exploring different factors affecting the dispersion of nanomaterials within the composites.

3.5 REFERENCES

[1] L. Wang, F. Aslani, A review on material design, performance, and practical application of electrically conductive cementitious composites, Constr. Build. Mater. 229 (2019) 116892. https://doi.org/10.1016/j.conbuildmat.2019.116892.

[2] W. Dong, W. Li, Z. Tao, K. Wang, Piezoresistive properties of cement-based sensors: Review and perspective, Constr. Build. Mater. 203 (2019) 146–163. https://doi.org/10.1016/j.conbuildmat.2019.01.081.

[3] S. Ding, S. Dong, A. Ashour, B. Han, Development of sensing concrete: Principles, properties and its applications, J. Appl. Phys. 126 (2019). https://doi.org/10.1063/1.5128242.

[4] F. Ubertini, A. D'Alessandro, Concrete with self-sensing properties, in: Eco-Efficient Repair Rehabil. Concr. Infrastructures, Elsevier, 2018: pp. 501–530. https://doi.org/10.1016/B978-0-08-102181-1.00018-6.

[5] G.H. Nalon, J.C.L. Ribeiro, E.N.D. de Araújo, L.G. Pedroti, J.M.F. de Carvalho, R.F. Santos, A. Aparecido-Ferreira, Effects of different kinds of carbon black nanoparticles on the piezoresistive and mechanical properties of cement-based composites, J. Build. Eng. 32 (2020) 101724. https://doi.org/10.1016/J.JOBE.2020.101724.

[6] Y. Huang, H. Li, S. Qian, Self-sensing properties of Engineered Cementitious Composites, Constr. Build. Mater. 174 (2018) 253–262. https://doi.org/10.1016/j.conbuildmat.2018.04.129.

[7] Y. Dai, M. Sun, C. Liu, Z. Li, Electromagnetic wave absorbing characteristics of carbon black cement-based composites, Cem. Concr. Compos. 32 (2010) 508–513. https://doi.org/10.1016/j.cemconcomp.2010.03.009.

[8] M.-G. Pârvan, G. Voicu, A.-I. Bădănoiu, Study of hydration and hardening processes of self-sensing cement-based materials with carbon black content, J. Therm. Anal. Calorim. 139 (2020) 807–815. https://doi.org/10.1007/s10973-019-08535-8.

[9] S. Ding, X. Wang, L. Qiu, Y. Ni, X. Dong, Y. Cui, A. Ashour, B. Han, J. Ou, Self-Sensing Cementitious Composites with Hierarchical Carbon Fiber-Carbon Nanotube Composite Fillers for Crack Development Monitoring of a Maglev Girder, Small. 19 (2023). https://doi.org/10.1002/smll.202206258.

[10] S. Ding, Y. Xiang, Y.-Q. Ni, V.K. Thakur, X. Wang, B. Han, J. Ou, In-situ synthesizing carbon nanotubes on cement to develop self-sensing cementitious composites for smart high-speed rail infrastructures, Nano Today. 43 (2022) 101438. https://doi.org/10.1016/j.nantod.2022.101438.

[11] H. Ridaoui, A. Jada, L. Vidal, J.-B. Donnet, Effect of cationic surfactant and block copolymer on carbon black particle surface charge and size, Colloids Surfaces A Physicochem. Eng. Asp. 278 (2006) 149–159. https://doi.org/10.1016/j.colsurfa.2005.12.013.

[12] A.O. Monteiro, A. Loredo, P.M.F.J. Costa, M. Oeser, P.B. Cachim, A pressure-sensitive carbon black cement composite for traffic monitoring, Constr. Build. Mater. 154 (2017) 1079–1086. https://doi.org/10.1016/J.CONBUILDMAT.2017.08.053.

[13] A.O. Monteiro, P.B. Cachim, P.M.F.J. Costa, Self-sensing piezoresistive cement composite loaded with carbon black particles, Cem. Concr. Compos. 81 (2017) 59–65. https://doi.org/10.1016/J.CEMCONCOMP.2017.04.009.

[14] B. Han, S. Ding, X. Yu, Intrinsic self-sensing concrete and structures: A review, Measurement. 59 (2015) 110–128. https://doi.org/10.1016/j.measurement.2014.09.048.

[15] M. Mardani, S. Hossein Hosseini Lavassani, M. Adresi, A. Rashidi, Piezoresistivity and mechanical properties of self-sensing CNT cementitious nanocomposites: Optimizing the effects of CNT dispersion and surfactants, Constr. Build. Mater. 349 (2022) 128127. https://doi.org/10.1016/j.conbuildmat.2022.128127.

[16] V.J. GARCÍA, C.O. MÁRQUEZ, A.R. ZÚÑIGA-SUÁREZ, B.C. ZÚÑIGA-TORRES, P.J. RÍOS-GÓNZALEZ, Mechanical and electrical properties of MWCNTs - high early strength cement - mortars composite: Dispersion of CNTs and effect of chemical admixtures, An. Acad. Bras. Cienc. 93 (2021). https://doi.org/10.1590/0001-3765202120200924.

[17] J. da S. Andrade Neto, T.A. Santos, S. de A. Pinto, C.M.R. Dias, D.V. Ribeiro, Effect of the combined use of carbon nanotubes (CNT) and metakaolin on the properties of cementitious matrices, Constr. Build. Mater. 271 (2021) 121903. https://doi.org/10.1016/j.conbuildmat.2020.121903.

[18] H. Qin, S. Ding, A. Ashour, Q. Zheng, B. Han, Revolutionizing infrastructure: The evolving landscape of electricity-based multifunctional concrete from concept to practice, Prog. Mater. Sci. 145 (2024) 101310. https://doi.org/10.1016/j.pmatsci.2024.101310.

[19] A.H. Korayem, N. Tourani, M. Zakertabrizi, A.M. Sabziparvar, W.H. Duan, A review of dispersion of nanoparticles in cementitious matrices: Nanoparticle geometry perspective, Constr. Build. Mater. 153 (2017) 346–357. https://doi.org/10.1016/j.conbuildmat.2017.06.164.

[20] H. Kato, A. Nakamura, M. Shimizu, Effect of surfactant micelle size on the dispersibility of aqueous carbon black particle suspensions prepared by ultrasonication, Powder Technol. 399 (2022) 117206. https://doi.org/10.1016/j.powtec.2022.117206.

[21] L. Assi, A. Alsalman, D. Bianco, P. Ziehl, J. El-Khatib, M. Bayat, F.H. Hussein, Multiwall carbon nanotubes (MWCNTs) dispersion & mechanical effects in OPC mortar & paste: A review, J. Build. Eng. 43 (2021) 102512. https://doi.org/10.1016/j.jobe.2021.102512.

[22] L. Vaisman, H.D. Wagner, G. Marom, The role of surfactants in dispersion of carbon

nanotubes, Adv. Colloid Interface Sci. 128–130 (2006) 37–46. https://doi.org/10.1016/j.cis.2006.11.007.

[23] F. Collins, J. Lambert, W.H. Duan, The influences of admixtures on the dispersion, workability, and strength of carbon nanotube–OPC paste mixtures, Cem. Concr. Compos. 34 (2012) 201–207. https://doi.org/10.1016/j.cemconcomp.2011.09.013.

[24] B. Zou, S.J. Chen, A.H. Korayem, F. Collins, C.M. Wang, W.H. Duan, Effect of ultrasonication energy on engineering properties of carbon nanotube reinforced cement pastes, Carbon N. Y. 85 (2015) 212–220. https://doi.org/10.1016/J.CARBON.2014.12.094.

[25] J.E.L. de SIQUEIRA, P.J.P. GLEIZE, Effect of carbon nanotubes sonication on mechanical properties of cement pastes, Rev. IBRACON Estruturas e Mater. 13 (2020) 455–463. https://doi.org/10.1590/s1983-41952020000200013.

[26] L.M. Echeverry-Cardona, N. Álzate, E. Restrepo-Parra, R. Ospina, J.H. Quintero-Orozco, Time-Stability Dispersion of MWCNTs for the Improvement of Mechanical Properties of Portland Cement Specimens, Materials (Basel). 13 (2020) 4149. https://doi.org/10.3390/ma13184149.

[27] L. Oliveira de Souza, M. Cordazzo, L.M. Silva de Souza, G. Tonoli, F. de Andrade Silva, V. Mechtcherine, Investigation of dispersion methodologies of microcrystalline and nano-fibrillated cellulose on cement pastes, Cem. Concr. Compos. 126 (2022) 104351. https://doi.org/10.1016/j.cemconcomp.2021.104351.

[28] I. Papanikolaou, L. Ribeiro de Souza, C. Litina, A. Al-Tabbaa, Investigation of the dispersion of multi-layer graphene nanoplatelets in cement composites using different superplasticiser treatments, Constr. Build. Mater. 293 (2021) 123543. https://doi.org/10.1016/j.conbuildmat.2021.123543.

[29] W. Dong, W. Li, L. Shen, D. Sheng, Piezoresistive behaviours of carbon black cement-based sensors with layer-distributed conductive rubber fi bres, Mater. Des. 182 (2019) 108012. https://doi.org/10.1016/j.matdes.2019.108012.

[30] A. D'Alessandro, A. Meoni, F. Ubertini, Innovative Composites with Carbon Nanofillers for Self-Sensing Structural RC Beams, Nano Hybrids Compos. 19 (2018) 12–22. https://doi.org/10.4028/www.scientific.net/NHC.19.12.

[31] B. Han, L. Zhang, J. Ou, Influence of water content on conductivity and piezoresistivity of cement-based material with both carbon fiber and carbon black, J. Wuhan Univ. Technol. Sci. Ed. 25 (2010) 147–151. https://doi.org/10.1007/s11595-010-1147-z.

[32] H. Dehghanpour, K. Yilmaz, M. Ipek, Evaluation of recycled nano carbon black and

waste erosion wires in electrically conductive concretes, Constr. Build. Mater. 221 (2019) 109–121. https://doi.org/10.1016/j.conbuildmat.2019.06.025.

[33] A. Dinesh, P. Saravanakumar, B. Rahul Prasad, S. Kilbert Raj, Carbon black based self-sensing cement composite for structural health monitoring – A review on strength and conductive characteristics, Mater. Today Proc. (2023). https://doi.org/10.1016/j.matpr.2023.03.661.

[34] L. Liu, J. Xu, T. Yin, Y. Wang, H. Chu, Improving electrical and piezoresistive properties of cement-based composites by combined addition of nano carbon black and nickel nanofiber, J. Build. Eng. 51 (2022) 104312. https://doi.org/10.1016/j.jobe.2022.104312.

[35] Y. Guo, W. Li, W. Dong, Z. Luo, F. Qu, F. Yang, K. Wang, Self-sensing performance of cement-based sensor with carbon black and polypropylene fibre subjected to different loading conditions, J. Build. Eng. 59 (2022) 105003. https://doi.org/10.1016/j.jobe.2022.105003.

[36] G. Henrique Nalon, J.C. Lopes Ribeiro, L. Gonçalves Pedroti, R. Marcio da Silva, E. Nery Duarte de Araújo, G. Emilio Soares de Lima, Smart laying mortars for masonry structures: effects of lime/cement ratio and carbon nanomaterials content on self-sensing behavior, Cem. Concr. Compos. 145 (2024) 105351. https://doi.org/10.1016/j.cemconcomp.2023.105351.

[37] G. Marchetti, C. Castellano, V. Bonavetti, E.F. Irassar, Tools for designing the early-age properties of fly ash and limestone filler ternary systems, Constr. Build. Mater. 347 (2022) 128552. https://doi.org/10.1016/J.CONBUILDMAT.2022.128552.

[38] A.A. de Siqueira, G.C. Cordeiro, Properties of binary and ternary mixes of cement, sugarcane bagasse ash and limestone, Constr. Build. Mater. 317 (2022) 126150. https://doi.org/10.1016/J.CONBUILDMAT.2021.126150.

[39] H. Wang, F. Shi, J. Shen, A. Zhang, L. Zhang, H. Huang, J. Liu, K. Jin, L. Feng, Z. Tang, Research on the self-sensing and mechanical properties of aligned stainless steel fiber-reinforced reactive powder concrete, Cem. Concr. Compos. 119 (2021) 104001. https://doi.org/10.1016/J.CEMCONCOMP.2021.104001.

[40] J. Han, J. Cai, J. Pan, Y. Sun, Study on the conductivity of carbon fiber self-sensing high ductility cementitious composite, J. Build. Eng. 43 (2021) 103125. https://doi.org/10.1016/J.JOBE.2021.103125.

[41] G.H. Nalon, J.C. Lopes Ribeiro, L.G. Pedroti, E.N. Duarte de Araújo, J.M. Franco de Carvalho, G.E. Soares de Lima, L. de Moura Guimarães, Residual piezoresistive

properties of mortars containing carbon nanomaterials exposed to high temperatures, Cem. Concr. Compos. 121 (2021) 104104. https://doi.org/10.1016/J.CEMCONCOMP.2021.104104.

[42] A. Downey, A. D'Alessandro, F. Ubertini, S. Laflamme, R. Geiger, Biphasic DC measurement approach for enhanced measurement stability and multi-channel sampling of self-sensing multi-functional structural materials doped with carbon-based additives, Smart Mater. Struct. 26 (2017) 065008. https://doi.org/10.1088/1361-665X/aa6b66.

[43] A. Meoni, A. D'Alessandro, R. Kruse, L. De Lorenzis, F. Ubertini, Strain field reconstruction and damage identification in masonry walls under in-plane loading using dense sensor networks of smart bricks: Experiments and simulations, Eng. Struct. 239 (2021) 112199. https://doi.org/10.1016/J.ENGSTRUCT.2021.112199.

[44] J.M. Franco de Carvalho, W. Schmidt, H.C. Kühne, R.A.F. Peixoto, Influence of high-charge and low-charge PCE-based superplasticizers on Portland cement pastes containing particle-size designed recycled mineral admixtures, J. Build. Eng. 32 (2020) 101515. https://doi.org/10.1016/J.JOBE.2020.101515.

[45] K.L. Scrivener, R. Snellings, B. Lothenbach, A practical guide to microstructural analysis of cementitious materials, CRC Press, Boca Raton, 2016.

[46] H.N. Yoon, D. Jang, T. Kil, H.K. Lee, Influence of various deterioration factors on the electrical properties of conductive cement paste, Constr. Build. Mater. 367 (2023) 130289. https://doi.org/10.1016/J.CONBUILDMAT.2022.130289.

[47] H. Li, H. Chen, M. Wei, R. Wang, N. Lei, Q. Wang, Design and preparation of double-layer iron ore tailings cement-based electromagnetic wave absorbing materials containing carbon black and steel fiber, Constr. Build. Mater. 364 (2023) 129972. https://doi.org/10.1016/J.CONBUILDMAT.2022.129972.

[48] Y. Ding, Z. Chen, Z. Han, Y. Zhang, F. Pacheco-torgal, Nano-carbon black and carbon fiber as conductive materials for the diagnosing of the damage of concrete beam, Constr. Build. Mater. 43 (2013) 233–241. https://doi.org/10.1016/j.conbuildmat.2013.02.010.

[49] A. Hussain, Y. Ding, G. Liu, A. Naqi, Study on self-monitoring of multiple cracked concrete beams with multiphase conductive materials subjected to bending, (2019).

[50] S. Ding, Y. Ruan, X. Yu, B. Han, Y.Q. Ni, Self-monitoring of smart concrete column incorporating CNT/NCB composite fillers modified cementitious sensors, Constr. Build. Mater. 201 (2019) 127–137. https://doi.org/10.1016/J.CONBUILDMAT.2018.12.203.

[51] G.H. Nalon, R.F. Santos, G.E.S. de Lima, I.K.R. Andrade, L.G. Pedroti, J.C.L. Ribeiro, J.M. Franco de Carvalho, Recycling waste materials to produce self-sensing concretes

for smart and sustainable structures: A review, Constr. Build. Mater. 325 (2022) 126658. https://doi.org/10.1016/J.CONBUILDMAT.2022.126658.

[52] A.O. Monteiro, P.B. Cachim, P.M.F.J. Costa, Carbon nanoparticles cement-based materials for service life monitoring, in: Conf. Segm. Serv. Life Cem. Mater. Struct., RILEM, Lyngby, 2016: pp. 195–202.

[53] A.O. Monteiro, A. Loredo, P.M.F.J. Costa, M. Oeser, P.B. Cachim, A pressure-sensitive carbon black cement composite for traffic monitoring, Constr. Build. Mater. 154 (2017) 1079–1086. https://doi.org/10.1016/j.conbuildmat.2017.08.053.

[54] B. Chen, K. Wu, W. Yao, Conductivity of carbon fiber reinforced cement-based composites, Cem. Concr. Compos. 26 (2004) 291–297. https://doi.org/10.1016/S0958-9465(02)00138-5.

[55] Y. Li, J. Yin, Q. Yuan, T. Huang, J. He, J. Li, Fresh and hardened properties of cement paste and mortar incorporating calcined cutter soil mixing residue, Constr. Build. Mater. 357 (2022) 129376. https://doi.org/10.1016/J.CONBUILDMAT.2022.129376.

[56] S. Yu, J. Sanjayan, H. Du, Effects of cement mortar characteristics on aggregate-bed 3D concrete printing, Addit. Manuf. 58 (2022) 103024. https://doi.org/10.1016/J.ADDMA.2022.103024.

[57] Y. Rashidi, M. Ranjkesh Rashteh Roudi, A. Habibnejad Korayem, E. Shamsaei, Investigation of ultrasonication energy effect on workability, mechanical properties and pore structure of halloysite nanotube reinforced cement mortars, Constr. Build. Mater. 304 (2021) 124610. https://doi.org/10.1016/J.CONBUILDMAT.2021.124610.

[58] M.S. Strano, V.C. Moore, M.K. Miller, M.J. Allen, E.H. Haroz, C. Kittrell, R.H. Hauge, R.E. Smalley, The Role of Surfactant Adsorption during Ultrasonication in the Dispersion of Single-Walled Carbon Nanotubes, J. Nanosci. Nanotechnol. 3 (2003) 81–86. https://doi.org/10.1166/jnn.2003.194.

[59] J.S. Kim, Enhanced effects of carbon-based conductive materials on the piezoresistive characteristics of cementitious composites, Constr. Build. Mater. 341 (2022) 127804. https://doi.org/10.1016/j.conbuildmat.2022.127804.

[60] A.C. Zaman, F. Kaya, C. Kaya, A study on optimum surfactant to multiwalled carbon nanotube ratio in alcoholic stable suspensions via UV–Vis absorption spectroscopy and zeta potential analysis, Ceram. Int. 46 (2020) 29120–29129. https://doi.org/10.1016/j.ceramint.2020.08.085.

[61] M. Sharif Sh., F. Golestani Fard, E. Khatibi, H. Sarpoolaky, Dispersion and stability of carbon black nanoparticles, studied by ultraviolet–visible spectroscopy, J. Taiwan Inst.

Chem. Eng. 40 (2009) 524–527. https://doi.org/10.1016/j.jtice.2009.03.006.

[62] C. Jäger, T. Henning, R. Schlögl, O. Spillecke, Spectral properties of carbon black, J. Non. Cryst. Solids. 258 (1999) 161–179. https://doi.org/10.1016/S0022-3093(99)00436-6.

[63] M.-G. Parvan, G. Voicu, A.-I. Badanoiu, V.O. Fruth, Self-sensing Piezoresistive Composites Based on Cement Incorporating Low Dosage of Carbon Black Used as Multifunctional Construction Materials, Rev. Chim. 71 (2020) 30–44. https://doi.org/10.37358/RC.20.5.8110.

[64] Q. Zhang, C. Luan, C. Yu, Y. Huang, Z. Zhou, Mechanisms of carbon black in multifunctional cement matrix: Hydration and microstructure perspectives, Constr. Build. Mater. 346 (2022) 128455. https://doi.org/10.1016/J.CONBUILDMAT.2022.128455.

[65] G.E.S. de Lima, G.H. Nalon, R.F. Santos, J.C.L. Ribeiro, J.M.F. de Carvalho, L.G. Pedroti, E.N.D. de Araújo, Microstructural Investigation of the Effects of Carbon Black Nanoparticles on Hydration Mechanisms, Mechanical and Piezoresistive Properties of Cement Mortars, Mater. Res. 24 (2021). https://doi.org/10.1590/1980-5373-mr-2020-0539.

[66] H. Du, S.D. Pang, Dispersion and stability of graphene nanoplatelet in water and its influence on cement composites, Constr. Build. Mater. 167 (2018) 403–413. https://doi.org/10.1016/J.CONBUILDMAT.2018.02.046.

[67] L. Wang, G. Li, C. He, Y. Tang, B. Yi, Preparation and properties of nano-carbon black modified ultra-high-performance concrete, Case Stud. Constr. Mater. 17 (2022) e01378. https://doi.org/10.1016/J.CSCM.2022.E01378.

[68] A. Tugelbayev, J.-H. Kim, J.U. Lee, C.-W. Chung, The effect of acid treated multi-walled carbon nanotubes on the properties of cement paste prepared by ultrasonication with polycarboxylate ester, J. Build. Eng. 64 (2023) 105638. https://doi.org/10.1016/J.JOBE.2022.105638.

[69] H. Zhang, J. Kou, C. Sun, P. Wang, J. Lin, J. Li, Y. Jiang, Optimization of cemented paste backfill with carbon nanotubes as a sustainable treatment for lead-containing tailings, Powder Technol. 415 (2023) 118152. https://doi.org/10.1016/J.POWTEC.2022.118152.

4 AVALIAÇÃO DO TEOR DE SURFACTANTE NA DISPERSÃO DE CBN PARA OTIMIZAÇÃO DAS PROPRIEDADES ELETROMECÂNICAS DE COMPÓSITOS CIMENTÍCIOS NANOMODIFICADOS SENSORES

Resumo: *Os polímeros à base de éter policarboxilato (PCE) são poderosos aditivos com ação superplastificante e redutora do consumo de água. Estudos prévios utilizaram o PCE para garantir apropriada dispersão de nanopartículas de carbon black (CBN) durante a produção de compósitos cimentícios nanomodificados sensores (CCNS), adotando consumos deste aditivo de forma arbitrária. A avaliação dos efeitos de diferentes dosagens de PCE na qualidade e estabilidade de dispersões de CBN e seus impactos nas propriedades eletromecânicas de CCNS ainda não foram explorados. Desta forma, o presente estudo desenvolveu uma investigação dos efeitos do teor de PCE na dispersão de CBN e seus impactos nas propriedades elétricas, mecânicas e reológicas de CCNS produzidos com diferentes razões PCE/CBN (em massa). A razão PCE/CBN igual a 0.4 forneceu o melhor desempenho conjunto entre as propriedades elétricas e mecânicas avaliadas. O comportamento reológico foi significativamente afetado pela variação do consumo de PCE, indicando que razões PCE/CBN entre 0.2 a 0.4 são a faixa mais indicada para a produção de CCNS. As análises de DLS, ZPT e UV-VIS possibilitaram uma avaliação coerente do grau de dispersão e estabilidade das nanosuspensões de CBN. As imagens de FEG-MEV apresentaram boa interação com as técnicas analíticas. O conjunto dos resultados analisados sugere que a razão PCE/CBN de 0.4 foi capaz de otimizar as características eletromecânicas e reológicas dos CCNS. Esta razão PCE/CBN produziu nanosuspensões com ótima qualidade de dispersão e estabilidade.*

Palavras-chave: *materiais cimentícios sensores, nanopartículas de carbon black, dispersão de nanopartículas, teor de surfactante, aditivo superplastificante, piezoresistividade.*

4.1 INTRODUÇÃO

O monitoramento das condições de serviço de uma estrutura ao longo de sua vida útil é essencial para manter um nível de desempenho e segurança adequados [1]. Desta forma, o monitoramento da integridade estrutural (*Structural Health Monitoring* - SHM) é uma importante ferramenta não destrutiva, que permite acompanhar em tempo real parâmetros de controle que poderiam levar a formação de futuros mecanismos de falha da estrutura [2]. Devido à sua elevada condutividade elétrica nanopartículas de *Carbon Black* (CBN) podem ser adicionadas à matriz cimentícia para a produção de compósitos cimentícios nanomodificados sensores (CCNS), capazes de monitorar tensões e deformações com uma melhor integração entre o sensor e a estrutura do que sistemas tradicionais de SHM [3–7].

Nos últimos anos, foram produzidos muitos estudos com foco na incorporação de diversos tipos de materiais condutivos e seus efeitos nas propriedades mecânicas e sensoras de CCNS [8–14]. Entretanto, a otimização da dispersão das nanopartículas, visando melhorar as habilidades sensoras sem também causar significativos prejuízos ao comportamento mecânico do material, não fez parte do escopo das pesquisas que empregaram CBN para a construção da rede condutora no interior dos compósitos. Uma dispersão apropriada é um elemento chave para a produção de CCNS com respostas elétricas estáveis e reprodutíveis, além de melhoras no comportamento eletromecânico do material aumentando o número de caminhos condutivos e densificando a matriz cimentícia [15–17].

Os polímeros à base de éter policarboxilato (PCE) são poderosos aditivos com ação superplastificante e redutora do consumo de água, amplamente utilizados na produção de artefatos cimentícios [18]. Os efeitos deste polímero como um agente dispersante também foram investigados em diversas pesquisas [19–21]. O PCE é formado por um grupo carboxilato aniônico que interage por adsorção com a superfície do grão de cimento criando um efeito de dispersão por repulsão eletrostática e também por cadeias laterais não iônicas que proporcionam o efeito de dispersão por impedimento estérico [18,22].

Diferentes tipos de surfactantes já se mostraram eficazes para a quebra de aglomerados de nanotubos de carbono (CNT) devido a mecanismos de descompactação ("*unzipping mechanisms*"), uma vez que a repulsão eletrostática ou estérica associada às moléculas de surfactante compensam as forças de Van der Waals entre os nanomateriais [23–25]. Devido às excelentes opções de PCE disponíveis no mercado e a ótima compatibilidade destes aditivos com sistemas cimentícios, muitos pesquisadores vêm utilizando o PCE não apenas para a

interação com os grãos de cimento e melhora na trabalhabilidade, mas também para a dispersão de nanomateriais incorporados nas matrizes cimentícias [26].

O efeito de diferentes teores de variados tipos de surfactantes na dispersão de CNT foi investigado em vários trabalhos anteriores [27–32]. Quando baixas dosagens são empregadas, menos moléculas de surfactantes são adsorvidas na superfície de CNT, o que compromete a proteção contra a aglomeração. Em proporções mais altas, pode ocorrer a floculação de surfactante ou a formação de micelas. Apesar dos vários trabalhos focados na dispersão de CNT em matrizes cimentícias, os efeitos de diferentes teores de surfactantes na qualidade da dispersão de CBN ainda são desconhecidos. Apesar disso, estudos anteriores já utilizaram o PCE na produção de CCNS com CBN, adotando consumos deste aditivo de forma arbitrária e empírica, sem estabelecer um teor ótimo para a dispersão das nanopartículas [33–35].

A avaliação dos efeitos de diferentes dosagens de PCE na qualidade e estabilidade de dispersões de CBN e seus impactos na resposta piezoresistiva e mecânica dos compósitos produzidos com estas nanosuspensões ainda não foram investigados em trabalhos anteriores. Desta forma, o presente estudo desenvolveu uma investigação dos efeitos do teor de PCE na dispersão de CBN e seus impactos nas propriedades de CCNS. As principais contribuições geradas a partir deste trabalho foram: (i) avaliação conjunta do comportamento eletromecânico e reológico de argamassas produzidas com CBN dispersas com diferentes teores de PCE; (ii) análise da qualidade da dispersão de CBN proporcionada pelos diferentes teores de PCE, utilizando-se uma combinação de quatro diferentes técnicas; e (iii) identificação da relação PCE/CBN ótima para produção de CCNS.

4.2 MATERIAIS E MÉTODOS

4.2.1 Materiais

Para produção dos materiais cimentícios deste estudo, foi utilizado um aditivo superplastificante comercial líquido à base de éter policarboxilato (PCE) com pH de 5.7 e densidade de 1.12 g/cm³. Como *nanofiller* condutivo foram selecionadas nanopartículas de *Carbon Black* (CBN) tipo N234, com tamanho médio de partículas de 20 nm e área superficial específica de 120 m²/g. O aglomerante utilizado foi o cimento Portland CP V-ARI (equivalente ASTM C150 Tipo III). A areia natural utilizada é de origem quartzosa, com massa específica de 2.64 g/cm³ e diâmetro máximo de 2.38 mm. Além disso, foi utilizada água destilada com pH 6.5 em todas as etapas do estudo.

4.2.2 Produção dos corpos de prova

Argamassas nanomodificadas sensoras foram produzidas a partir de nanosuspensões preparadas com um sonicador do tipo sonda com frequência ultrassônica de 20 kHz e potência de 50 W. Para produção de variadas séries de corpos de prova (CP`s) foram utilizadas cinco diferentes razões PCE/CBN, conforme indicado na Tabela 1. Por consequência disso, foram adotados cinco traços diferentes, com uma relação areia/cimento de 1.95 (em massa), água/cimento de 0.56 e um consumo de CBN de 9% em relação ao peso de cimento (Tabela 1).

Tabela 1 – Variação do teor de PCE e consumo de materiais

Série	Razão PCE/CBN (em massa)	Consumo (kg/m³)				
		Cimento	Areia	Água	CBN	PCE
PCE-0	0.0	596.99	1164.18	333.18	53.73	0.00
PCE-1	0.1	594.14	1158.62	331.59	53.47	5.35
PCE-2	0.2	591.31	1153.12	330.02	53.22	10.64
PCE-4	0.4	585.75	1142.26	326.91	52.72	21.09
PCE-8	0.8	574.92	1121.15	320.87	51.74	41.39

Fonte: Autor (2024)

As nanosuspensões foram preparadas fazendo a mistura de CBN, água e os vários teores de PCE, sendo aplicada uma energia de sonicação de 240 J/mL. Na sequência, a nanosuspensão foi levada para um misturador planetário mecânico onde foram adicionados o cimento e a areia durante mistura de cerca de 10 minutos. Ao fim da mistura, foi retirada uma parcela da argamassa para avaliação da plasticidade no ensaio de *Mini-Flow*, utilizando um cone tipo Kantro [36,37].

Após o processo de mistura, a argamassa fresca foi vertida em moldes plásticos, preparados com desmoldante para auxiliar no processo de desforma. Na sequência, o material foi adensado em mesa vibratória por um tempo de 10 segundos. Antes de encaminhar para câmara úmida, os CP`s destinados aos ensaios eletromecânicos passaram por uma etapa adicional, na qual foram embutidos dois eletrodos de cobre (1.4 cm x 3.0 cm x 0.1 cm) na região central de cada CP, separados entre si de cerca de 0.8 cm. Os moldes então foram encaminhados para câmara úmida (umidade relativa >85% e temperatura ambiente de 20 ± 5 ºC), onde foram desformados após 72 horas e permaneceram até completar a idade de 28 dias. Para cada uma das séries foram produzidos três prismas com dimensões de 2.5 cm x 2.5 cm x 7.5 cm (com eletrodos) utilizados nos ensaios para avaliação das propriedades piezoresistivas, três cubos

com aresta de 2.5 cm (sem eletrodos) para os ensaios de resistência mecânica à compressão e um cilindro de 3.5 cm x 7.0 cm para análise microestrutural.

4.2.3 Análise eletromecânica

Para eliminar eventual efeito indesejável na resposta piezoresistiva devido à condução iônica causada pela água livre dos poros da matriz cimentícia, os CP`s foram secos em estufa a aproximadamente 60 ºC por 72 horas e, após isso, foram retirados e resfriados até a temperatura ambiente [38,39]. Na sequência, os CP`s com eletrodo passaram por um ensaio de corrente contínua (CC) para avaliação da resistividade elétrica, além de um segundo ensaio utilizando corrente contínua bifásica (B-CC) para medição da piezoresistividade. Neste segundo caso, os CP`s foram submetidos à aplicação de ciclos de carregamento mecânico de compressão durante as medições elétricas.

Na execução dos ensaios, os CP`s foram conectados em série a um resistor de referência de 1 kΩ (R_{ref}). No ensaio CC, foi aplicada uma tensão constante de 5 V com o auxílio de uma placa eletrônica Arduino Mega (modelo 2560 R3). Já no teste B-CC, esta mesma placa eletrônica foi utilizada para gerar um sinal periódico na forma de onda quadrada de ±5 V e frequência de 6 Hz [7,40], visando reduzir ao máximo os efeitos de polarização. Um instrumento virtual desenvolvido no Labview foi utilizado para medir as quedas de tensão entre o compósito sensor (U_m) e o resistor de referência (U_{ref}). Os dados foram coletados por dois módulos NI-9219 conectados a um sistema de aquisição de dados NI cDAQ-9178. Assim, utilizando as Equações 1 e 2, a corrente elétrica do circuito (i) e a resistência elétrica do compósito (R_m) foram determinadas. Para o caso do ensaio B-CC, i e R_m foram obtidos utilizando os valores de U_m e U_{ref} medidos a 80% do valor da faixa constante positiva da onda quadrada gerada [40–42]. Com a distância entre os eletrodos (L) e sua área efetiva em contato com a argamassa (A), a resistividade elétrica foi calculada utilizando a Equação 3.

Equação 4
$$i = \frac{U_{ref}}{R_{ref}}$$

Equação 5
$$R_m = \frac{U_m}{i}$$

Equação 6
$$\rho = \frac{R_m \ A}{L}$$

O comportamento piezoresistivo dos CCNS foi avaliado por meio de ciclos de carga-descarga, utilizando uma máquina universal de ensaios, aplicando o carregamento em CP`s prismáticos (com eletrodo) a uma taxa constante de 0.50 MPa/s. As deformações longitudinais foram lidas com extensômetros do tipo *clip-gauge*, instalados em posições diametralmente opostas em relação ao eixo central dos CP`s. As variações na resistividade elétrica (FCR) devido aos ciclos de carregamento foram obtidas pelo método B-CC já descrito. O coeficiente angular obtido na equação de regressão linear que correlaciona o valor FCR e de Deformação, corresponde ao fator *Gauge* (GF) dos CCNS.

No início do ensaio, os CP`s eram posicionados sobre um filme isolante instalado no centro do prato da máquina de ensaios. Na sequência, era aplicada uma pequena pré-carga para garantir a fixação adequada do conjunto. Os CCNS então eram submetidos a três ciclos de carregamento com amplitude máxima correspondente a 30% da carga de ruptura prevista. Na sequência, era aplicado um ciclo com três estágios progressivos de carregamento, sendo cada patamar correspondente a 10%, 20% e 30% da carga de ruptura prevista, respectivamente.

O Teste de Grubbs, a um nível de significância de 5%, foi aplicado aos dados experimentais obtidos de resistividade elétrica, fator *Gauge* e resistência mecânica à compressão. Este teste tem por objetivo a verificação da existência de *outliers* no conjunto de dados amostrais.

4.2.4 Análise reológica

A análise reológica do material foi realizada por meio de dois ensaios, o *Mini-Flow* com auxílio de um tronco-cone tipo Kantro e a viscosimetria utilizando um viscosímetro Fann modelo 35A. No caso do *Mini-Flow*, conforme tratado na seção 4.2.2, a medida foi realizada em argamassas, instantes antes da moldagem dos CP`s. Já no caso da viscosimetria, devido a limitações de torque do equipamento, a areia foi retirada das misturas e a medida foi realizada em pastas de cimento. As proporções entre os materiais informadas na seção 4.2.2 foram mantidas. Os ensaios foram realizados em ambiente climatizado, com umidade relativa de 60 ± 3% e temperatura ambiente de 21 ± 1 ºC. Para as análises deste estudo, foi considerado que o comportamento reológico das pastas e argamassas produzida segue o modelo de Bingham.

O ensaio de *Mini-Flow* foi realizado colocando o molde Kantro no centro de uma *Flow-Table* e preenchendo com três camadas de igual altura de argamassa fresca, sendo estas adensadas, respectivamente, com cinco, três e um golpes de uma haste metálica. Em seguida, o

molde era removido e eram aplicadas trinta quedas na *Flow-Table* em um tempo de 30 segundos. Então eram tomadas três medidas em posições distintas para a determinação do índice de espalhamento médio.

Para o ensaio de viscosimetria, foram preparados aproximadamente 500 mL da pasta para cada uma das séries, seguindo o mesmo procedimento descrito na seção 4.2.2 para produção das argamassas. A pasta foi despejada no jarro do equipamento até atingir o volume preestabelecido (350 mL) neste recipiente. O equipamento era ligado e, após a estabilização da leitura, o torque era registrado. A análise dos resultados foi realizada por meio da inclinação das curvas Torque vs. Velocidade angular (correlacionado com a viscosidade plástica) e do ponto de interceptação do eixo das ordenadas pelas curvas (correlacionado com a tensão de escoamento) [18].

4.2.5 Análise dos efeitos do teor de PCE na dispersão de CBN

Com o objetivo de explorar a qualidade da dispersão de CBN associada ao uso de diferentes teores de PCE, foram preparadas diferentes nanosuspensões representativas daquelas utilizadas na produção das argamassas. Inicialmente, misturou-se em um béquer uma quantidade de 0.200 g de PCE e 100.000 g de água, de modo a se obter uma solução de PCE. Em cinco diferentes tubos de ensaio colocou-se 0.025 g de CBN. A seguir, foi adicionada em cada tubo de ensaio uma determinada massa da solução de PCE: 0.000 g, 1.250 g, 2.500 g, 5.000 g e 10.000 g. Nestes tubos de ensaio também foram colocadas quantidades de 24.975 g, 23.725 g, 22.475 g, 19.975 g e 14.975 g de água, respectivamente. Assim, foi possível obter misturas com massa total igual a 25.000 g e razões PCE/CBN (em massa) de 0.0, 0.1, 0.2, 0.4 e 0.8, respectivamente, as quais correspondem diretamente àquelas empregadas na fabricação dos compósitos cimentícios (Tabela 1).

A seguir, cada diferente mistura foi submetida a uma energia de sonicação de 240 J/mL e diluída (fator de diluição igual a 125), a fim de tornar possível a execução de análises de DLS, UV-VIS e Potencial Zeta. Nessa diluição, retirou-se de cada diferente suspensão uma alíquota de 0.200 mL com uma micropipeta automática, a qual foi adicionada à 25.000 mL de água em um outro tubo de ensaio com tampa. Após agitação manual, as misturas obtidas foram submetidas às análises de espalhamento dinâmico de luz (DLS), espectroscopia no ultravioleta visível (UV-VIS) e potencial Zeta (ZPT).

O DLS foi utilizado para estudar os efeitos do uso de diferentes teores de PCE no raio hidrodinâmico e na distribuição do tamanho dos agregados de CBN. Foi utilizado um

Espectrômetro DLS Brookhaven Instruments com correlacionador Turbocorr de 522 canais, posicionamento angular de 90º e laser HeNe (632.8 nm) de 75 mW de potência.

Um espectrômetro UV-VIS FluoroMax HORIBA foi utilizado para determinar os efeitos do uso de diferentes teores de PCE na absorbância resultante da luz absorvida pelas CBN nas nanosuspensões. Foi selecionado pelo monocromador uma lâmpada com comprimento de onda de 350 nm, para uma faixa de leitura entre 250 nm e 750 nm.

Um analisador de ZPT modelo Zetasizer Nano ZS foi utilizado para avaliar os efeitos do uso de diferentes teores de PCE nas nanosuspensões. O dispersante selecionado foi a água, sendo adotados os parâmetros fornecidos pelo equipamento (constante dielétrica de 78.5 e viscosidade de 0.8872 cP). A aproximação de Smoluchowski (1.5) adotada para a Função de Henry, uma vez que amostras analisadas foram consideradas como meios aquosos de concentração moderada de eletrólitos.

A análise microestrutural foi realizada em CP`s cilíndricos, conforme relatado na seção 4.2.2. Estes CP`s foram cortados utilizando uma serra e um disco apropriado para corte de materiais cimentícios. Foi retirada uma lâmina com espessura de aproximadamente 0.4 cm, extraída da parte central do cilindro [43]. Na sequência, para interromper o processo de hidratação do material, as lâminas foram imersas em álcool isopropílico e armazenadas em recipientes individuais com tampa.

As amostras destinadas à microscopia foram previamente preparadas visando garantir condições adequadas para obtenção das imagens. Inicialmente as lâminas foram retiradas do isopropanol e imediatamente foi extraído da porção central um pequeno cubo com lado de cerca de 0.4 cm. Essa amostra foi fixada em um *stub* previamente preparado com fita condutora de carbono. Na sequência, a amostra foi revestida por *sputtering* com uma fina camada de ouro aplicada por um metalizador Quorum Q150RS. Foram obtidas imagens por elétrons secundários das amostras, utilizando um Microscópio Eletrônico de Varredura com Emissão de Campo (FEG-SEM) TESCAN MIRA, com resolução de 1.2 nm a 30 keV. Esta análise teve por objetivo avaliar de forma qualitativa a influência do teor de PCE na interação entre o CBN e a matriz cimentícia endurecida, complementando os resultados de DLS, UV-VIS e ZPT.

4.3 RESULTADOS E DISCUSSÕES

4.3.1 Comportamento eletromecânico

O comportamento eletromecânico dos diferentes compósitos cimentícios nanomodificados foi avaliado por meio da análise da resistividade elétrica, resistência mecânica à compressão e comportamento piezoresistivo. Inicialmente, os dados amostrais obtidos foram submetidos ao Teste de Grubbs para verificação da presença de *outliers*. O teste foi aplicado a um nível de significância de 5% e rejeitou a hipótese de existência de valor atípicos entre os resultados.

Na Figura 1 é apresentada a correlação entre a resistividade elétrica e a resistência à compressão em função da razão PCE/CBN, enquanto na Tabela 2 são mostrados os valores médios obtidos para as propriedades eletromecânicas. O valor máximo de resistividade elétrica média foi de 837.02 Ω.cm para a série PCE-2, com um coeficiente de variação de 20.51%. Este elevado valor de resistividade elétrica quando comparado com as demais séries, associado a uma acentuada variabilidade, possivelmente está relacionado com os problemas ocasionados no adensamento durante a moldagem dos CP`s, com menor dosagem de PCE, os quais serão discutidos de forma mais detalhada na próxima seção.

Entre as séries PCE-2 e PCE-8, foi observada uma redução gradativa da resistividade elétrica média da ordem de 51%. Entretanto, o menor valor de resistividade elétrica média obtido foi de 356.72 Ω.cm para a série PCE-0. Estes resultados podem ser explicados por um aprimoramento inicial do processo de moldagem, que tende a reduzir a quantidade de vazios no compósito e aumentar a quantidade de produtos de hidratação não condutivos que bloqueiam caminhos condutivos entre CBN, o que tende a causar aumentos de resistividade elétrica quando a razão PCE/CBN aumentou de 0 para 0.2 (em massa).

A partir do momento em que os problemas de adensamento foram superados, ficou evidente a contribuição do PCE para melhorar a qualidade da dispersão de nanomateriais e refinar a rede condutiva no interior da matriz cimentícia, o que causou uma redução da resistividade elétrica, mas por outro lado provocou uma maior variação na resposta piezoresistiva, como será discutido mais à frente nesta seção. Apesar disso, os valores de resistividade elétrica média observados estão na mesma ordem de grandeza daqueles observados em outras pesquisas que também estudaram argamassas sensoras [44,45].

Figura 1 – Relação entre resistividade elétrica e resistência à compressão em função da razão PCE/CBN.

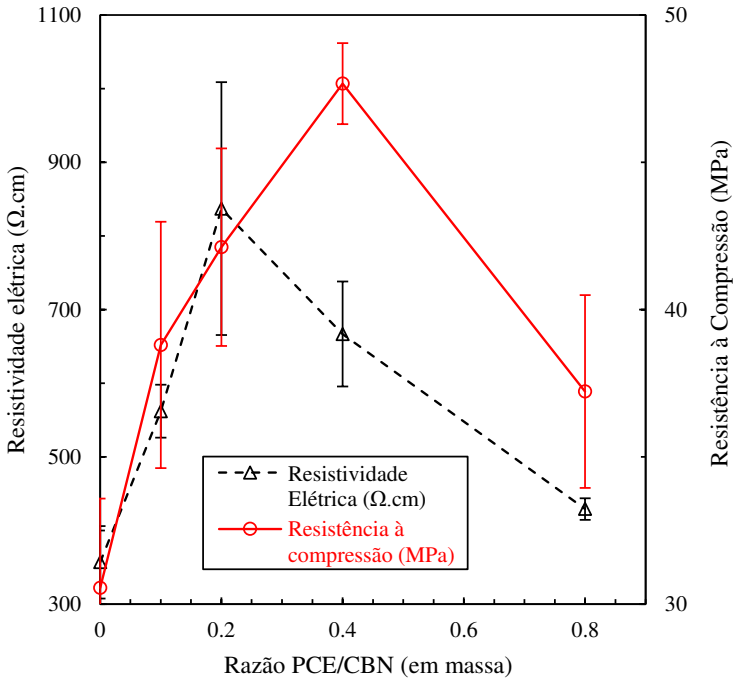

Fonte: Autor (2024)

Quanto à resistência à compressão média, foi observado um crescimento de 30.54 MPa da série PCE-0 para 47.67 MPa da série PCE-4, seguido de uma redução para 37.22 MPa da série PCE-8. Até certo ponto, o aumento da razão PCE/CBN ajustou de forma mais adequada a trabalhabilidade da argamassa, corrigindo problemas de moldagem. Isto também favoreceu a manutenção da dispersão das nanopartículas e causou um aumento da resistência à compressão de até 56.1% com relação à série de referência. Entretanto, o aumento excessivo de PCE no sistema trouxe impactos negativos para o processo de hidratação da matriz cimentícia, como será discutido de forma mais detalhada nas seções posteriores. A série PCE-4 foi a que demonstrou o melhor desempenho mecânico, sugerindo que a razão PCE/CBN igual a 0.4 proporcionou o melhor equilíbrio entre dispersão das nanopartículas e plasticidade da argamassa.

Tabela 2 – Propriedades eletromecânicas dos CCNS

Série	Relação PCE/CBN (em massa)	Resistividade elétrica (Ω.cm)		Resistência à compressão (MPa)		Fator *Gauge*	
		Média	Desvio Padrão	Média	Desvio Padrão	Média	Desvio Padrão
PCE-0	0.0	356.72	49.09	30.54	3.03	183.33	51.29
PCE-1	0.1	561.82	35.99	38.80	4.18	244.00	26.15
PCE-2	0.2	837.02	171.71	42.12	3.35	148.33	17.39
PCE-4	0.4	666.64	71.31	47.67	1.38	161.33	31.01
PCE-8	0.8	429.14	14.64	37.22	3.27	134.67	7.64

Fonte: Autor (2024)

Na Figura 2 são apresentadas as relações entre a variação relativa da resistividade elétrica (FCR) e a deformação, obtidas nos ensaios piezoresistivos. Em todos os gráficos foi adotada a mesma escala para os eixos vertical e horizontal, sendo que as repetições de uma mesma série foram plotadas em um mesmo gráfico (CP1 – Azul; CP2 – Laranja; CP3 – Verde). Todos os ensaios foram realizados no regime elástico-linear e atingiram deformações máximas da ordem de 800 με. A resposta elétrica apresentou boa repetibilidade e baixa histerese, sendo as variações máximas de FCR de cerca de 12%. Foram ajustados modelos de regressão linear para descrever o comportamento da relação FRC vs deformação de cada uma das repetições. O coeficiente angular de cada um dos modelos de regressão obtidos representa o GF do material e foi apresentado na Tabela 2. Considerando os valores obtidos para o coeficiente de determinação (R^2) dos modelos de regressão linear, é possível afirmar que estes modelos foram capazes de descrever de forma satisfatória o comportamento dos dados amostrais.

A série PCE-0 apresentou os valores mais baixos de deformação, sendo que apenas o CP1-PCE-0 atingiu valores de FCR superiores a 8%. Em especial, esta série foi a que apresentou uma maior variação do coeficiente angular entre as repetições. Este fato provavelmente está relacionado aos problemas de moldagem observados durante a produção dos compósitos, sendo estes tratados com maiores detalhes na seção posterior. As séries PCE-1 e PCE-2, apresentaram modelos de regressão que representam de forma adequada a relação FCR vs deformação, obtendo valores de R^2 que variaram de 0.9790 a 0.9879. A série PCE-4 foi a que atingiu os maiores valores de deformação e FCR, o que está relacionado à elevada resistência à compressão dessa série (quanto maior a resistência à compressão do material, maior foi a amplitude de carregamento durante os ensaios piezoresistivos e, consequentemente, maiores os níveis de deformação e FCR do material). Por outro lado, a série PCE-8 foi a que apresentou o menor valor de R^2, no caso do CP1-PCE-8 (R^2 = 0.9197). Esta elevada variabilidade quando comparada com os demais CP`s, possivelmente está relacionada à baixa viscosidade dessa mistura, conforme será melhor explicado na seção 4.3.2 (Comportamento reológico).

Figura 2 – Relação entre FCR e Deformação das argamassas (Codificação de cores: CP1 – Azul; CP2 – Laranja; CP3 – Verde): (A) PCE-0; (B) PCE-1; (C) PCE-2; (D) PCE-4; (E) PCE-8.

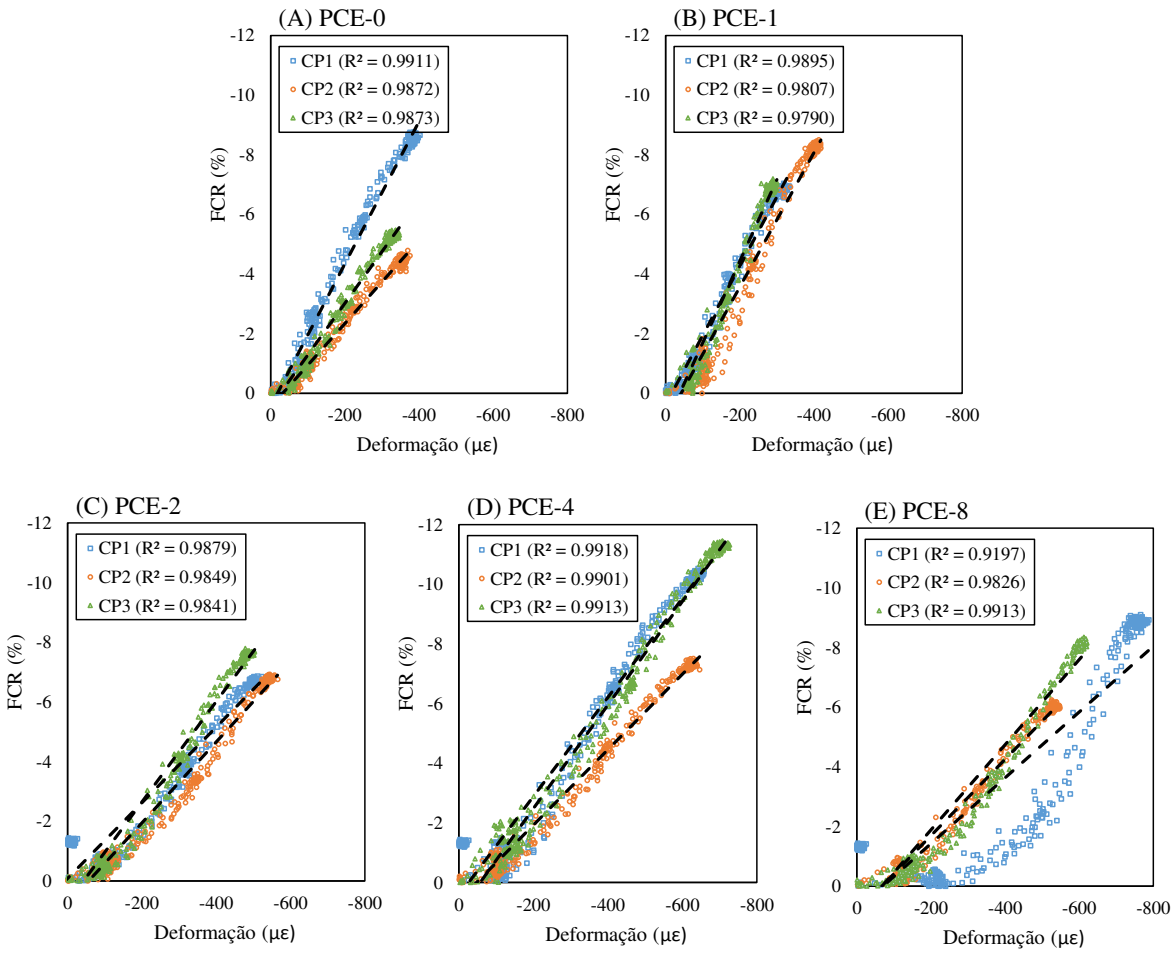

Fonte: Autor (2024)

A relação entre a resistividade elétrica e o GF em função da razão PCE/CBN é apresentada na Figura 3. Os valores médios obtidos para o GF variaram de 134.67 (PCE-8) a 244.00 (PCE-1), e estão em conformidade com valores observados na literatura [7,46–49]. De forma geral, os valores de GF observados indicam uma boa sensibilidade para monitorar deformações dos CCNS produzidos. A série PCE-0 apresentou um GF médio de 183.33, entretanto com um coeficiente de variação de 27.97%, o maior dentre todas as séries do estudo. Este comportamento já foi discutido anteriormente e está associado à variabilidade do coeficiente angular das repetições desta série. A série PCE-1 alcançou o maior valor de GF médio (244.00), que teve um coeficiente de variação de 10.72%. Entretanto, esta série apresentou valores de resistência à compressão mais baixos, o que consequentemente fez com o que elemento sensor atingisse deformações significativamente menores que séries com razão PCE/CBN superiores a 0.2. As séries PCE-4 e PCE-8 alcançaram valores de GF de 161.33 e 134.67, respectivamente. Esta redução no valor de GF da série PCE-8 já era esperada, uma vez

o teor excessivo de PCE desta série, impactou seu comportamento reológico e suas propriedades mecânicas.

Figura 3 – Relação entre resistividade elétrica e fator *Gauge* em função da razão PCE/CBN.

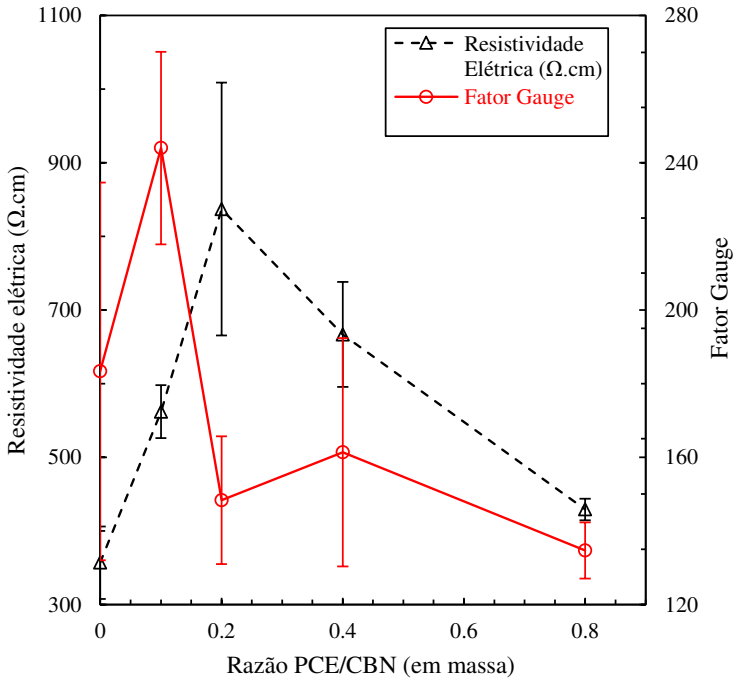

Fonte: Autor (2024)

Os resultados dos ensaios eletromecânicos sugerem que a faixa da razão PCE/CBN estudada foi capaz de produzir CCNS com habilidades sensoras adequadas para o monitoramento de deformações. A queda progressiva de resistividade elétrica (após contornados os problemas de moldagem) e a qualidade da resposta piezoresistiva indicam que a condução eletrônica (tunelamento quântico e contato) foi o mecanismo dominante de transporte de elétrons nas argamassas estudadas. Este bom comportamento piezoresistivo observado é um indício de que a etapa de sonicação foi eficiente em dispersar as nanopartículas [50] e que a adição de PCE contribuiu de forma satisfatória com a manutenção desta dispersão.

A variação da razão PCE/CBN influenciou de forma significativa o comportamento eletromecânico das argamassas sensoras. A razão PCE/CBN de 0.8 impactou de forma negativa o desempenho mecânico do material. Razões PCE/CBN menores que 0.2 apresentaram uma boa resposta piezoresistiva, entretanto os elementos sensores atingiram níveis de resistência à compressão mais modestos. De forma geral, a razão PCE/CBN igual a 0.4 foi a que forneceu o melhor desempenho conjunto entre as propriedades elétricas e mecânicas avaliadas. Desta forma, esta razão seria a mais apropriada para a produção de CCNS.

4.3.2 Comportamento reológico

Para a análise reológica dos CCNS, foi considerado que as pastas e argamassas produzidas se comportam segundo o modelo de Bingham [51,52]. Este modelo é uma forma simples de descrever o comportamento plástico de um fluido não-Newtoniano, utilizando como parâmetros a tensão de escoamento e a viscosidade plástica [53,54]. A inclinação da curva Torque vs. Velocidade angular está relacionada com a viscosidade plástica do material, enquanto o ponto de interceptação do eixo das ordenadas pela curva está relacionado com a tensão de escoamento [18].

As curvas Torque vs. Velocidade angular das pastas e o comportamento reológico em função da relação PCE/CBN, são apresentados na Figura 4. Os efeitos da variação da relação PCE/CBN são nítidos com a mudança do coeficiente angular apresentado na Figura 4A. Em todas as misturas, o ponto de intercessão das curvas com eixo das ordenadas (Torque) foi próximo a zero, evidenciando a ação do PCE, praticamente anulando a tensão de escoamento das pastas [18]. A série PCE-0, na qual não foi adicionado PCE, teve a curva de maior inclinação, o que sugere a maior viscosidade plástica. Em contrapartida, a série PCE-8, na qual foi adicionado 8% de PCE em relação à massa de CBN, apresentou a menor inclinação, sendo o coeficiente angular cerca de 9.5 vezes menor que o da série PCE-0, indicando uma redução drástica da viscosidade plástica da pasta.

Figura 4 – Curvas Torque vs. Velocidade angular das pastas estudadas (A) e comportamento reológico em função da razão PCE/CBN (B).

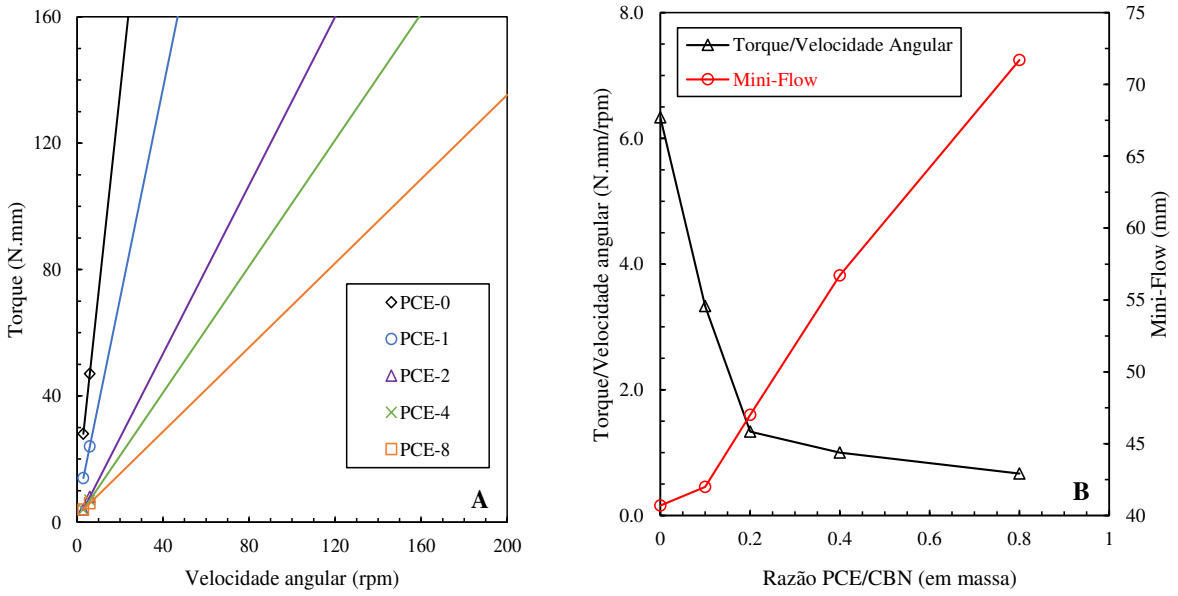

Fonte: Autor (2024)

Na figura 4B é apresentado o comportamento reológico por meio das relações entre razão Torque/Velocidade angular (correlacionado à viscosidade plástica), o espalhamento (*Mini-Flow*) e a razão PCE/CBN. De forma geral, o aumento da razão PCE/CBN levou a uma redução da razão Torque/Velocidade angular e aumento do espalhamento. A título de exemplificar, a série PCE-1 apresentou uma razão Torque/Velocidade angular da ordem de 3.3 vezes maior que a da série PCE-4, enquanto o espalhamento foi cerca de 26% menor em comparação com a mesma série. As séries PCE-0 e PCE-1, devido a sua elevada viscosidade, apresentaram consistência inadequada para a moldagem e adensamento. Já a série PCE-8, devido à baixa viscosidade, apresentou uma grande dificuldade para permitir o posicionamento adequado dos eletrodos. A série PCE-4 apresentou as melhores condições de moldagem e adensamento, com espalhamento de 56.7 mm.

Estudos que investigaram os efeitos de diferentes surfactantes na trabalhabilidade de matrizes cimentícias contendo nanoplaquetas de grafeno e nanotubos de carbono [16,19] observaram um comportamento semelhante. Papanikolau et al. [19] indicam que dosagens mais baixas de surfactantes podem não ser capazes de dispersar as nanopartículas e manter um equilíbrio adequado entre a dispersão e a viscosidade do material. Apesar do aumento do teor de PCE melhorar a trabalhabilidade das matrizes cimentícias nanomodificadas, dosagens muito elevadas de PCE favorecem o processo de exsudação, causando uma distribuição desigual das partículas sólidas na matriz cimentícia [19,55]. Como o PCE causa uma redução acentuada da tensão de escoamento, o sistema passa a não suportar mais o peso próprio da pasta, favorecendo o processo de sedimentação e consequentemente aumentando a exsudação [55].

A variação da razão PCE/CBN teve impactos diretos no comportamento reológico das misturas. Os problemas de moldagem observados para as razões PCE/CBN menores que 0.2 causaram uma maior dispersão nos valores de resistividade elétrica discutidos na seção anterior. Já a razão PCE/CBN da ordem de 0.8, afetaram negativamente as propriedades mecânicas do material. Desta forma, considerando-se também os resultados dos ensaios eletromecânicos, é possível notar que o comportamento reológico observado mais adequado para a produção de CCNS foi para a faixa da razão PCE/CBN entre 0.2 a 0.4.

4.3.3 Efeitos da razão PCE/CBN na dispersão de CBN

A relação entre o tamanho médio dos agregados de CBN e o ZPT em função da variação da razão PCE/CBN é apresentada na Figura 5. Segundo os resultados observados de DLS, o aumento da razão PCE/CBN implicou em uma significativa redução no tamanho médio dos

agregados de CBN. O tamanho médio observado na série PCE-0 foi de 2261.0 nm, enquanto na série PCE-8 foi de 189.0 nm, o que representa uma redução de aproximadamente 12 vezes. O aumento da quantidade de PCE disponível na nanosuspensão, permite que uma maior quantidade de moléculas de PCE passe a interagir com as CBN, otimizando o efeito da sonicação e evitando a reaglomeração das nanopartículas [19,23–25]. No caso de nanotubos de carbono, estudos prévios já verificaram que a cobertura da superfície destes nanomateriais com moléculas de surfactantes é capaz de aprimorar a qualidade da dispersão, uma vez que estas se orientam de tal forma que sua extremidade hidrofóbica se volta para a superfície dos nanotubos de carbono e a extremidade hidrofílica se curva para a fase aquosa, o que tende a evitar a tendência de reaglomeração dos nanomateriais por forças de Van der Waals [23,56].

A estabilidade das nanosuspensões pode ser determinada pelo ZPT, que está ligado ao grau de repulsão eletrostática entre as partículas em uma solução. Desta forma, quanto maior o valor de ZPT (em módulo), maiores serão as energias de repulsão, reduzindo ou até eliminando a reaglomeração das nanopartículas [57,58]. Um ZPT da ordem de 30 mV já é suficiente para manter a estabilidade de uma suspensão com partículas menores que 1 μm por um curto prazo de tempo [57,59]. De forma geral, um aumento da razão PCE/CBN implicou em um aumento do ZPT, o que está de acordo com o observado na literatura para materiais cimentícios [60]. Na série PCE-0, foi observado o valor de -22.73 mV para o ZPT, o menor valor médio (em módulo) dentre as dispersões avaliadas. Por outro lado, a série PCE-8 atingiu o maior valor médio (em módulo), um ZPT de -29.67 mV, o que representou um aumento absoluto da ordem de 30%. As maiores dispersões dos dados foram observadas nas séries PCE-2 e PCE-8, com desvio padrão de 0.62 mV e 0.67 mV, respectivamente. Entretanto, as variações dos resultados são inferiores às observadas na literatura para outros nanomateriais [61,62].

Figura 5 – Relação entre o tamanho dos agregados de CBN e o potencial zeta em função da razão PCE/CBN.

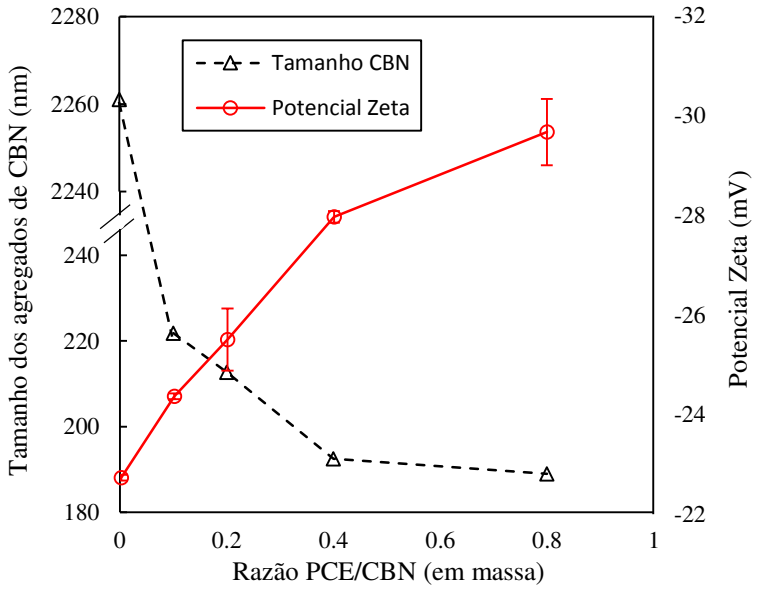

Fonte: Autor (2024)

O espectrograma de absorbância na faixa do UV-VIS obtido para as diferentes razões PCE/CBN, considerando que a comparação das concentrações ocorreu dentro do limite de validade da Lei de Lambert-Beer, é apresentado na Figura 6. Com o aumento desta razão, foi observado um comportamento geral de aumento na absorção de luz das soluções, sugerindo que teores mais elevados de PCE foram eficientes em manter as partículas dispersas no sistema. A absorção de luz máxima ocorreu na faixa de comprimentos de onda de 250 nm a 270 nm, conforme indicado em destaque na Figura 6. Essa faixa de absorção está ligada a transições eletrônicas tipo π-π* relacionadas a nanomateriais à base de carbono sendo que um aumento na quantidade de excitações π-π* pode ser associado a uma maior área de CBN exposta à radiação UV [63,64].

Diferentemente dos resultados das análises de DLS e ZPT, foi observado que a maior absorção de luz UV ocorreu na série PCE-2. Esta resposta aparentemente anômala, pode indicar que esta razão PCE/CBN também pôde ter sido bastante eficiente para manter o equilíbrio das nanosuspensões. Este resultado aparentemente está em conformidade com o já discutido na seção 4.2.2, que indicou que o equilíbrio mais adequado entre dispersão de CBN e viscosidade das argamassas, foi observado para a faixa da razão PCE/CBN entre 0.2 a 0.4. Para a série PCE-0, os níveis de absorção de luz UV foram drasticamente mais baixos que os observados em todas as séries em que foi empregado o surfactante, o que sugere que a ausência de PCE não apenas favoreceu a imediata reaglomeração das nanopartículas após o processo de sonicação, mas também limitou o potencial de dispersão de CBN por métodos ultrassônicos,

reduzindo a área superficial de CBN capaz de absorver a luz UV. As séries PCE-4 e PCE-8, atingiram níveis de absorção de luz máximos próximos dos níveis da série PCE-2, o que sugere que estas séries também apresentam boas condições de qualidade de dispersão de CBN.

Figura 6 – Espectrograma de absorbância no UV-VIS para diferentes níveis de energia de sonicação.

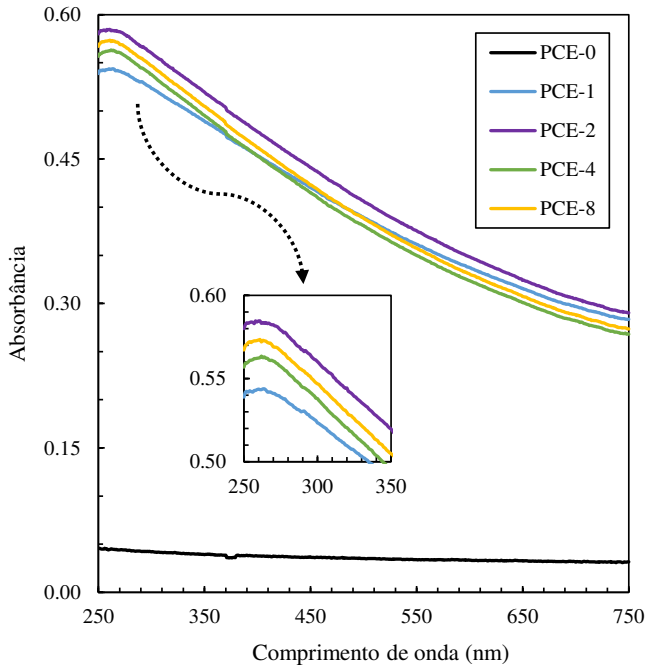

Fonte: Autor (2024)

A avaliação dos efeitos do teor de PCE na dispersão das CBN em meio aquoso foi complementada por uma análise microestrutural após o período de cura de 28 dias. Desta forma, foram utilizadas micrografias obtidas por meio de FEG-MEV para realizar uma avaliação qualitativa da interação entre o CBN e esta matriz.

As imagens de FEG-MEV das argamassas, com ampliação de 80 kx (escala gráfica de 1 µm), são apresentadas na Figura 7. Analisando as imagens, foram identificados sinais da presença de cristais com morfologia compatível com a etringita, hidróxido de cálcio (CH) e a calcita ($CaCO_3$). A presença de etringita em idades mais avançadas pode ocorrer em cimentos que contenham calcita, uma vez que a formação de monocarbonatos causa uma estabilização indireta da etringita e impede sua precipitação em monossulfatos [65,66]. Não foram identificadas formações que possam indicar a presença de contaminações, defeitos ou descontinuidades incomuns de uma matriz cimentícia. Foi observado um grande número de estruturas em formato de cachos, formadas por conjuntos de esferas, dispersas em uma formação floculada característica do gel de silicatos de cálcio hidratados (C-S-H), indicando uma interação adequada entre C-S-H e CBN.

O aumento da relação PCE/CBN sugere que inicialmente ocorreu um refinamento da matriz cimentícia, uma vez que foi observado um ganho de resistência mecânica à compressão média de cerca de 56% da série PCE-0 para PCE-4. Entretanto, também se observa uma redução da ordem de 22% da série PCE-4 para PCE-8 para esta mesma propriedade. Este efeito deletério no comportamento mecânico já foi reportado em outros trabalhos e indica que dosagens elevadas de PCE impactam negativamente o processo de hidratação do cimento [60,67,68], conforme discutido na seção 4.3.1. O PCE, quando em excesso na mistura, interage com os grãos de cimento impedindo que a água consiga acessar os grãos e iniciar a sua dissolução, causando um atraso no processo de hidratação da pasta.

Figura 7 – Micrografias das argamassas com ampliação de 80 kx (escala gráfica de 1 µm): (A) PCE-0; (B) PCE-1; (C) PCE-2; (D) PCE-4; (E) PCE-8.

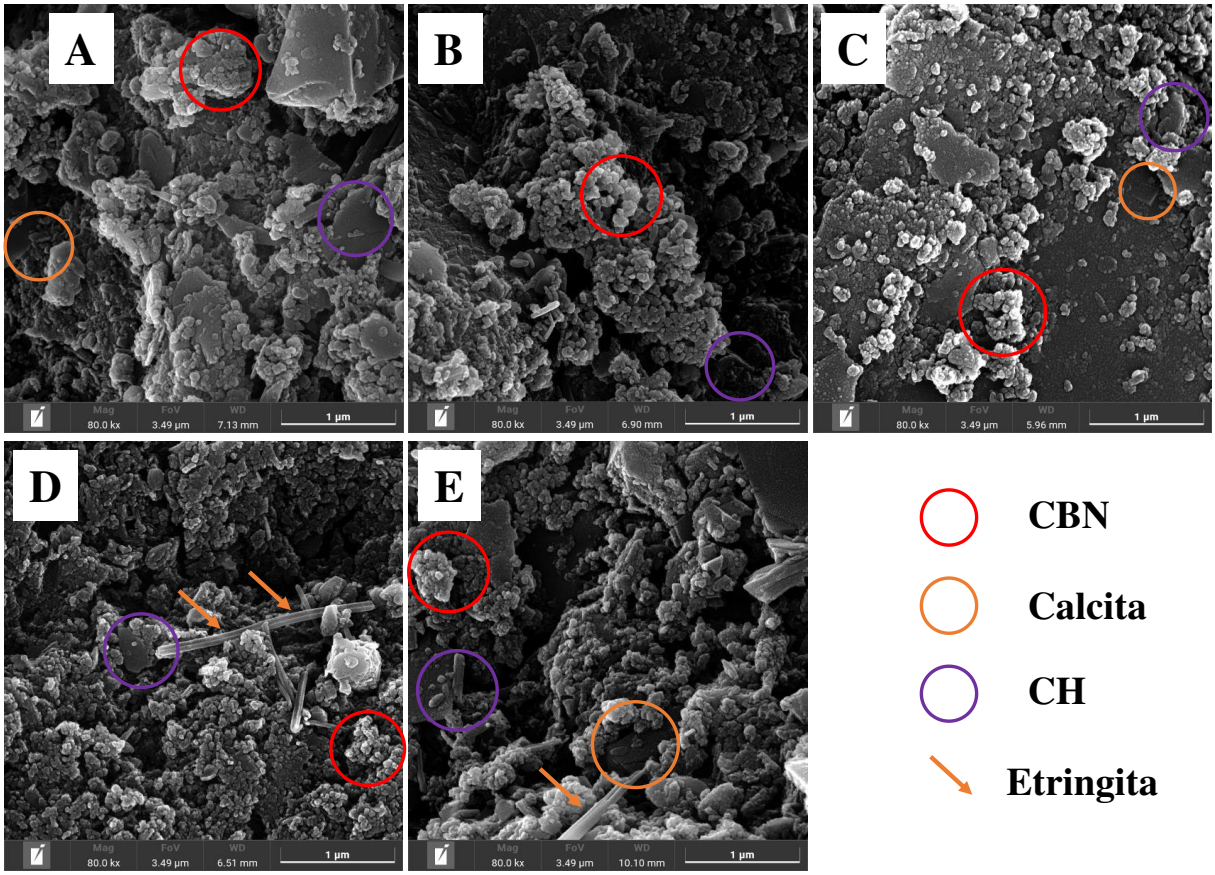

Fonte: Autor (2024)

Na Figura 8, são apresentadas as imagens de FEG-MEV das argamassas com ampliação de 200 kx (escala gráfica de 200 nm). Fica evidenciado que o aumento do teor de PCE disponível no sistema potencializou os efeitos da sonicação, garantindo que os agregados de CBN não se reaglomerassem rapidamente, em conformidade com os resultados obtidos para o DLS (Figura 5), o que tende a evitar o surgimento de pontos de fraqueza no interior da matriz. Também é possível verificar na Figura 8, uma grande quantidade de estruturas dispersas

compatíveis com os agregados de CBN, de tamanho cada vez menor com o aumento da razão PCE/CBN, o que reforça o fato constatado pelas análises prévias (DLS, ZPT e UV-VIS) de que o aumento da quantidade de PCE no sistema reduziu a reaglomeração de CBN. A redução da resistividade elétrica observada para as relações PCE/CBN de 0.2 a 0.8, indicam que ocorreu uma maior formação de caminhos condutivos (Figura 1), possivelmente relacionada à maior estabilidade das nanosuspensões, em conformidade com os resultados de ZPT. Uma maior estabilidade das nanosuspensões mantém as CBN adequadamente dispersas, estabelecendo condições favoráveis para que estas partículas funcionem como pontos de nucleação para os hidratos do cimento [69–71]. Este efeito tem impacto direto na melhoria das propriedades mecânicas do material, o que já foi discutido de forma mais detalhada anteriormente e pôde ser observado na Figura 1.

Figura 8 – Micrografias das argamassas com ampliação de 200 kx (escala gráfica de 200 nm): (A) PCE-0; (B) PCE-1; (C) PCE-2; (D) PCE-4; (E) PCE-8.

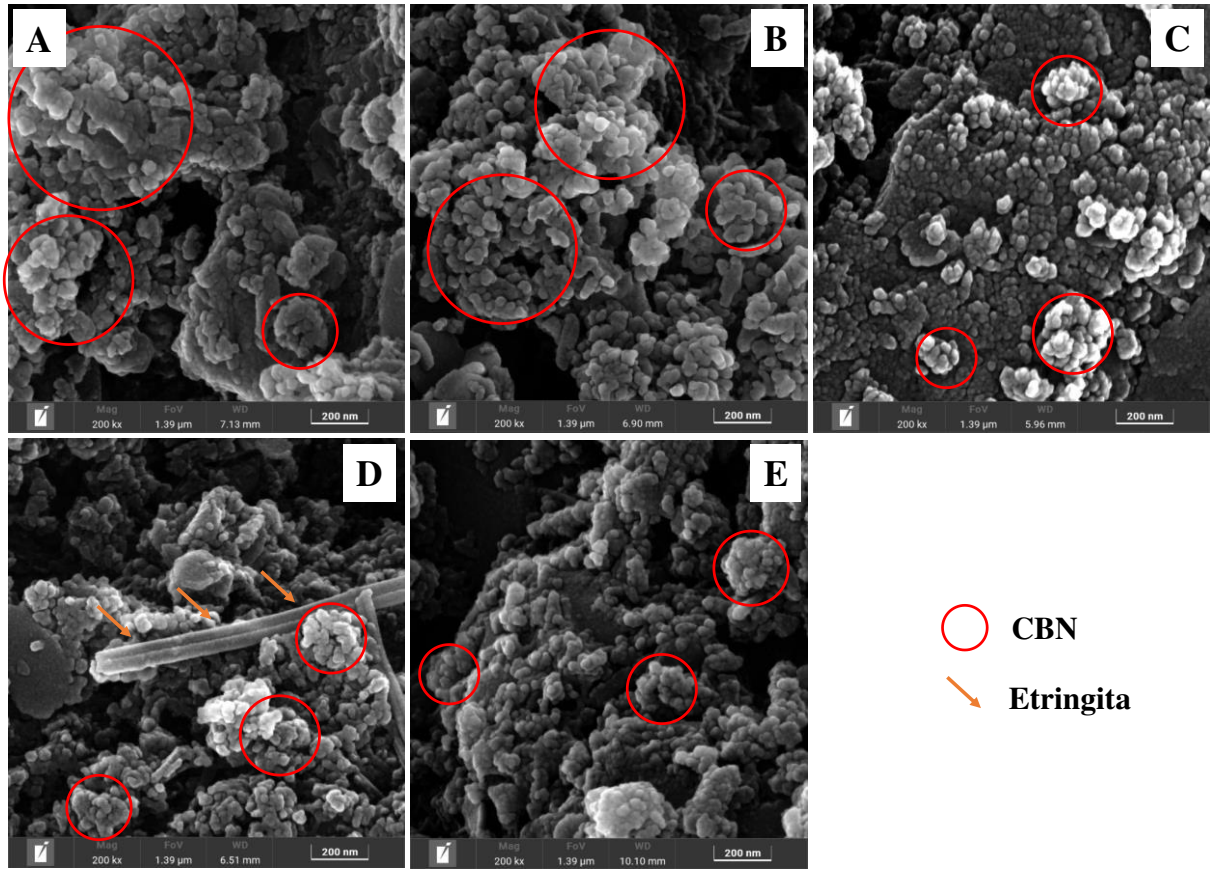

Fonte: Autor (2024)

Apesar dos resultados combinados de DLS e ZPT indicarem uma acentuada redução do tamanho médio dos aglomerados de CBN e uma boa estabilidade dos CCNS com razão PCE/CBN maior que 0.4, os maiores valores de GF médio foram obtidos para as séries PCE-0 e PCE-1, 183.3 e 244.0 respectivamente. Entretanto, a série PCE-0 apresentou um coeficiente

de variação de 27.97%, o maior entre as misturas estudadas. Este fato indica que a ausência de PCE, além de afetar a plasticidade da mistura e prejudicar a moldagem, também favoreceu a reaglomeração das CBN e prejudicou a formação de caminhos condutivos, impactando negativamente na condução eletrônica por tunelamento, a qual é responsável pela resposta sensora de matrizes cimentícias nanomodificadas [5,15,72].

As análises de DLS, ZPT e UV-VIS possibilitaram uma avaliação coerente do grau de dispersão e estabilidade das nanosuspensões de CBN. Os efeitos provocados pela variação da razão PCE/CBN alteraram de forma significativa o comportamento da dispersão de CBN. As imagens de FEG-MEV apresentaram boa interação com a resposta das técnicas analíticas, indicando seu potencial uso como ferramenta complementar qualitativa para compreensão da disposição das CBN na matriz cimentícia em seu estado endurecido. Quanto à relação PCE/CBN, valores menores que 0.2 causaram uma maior chance de reaglomeração devido ao seu ZPT mais baixo quando comparado às demais relações PCE/CBN. Por outro lado, os menores tamanhos médios de agregados de CBN, foram observados para relações PCE/CBN superiores a 0.4. Entretanto, a relação igual a 0.8 causou queda na resistência mecânica quando se compara com a série anterior. A análise conjunta do desempenho eletromecânico dos compósitos cimentícios e da qualidade de dispersão das nanosuspensões indica que as relações PCE/CBN entre 0.2 e 0.4 são as mais adequadas para a produção de CCNS.

4.4 CONCLUSÕES

Os impactos da variação da razão PCE/CBN no comportamento eletro-mecânico e reológico de CCNS foram investigados no presente trabalho. Além disso, este estudo realizou uma análise da qualidade das nanosuspensões proporcionada por diferentes teores de surfactante. As principais conclusões do estudo são as seguintes:

(1) O comportamento eletromecânico das argamassas sensoras sofreu forte influência da variação da razão PCE/CBN. A quantidade excessiva de PCE (razão PCE/CBN igual a 0.8), causou uma redução na resistência à compressão do material. Apesar da boa resposta piezoresistiva, os elementos sensores produzidos com uma razão PCE/CBN menores que 0.2, apresentaram menores valores de resistência mecânica. De forma geral, a razão PCE/CBN igual a 0.4 foi a que proporcionou o melhor desempenho conjunto entre as propriedades elétricas e mecânicas avaliadas.

(2) A variação da razão PCE/CBN teve impactos diretos no comportamento reológico das misturas. Razões PCE/CBN menores que 0.2 apresentaram consistência inadequada para a moldagem e adensamento. A razão PCE/CBN igual a 0.8, afetou negativamente as propriedades mecânicas do material, devido à elevada dosagem de PCE. O comportamento reológico observado mais adequado para a produção de CCNS foi para a faixa da razão PCE/CBN entre 0.2 a 0.4.

(3) O grau de dispersão e estabilidade das nanosuspensões foi avaliado de forma satisfatória com as técnicas de DLS, ZPT e UV-VIS. A variação da razão PCE/CBN alterou de forma significativa o comportamento da dispersão de CBN. As imagens de FEG-MEV apresentaram boa interação com a resposta das técnicas analíticas, proporcionando uma boa avaliação da matriz cimentícia endurecida. As técnicas indicaram que relações PCE/CBN menores que 0.2 levaram a uma maior tendência de reaglomeração de CBN. Por outro lado, os menores tamanhos médios de agregados de CBN, foram observados para relações PCE/CBN superiores a 0.4. A análise das nanosuspensões indicou que as relações PCE/CBN entre 0.2 e 0.4 são as mais adequadas para a produção de CCNS.

(4) O conjunto dos resultados analisados neste trabalho sugerem que a razão PCE/CBN de 0.4 foi capaz de otimizar as características eletromecânicas e reológicas dos CCNS. Esta razão PCE/CBN produziu nanosuspensões com ótima qualidade de dispersão e estabilidade, o que implicou em uma matriz cimentícia mais refinada e em um aumento dos caminhos condutivos.

A fim de avançar neste campo do conhecimento, são sugeridas futuras pesquisas para investigar os efeitos do uso de diferentes razões PCE/CBN na durabilidade dos CCNS e os impactos da aplicação de diferentes tipos de surfactantes em nanosuspensões e em suas implicações nas propriedades eletromecânicas dos compósitos sensores.

4.5 REFERÊNCIAS

[1] M. Siahkouhi, G. Razaqpur, N.A. Hoult, M. Hajmohammadian Baghban, G. Jing, Utilization of carbon nanotubes (CNTs) in concrete for structural health monitoring (SHM) purposes: A review, Constr. Build. Mater. 309 (2021) 125137. https://doi.org/10.1016/j.conbuildmat.2021.125137.

[2] M. Mishra, P.B. Lourenço, G.V. Ramana, Structural health monitoring of civil engineering structures by using the internet of things: A review, J. Build. Eng. 48 (2022) 103954. https://doi.org/10.1016/j.jobe.2021.103954.

[3] L. Wang, F. Aslani, A review on material design, performance, and practical application of electrically conductive cementitious composites, Constr. Build. Mater. 229 (2019) 116892. https://doi.org/10.1016/j.conbuildmat.2019.116892.

[4] W. Dong, W. Li, Z. Tao, K. Wang, Piezoresistive properties of cement-based sensors: Review and perspective, Constr. Build. Mater. 203 (2019) 146–163. https://doi.org/10.1016/j.conbuildmat.2019.01.081.

[5] S. Ding, S. Dong, A. Ashour, B. Han, Development of sensing concrete: Principles, properties and its applications, J. Appl. Phys. 126 (2019). https://doi.org/10.1063/1.5128242.

[6] F. Ubertini, A. D'Alessandro, Concrete with self-sensing properties, in: Eco-Efficient Repair Rehabil. Concr. Infrastructures, Elsevier, 2018: pp. 501–530. https://doi.org/10.1016/B978-0-08-102181-1.00018-6.

[7] G.H. Nalon, J.C.L. Ribeiro, E.N.D. de Araújo, L.G. Pedroti, J.M.F. de Carvalho, R.F. Santos, A. Aparecido-Ferreira, Effects of different kinds of carbon black nanoparticles on the piezoresistive and mechanical properties of cement-based composites, J. Build. Eng. 32 (2020) 101724. https://doi.org/10.1016/J.JOBE.2020.101724.

[8] W. Li, W. Dong, L. Shen, A. Castel, S.P. Shah, Conductivity and piezoresistivity of nano-carbon black (NCB) enhanced functional cement-based sensors using polypropylene fibres, Mater. Lett. 270 (2020) 127736. https://doi.org/10.1016/j.matlet.2020.127736.

[9] W. Dong, W. Li, K. Wang, Y. Guo, D. Sheng, S.P. Shah, Piezoresistivity enhancement of functional carbon black filled cement-based sensor using polypropylene fibre, Powder Technol. 373 (2020) 184–194. https://doi.org/10.1016/j.powtec.2020.06.029.

[10] W. Dong, W. Li, K. Wang, B. Han, D. Sheng, S.P. Shah, Investigation on physicochemical and piezoresistive properties of smart MWCNT/cementitious

composite exposed to elevated temperatures, Cem. Concr. Compos. 112 (2020) 103675. https://doi.org/10.1016/j.cemconcomp.2020.103675.

[11] L. Zhang, S. Ding, B. Han, X. Yu, Y.-Q. Ni, Effect of water content on the piezoresistive property of smart cement-based materials with carbon nanotube/nanocarbon black composite filler, Compos. Part A Appl. Sci. Manuf. 119 (2019) 8–20. https://doi.org/10.1016/j.compositesa.2019.01.010.

[12] D.-Y. Yoo, I. You, H. Youn, S.-J. Lee, Electrical and piezoresistive properties of cement composites with carbon nanomaterials, J. Compos. Mater. 52 (2018) 3325–3340. https://doi.org/10.1177/0021998318764809.

[13] A. D'Alessandro, D. Coffetti, E. Crotti, L. Coppola, A. Meoni, F. Ubertini, Self-Sensing Properties of Green Alkali-Activated Binders with Carbon-Based Nanoinclusions, Sustainability. 12 (2020) 9916. https://doi.org/10.3390/su12239916.

[14] A. Belli, A. Mobili, T. Bellezze, F. Tittarelli, P. Cachim, Evaluating the Self-Sensing Ability of Cement Mortars Manufactured with Graphene Nanoplatelets, Virgin or Recycled Carbon Fibers through Piezoresistivity Tests, Sustainability. 10 (2018) 4013. https://doi.org/10.3390/su10114013.

[15] B. Han, S. Ding, X. Yu, Intrinsic self-sensing concrete and structures: A review, Measurement. 59 (2015) 110–128. https://doi.org/10.1016/j.measurement.2014.09.048.

[16] M. Mardani, S. Hossein Hosseini Lavassani, M. Adresi, A. Rashidi, Piezoresistivity and mechanical properties of self-sensing CNT cementitious nanocomposites: Optimizing the effects of CNT dispersion and surfactants, Constr. Build. Mater. 349 (2022) 128127. https://doi.org/10.1016/j.conbuildmat.2022.128127.

[17] J. da S. Andrade Neto, T.A. Santos, S. de A. Pinto, C.M.R. Dias, D.V. Ribeiro, Effect of the combined use of carbon nanotubes (CNT) and metakaolin on the properties of cementitious matrices, Constr. Build. Mater. 271 (2021) 121903. https://doi.org/10.1016/j.conbuildmat.2020.121903.

[18] J.M. Franco de Carvalho, W. Schmidt, H.C. Kühne, R.A.F. Peixoto, Influence of high-charge and low-charge PCE-based superplasticizers on Portland cement pastes containing particle-size designed recycled mineral admixtures, J. Build. Eng. 32 (2020) 101515. https://doi.org/10.1016/J.JOBE.2020.101515.

[19] I. Papanikolaou, L. Ribeiro de Souza, C. Litina, A. Al-Tabbaa, Investigation of the dispersion of multi-layer graphene nanoplatelets in cement composites using different superplasticiser treatments, Constr. Build. Mater. 293 (2021) 123543. https://doi.org/10.1016/j.conbuildmat.2021.123543.

[20] K. Samimi, M. Pakan, J. Eslami, L. Asgharnejad, Investigation of two different water-dispersed graphene on the performance of graphene/cement paste: Surfactant and superplasticizer effect, Constr. Build. Mater. 349 (2022) 128756. https://doi.org/10.1016/j.conbuildmat.2022.128756.

[21] X. Yan, D. Zheng, H. Yang, H. Cui, M. Monasterio, Y. Lo, Study of optimizing graphene oxide dispersion and properties of the resulting cement mortars, Constr. Build. Mater. 257 (2020) 119477. https://doi.org/10.1016/j.conbuildmat.2020.119477.

[22] L. Lei, M. Palacios, J. Plank, A.A. Jeknavorian, Interaction between polycarboxylate superplasticizers and non-calcined clays and calcined clays: A review, Cem. Concr. Res. 154 (2022) 106717. https://doi.org/10.1016/j.cemconres.2022.106717.

[23] L. Assi, A. Alsalman, D. Bianco, P. Ziehl, J. El-Khatib, M. Bayat, F.H. Hussein, Multiwall carbon nanotubes (MWCNTs) dispersion & mechanical effects in OPC mortar & paste: A review, J. Build. Eng. 43 (2021) 102512. https://doi.org/10.1016/j.jobe.2021.102512.

[24] M.S. Strano, V.C. Moore, M.K. Miller, M.J. Allen, E.H. Haroz, C. Kittrell, R.H. Hauge, R.E. Smalley, The Role of Surfactant Adsorption during Ultrasonication in the Dispersion of Single-Walled Carbon Nanotubes, J. Nanosci. Nanotechnol. 3 (2003) 81–86. https://doi.org/10.1166/jnn.2003.194.

[25] L. Vaisman, H.D. Wagner, G. Marom, The role of surfactants in dispersion of carbon nanotubes, Adv. Colloid Interface Sci. 128–130 (2006) 37–46. https://doi.org/10.1016/j.cis.2006.11.007.

[26] C. Liu, X. Huang, Y.-Y. Wu, X. Deng, Z. Zheng, Z. Xu, D. Hui, Advance on the dispersion treatment of graphene oxide and the graphene oxide modified cement-based materials, Nanotechnol. Rev. 10 (2021) 34–49. https://doi.org/10.1515/ntrev-2021-0003.

[27] M.S. Konsta-Gdoutos, Z.S. Metaxa, S.P. Shah, Highly dispersed carbon nanotube reinforced cement based materials, Cem. Concr. Res. 40 (2010) 1052–1059. https://doi.org/10.1016/j.cemconres.2010.02.015.

[28] V.J. GARCÍA, C.O. MÁRQUEZ, A.R. ZÚÑIGA-SUÁREZ, B.C. ZÚÑIGA-TORRES, P.J. RÍOS-GÓNZALEZ, Mechanical and electrical properties of MWCNTs - high early strength cement - mortars composite: Dispersion of CNTs and effect of chemical admixtures, An. Acad. Bras. Cienc. 93 (2021). https://doi.org/10.1590/0001-3765202120200924.

[29] M. Liebscher, R. Fuge, C. Schröfl, A. Lange, A. Caspari, C. Bellmann, V. Mechtcherine, J. Plank, A. Leonhardt, Temperature- and pH-Dependent Dispersion of Highly Purified

Multiwalled Carbon Nanotubes Using Polycarboxylate-Based Surfactants in Aqueous Suspension, J. Phys. Chem. C. 121 (2017) 16903–16910. https://doi.org/10.1021/acs.jpcc.7b05534.

[30] M. Liebscher, A. Lange, C. Schröfl, R. Fuge, V. Mechtcherine, J. Plank, A. Leonhardt, Impact of the molecular architecture of polycarboxylate superplasticizers on the dispersion of multi-walled carbon nanotubes in aqueous phase, J. Mater. Sci. 52 (2017) 2296–2307. https://doi.org/10.1007/s10853-016-0522-3.

[31] O. Mendoza, G. Sierra, J.I. Tobón, Influence of super plasticizer and Ca(OH)2 on the stability of functionalized multi-walled carbon nanotubes dispersions for cement composites applications, Constr. Build. Mater. 47 (2013) 771–778. https://doi.org/10.1016/j.conbuildmat.2013.05.100.

[32] G.M. Kim, I.W. Nam, H.N. Yoon, H.K. Lee, Effect of superplasticizer type and siliceous materials on the dispersion of carbon nanotube in cementitious composites, Compos. Struct. 185 (2018) 264–272. https://doi.org/10.1016/j.compstruct.2017.11.011.

[33] W. Dong, W. Li, N. Lu, F. Qu, K. Vessalas, D. Sheng, Piezoresistive behaviours of cement-based sensor with carbon black subjected to various temperature and water content, Compos. Part B Eng. 178 (2019) 107488. https://doi.org/10.1016/j.compositesb.2019.107488.

[34] A. Hussain, Y. Ding, G. Liu, A. Naqi, Study on self-monitoring of multiple cracked concrete beams with multiphase conductive materials subjected to bending, (2019).

[35] Y. Huang, H. Li, S. Qian, Self-sensing properties of Engineered Cementitious Composites, Constr. Build. Mater. 174 (2018) 253–262. https://doi.org/10.1016/j.conbuildmat.2018.04.129.

[36] G. Marchetti, C. Castellano, V. Bonavetti, E.F. Irassar, Tools for designing the early-age properties of fly ash and limestone filler ternary systems, Constr. Build. Mater. 347 (2022) 128552. https://doi.org/10.1016/J.CONBUILDMAT.2022.128552.

[37] A.A. de Siqueira, G.C. Cordeiro, Properties of binary and ternary mixes of cement, sugarcane bagasse ash and limestone, Constr. Build. Mater. 317 (2022) 126150. https://doi.org/10.1016/J.CONBUILDMAT.2021.126150.

[38] H. Wang, F. Shi, J. Shen, A. Zhang, L. Zhang, H. Huang, J. Liu, K. Jin, L. Feng, Z. Tang, Research on the self-sensing and mechanical properties of aligned stainless steel fiber-reinforced reactive powder concrete, Cem. Concr. Compos. 119 (2021) 104001. https://doi.org/10.1016/J.CEMCONCOMP.2021.104001.

[39] J. Han, J. Cai, J. Pan, Y. Sun, Study on the conductivity of carbon fiber self-sensing high

ductility cementitious composite, J. Build. Eng. 43 (2021) 103125. https://doi.org/10.1016/J.JOBE.2021.103125.

[40] G.H. Nalon, J.C. Lopes Ribeiro, L.G. Pedroti, E.N. Duarte de Araújo, J.M. Franco de Carvalho, G.E. Soares de Lima, L. de Moura Guimarães, Residual piezoresistive properties of mortars containing carbon nanomaterials exposed to high temperatures, Cem. Concr. Compos. 121 (2021) 104104. https://doi.org/10.1016/J.CEMCONCOMP.2021.104104.

[41] A. Downey, A. D'Alessandro, F. Ubertini, S. Laflamme, R. Geiger, Biphasic DC measurement approach for enhanced measurement stability and multi-channel sampling of self-sensing multi-functional structural materials doped with carbon-based additives, Smart Mater. Struct. 26 (2017) 065008. https://doi.org/10.1088/1361-665X/aa6b66.

[42] A. Meoni, A. D'Alessandro, R. Kruse, L. De Lorenzis, F. Ubertini, Strain field reconstruction and damage identification in masonry walls under in-plane loading using dense sensor networks of smart bricks: Experiments and simulations, Eng. Struct. 239 (2021) 112199. https://doi.org/10.1016/J.ENGSTRUCT.2021.112199.

[43] K.L. Scrivener, R. Snellings, B. Lothenbach, A practical guide to microstructural analysis of cementitious materials, CRC Press, Boca Raton, 2016.

[44] H.N. Yoon, D. Jang, T. Kil, H.K. Lee, Influence of various deterioration factors on the electrical properties of conductive cement paste, Constr. Build. Mater. 367 (2023) 130289. https://doi.org/10.1016/J.CONBUILDMAT.2022.130289.

[45] H. Li, H. Chen, M. Wei, R. Wang, N. Lei, Q. Wang, Design and preparation of double-layer iron ore tailings cement-based electromagnetic wave absorbing materials containing carbon black and steel fiber, Constr. Build. Mater. 364 (2023) 129972. https://doi.org/10.1016/J.CONBUILDMAT.2022.129972.

[46] G.H. Nalon, R.F. Santos, G.E.S. de Lima, I.K.R. Andrade, L.G. Pedroti, J.C.L. Ribeiro, J.M. Franco de Carvalho, Recycling waste materials to produce self-sensing concretes for smart and sustainable structures: A review, Constr. Build. Mater. 325 (2022) 126658. https://doi.org/10.1016/J.CONBUILDMAT.2022.126658.

[47] A.O. Monteiro, P.B. Cachim, P.M.F.J. Costa, Carbon nanoparticles cement-based materials for service life monitoring, in: Conf. Segm. Serv. Life Cem. Mater. Struct., RILEM, Lyngby, 2016: pp. 195–202.

[48] A.O. Monteiro, A. Loredo, P.M.F.J. Costa, M. Oeser, P.B. Cachim, A pressure-sensitive carbon black cement composite for traffic monitoring, Constr. Build. Mater. 154 (2017) 1079–1086. https://doi.org/10.1016/j.conbuildmat.2017.08.053.

[49] A.O. Monteiro, P.B. Cachim, P.M.F.J. Costa, Self-sensing piezoresistive cement composite loaded with carbon black particles, Cem. Concr. Compos. 81 (2017) 59–65. https://doi.org/10.1016/J.CEMCONCOMP.2017.04.009.

[50] A.O. Monteiro, A. Loredo, P.M.F.J. Costa, M. Oeser, P.B. Cachim, A pressure-sensitive carbon black cement composite for traffic monitoring, Constr. Build. Mater. 154 (2017) 1079–1086. https://doi.org/10.1016/J.CONBUILDMAT.2017.08.053.

[51] Y. Li, J. Yin, Q. Yuan, T. Huang, J. He, J. Li, Fresh and hardened properties of cement paste and mortar incorporating calcined cutter soil mixing residue, Constr. Build. Mater. 357 (2022) 129376. https://doi.org/10.1016/J.CONBUILDMAT.2022.129376.

[52] S. Yu, J. Sanjayan, H. Du, Effects of cement mortar characteristics on aggregate-bed 3D concrete printing, Addit. Manuf. 58 (2022) 103024. https://doi.org/10.1016/J.ADDMA.2022.103024.

[53] B. Zhaidarbek, A. Tleubek, G. Berdibek, Y. Wang, Analytical predictions of concrete pumping: Extending the Khatib–Khayat model to Herschel–Bulkley and modified Bingham fluids, Cem. Concr. Res. 163 (2023) 107035. https://doi.org/10.1016/j.cemconres.2022.107035.

[54] J.M. Beltrán, L. Chica, On fresh state behavior of foamed cement pastes and its influence on hardened performance, Constr. Build. Mater. 368 (2023) 130518. https://doi.org/10.1016/j.conbuildmat.2023.130518.

[55] Y. Ji, L. Pel, Z. Sun, The microstructure development during bleeding of cement paste: An NMR study, Cem. Concr. Res. 125 (2019) 105866. https://doi.org/10.1016/j.cemconres.2019.105866.

[56] R. Rastogi, R. Kaushal, S.K. Tripathi, A.L. Sharma, I. Kaur, L.M. Bharadwaj, Comparative study of carbon nanotube dispersion using surfactants, J. Colloid Interface Sci. 328 (2008) 421–428. https://doi.org/10.1016/j.jcis.2008.09.015.

[57] S. Kriegseis, A.Y. Vogl, L. Aretz, T. Tonnesen, R. Telle, Zeta potential and long-term stability correlation of carbon-based suspensions for material jetting, Open Ceram. 4 (2020) 100037. https://doi.org/10.1016/j.oceram.2020.100037.

[58] J.S. Kim, Enhanced effects of carbon-based conductive materials on the piezoresistive characteristics of cementitious composites, Constr. Build. Mater. 341 (2022) 127804. https://doi.org/10.1016/j.conbuildmat.2022.127804.

[59] R. Xu, C. Wu, H. Xu, Particle size and zeta potential of carbon black in liquid media, Carbon N. Y. 45 (2007) 2806–2809. https://doi.org/10.1016/j.carbon.2007.09.010.

[60] H. Feng, Z. Feng, W. Wang, Z. Deng, B. Zheng, Impact of polycarboxylate

superplasticizers (PCEs) with novel molecular structures on fluidity, rheological behavior and adsorption properties of cement mortar, Constr. Build. Mater. 292 (2021) 123285. https://doi.org/10.1016/j.conbuildmat.2021.123285.

[61] M. Kosmulski, E. Mączka, Zeta potential in dispersions of titania nanoparticles in moderately polar solvents stabilized with anionic surfactants, J. Mol. Liq. 355 (2022) 118972. https://doi.org/10.1016/j.molliq.2022.118972.

[62] H. Guo, Z. Wang, Q. Liang, G. Li, Improvement of stability and mechanical properties of cement asphalt emulsion composites using nano fibrillated celluloses, Cem. Concr. Compos. 125 (2022) 104330. https://doi.org/10.1016/j.cemconcomp.2021.104330.

[63] M. Sharif Sh., F. Golestani Fard, E. Khatibi, H. Sarpoolaky, Dispersion and stability of carbon black nanoparticles, studied by ultraviolet–visible spectroscopy, J. Taiwan Inst. Chem. Eng. 40 (2009) 524–527. https://doi.org/10.1016/j.jtice.2009.03.006.

[64] C. Jäger, T. Henning, R. Schlögl, O. Spillecke, Spectral properties of carbon black, J. Non. Cryst. Solids. 258 (1999) 161–179. https://doi.org/10.1016/S0022-3093(99)00436-6.

[65] H. Suh, H. Jee, J. Kim, R. Kitagaki, S. Ohki, S. Woo, K. Jeong, S. Bae, Influences of rehydration conditions on the mechanical and atomic structural recovery characteristics of Portland cement paste exposed to elevated temperatures, Constr. Build. Mater. 235 (2020) 117453. https://doi.org/10.1016/j.conbuildmat.2019.117453.

[66] Y. Wei, W. Yao, X. Xing, M. Wu, Quantitative evaluation of hydrated cement modified by silica fume using QXRD, 27Al MAS NMR, TG–DSC and selective dissolution techniques, Constr. Build. Mater. 36 (2012) 925–932. https://doi.org/10.1016/j.conbuildmat.2012.06.075.

[67] D.B.P. Silva, N.B. Lima, V.M.E. Lima, A.M.L. Estolano, H.C.B. Nascimento, P. Vilemen, E. Padron-Hernández, A.M.P. Carneiro, N.B.D. Lima, Y.V. Povoas, Producing a gypsum-based self-leveling mortar for subfloor modified by polycarboxylate admixture (PCE), Constr. Build. Mater. 364 (2023) 130007. https://doi.org/10.1016/j.conbuildmat.2022.130007.

[68] J. Wang, J. Liao, X. Kong, J. Yin, Characterization of the nanoparticles formed in aqueous phase of hydrating cement pastes in the presence of PCEs, Cem. Concr. Res. 165 (2023) 107087. https://doi.org/10.1016/j.cemconres.2022.107087.

[69] L. Wang, G. Li, C. He, Y. Tang, B. Yi, Preparation and properties of nano-carbon black modified ultra-high-performance concrete, Case Stud. Constr. Mater. 17 (2022) e01378. https://doi.org/10.1016/J.CSCM.2022.E01378.

[70] A. Tugelbayev, J.-H. Kim, J.U. Lee, C.-W. Chung, The effect of acid treated multi-walled carbon nanotubes on the properties of cement paste prepared by ultrasonication with polycarboxylate ester, J. Build. Eng. 64 (2023) 105638. https://doi.org/10.1016/J.JOBE.2022.105638.

[71] H. Zhang, J. Kou, C. Sun, P. Wang, J. Lin, J. Li, Y. Jiang, Optimization of cemented paste backfill with carbon nanotubes as a sustainable treatment for lead-containing tailings, Powder Technol. 415 (2023) 118152. https://doi.org/10.1016/J.POWTEC.2022.118152.

[72] Z. Tian, Y. Li, J. Zheng, S. Wang, A state-of-the-art on self-sensing concrete: Materials, fabrication and properties, Compos. Part B Eng. 177 (2019) 107437. https://doi.org/10.1016/j.compositesb.2019.107437.

5 ESTUDO EXPERIMENTAL DA COMPATIBILIDADE MECÂNICA ENTRE COMPÓSITOS CIMENTÍCIOS NANOMODIFICADOS SENSORES (CCNS) E VIGAS DE CONCRETO ARMADO

Resumo: *Diferentes estudos vêm explorando a aplicação de compósitos cimentícios nanomodificados sensores (CCNS) para o monitoramento do desempenho estrutural de vigas de concreto armado. De forma geral, esses trabalhos estão focados principalmente em testar a resposta de vigas de concreto produzidas com sensores cimentícios com diferentes características, como por exemplo variações dos teores de um filler condutivo, diferentes tipos de nanopartículas ou diferentes abordagens de instalação do sensor cimentício nas vigas. Contudo, nenhum destes trabalhos avaliou os efeitos da existência ou falta de compatibilidade de deformações entre os CCNS e o substrato em que eles são instalados. Para preencher a lacuna ainda existente na literatura, a presente pesquisa desenvolveu uma investigação da compatibilidade mecânica entre os CCNS e um elemento de concreto armado submetido à flexão. Os CCNS foram instalados em vigas de concreto com concretos de diferentes propriedades mecânicas (RC-20, RC-30 e RC-35), de modo a se obter cenários com distintas condições de incompatibilidade de deformações entre o sensor cimentício e o substrato onde é instalado. A habilidade de detecção de danos da viga pelo CCNS foi observada para todos os modelos estudados. Já a habilidade de monitoramento de deformação da viga pelo CCNS apresentou as melhores respostas para o caso do modelo RC-30, no qual o sensor possuía módulo de elasticidade ligeiramente inferior ao do concreto da viga. Para demais casos estudados, o sensor monitorou as deformações corretamente por uma faixa de carregamento menor (RC-20) ou demonstrou uma menor capacidade de registrar as deformações (RC-35). O conjunto de todos os resultados analisados sugere que CCNS apresentou a melhor compatibilidade mecânica para registro de deformações e danos com a viga do modelo RC-30.*

Palavras-chave: *compatibilidade mecânica, vigas de concreto, compósito cimentício nanomodificado sensor, piezoresistividade.*

5.1 INTRODUÇÃO

Em uma estrutura, parâmetros como deformação, tensão, vibração e deslocamentos podem ser monitorados por meio do uso de diferentes tipos de dispositivos sensores específicos. O processo de avaliação contínua do comportamento destes parâmetros ao longo do ciclo de vida de uma estrutura é conhecido como monitoramento da integridade estrutural (SHM, do inglês *Structural Health Monitoring*). As informações obtidas com sistemas de SHM permitem o planejamento adequado de ações de manutenção, detecção precoce de danos e garantia da segurança, confiabilidade e longevidade das estruturas [1–4].

O desenvolvimento de compósitos cimentícios nanomodificados sensores (CCNS) tem sido objeto de estudos recentes [5–8]. A incorporação de nanomateriais de alta condutividade elétrica, associada a uma dispersão adequada desses materiais na matriz cimentícia, permite a formação de uma extensa rede condutora, reduzindo a resistividade elétrica do compósito a valores próximos àquela de semicondutores [9]. Assim, quando o material se deforma, são causadas alterações em sua resistividade elétrica, fazendo que o compósito se comporte como um elemento sensor, possibilitando realizar medições de deformação e tensão. Mudanças de resistividade elétrica também decorrem de danos causados por fissuração na matriz cimentícia, de forma que os CCNS também podem ser utilizados para a autodetecção da propagação de fissuras em elementos de concreto [10,11].

O uso de nanomateriais à base de carbono como *filler* condutivo tem sido recorrente no desenvolvimento de CCNS [12–17]. Dentre esses materiais, nanopartículas de carbon black (CBN) têm se destacado devido ao seu baixo custo, elevada condutividade elétrica, boa estabilidade de sinal, facilidade de aplicação [7,18–22] e, se utilizadas em proporções adequadas, contribuem com o refinamento da matriz cimentícia, com possíveis impactos positivos nas propriedades mecânicas e elétricas do compósito [12,23].

Atualmente, diferentes trabalhos na literatura vêm explorando a aplicação de CCNS para o monitoramento do desempenho estrutural de vigas de concreto armado [24–30]. De forma geral, esses trabalhos estão focados principalmente em testar a resposta de vigas de concreto produzidas com sensores cimentícios com diferentes características, como por exemplo variações dos teores de um *filler* condutivo, diferentes tipos de nanopartículas ou diferentes abordagens de instalação do sensor cimentício nas vigas [2,25–29].

Contudo, nenhum destes trabalhos avaliou os efeitos da existência ou falta de compatibilidade de deformações entre os CCNS e o substrato em que eles são instalados. Neste sentido, um campo promissor de trabalho está ligado a investigação de questões relacionadas à

compatibilidade entre o sensor e o elemento que se pretende monitorar. Para preencher a lacuna ainda existente na literatura, a presente pesquisa se concentrou na análise das interações mecânicas entre CCNS e vigas de concreto com diferentes combinações de classes de resistência. Dos muitos problemas que a escolha inadequada de um sensor pode acarretar, pode-se citar a obtenção de dados imprecisos, concentrações indesejáveis de tensões, perda prematura do sensor, problemas de aderência e, em caso mais severos, um acidente com a estrutura monitorada.

Desta forma, no presente estudo desenvolve-se uma investigação da compatibilidade mecânica entre os CCNS e um elemento de concreto armado submetido à flexão. As seguintes contribuições originaram do desenvolvimento deste trabalho: (i) análise comparativa das deformações medidas por CCNS e *strain gauge* comerciais; (ii) avaliação do comportamento mecânico e piezoresistivo de CCNS embutidos em vigas com diferentes características mecânicas, após aplicação de carregamentos de diferentes magnitudes; (iii) avaliação da capacidade de um CCNS em identificar danos em vigas com diferentes características mecânicas. Os resultados encontrados nesta pesquisa fornecem uma série de diretrizes essenciais para a seleção e aplicação prática de CCNS, aumentando a confiabilidade de sua resposta elétrica e a segurança das estruturas de concreto.

5.2 MATERIAIS E MÉTODOS

5.2.1 Materiais

Neste estudo, para produção das argamassas sensoras, foram utilizados os seguintes materiais: cimento Portland CP V-ARI, equivalente ao cimento Portland ASTM C150 Tipo III; areia natural quartzosa, com diâmetro máximo de 2.38 mm; CBN tipo N234, com tamanho médio de partículas de 20 nm e área superficial específica de 120 m^2/g; aditivo superplastificante à base de éter policarboxilato (PCE) com densidade de 1.12 g/cm^3; e água destilada com pH 6.5.

Para produção dos concretos, foram utilizados o mesmo cimento e areia das argamassas sensoras, além de uma brita de origem gnáissica com diâmetro máximo de 9.5 mm; aditivo plastificante multifuncional com densidade de 1.10 g/cm^3; e água potável. Na produção das armaduras dos modelos experimentais, foram utilizadas barras de aço CA-50 e CA-60, semelhante as barras de aço ASTM A615, categoria 1, Graus 60 e 75, respectivamente.

Por fim, seguindo recomendação da literatura [31], foi utilizado um adesivo estrutural de base epóxi, com densidade de 1.70 g/cm³, para atuar como ponte de aderência, permitindo uma incorporação adequada do CCNS ao concreto fresco e ainda, atuando como material impermeabilizante, visando impedir o ingresso da água na matriz do sensor.

5.2.2 CCNS

5.2.2.1 Produção

Os compósitos sensores foram produzidos a partir de nanosuspensões preparadas com o auxílio de um sonicador com micro ponta de 3.0 mm, com frequência ultrassônica de 20 kHz e potência de 50 W. Na Tabela 1, pode-se observar o consumo dos materiais utilizados para produção da argamassa sensora, sendo adotada uma relação areia/cimento de 1.95 (em massa), água/cimento de 0.56 e um consumo de CBN de 9% em relação ao peso de cimento.

Tabela 1 – Consumo de materiais para produção de CCNS

Consumo (kg/m³)				
Cimento	Areia	Água	CBN	PCE
585.75	1142.26	326.91	52.72	21.09

Fonte: Autor (2024)

A nanosuspensão foi preparada realizando a dispersão de CBN em uma solução de água destilada e PCE, aplicando um tempo de sonicação suficiente para fornecer uma energia de 240 J/mL à mistura. Posteriormente, o material resultante foi transferido para um misturador planetário mecânico, onde cimento e areia foram incorporados e misturados por um período de 10 minutos. A argamassa fresca resultante foi despejada em moldes previamente preparados com desmoldante e, na sequência, foi adensada em mesa vibratória por 10 segundos. Por fim, foram embutidos dois eletrodos de cobre (1.4 cm x 3.0 cm x 0.1 cm) na região central de cada corpo de prova (CP), separados entre si de cerca de 0.8 cm.

Finalizado o processo de moldagem, os moldes foram colocados em câmara úmida com umidade relativa >85% e temperatura ambiente de 20 ± 5 ºC. Após 72 horas, os CP`s foram desmoldados e permaneceram em processo de cura em câmara úmida por 28 dias. Para a avaliação das propriedades piezoresistivas, foram confeccionados três prismas de argamassa sensora com dimensões de 2.5 cm x 2.5 cm x 7.5 cm (com eletrodos), designados como S1, S2

e S3. Para o ensaio de módulo de elasticidade, foram produzidos cinco prismas com dimensões de 2.5 cm x 2.5 cm x 7.5 cm (sem eletrodos).

5.2.2.2 Análise eletromecânica

Os CCNS passaram por um processo de calibração antes do processo de incorporação nas vigas de concreto, seguindo o mesmo procedimento utilizado em trabalhos anteriores [23,32,33], descrito de forma detalhada na sequência desta seção.

Com o objetivo de mitigar potenciais efeitos de condução iônica durante os ensaios, os CCNS foram submetidos à secagem em estufa a 60±10 ºC por 72 horas, seguidos de resfriamento até a temperatura ambiente [34,35]. Posteriormente, nos compósitos com eletrodos, foi realizado um ensaio bifásico de corrente contínua (B-CC), concomitante à aplicação de ciclos de carregamento mecânico, para mensurar a piezoresistividade.

No início dos testes, cada CCNS foi conectado em série a um resistor de referência de 1 kΩ (R_{ref}). Visando reduzir possíveis efeitos de polarização, a mesma placa foi utilizada para gerar um sinal periódico, em forma de onda quadrada, de ±5 V com frequência de 6 Hz [33,36].

Um instrumento virtual foi desenvolvido no *LabVIEW* para medir as quedas de tensão entre o compósito sensor (U_m) e o resistor de referência (U_{ref}). A aquisição dos dados foi realizada utilizando um chassi *National Instruments* NI cDAQ-9178 e dois módulos NI-9219. A corrente elétrica do circuito (i) e a resistência elétrica do compósito (R_m) foram determinadas por meio das Equações 1 e 2, respectivamente. Neste ensaio, i e R_m foram obtidos utilizando os valores de U_m e U_{ref} medidos nos instantes correspondentes a 80% de cada semi-onda positiva do sinal periódico gerado [33,37,38]. A resistividade elétrica foi calculada utilizando a Equação 3, considerando a distância entre os eletrodos (L) e sua área efetiva em contato com a argamassa (A).

Equação 1
$$i = \frac{U_{ref}}{R_{ref}}$$

Equação 2
$$R_m = \frac{U_m}{i}$$

Equação 3
$$\rho = \frac{R_m \ A}{L}$$

O comportamento piezoresistivo foi avaliado por meio da aplicação de ciclos de carga/descarga nos CCNS, utilizando uma máquina universal de ensaios EMIC DL-60000, com uma taxa de carregamento constante de 0.50 MPa/s. As variações relativas na resistividade elétrica (FCR) foram obtidas conforme método descrito previamente. Dois extensômetros elétricos EMIC, tipo *clip-gauge*, posicionados de forma simétrica ao eixo do CNSS, registraram as deformações longitudinais. O coeficiente angular calculado para a curva FCR vs Deformação, foi definido como o fator *Gauge* (GF) dos CNSS.

Os CNSS foram posicionados na máquina universal de ensaios entre filmes plásticos eletricamente isolantes, seguindo-se a aplicação de uma pré-carga. Na sequência, os compósitos foram submetidos a dois diferentes processos de carregamento: o primeiro, com três ciclos iguais de carga/descarga, com amplitude máxima de 30% da carga de ruptura estimada do material; o segundo, com três patamares progressivos, aplicando-se cargas correspondentes a 10%, 20% e 30% do limite de ruptura.

Os dados obtidos no ensaio piezoresistivo foram tratados com um filtro de Savitzky-Golay, conforme observado em estudos anteriores [39–42]. Esta técnica de suavização visa reduzir a relação sinal/ruído por meio da convolução do conjunto de dados, realizando um ajuste polinomial por mínimos quadrados e preservando as características do sinal original.

5.2.3 Vigas de concreto equipadas com CCNS

5.2.3.1 Características dos modelos experimentais

Para a avaliação da compatibilidade mecânica entre os compósitos sensores e o elemento estrutural de concreto monitorado, foram produzidas três vigas de concreto armado para realização de testes eletromecânicos. Os modelos experimentais foram designados como RC-20, RC-30 e RC-35.

As vigas foram pré-dimensionadas no Domínio 3 (seção subarmada), de forma que o modo de colapso esperado seria por deformação excessiva das armaduras. Os modelos experimentais foram produzidos com dimensões nominais de 10x10x105 cm, sendo que o vão efetivo no ensaio de flexão de 4 pontos foi de 100.0 cm. A armadura longitudinal de tração foi composta por duas barras de aço CA-50, de diâmetro variável de acordo com a resistência do concreto da viga (Ø8.0 mm e Ø10.0 mm). A armadura longitudinal de compressão foi composta por duas barras de aço CA-60 de diâmetro Ø5.0 mm. Para armadura transversal, foram

utilizadas barras CA-60 com diâmetro Ø5.0 mm, espaçadas a cada 10.0 cm. O cobrimento da armadura foi de 1.0 cm. Na Figura 1, apresenta-se o detalhamento típico das armaduras dos modelos experimentais.

Figura 1 – Detalhamento das armaduras dos modelos experimentais
(dimensões em milímetros).

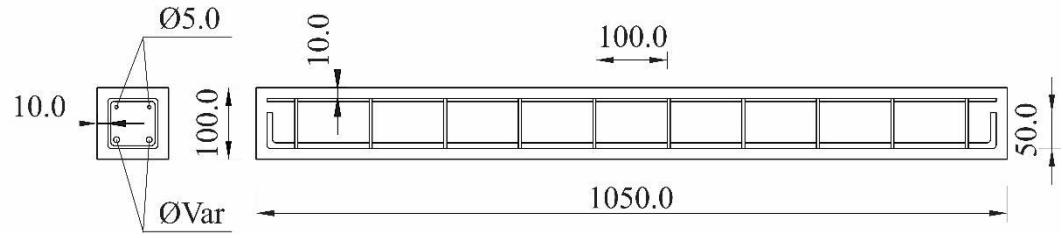

Fonte: Autor (2024)

Na Tabela 2, apresenta-se de forma resumida, o conjunto das características dos modelos experimentais produzidos.

Tabela 2 – Características dos modelos experimentais

Série	Dimensões da viga (cm)	Resistência à compressão média do concreto (MPa)	Módulo de elasticidade médio do concreto (GPa)	Armadura longitudinal de tração (mm)	Armadura longitudinal de compressão (mm)	Armadura transversal (mm)
RC-20	10x10x105	19.75	21.81	Ø8.0	Ø5.0	Ø5.0
RC-30		28.52	25.01	Ø10.0		
RC-35		35.31	29.25	Ø10.0		

Fonte: Autor (2024)

5.2.3.2 Características do concreto e aço das vigas

O concreto utilizado foi produzido de acordo com a norma ABNT NBR 12655:2022 [43], sendo adotados três traços de referência para o estudo, compatíveis com as classes de resistência C20, C30 e C35. A consistência do concreto fresco foi determinada conforme a norma ABNT NBR 16889:2020 [44] . A resistência mecânica à compressão e o módulo de elasticidade secante do concreto foram avaliados segundo as normas ABNT NBR 5739:2018 [45] e ABNT NBR 8522-1:2021 [46], respectivamente. Estes ensaios foram realizados na mesma data do ensaio de flexão das vigas. Na Tabela 3, são apresentados os traços adotados para a produção dos concretos. Na Tabela 2, constam as propriedades mecânicas dos concretos utilizados nos modelos experimentais.

Tabela 3 – Consumo dos materiais para produção dos concretos (kg/m³)

Série	Cimento	Agregado miúdo	Agregado graúdo	Água	Aditivo plastificante	Slump (mm)
RC-20	270	875	950	216	1.62	165
RC-30	306	835	964	214	2.14	185
RC-35	350	788	981	210	2.80	195

Fonte: Autor (2024)

Conforme descrito na seção 5.2.1, as armaduras dos modelos experimentais foram produzidas com barras de aço CA-50 e CA-60. Os limites de escoamento e resistência das barras foram avaliados segundo a norma ABNT NBR ISO 6892:2024 [47] e são apresentados na Tabela 4.

Tabela 4 – Característica das barras de aço

Diâmetro (mm)	Tipo	Tensão de escoamento (MPa)	Tensão de ruptura (MPa)
5.0	CA-60	655	732
8.0	CA-50	580	657
10.0	CA-50	570	654

Fonte: Autor (2024)

5.2.3.3 Instrumentação da viga

Para monitorar as deformações nas armaduras ao longo do ensaio, anteriormente à concretagem, cada uma das barras tracionadas recebeu um extensômetro elétrico para aço (SG-T) em sua região central. No centro da peça, na parte superior, foi instalado um extensômetro elétrico para concreto (SG-C), para monitoramento das deformações e realizar um comparativo com as medições do CCNS. Na Figura 2, é indicado o esquema geral da instrumentação adotada para o ensaio.

Figura 2 – Detalhamento da instrumentação da viga

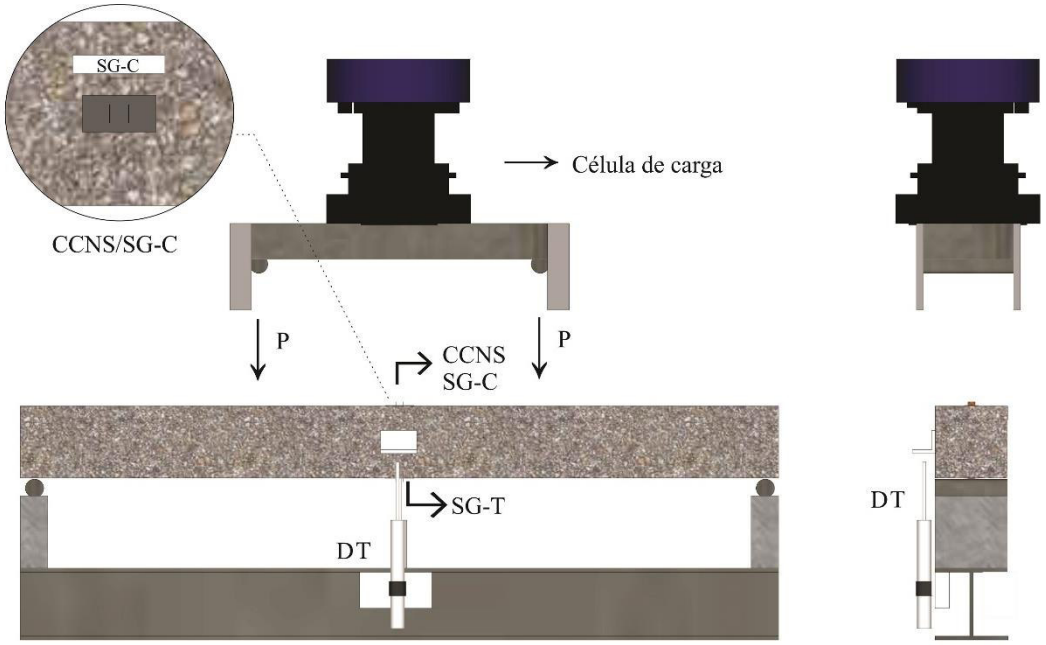

Fonte: Autor (2024)

5.2.3.4 Produção das vigas de concreto

Todas as vigas fossem moldadas em uma única etapa de concretagem. As armaduras foram produzidas conforme descrito na seção 5.2.3.1, sendo que cada uma das barras tracionadas recebeu um extensômetro elétrico (SG-T). Antes do início do processo de moldagem, as formas foram limpas e um desmoldante foi aplicado internamente.

Os compósitos sensores foram previamente secos em estufa seguindo o mesmo procedimento relatado na seção 5.2.2.2 e, após seu resfriamento a temperatura ambiente, suas propriedades eletromecânicas foram determinadas conforme descrito na seção 5.2.3. Na sequência, foram aplicadas na superfície do CCNS duas finas camadas de adesivo estrutural epóxi, sendo pulverizada uma pequena quantidade de areia imediatamente após a aplicação do adesivo, visando garantir boas condições de aderência entre o sensor e o concreto da viga. Conforme relatado em trabalhos anteriores, a ponte de aderência feita com o adesivo epóxi, também atua como agente impermeabilizante e isolante elétrico do compósito [10,31,48]. Com as armaduras posicionadas na forma, o concreto foi lançado, sendo o adensamento realizado em mesa vibratória por 10 segundos. Na sequência, o CCNS foi cuidadosamente instalado no centro da viga e o conjunto foi novamente adensado por mais 5 segundos. Na Figura 3, é apresentada a sequência de etapas de produção das vigas.

Figura 3 – Produção dos modelos experimentais

Fonte: Autor (2024)

Os modelos experimentais então foram identificados com etiquetas e mantidos por 48 horas umedecidos, cobertos por lona plástica. Na sequência, as peças foram desformadas e armazenadas em câmara úmida, com umidade relativa superior a 85% e temperatura de 20 ± 5 °C, até completar 28 dias. Passado este período, as vigas foram retiradas da câmara úmida e permaneceram em uma sala em condições ambiente por 90 dias. Por fim, seguindo o mesmo procedimento descrito na seção 5.2.3, visando mitigar potenciais efeitos de condução iônica durante os ensaios, os elementos foram submetidos à secagem em estufa a 60 ºC por 72 horas, seguidos de resfriamento até a temperatura ambiente. Os corpos de prova cilíndricos de concreto de 10x20 cm foram mantidos nas mesmas condições ambientais dos modelos experimentais durante todo o processo, sendo ensaiados na mesma data que as vigas.

5.2.3.5 Procedimentos do ensaio de flexão

Para aplicação do carregamento, os elementos foram posicionados no eixo de uma máquina universal servo controlada EMIC DL 60000, sobre uma viga de reação de aço previamente instalada, conforme Figura 4. O carregamento foi promovido pela ação do atuador, aplicando carga em dois pontos do bordo superior da viga, com controle de deslocamentos, a uma taxa de 0.02 mm/s. O ensaio foi configurado para uma flexão a quatro pontos, ficando os pontos de aplicação de carga posicionados a 25.0 cm da linha de eixo dos apoios. Um transdutor de deslocamento (DT), foi posicionado no centro do vão da viga, para registrar a flecha ao longo do ensaio. Nas extremidades da viga de reação foram posicionados dois transdutores de deslocamento auxiliares para verificar a ocorrência de algum deslocamento indesejado,

permitindo sua compensação, caso necessário. Entre o atuador da máquina de ensaios universal e a viga, foi posicionada uma célula de carga com capacidade de 200 kN, para registro do carregamento ao longo do ensaio. A aquisição dos dados obtidos pela célula de carga, extensômetros elétricos e transdutores de deslocamento foi realizada utilizando um sistema HBM Quantum X, com os módulos MX840A e MX1615.

Figura 4 – Procedimento de ensaio: (a) visão geral da montagem; (b) detalhe da instrumentação

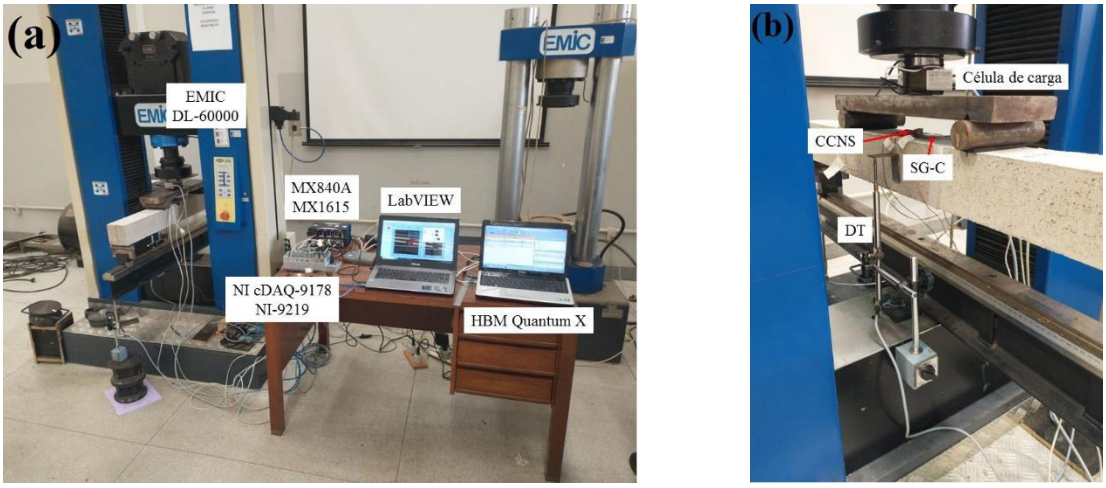

Fonte: Autor (2024)

As vigas foram submetidas a dois padrões de carregamento: o primeiro, que correspondeu a aplicação de 3 ciclos de carga/descarga de 2.5 kN (P0), 2.5 kN (P1), 5 kN (P2), 10 kN (P3), 15 kN (P4) e 20 kN (P5) e; o segundo, com aplicação de carregamentos progressivos de 10%, 20% e 30% da carga prevista para o ciclo de carga/descarga, seguido de um passo adicional até a ruptura do elemento, para o estágio de carregamento P5. O nível P0 foi aplicado com a mesma amplitude de carga do nível P1, com o objetivo de realizar os ajustes e as compensações de acomodações iniciais do conjunto. As variações de resistividade elétrica no CCNS foram medidas durante o ensaio, utilizando-se os mesmos procedimentos e equipamentos descritos na seção 5.2.2.2.

5.3 RESULTADOS E DISCUSSÕES

5.3.1 Caracterização dos CCNS

As relações entre FCR e Deformação observadas nos ensaios piezoresistivos dos CCNS (S1, S2 e S3) sujeitos à compressão uniaxial, são apresentadas na Figura 5. A calibração dos CCNS foi realizada dentro do regime elástico-linear, sendo obtida uma resposta elétrica com

baixo nível de histerese e um bom grau de repetibilidade. Foram ajustados modelos de regressão linear ao conjunto de dados, sendo o GF assumido como o coeficiente angular das equações obtidas para cada um desses modelos. Para todos os casos, foi obtido um excelente coeficiente de determinação (R^2), o que indica que os modelos de regressão linear foram capazes de descrever adequadamente o comportamento dos dados, não sendo necessário utilizar modelos de regressão mais complexos, como reportado por outros autores [29,49,50].

Figura 5 – Relação entre FCR e Deformação dos CCNS

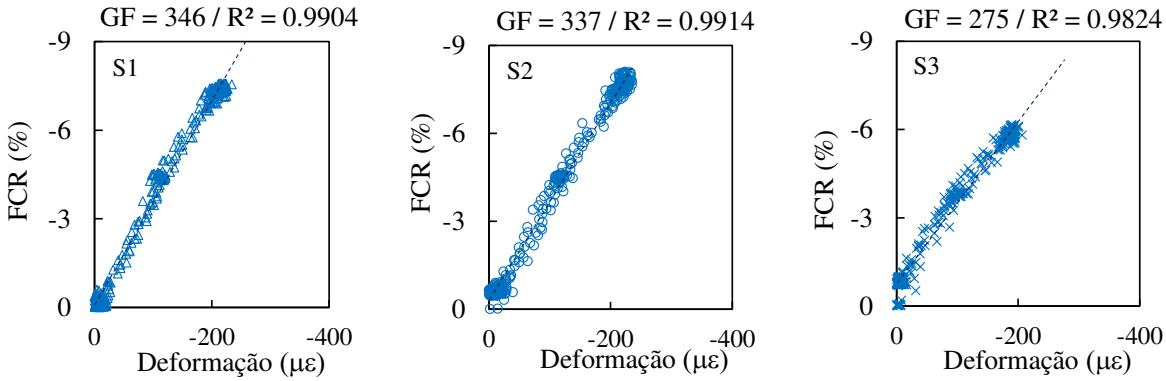

Fonte: Autor (2024)

De forma geral, os CCNS atingiram níveis de deformação semelhantes, sendo que o sensor S3 obteve uma amplitude um pouco menor para o FCR, o que implicou em uma redução da ordem de 20% no valor de GF desse sensor, quando comparado ao valor médio de GF dos sensores S1 e S2 ($GF_{1,2}$ = 341.5). Essas variações no valor de GF podem ser atribuídas a natureza heterogênea da argamassa sensora e a pequenas variabilidades causadas pelo processo de produção dos CCNS. Comportamento semelhante pode ser observado em outros trabalhos presentes na literatura, que também reportaram elevada variabilidade nos valores de propriedades autossensoras de compósitos cimentícios [23,51,52]. Os CCNS S1, S2 e S3, foram embutidos nas vigas RC-35, RC-30 e RC-20, respectivamente.

Figura 6 – Módulo de elasticidade do CCNS e do concreto das vigas

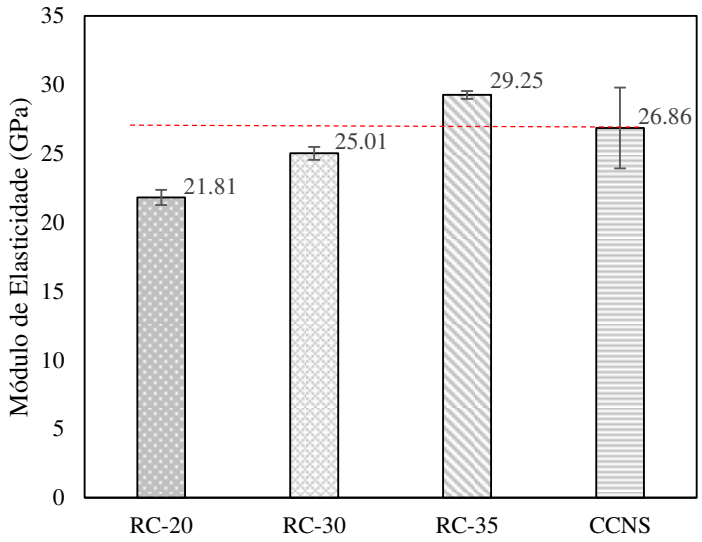

Fonte: Autor (2024)

Na mesma idade do ensaio de flexão das vigas, o módulo de elasticidade do CCNS foi determinado, sendo obtido o valor médio de 26.86 GPa. Na Figura 6, são apresentados os módulos de elasticidade do concreto dos modelos experimentais e do CCNS. Nota-se que o módulo de elasticidade médio dos CCNS foi 18.8% superior que o da série RC-20, 6.89% superior que o da série RC-30 e 8.90% menor que o da série RC-35, o que representa diferentes cenários de incompatibilidade de deformações passíveis de investigação no presente trabalho.

5.3.2 Avaliação da compatibilidade mecânica

5.3.2.1 Análise do mecanismo de falha das vigas

Conforme descrito na seção 5.3.2.1, as vigas foram pré-dimensionadas, de forma que o modo de colapso esperado seria por deformação excessiva das armaduras, com esmagamento do concreto. Para essa situação, tida como ideal, ocorre o melhor aproveitamento do potencial de resistência dos materiais, mantendo as condições de segurança, caracterizada por uma ruptura dúctil. Na Figura 7, é apresentado o conjunto dos modelos experimentais após a realização do ensaio de flexão.

Figura 7 – Mecanismo de falha das vigas

Fonte: Autor (2024)

Quando as armaduras tracionadas atingiram a deformação correspondente à tensão de escoamento informada na Tabela 4, as deformações no concreto registradas pelo SG-T eram da ordem de 1592.3 με (RC-20), 2139.3 με (RC-30) e 2008.9 με (RC-35). As medições obtidas pelo SG-T, no instante da ruptura do concreto, foram 13240.3 με, 8959.2 με e 12509.3 με para as vigas RC-20, RC-30 e RC-35, respectivamente. Assim, para todos os casos estudados, foi possível verificar que a ruptura ocorreu pelo mesmo mecanismo de falha, no qual as armaduras de tração atingiram o patamar de escoamento, seguido do esmagamento do concreto comprimido. Logo, as dimensões da viga e a taxa de armadura escolhidas para cada modelo foram capazes de assegurar um mesmo modo de ruptura para todos os corpos de prova, o que viabiliza comparações coerentes nas seções seguintes. No caso da viga RC-20, a carga máxima registrada foi de 25.02 kN, com uma flecha máxima no meio do vão de 9.48 mm. Para a viga RC-30, a carga de ruptura foi de 38.74 kN, com uma fecha de 10.03 mm. Por fim, para a viga RC-35, o colapso se deu para uma carga de 39.29 kN e fecha de 10.49 mm.

5.3.2.2 Análise da interface CCNS-Concreto

A qualidade da interface entre o CCNS e o concreto de substrato é uma das características fundamentais para permitir uma adequada transferência de esforços e, consequentemente possibilitar uma avaliação correta da compatibilidade entre o sensor cimentício e o elemento estrutural monitorado. Com o objetivo de obter uma interface coesa, conforme descrito na seção 5.2.3.4, foi utilizado um adesivo estrutural de base epóxi somado a uma fina camada de areia, criando assim uma ponte de aderência apropriada entre o compósito e o concreto fresco. Na Figura 8, são apresentados cortes transversais das vigas estudadas, onde é possível observar a interface entre o CCNS e o concreto endurecido.

Figura 8 – Interface CCNS-Concreto

RC-20 RC-30 RC-35

Fonte: Autor (2024)

A análise das imagens da Figura 8, indica que o tratamento adotado para melhorar a aderência entre o CCNS e o concreto ocorreu de forma satisfatória. O filme formado pelo adesivo epóxi formou uma zona de transição entre os materiais com aspecto homogêneo e coeso, semelhante ao reportado por outros autores [26]. Os resultados do ensaio de flexão, que discutidos nas seções posteriores, corroboram a hipótese de que a viga foi capaz de transmitir os esforços adequadamente para o CCNS. O corte da seção transversal das vigas ocorreu após a realização do ensaio de flexão, entretanto não foram verificados danos visíveis a olho nu na interface entre os materiais.

5.3.2.3 Análise da capacidade do CCNS para monitoramento de deformações e danos

Para analisar a variação do GF do sensor cimentício após os ciclos de carregamento com diferentes magnitudes, este parâmetro foi recalculado após cada estágio de carga, considerando o valor de FCR medido no CCNS e a deformação de referência obtida por meio do SG-C. Na Figura 9, são apresentados os gráficos com as relações entre FCR e deformação para a viga RC-20.

Figura 9 – Viga RC-20: Relação entre FCR e Deformação

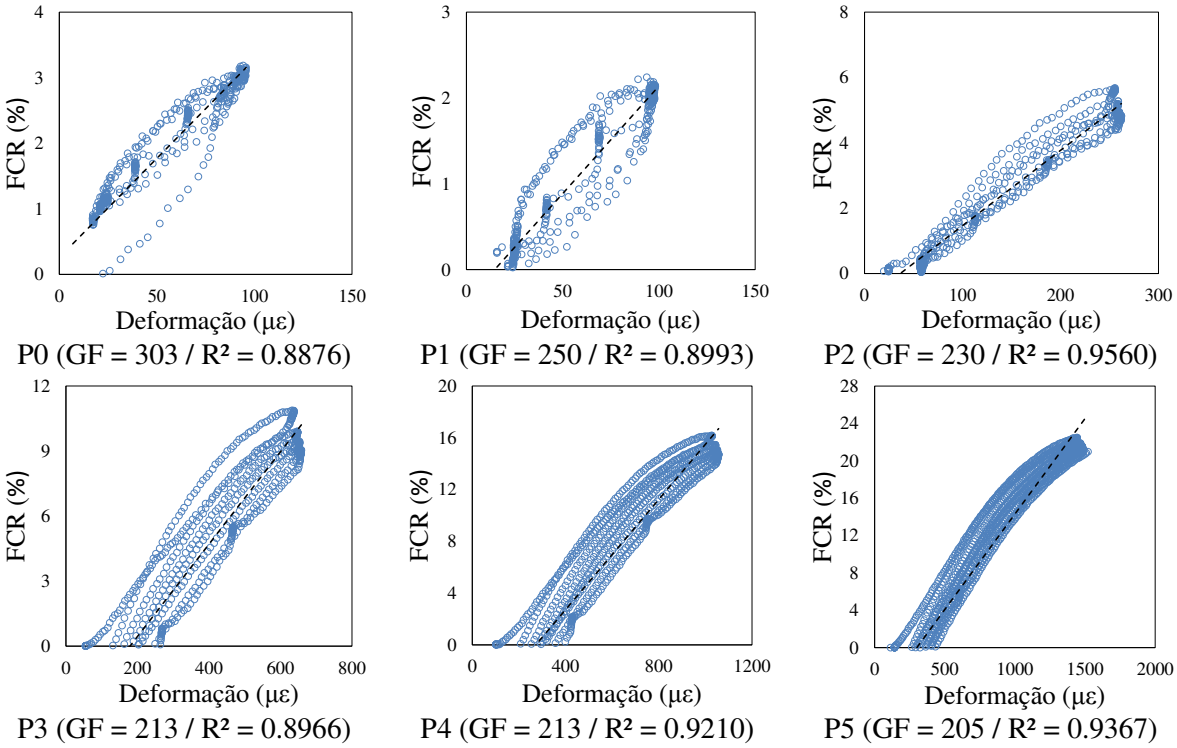

Fonte: Autor (2024)

No primeiro estágio de carregamento (P0), é perceptível uma maior dispersão dos dados, possivelmente relacionada a acomodações iniciais do ensaio. Para esta etapa, o GF calculado ($GF_0 = 303$), foi cerca de 10.2% superior ao GF obtido durante a calibração do sensor cimentício antes de sua instalação na viga (GF-C = 275). No segundo estágio de carga (P1), nota-se uma redução na dispersão dos dados e uma queda de 17.5% do valor de GF. A partir desse ponto, observou-se uma progressiva queda linear do GF, até atingir o estágio P3 ($GF_3 = 213$). Na etapa final, o valor de GF sofreu mais uma pequena redução de 3.8% ($GF_5 = 205$).

A redução progressiva do valor de GF após o estágio de carga P2, está associada à evolução da fissuração da matriz cimentícia ao longo das etapas de carregamento. O processo de degradação da matriz interrompe parte dos caminhos condutivos do compósito, aumentando sua resistividade elétrica e, por consequência, reduzindo o valor de FCR esperado para um mesmo nível de deformação, o que leva a uma redução nos valores de GF.

Na Figura 10, é apresentado o monitoramento das deformações do concreto da viga RC-20 ao longo do tempo. A curva cinza, representa o sinal original do CCNS obtido durante o ensaio de flexão. A curva azul, reproduz o sinal do CCNS após passar pelo tratamento de suavização, descrito no item 5.2.2.2. É possível verificar que o ruído do sinal original manteve sua amplitude ao longo do ensaio, ficando praticamente imperceptível com o aumento do nível de deformação, melhor evidenciado nos estágios de carregamento P3 a P5. Por fim, a curva

laranja representa a resposta do *strain guage* (SG-C) posicionado na face superior da viga, conforme descrito na seção 5.2.3.3.

Figura 10 – Viga RC-20: Monitoramento da deformação ao longo do tempo
(Codificação de cores: CCNS original – Cinza; CCNS suavizado – Azul; SG-C – Laranja)

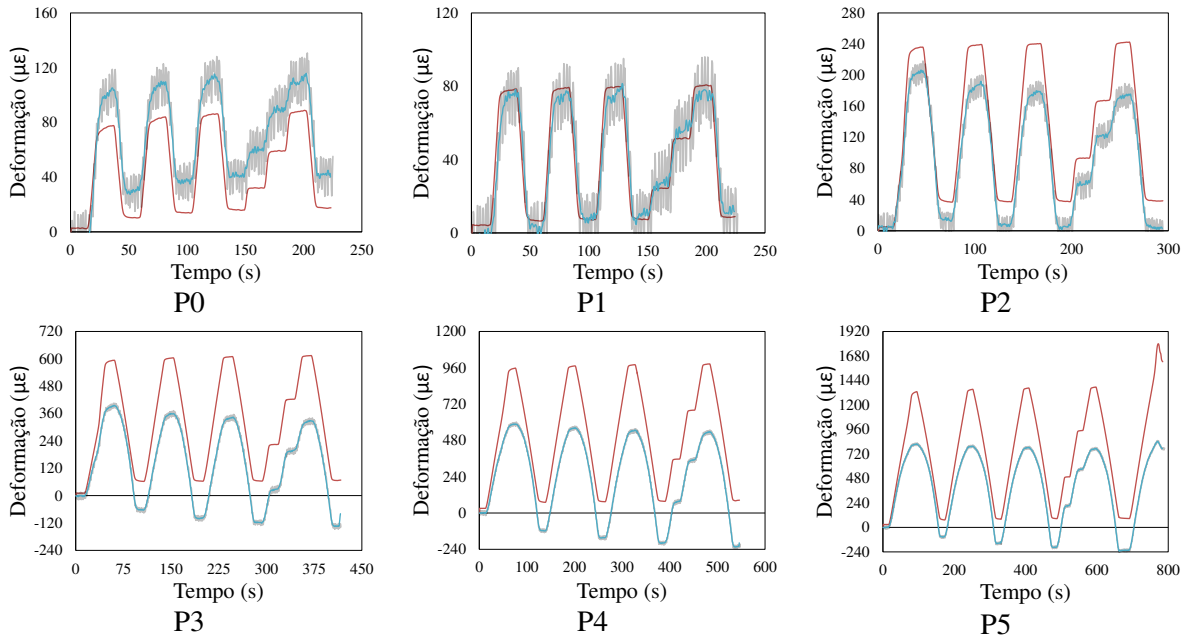

Fonte: Autor (2024)

Analisando conjuntamente as Figuras 9 e 10, é possível verificar que após o ciclo de ajuste inicial (P0), o CCNS foi capaz de monitorar adequadamente as deformações até o carregamento do estágio P1, registrando resposta semelhando do SG-C (curva laranja). Este comportamento indica que a viga de concreto ainda não havia ultrapassado os limites do regime elástico-linear. Entretanto, como o módulo de elasticidade do CCNS é 18.8% maior do que o do concreto do modelo RC-20, é possível observar que as deformações medidas com o CCNS são menores que as registradas com o SG-C.

A partir do carregamento de nível P2, os resultados sugerem que o CCNS inicia um processo de formação de fissuras. A partir desse estágio, a resposta elétrica do CCNS não mais representa apenas os efeitos das deformações de compressão, mas também os efeitos da formação e propagação de fissuras. É possível verificar que, a partir do estágio P2, as curvas de deformação continuam alcançando as mesmas amplitudes. Entretanto, a cada ciclo de carga/descarga, a curva FCR versus Tempo, sofria ligeiros deslocamentos para baixo. Este comportamento sugere que o CCNS é capaz de monitorar o surgimento de danos em uma estrutura sujeita a carregamentos excessivos repetitivos. Por estar embutido na estrutura monitorada e, por ser produzido com a mesma matriz do substrato, espera-se que o CCNS sofra danos correlacionados aos gerados na viga de concreto. As alterações causadas na matriz do

CCNS levam a um aumento da resistividade elétrica e, consequentemente, a uma modificação nos valores máximos de FCR observados durante o ensaio, o que implica no deslocamento observado nas curvas da Figura 10.

O comportamento do SG-C é retratado pela curva laranja, conforme Figura 10. Nota-se que SG-C e CCNS atingem amplitudes semelhantes de deformação, com destaque para o estágio P1, onde ambos os sensores exibem respostas semelhantes. Entretanto, para os estágios de carregamento seguintes, o SG-C não apresenta o deslocamento do seu sinal como acontece com o CCNS. Por se tratar de um *strain gauge* comercial convencional colado na superfície da viga, este tipo de sensor não é capaz de detectar danos internos causados na matriz cimentícia. Assim, o sensor apresentou o mesmo padrão de resposta para todos os níveis de carregamento ao longo do ensaio, relacionado às deformações medidas na superfície da viga.

Na Figura 11, são apresentados os gráficos com as relações entre FCR e deformação para a viga RC-30. O primeiro estágio de carregamento apresentou comportamento semelhante ao observado na série RC-20, entretanto com uma dispersão um pouco menor, como pode ser observado por meio da comparação entre os coeficientes de correlação das duas séries.

O GF calculado para o estágio de carregamento P0 ($GF_0 = 402$), foi 16.2% superior ao GF obtido durante a calibração (GF-C = 337). O GF para os estágios P1 e P2 foi cerca de 7.7% e 0.9% superior ao observado na referência de calibração, respectivamente. Para os demais estágios de carregamento, foi observado um aumento no grau de dispersão dos dados semelhante ao da série RC-20. Conforme discutido anteriormente, esse comportamento está associado às alterações causadas nos caminhos condutivos pelo processo de deterioração da matriz cimentícia.

Figura 11 – Viga RC-30: Relação entre FCR e Deformação

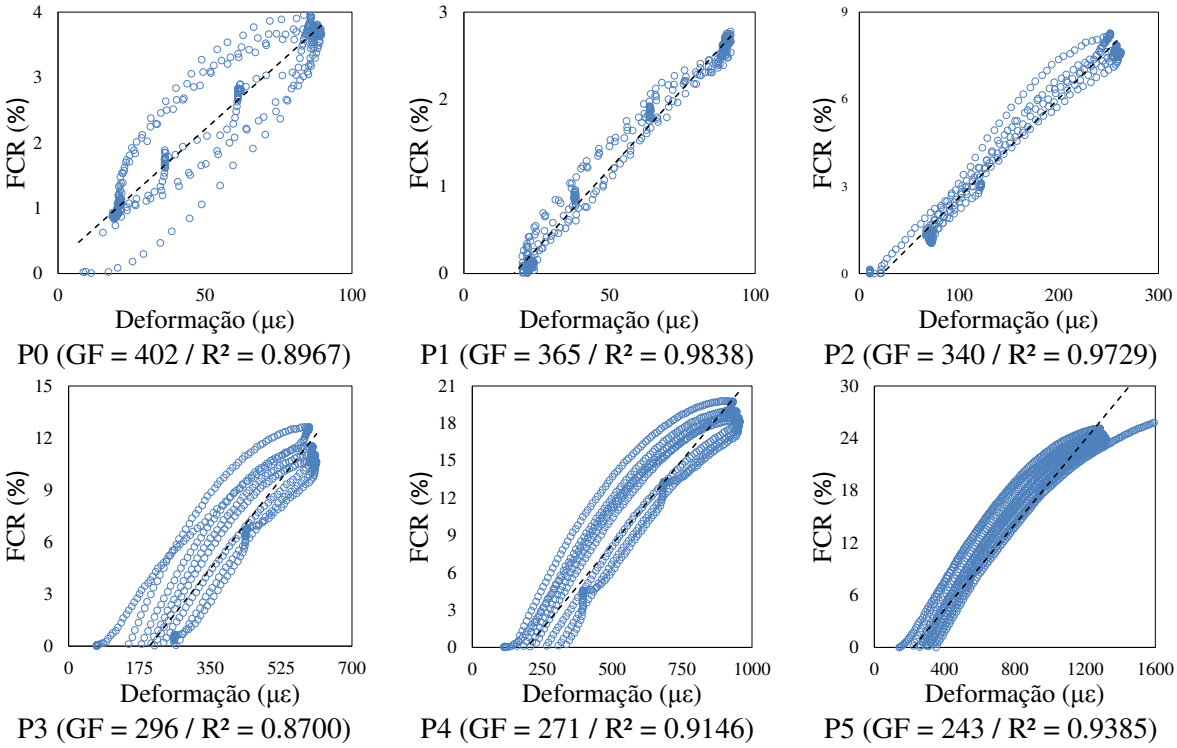

Fonte: Autor (2024)

O monitoramento das deformações ao longo do tempo para a viga RC-30 é apresentado na Figura 12. De forma geral, a relação ruído/sinal manteve sua amplitude ao longo de cada ensaio, apresentando a impressão de atenuação para os estágios de carregamento P3 a P5, devido as variações de escala do eixo vertical dos gráficos. Por meio da análise conjunta das Figuras 11 e 12, nota-se que o CCNS monitorou de forma eficiente as deformações do estágio de carregamento P1 e nos dois primeiros ciclos de carga/descarga do estágio P2. Este comportamento é um indicativo que, para esse nível de carregamento, a viga se encontrava no regime elástico-linear. Como o módulo de elasticidade do CCNS é cerca de 6.9% maior do que o do modelo RC-30, é possível observar que as deformações registradas com o CCNS foram levemente maiores que as do SG-C, para o estágio P1 e em parte do P2.

A partir da segunda metade do estágio de carregamento P2, fica mais nítido que a viga apresentou sinais do início do processo de fissuração da matriz cimentícia. Comportamento semelhante ao observado para o modelo RC-20 pode ser notado, onde verifica-se que as curvas de deformação, medidas pelo *strain gauge* comercial, continuam alcançando as mesmas amplitudes, enquanto a cada novo ciclo de carga/descarga, a curva FCR versus Tempo se desloca para baixo. Quando atinge esta fase, a resposta elétrica do compósito passa a caracterizar não apenas o estado de compressão em que se encontra, mas também o nível de fissuração que apresenta. Logo, os resultados sugerem que o CCNS é capaz de monitorar danos

causados pela formação de fissuras na matriz cimentícia. Para o *strain gauge* comercial SG-C, da mesma forma que relatado para o modelo anterior, não foram observadas alterações no sinal de resposta que possam ser associadas a uma habilidade de monitoramento de danos.

Figura 12 – Viga RC-30: Monitoramento da deformação ao longo do tempo
(Codificação de cores: CCNS original – Cinza; CCNS suavizado – Azul; SG-C – Laranja)

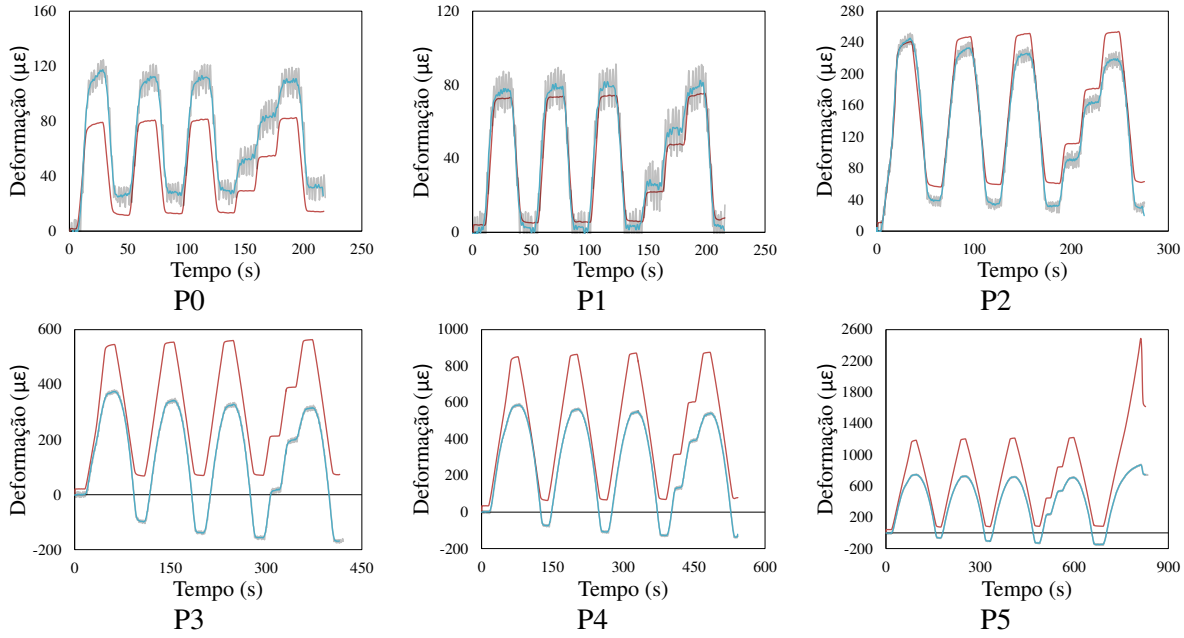

Fonte: Autor (2024)

Na Figura 13, são apresentados os gráficos com as relações entre FCR e deformação para a viga RC-35. Assim como observado nas séries anteriores, o estágio P0 auxiliou na redução da dispersão dos dados, por meio de acomodações iniciais e ajustes de posicionamento do conjunto na máquina de ensaios. Essa abordagem se mostrou eficiente em todos os casos estudados nesse trabalho.

O GF calculado para o estágio de carregamento P0 (GF_0 = 260), foi cerca de 33.1% inferior ao GF obtido durante a calibração (GF-C = 346). O GF para os estágios P1 e P2 foi cerca de 34.1% e 31.6% inferiores ao observado na referência de calibração, respectivamente. Para os estágios P3 e P4, foi observado um aumento no grau de dispersão dos dados, semelhante ao que ocorreu nas séries já analisadas. Conforme discutido anteriormente, esse comportamento está associado às mudanças que o processo de fissuração gradual da matriz cimentícia causa nos caminhos condutivos do CCNS.

Figura 13 – Viga RC-35: Relação entre FCR e Deformação

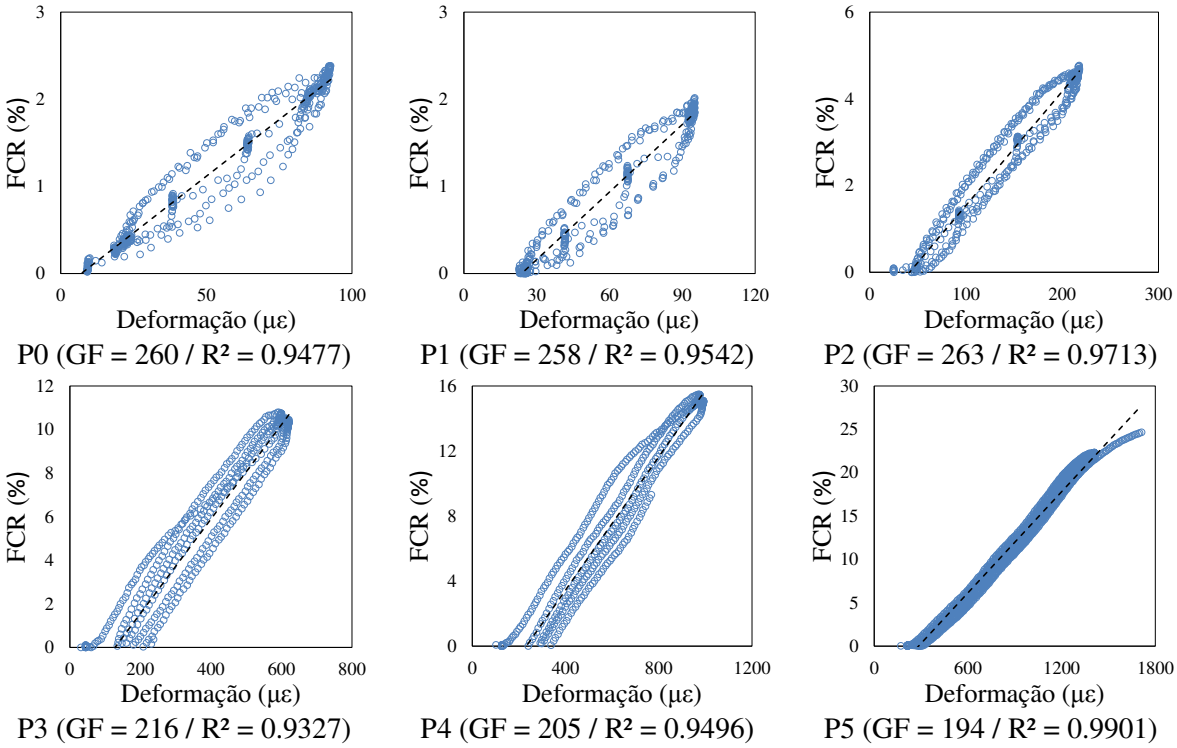

Fonte: Autor (2024)

O monitoramento das deformações ao longo do tempo para a viga RC-30 é apresentado na Figura 14. De forma geral, a relação ruído/sinal manteve sua amplitude ao longo de cada ensaio, apresentando uma impressão de maior atenuação para os estágios de carregamento P3 a P5, devido à ampliação da escala do eixo vertical dos gráficos. Por meio da análise conjunta das Figuras 13 e 14, diferente do que foi observado nas séries anteriores, o CCNS não foi capaz de atingir o mesmo nível de deformação medido pelo *strain gauge* comercial. Como o módulo de elasticidade do CCNS é cerca de 8.9% menor do que o do modelo RC-35, é possível que tenha ocorrido uma restrição na transmissão dos esforços do concreto para o sensor, impactando na resposta de deformação.

No estágio de carregamento P2, a evidência do possível desenvolvimento de microfissuração é mais sutil, ficando tal efeito, mais evidente no estágio P3. Este comportamento está relacionado ao fato desse modelo experimental possuir uma maior rigidez quando comparada com a dos demais modelos e com a do CCNS. No entanto, da mesma forma que foi observado anteriormente, as curvas de deformação, medidas pelo *strain gauge* comercial, continuam alcançando as mesmas amplitudes, enquanto a cada novo ciclo de carga/descarga, a curva FCR versus Tempo se desloca para baixo. Nessa fase, a resposta elétrica do CCNS é influenciada pela deformação causada pela compressão do sensor e pelas mudanças dos caminhos condutivos causadas pelo processo de fissuração na matriz do compósito. Logo,

o CCNS é capaz de monitorar danos causados pela deterioração da matriz cimentícia provocada pela formação de fissuras. Para o *strain gauge* comercial SG-C, da mesma forma que reportado para os modelos anteriores, não foram observadas alterações no sinal de resposta que possam ser associadas a uma habilidade de monitoramento de danos.

Figura 14 – Viga RC-35: Monitoramento da deformação ao longo do tempo
(Codificação de cores: CCNS original – Cinza; CCNS suavizado – Azul; SG-C – Laranja)

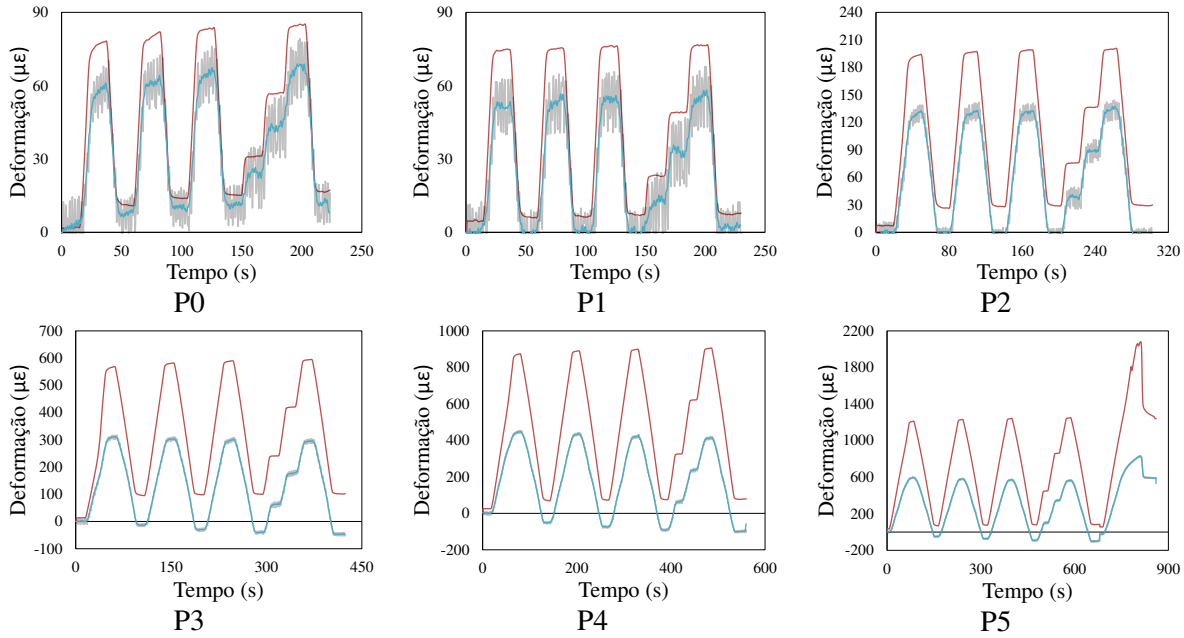

Fonte: Autor (2024)

5.3.2.4 Análise da compatibilidade entre os CCNS e as vigas de concreto

Na seção anterior, foram discutidos os aspectos relacionados à variação do GF com o aumento do nível de carregamento dos modelos experimentais e as habilidades de monitoramento de deformação e danos do CCNS. Nessa seção, os resultados foram sintetizados na Figura 15, com o objetivo de analisar para qual dos casos estudados o CCNS apresentou as melhores condições de compatibilidade mecânica. Para esta análise, os dados do nível de carregamento P0 não foram considerados pois, como discutido na seção anterior, esse nível foi responsável apenas por garantir as acomodações iniciais do conjunto para a realização do ensaio e, mantê-lo nesta análise, poderia induzir um viés na conclusão.

Na Figura 15, a curva GF-T representa a variação do GF ao longo dos diferentes estágios de carregamento a que as vigas foram submetidas. A linha GF-C indica o GF obtido na calibração dos CCNS, em ensaios de compressão uniaxial. Por fim, a linha GF-Ta, marca a posição do valor médio do GF-T das faixas de carregamento P1 e P2. Estas faixas foram

escolhidas para a análise, pois apenas elas se restringiram às proximidades do regime elástico-linear dos CCNS.

Figura 15 – Variação do GF em função dos estágios de carregamento

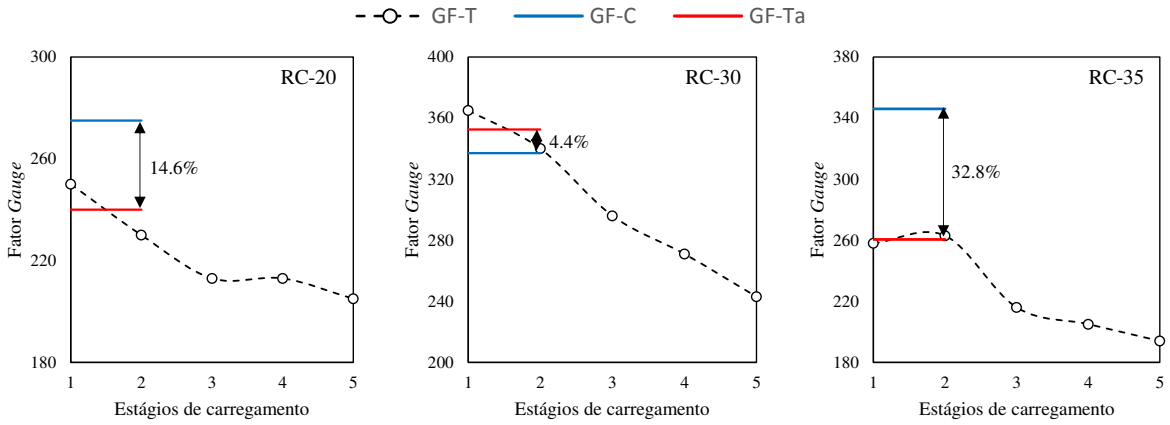

RC-20 RC-30 RC-35

Fonte: Autor (2024)

Para o caso da viga RC-20, nota-se que o valor de GF-C apresentou uma diferença de 14.6% em relação a GF-Ta. O modelo de regressão que ofereceu o melhor ajuste para GF-T foi um modelo polinomial de grau 2. Para o caso da viga RC-30, foi observada uma diferença de apenas 4.4% de GF-C em relação ao GF-C. O GF-T, apresentou o melhor ajuste ao modelo de regressão linear. Por fim, para a viga RC-35, a diferença entre GF-C e GF-T, foi da ordem de 32.8%. Para este caso, o ajuste mais adequado para o GF-T ocorreu para um modelo de regressão polinomial de quarto grau.

Conforme pode ser observado nas discussões apresentadas na seção 5.3.2.3, os estágios de carregamento P1 e P2, marcam a faixa de carga correspondente ao regime elástico e, eventualmente, o início da transição para o regime plástico. Analisando especificamente esses estágios de carregamento nas Figuras 10, 12 e 14, nota-se que o modelo RC-30 apresentou a melhor habilidade para o monitoramento de deformação no regime elástico-linear, de modo que os valores de GF obtidos nos estágios de carregamento 1 e 2 (365 e 340, respectivamente) foram bem próximos ao valor de GF obtido no ensaio de compressão inicial (337). Este comportamento possivelmente está relacionado com o fato de o CCNS possuir um módulo de elasticidade médio ligeiramente superior (+6.89%) ao do concreto do modelo RC-30. Para o caso oposto, no qual o módulo de elasticidade do CCNS foi inferior ao do concreto (-8.90%), não foi observada a mesma situação de compatibilidade.

Quanto à habilidade de monitoramento de danos, a análise das Figuras 10, 12 e 14, também indica que em todos os modelos foi possível observar esse comportamento. Não foram

observadas diferenças significativas de comportamento para essa habilidade considerando a diferença do módulo de elasticidade para ciclo de carregamento de curta duração. Assim, futuros estudos dedicados à aplicação de carregamentos cíclicos de longa duração são necessários para compreender melhor os efeitos da deterioração na matriz no comportamento piezoresistivo do sensor e seus impactos na capacidade de monitorar danos.

5.4 CONCLUSÕES

No presente trabalho foi desenvolvida uma investigação da compatibilidade mecânica entre os CCNS e vigas de concreto armado submetidas à flexão. As principais conclusões obtidas no estudo são as seguintes:

(1) As respostas obtidas no processo de calibração dos CNCS indicaram que a metodologia adotada na produção dos sensores foi adequada para a aplicação proposta, sendo a variabilidade de respostas mecânicas e sensoras observadas, compatíveis com aquelas tipicamente observada em estudos anteriores;

(2) A análise da interface CCNS-concreto, evidenciou que o uso do adesivo estrutural de base epóxi com adição de uma fina camada de areia, foi uma solução eficaz para estabelecer apropriada ponte de aderência entre os materiais, garantindo que os esforços fossem transmitidos de uma maneira adequada;

(3) A habilidade de monitoramento de deformações da viga de concreto pelo CCNS apresentou as melhores respostas para o caso do modelo RC-30, no qual o sensor possuía módulo de elasticidade ligeiramente inferior ao do concreto da viga. Para este caso, o sensor foi capaz de registrar as deformações de forma adequada por uma maior faixa de carregamento. Para os demais casos estudados, o sensor monitorou as deformações corretamente por uma faixa de carregamento menor (RC-20) ou demonstrou uma menor capacidade de registrar a amplitude das deformações (RC-35);

(4) A habilidade de monitoramento de danos da viga de concreto pelo CCNS foi observada para todos os modelos estudados, uma vez que a aplicação de carregamento na faixa do regime plástico do material, proporcionou reduções progressivas na amplitude de FCR e, consequentemente, decréscimos no valor do GF do CCNS;

(5) O conjunto de todos os resultados analisados sugere que CCNS apresentou a melhor compatibilidade mecânica com a viga do modelo RC-30, com base nas respostas obtidas para automonitoramento de deformações e autodetecção de danos. Um módulo de

elasticidade médio ligeiramente menor que o do elemento que se deseja monitorar, foi fundamental para a obtenção de uma resposta mais coerente do sensor.

Para promover mais avanços neste campo do conhecimento, os autores sugerem investigar os efeitos da compatibilidade mecânica entre os CCNS e elementos de concreto armado submetidos à carregamentos cíclicos de longa duração e a deformações causadas por efeitos de variação de temperatura.

5.5 REFERÊNCIAS

[1] D. Xu, X. Xu, M.C. Forde, A. Caballero, Concrete and steel bridge Structural Health Monitoring—Insight into choices for machine learning applications, Constr. Build. Mater. 402 (2023) 132596. https://doi.org/10.1016/J.CONBUILDMAT.2023.132596.

[2] A. Dinesh, D. Suji, M. Pichumani, Performance evaluation of graphite-integrated smart-engineered cementitious composite for health monitoring of structural components, J. Build. Eng. 69 (2023) 106228. https://doi.org/10.1016/J.JOBE.2023.106228.

[3] A.A.E. Elseady, Y. Zhuge, X. Ma, C.W.K. Chow, I. Lee, J. Zeng, N. Gorjian, Development of self-sensing cementitious composites by incorporating a two-dimensional carbon-fibre textile network for structural health monitoring, Constr. Build. Mater. 415 (2024) 135049. https://doi.org/10.1016/J.CONBUILDMAT.2024.135049.

[4] J. Zhang, M. Huang, N. Wan, Z. Deng, Z. He, J. Luo, Missing measurement data recovery methods in structural health monitoring: The state, challenges and case study, Measurement. 231 (2024) 114528. https://doi.org/10.1016/j.measurement.2024.114528.

[5] S. Ding, S. Dong, A. Ashour, B. Han, Development of sensing concrete: Principles, properties and its applications, J. Appl. Phys. 126 (2019). https://doi.org/10.1063/1.5128242.

[6] A. D'Alessandro, A. Meoni, F. Ubertini, A. Luigi Materazzi, Strain Measurement in a Reinforced Concrete Beam Using Embedded Smart Concrete Sensors, in: 2020: pp. 289–300. https://doi.org/10.1007/978-3-030-23748-6_22.

[7] W. Dong, W. Li, Z. Tao, K. Wang, Piezoresistive properties of cement-based sensors: Review and perspective, Constr. Build. Mater. 203 (2019) 146–163. https://doi.org/10.1016/j.conbuildmat.2019.01.081.

[8] Y. Wang, L. Zhang, B. Han, S. Sun, Y. Qin, X. Han, G. Yang, M. Li, X. Fan, W. Peng, Advances in self-sensing cement-based composites containing nano materials for smart

civil infrastructures, Measurement. 230 (2024) 114514. https://doi.org/10.1016/j.measurement.2024.114514.

[9] I. You, D.Y. Yoo, S. Kim, M.J. Kim, G. Zi, Electrical and self-sensing properties of ultra-high-performance fiber-reinforced concrete with carbon nanotubes, Sensors (Switzerland). 17 (2017). https://doi.org/10.3390/s17112481.

[10] G.H. Nalon, J.C.L. Ribeiro, R.M. da Silva, L.G. Pedroti, E.N.D. de Araújo, Self-sensing concrete masonry structures with intrinsic abilities of strain monitoring and damage detection, Structures. 59 (2024) 105760. https://doi.org/10.1016/j.istruc.2023.105760.

[11] E. Demircilioğlu, E. Teomete, O.E. Ozbulut, S. Kahraman, Cross tension and compression loading and large-scale testing of strain and damage sensing smart concrete, Constr. Build. Mater. 316 (2022) 125784. https://doi.org/10.1016/j.conbuildmat.2021.125784.

[12] L. Wang, F. Aslani, A review on material design, performance, and practical application of electrically conductive cementitious composites, Constr. Build. Mater. 229 (2019) 116892. https://doi.org/10.1016/j.conbuildmat.2019.116892.

[13] D.D.L. Chung, Electrical applications of carbon materials, J. Mater. Sci. 39 (2004) 2645–2661. https://doi.org/10.1023/B:JMSC.0000021439.18202.ea.

[14] S.-H. Lee, J.H. Kim, S.-J. Han, S.-T. Yi, K.S. Kim, Self-sensing capability of ultra-high performance fiber-reinforced concrete with multiwalled carbon nanotubes, J. Build. Eng. 86 (2024) 108972. https://doi.org/10.1016/j.jobe.2024.108972.

[15] L. Wang, F. Aslani, Structural performance of reinforced concrete beams with 3D printed cement-based sensor embedded and self-sensing cementitious composites, Eng. Struct. 275 (2023) 115266. https://doi.org/10.1016/j.engstruct.2022.115266.

[16] X. Wang, A. Al-Tabbaa, S.K. Haigh, Measurement techniques for self-sensing cementitious composites under flexure, Cem. Concr. Compos. 142 (2023) 105215. https://doi.org/10.1016/j.cemconcomp.2023.105215.

[17] A. Hussain, Y. Xiang, T. Yu, F. Zou, Nanocarbon black-based ultra-high-performance concrete (UHPC) with self-strain sensing capability, Constr. Build. Mater. 359 (2022) 129496. https://doi.org/10.1016/j.conbuildmat.2022.129496.

[18] H. Li, H. Xiao, J. Ou, Effect of compressive strain on electrical resistivity of carbon black-filled cement-based composites, Cem. Concr. Compos. 28 (2006) 824–828. https://doi.org/10.1016/j.cemconcomp.2006.05.004.

[19] A.O. Monteiro, Development of a multifunctional carbon black/cement composite for traffic monitoring, Universidade de Aveiro, 2018.

[20] Y. Huang, H. Li, S. Qian, Self-sensing properties of Engineered Cementitious Composites, Constr. Build. Mater. 174 (2018) 253–262. https://doi.org/10.1016/j.conbuildmat.2018.04.129.

[21] Z. Zhou, N. Xie, X. Cheng, L. Feng, P. Hou, S. Huang, Z. Zhou, Electrical properties of low dosage carbon nanofiber/cement composite: Percolation behavior and polarization effect, Cem. Concr. Compos. 109 (2020) 103539. https://doi.org/10.1016/j.cemconcomp.2020.103539.

[22] D.-Y. Yoo, I. You, H. Youn, S.-J. Lee, Electrical and piezoresistive properties of cement composites with carbon nanomaterials, J. Compos. Mater. 52 (2018) 3325–3340. https://doi.org/10.1177/0021998318764809.

[23] G.E.S. de Lima, G.H. Nalon, R.F. Santos, J.C.L. Ribeiro, J.M.F. de Carvalho, L.G. Pedroti, E.N.D. de Araújo, Microstructural Investigation of the Effects of Carbon Black Nanoparticles on Hydration Mechanisms, Mechanical and Piezoresistive Properties of Cement Mortars, Mater. Res. 24 (2021). https://doi.org/10.1590/1980-5373-mr-2020-0539.

[24] L. Wang, F. Aslani, Structural performance of reinforced concrete beams with 3D printed cement-based sensor embedded and self-sensing cementitious composites, Eng. Struct. 275 (2023) 115266. https://doi.org/10.1016/j.engstruct.2022.115266.

[25] R. kant Rao, S. Sasmal, Smart nano-engineered cementitious composite sensors for vibration-based health monitoring of large structures, Sensors Actuators A. Phys. 311 (2020) 112088. https://doi.org/10.1016/j.sna.2020.112088.

[26] W. Dong, W. Li, Z. Luo, G. Long, K. Vessalas, D. Sheng, Structural response monitoring of concrete beam under flexural loading using smart carbon black / cement-based sensors, (2020).

[27] N. Yang, Q. Sun, Study on the Self-Monitoring of Bending Fatigue Cumulative Damage for Carbon Nanofiber Polyurethane Cement, Appl. Sci. 9 (2019) 1–20.

[28] M.H. Sarwary, G. Yıldırım, A. Al-Dahawi, Ö. Anıl, K.A. Khiavi, K. Toklu, M. Şahmaran, Self-Sensing of Flexural Damage in Large-Scale Steel-Reinforced Mortar Beams, ACI Mater. J. 116 (2019). https://doi.org/10.14359/51715581.

[29] A. Hussain, Y. Ding, G. Liu, A. Naqi, Study on self-monitoring of multiple cracked concrete beams with multiphase conductive materials subjected to bending, (2019).

[30] Y. Ding, G. Liu, A. Hussain, F. Pacheco-torgal, Y. Zhang, Effect of steel fiber and carbon black on the self-sensing ability of concrete cracks under bending Effect of steel fiber and carbon black on the self-sensing ability of concrete cracks under bending, Constr.

Build. Mater. 207 (2019) 630–639. https://doi.org/10.1016/j.conbuildmat.2019.02.160.

[31] G. Henrique Nalon, J. Carlos Lopes Ribeiro, E. Nery Duarte de Araújo, R. Marcio da Silva, L. Gonçalves Pedroti, G. Emilio Soares de Lima, Concrete units for strain-monitoring in civil structures: Installation of cement-based sensors using different approaches, Constr. Build. Mater. 394 (2023) 132169. https://doi.org/10.1016/j.conbuildmat.2023.132169.

[32] G.H. Nalon, J.C. Lopes Ribeiro, E.N. Duarte de Araújo, R. Marcio da Silva, L.G. Pedroti, Effects of shrinkage-reducing admixtures and expansive agents on the self-sensing behavior of nanomodified cement-based materials, J. Build. Eng. 78 (2023) 107648. https://doi.org/10.1016/J.JOBE.2023.107648.

[33] G.H. Nalon, J.C. Lopes Ribeiro, L.G. Pedroti, E.N. Duarte de Araújo, J.M. Franco de Carvalho, G.E. Soares de Lima, L. de Moura Guimarães, Residual piezoresistive properties of mortars containing carbon nanomaterials exposed to high temperatures, Cem. Concr. Compos. 121 (2021) 104104. https://doi.org/10.1016/J.CEMCONCOMP.2021.104104.

[34] H. Wang, F. Shi, J. Shen, A. Zhang, L. Zhang, H. Huang, J. Liu, K. Jin, L. Feng, Z. Tang, Research on the self-sensing and mechanical properties of aligned stainless steel fiber-reinforced reactive powder concrete, Cem. Concr. Compos. 119 (2021) 104001. https://doi.org/10.1016/J.CEMCONCOMP.2021.104001.

[35] J. Han, J. Cai, J. Pan, Y. Sun, Study on the conductivity of carbon fiber self-sensing high ductility cementitious composite, J. Build. Eng. 43 (2021) 103125. https://doi.org/10.1016/J.JOBE.2021.103125.

[36] G.H. Nalon, J.C.L. Ribeiro, E.N.D. de Araújo, L.G. Pedroti, J.M.F. de Carvalho, R.F. Santos, A. Aparecido-Ferreira, Effects of different kinds of carbon black nanoparticles on the piezoresistive and mechanical properties of cement-based composites, J. Build. Eng. 32 (2020) 101724. https://doi.org/10.1016/J.JOBE.2020.101724.

[37] A. Downey, A. D'Alessandro, F. Ubertini, S. Laflamme, R. Geiger, Biphasic DC measurement approach for enhanced measurement stability and multi-channel sampling of self-sensing multi-functional structural materials doped with carbon-based additives, Smart Mater. Struct. 26 (2017) 065008. https://doi.org/10.1088/1361-665X/aa6b66.

[38] A. Meoni, A. D'Alessandro, R. Kruse, L. De Lorenzis, F. Ubertini, Strain field reconstruction and damage identification in masonry walls under in-plane loading using dense sensor networks of smart bricks: Experiments and simulations, Eng. Struct. 239 (2021) 112199. https://doi.org/10.1016/J.ENGSTRUCT.2021.112199.

[39] Y. Huang, T. Xie, X. Xu, Q. Ding, Experimental study of creep Poisson ratio of hydraulic concrete under multi-age loading-unloading conditions, Constr. Build. Mater. 310 (2021) 125269. https://doi.org/10.1016/j.conbuildmat.2021.125269.

[40] R.N. Deo, A. Sounthararajah, J. Kodikara, Reflectance spectroscopy of asphalt pavement under moisture and diesel perturbations: A laboratory study, Constr. Build. Mater. 415 (2024) 135076. https://doi.org/10.1016/j.conbuildmat.2024.135076.

[41] B. Liu, F. Yue, B. Chen, X. Man, L. Chen, S. Jaisee, Study on bond performance, flexural and crack extension behavior of base concrete prisms strengthen with strain-hardening cementitious composites (SHCC) using DIC technology, Constr. Build. Mater. 251 (2020) 119035. https://doi.org/10.1016/j.conbuildmat.2020.119035.

[42] M.A. Dehghani Najvani, D. Heras Murcia, E. Soliman, M.M. Reda Taha, Early-age strength and failure characteristics of 3D printable polymer concrete, Constr. Build. Mater. 394 (2023) 132119. https://doi.org/10.1016/j.conbuildmat.2023.132119.

[43] Brazilian Association of Technical Standards, NBR 12655:2022 - Portland cement concrete - Preparation, control, receipt and acceptance, Rio de Janeiro, 2022.

[44] Brazilian Association of Technical Standards, NBR 16889:2020 - Fresh concrete - Slump test, Rio de Janeiro, 2020.

[45] Brazilian Association of Technical Standards, NBR 5739:2018 - Concrete - Compression test of cylindrical specimens, Rio de Janeiro, 2018.

[46] Brazilian Association of Technical Standards, NBR 8522-1:2021 - Hardened concrete - Determination of elasticity and deformation modulus - Part 1: Static modulus by compression, Rio de Janeiro, 2021.

[47] Brazilian Association of Technical Standards, NBR ISO 6892-1: 2024 - Metallic materials - Tensile testing - Part 1: Method od test at room temperature, Rio de Janeiro, 2024.

[48] H. Xiao, H. Li, J. Ou, Strain sensing properties of cement-based sensors embedded at various stress zones in a bending concrete beam, Sensors Actuators A. Phys. 167 (2011) 581–587. https://doi.org/10.1016/j.sna.2011.03.012.

[49] Y. Ding, Z. Chen, Z. Han, Y. Zhang, F. Pacheco-torgal, Nano-carbon black and carbon fiber as conductive materials for the diagnosing of the damage of concrete beam, Constr. Build. Mater. 43 (2013) 233–241. https://doi.org/10.1016/j.conbuildmat.2013.02.010.

[50] S. Ding, Y. Ruan, X. Yu, B. Han, Y.Q. Ni, Self-monitoring of smart concrete column incorporating CNT/NCB composite fillers modified cementitious sensors, Constr. Build. Mater. 201 (2019) 127–137. https://doi.org/10.1016/J.CONBUILDMAT.2018.12.203.

[51] R. kant Rao, B.S. Sindu, S. Sasmal, Synthesis , design and piezo-resistive characteristics of cementitious smart nanocomposites with different types of functionalized MWCNTs under long cyclic loading, Cem. Concr. Compos. 108 (2020) 103517. https://doi.org/10.1016/j.cemconcomp.2020.103517.

[52] B. Coppola, L. Di Maio, L. Incarnato, J.-M. Tulliani, Preparation and Characterization of Polypropylene/Carbon Nanotubes (PP/CNTs) Nanocomposites as Potential Strain Gauges for Structural Health Monitoring, Nanomaterials. 10 (2020) 814. https://doi.org/10.3390/nano10040814.

6 CONCLUSÕES E CONSIDERAÇÕES DA TESE

6.1 CONSIDERAÇÕES FINAIS

O presente trabalho teve como objetivo geral o desenvolvimento de um estudo para otimização da dispersão de nanopartículas visando a potencialização das propriedades de CCNS e a avaliação da compatibilidade mecânica destes compósitos em vigas de concreto armado.

Para atender este objetivo geral, foram realizadas investigações quanto:

(1) O estado da arte para produção, os mecanismos de hidratação e as propriedades mecânicas e piezoresistivas de argamassas sensoras;
(2) Os efeitos da variação da energia de sonicação na dispersão de CBN e no comportamento eletromecânico e reológico de CCNS. O desempenho mecânico e sensor dos compósitos foram explicados pela análise da qualidade de dispersão das nanosuspensões através de diferentes técnicas;
(3) Os impactos da variação da razão PCE/CBN no comportamento eletromecânico e reológico de CCNS. No estudo, foi realizada uma análise da qualidade das nanosuspensões proporcionada por diferentes teores de surfactante;
(4) A compatibilidade mecânica entre os CCNS e um elemento de concreto armado submetido à flexão. Esse estudo fornece diretrizes essenciais para a seleção e aplicação de CCNS.

6.2 PRINCIPAIS CONTRIBUIÇÕES DA PESQUISA

As principais contribuições que originaram do desenvolvimento deste trabalho foram:

(1) No estado da arte para produção, os mecanismos de hidratação e as propriedades mecânicas e piezoresistivas de argamassas sensoras: (i) identificação dos efeitos de diferentes materiais nos mecanismos de condutividade elétrica e resposta de autodetecção; (ii) identificação dos teores de diferentes materiais incorporados à matrizes cimentícias que podem proporcionar melhorias em algumas propriedades sensoras; e (iii) sugestão de resíduos de origem agrícola e industrial que podem ser alternativas promissoras para a produção de CCNS em futuras pesquisas;

(2) Nos efeitos da variação da energia de sonicação na dispersão de CBN: (i) avaliação conjunta do comportamento eletromecânico e reológico de argamassas produzidas com CBN dispersas com diferentes níveis de energia de sonicação; (ii) análise da qualidade da dispersão de CBN proporcionada pelos diferentes níveis de energia de sonicação, utilizando-se uma combinação de quatro diferentes técnicas; e (iii) identificação da energia de sonicação ótima para produção de CCNS contendo CBN;

(3) Nos impactos da variação da razão PCE/CBN no comportamento eletro-mecânico e reológico de CCNS: (i) avaliação conjunta do comportamento eletromecânico e reológico de argamassas produzidas com CBN dispersas com diferentes teores de PCE; (ii) análise da qualidade da dispersão de CBN proporcionada pelos diferentes teores de PCE, utilizando-se uma combinação de quatro diferentes técnicas; e (iii) identificação da relação PCE/CBN ótima para produção de CCNS;

(4) Na investigação da compatibilidade mecânica entre os CCNS e um elemento de concreto armado submetido à flexão: (i) análise comparativa das deformações medidas por CCNS e strain gauge comerciais; (ii) avaliação do comportamento mecânico e piezoresistivo de um CCNS embutido em vigas com diferentes características mecânicas, após aplicação de carregamentos de diferentes magnitudes; (iii) avaliação da capacidade de um CCNS em identificar danos em vigas com diferentes características mecânicas.

6.3 CONCLUSÕES FINAIS

As principais conclusões desta Tese foram:

(1) A análise dos efeitos da variação do teor de CBN nos mecanismos de hidratação, demonstrou que concentrações de 3% proporcionaram os melhores resultados para as propriedades mecânicas. Por outro lado, teores da ordem de 5% e 6% resultaram nas melhores características sensoras. A concentração ideal de CBN foi determinada em 5%, pois proporcionou excelente piezorresistividade sem comprometer significativamente as propriedades mecânicas;

(2) A análise dos efeitos da variação da energia de sonicação na dispersão de CBN indicou que energias da ordem de 240 J/mL foram as mais eficazes na produção de nanosuspensões com dispersões de alta eficiência. Este resultado sugere um refinamento da matriz cimentícia e um consequente aumento da rede condutora. Além disso, energias

dessa magnitude foram capazes de otimizar as propriedades eletromecânicas e reológicas dos CCNS;

(3) A análise da variação da razão PCE/CBN indicou que uma relação de 0.4 otimizou o comportamento eletromecânico e reológico dos CCNS. Essa razão propiciou a obtenção de nanosuspensões com dispersão e estabilidade mais adequadas, resultando em um refinamento da matriz cimentícia e em um aumento dos caminhos condutivos;

(4) O estudo da compatibilidade mecânica entre os CCNS e um elemento de concreto armado submetido à flexão, demonstrou que o sensor cimentício estudado possui habilidades satisfatórios para automonitoramento de deformações e autodetecção de danos. Um módulo de elasticidade médio ligeiramente menor que o do elemento que se deseja monitorar, é fundamental para a obtenção de uma resposta mais coerente do sensor.